Neuronal basis of multisensory integration

Hippolyte Moulle

PHD THESIS

SORBONNE UNIVERSITÉ

Field : Physique

Doctoral school n°564: Physique en Île-de-France

completed at

Laboratoire Jean Perrin

under the supervision of Volker BORMUTH

presented by

Hippolyte MOULLE

to acquire the following degree :

DOCTOR OF PHILOSOPHY SORBONNE UNIVERSITÉ

PhD subject :

Neuronal basis of multisensory integration

defended on the 6^{th} April 2023

in front of the jury :

M.	Ruben PORTUGUES	Rapporteur
M.	Yves BOUBENEC	Rapporteur
M.	Germán SUMBRE	Examinateur (président du jury)
Mme.	Elim HONG	Examinatrice
M.	Volker BORMUTH	Directeur de thèse

Monday 29th April, 2024, 17:39 version

Abstract

In a multisensory environment, our central nervous system is constantly dealing with a substantial amount of information. In this thesis, we wonder where and how stimuli are integrated in the brain, and the influence of multisensory integration on behaviour. Using a rotating setup associated with a screen and projector, we were able to investigate the effect of vestibular and visual cues on larval zebrafish. During unisensory and multisensory stimulations, we recorded the behaviour of the animals by tracking their eyes, and analyzed their neuronal response using light-sheet imaging. From a behavioural perspective, we found that the coherence of the stimuli had a strong impact on response, and that coherent vestibular and visual stimuli elicited a super-additive behaviour. Some neurons in the brain responded to both cues, and were stereotypically located. These neurons could be modeled linearly, and some of them were super-additive. This work helps understand how vestibular stimulation, a complex to evoke stimulus, is processed with visual input, at the whole-brain level. The multisensory area uncovered could define a basis for future studies on multisensory integration.

Keywords: multisensory integration · brain · neurons · behaviour · zebrafish · light-sheet microscopy · vestibular · visual · super-additive · adaptation

Résumé

Les humains et les animaux survivent en interagissant avec leur environnement. Nous intégrons constamment des stimuli extérieurs et répondons à ceux-ci pour optimiser notre comportement et nos chances de survie. Ce flux constant d'information doit être traité par notre cerveau et par notre système nerveux pour que la représentation que nous nous faisons de ce qui nous entoure soit la plus proche possible de la réalité. Avec 100 milliards de neurones dans un cerveau d'humain adulte, et 1 000 000 milliards de connexions estimées, il est difficile de se représenter la complexité des calculs opérés dans cet organe. Mais c'est grâce à cette intégration multisensorielle continue que nous pouvons définir des commandes motrices plus rapides et plus précises, et apprendre.

A l'aide de technologies d'imagerie, il a été montré que de nombreuses zones du cerveau que nous pension unimodales sont en réalité sièges d'intégration de multiples modalités. Le défi actuel du domaine des neurosciences est de pouvoir enregistrer des données neuronales couvrant le plus grand volume possible du cerveau afin d'avoir une idée des circuits neuronaux sous-jacents, tout en ayant une résolution temporelle suffisante pour ne pas perdre trop d'information. Grâce à la technologie de microscopie à nappe de lumière, combinée à des indicateurs calciques génétiquement encodés, cette possibilité est maintenant à notre portée. Avec comme modèle animal le poisson zèbre, dont certaines sous-espèces génétiquement modifiées sont transparentes, nous avons accès à des dizaines de milliers de neurones simultanément. Comme le comportement de cet animal à l'état larvaire est facilement définissable, il est possible de relier ses actions à des circuits neuronaux, et comprendre plus en détail comment son cerveau lui permet d'interagir avec son environnement.

Pour étudier l'intégration multisensorielle, il faut nécessairement simplifier le nombre de modalités étudiées, et se concentrer sur deux d'entre elles qui, présentées en même temps, peuvent avoir un impact sur la réponse comportementale. Dans cette thèse nous

avons choisi de nous concentrer sur les modalités vestibulaire et visuelle.

Le système vestibulaire est utilisé pour stabiliser le regard et le corps. Il est intrisèquement multisensoriel, et il a été montré chez le singe que de nombreux neurones des noyaux vestibulaires répondent à des stimuli visuels. Le système vestibulaire est localisé dans l'oreille interne, et est composé de canaux semi-circulaires qui détectent les accélérations angulaires, et des otolithes qui détectent les accélérations linéaires et gravitationnelles. Ces accélérations sont perçues par les cellules ciliées, qui convertissent les mouvements mécaniques du fluide inertiel avec lequel elles sont en contact en signaux nerveux. C'est grâce au système vestibulaire que nous pouvons stabiliser notre regard, par le biais du réflexe vestibulo-oculaire: l'utricule, un des otolithes, envoie une information de mouvement aux noyaux tangentiels, qui à leur tour stimulent les noyaux oculo-moteurs. Le système vestibulaire est fonctionnel à 3 jours chez la larve de poisson zèbre, et est bien conservé chez les vertébrés.

Le système visuel est également bien conservé chez les vertébrés, et la larve de poisson zèbre a une rétine fonctionnelle à 5 jours. Ce système permet à un autre réflexe d'exister: le réflexe optocinétique. Durant ce réflexe, les yeux suivent le mouvement visuel environnant. Le système visuel inclut l'oeil, composé notamment de la rétine, et des projections neuronales qui vont jusqu'au cortex visuel du cerveau. Dans la rétine, une organisation neuronale par couche permet de transformer un influx de photons en signal nerveux, en particulier grâce à l'action de photo-récepteurs, qui nous permettent de capter l'intensité lumineuse et les couleurs.

Dans le travail présenté ci-après, nous allons nous intéresser au comportement et à la réponse neuronale de la larve de poisson zèbre dans un environnement multisensoriel composé des modalités vestibulaire et visuelle. Nous commencerons par expliquer comment nous avons visualisé des données neuronales, avant d'étudier l'influence de la cohérence des stimuli sur l'animal. Nous étudierons ensuite comment le contraste visuel est intégré, et discuterons finalement de la capacité d'apprentissage dans un contexte multimodal.

En arrivant au laboratoire Jean Perrin, j'ai eu l'opportunité de récupérer des données neuronales de poissons zèbres issues de différents protocoles expérimentaux. Parmi les 38 différents poissons étudiés, 11 expériences avaient été faites sur le système vestibulaire, 1 sur le système visuel, 3 sur le système auditif, 9 sur la réponse au chaud, et 14 sur la

réponse au froid.

Mon objectif premier a été de trouver un moyen de relier efficacement la réponse neuronale à l'échelle du cerveau entier au stimulus. Comme je n'avais pas défini les expériences moi-même, les stimuli étaient variés. Les stimulations vestibulaire et visuelle étaient périodiques, en sinusoïde ou en créneau, la stimulation auditive était périodique en pulsation, et les stimulations en températures étaient des flux aléatoires d'eau chaude ou froide. Après avoir essayé plusieurs méthodes pour définir si un neurone répondait à un stimulus, j'ai finalement choisi la F-statistique, qui donne une valeur indicative de la performance d'une régression linéaire ou multilinéaire.

L'étape suivante a été de visualiser ces neurones. Pour pouvoir comparer ces jeux de données, j'ai défini une structure en grillage, dans laquelle chaque neurone du cerveau était associé au voxel dans lequel il était. J'ai ensuite conçu un programme qui permettait de superposer les neurones les plus sensibles aux stimuli proposés pour 2 poissons différents. Grâce à la structure en grillage proposée, les voxels incluant des neurones communs aux deux poissons, et donc potentiellement des zones multisensorielles du cerveau, étaient faciles à repérer. J'ai ajouté plusieurs autres fonctionnalités à ce programme, comme la possibilité de représenter les isovaleurs des F-statistiques pour un poisson donné, et les différentes zones du cerveau, prises dans un cerveau de référence.

J'ai finalement pu superposer les 38 jeux de données, et identifier des régions du cerveau potentiellement multisensorielles. L'une se situait antérieurement aux neurones oculomoteurs, une autre dans le cervelet, et la dernière était localisée dans le cerveau postérieur dorsal, une zone comprenant d'autres neurones moteurs.

Cette analyse a permis d'étudier un grand nombre de jeux de données, et un grand nombre de stimuli. Elle a permis d'identifier des régions intéressantes dans le cerveau, en terme d'intégration multisensorielle. Mais malheureusement, comme ces expériences n'avaient pas été faites sur les mêmes poissons, il n'était pour le moment pas possible de dire avec exactitude que des neurones étaient effectivement multisensoriels. C'est ce que la partie suivante de ma thèse a voulu creuser.

Mon deuxième objectif a été de localiser avec précision des neurones multisensoriels au sein du cerveau. Grâce aux stimuli vestibulaire et visuel présentés l'un après l'autre, puis en même temps, j'ai pu étudier les réponses comportementales et neuronales de la

larve de poisson zèbre. Dans les expériences que j'ai réalisées, la larve de poisson zèbre était immobilisée dans de l'agarose. Pour récupérer les informations comportementales, j'ai libéré les yeux de l'animal, et pour l'imagerie j'ai au préalable paralysé le poisson à l'aide de bungarotoxine. L'animal était tourné autour de son axe rostro-caudal par un moteur pour le stimulus vestibulaire, et un écran placé sous son corps permettait de projeter un motif à bandes blanches et noires pour le stimulus visuel. Pour les stimuli multisensoriels, on définit la cohérence entre les deux modalités grâce à un paramètre: la congruence. Une congruence de 1 veut dire qu'une stimulation visuelle (grâce au réflexe optocinétique) éliciterait la même réaction qu'une stimulation vestibulaire (grâce au réflexe vestibulo-oculaire): c'est un environnement multisensoriel cohérent, et c'est ce que nous expérimentons tous au quotidien. Nous appelons une congruence de 0 conflit, puisque malgré une rotation vestibulaire, le motif visuel est fixe dans le référentiel du poisson. Une congruence de -1, appelée opposition, signifie que le motif visuel est en opposition de la rotation, et une congruence de 2, appelée amplification, signifie que le motif visuel devrait déclencher un réflexe oculaire deux fois plus élevée que la rotation.

J'ai commencé par caractériser la réponse comportementale aux stimuli. Les réponses normalisées à des stimuli vestibulaires étaient environ 6 fois plus élevées que les réponses aux stimuli visuels, pour plusieurs amplitudes de stimulations. Ceci nous a montré que la réponse comportementale est très variable en fonction du type de modalité étudiée. Pour les réponses multisensorielles, alors que les réponses pour des stimulations en opposition et en conflit étaient sensiblement les mêmes que la réponse au vestibulaire, les réponses pour des stimulations cohérentes et amplifiées étaient bien supérieures au réponses au stimulus vestibulaire. De manière encore plus intéressante, pour des stimulations cohérentes, les réponses multisensorielles étaient plus élevées que la somme des réponses unisensorielles, nous montrant un comportement super-additif.

En analysant des données neuronales sur les mêmes types de stimulations, j'ai pu définir les neurones vestibulaires et visuels. Le nombre de neurones répondant à ces deux modalités était constant d'un poisson à l'autre, de même que leur localisation était stéréotypée et correspondait à la littérature. Une faible partie des neurones du cerveau répondait à la fois aux deux modalités, mais leur localisation dans le cerveau était une fois encore très stéréotypée. En définissant géographiquement cette région multisensorielle du cerveau, j'ai pu constater qu'elle incluait une proportion importante des régions motrices des yeux

et de la queue du poisson.

En modélisant la réponse des neurones répondant aux stimuli vestibulaire et visuel, il a été intéressant de remarquer que leur activité multisensorielle était linéaire par rapport à leurs activités unisensorielles. Par ailleurs, en utilisant un coefficient extrait de ce travail de modélisation, j'ai pu identifier des neurones super-additifs, c'est-à-dire des neurones dont la réponse à un stimulus multimodal était supérieure à la somme de leurs réponses aux stimuli unimodaux. En définissant une région super-additive du cerveau, il a été intéressant de constater que celle-ci incluait 50% de la région multisensorielle définie ci-dessus. Par ailleurs, cette région super-additive incluait également un nombre important de neurones moteurs, et notamment de neurones oculo-moteurs. Ceci nous a permis de faire le lien avec la réponse comportementale super-additive que nous avions observée plus tôt.

Ce travail a fourni une analyse poussée des réponses comportementales et neuronales de la larve de poisson zèbre, soumise à des stimuli vestibulaire et visuel. L'analyse du comportement nous a montré qu'il existait des mécanismes permettant d'adapter la réponse d'un organisme plus efficacement quand deux stimuli étaient cohérents, en particulier la super-additivité observée dans le cerveau. Nous avons ensuite pu voir que malgré l'existence de neurones multimodaux localisés dans différentes régions du cerveau, certaines régions en étaient plus densément peuplées. Ceci confirme l'aspect multimodal du cerveau dans son entièreté, tout en ayant des zones plus spécifiquement dédiées à l'intégration multisensorielle.

Je me suis ensuite intéressé à l'intégration du contraste visuel dans un environnement multisensoriel. J'ai utilisé le même protocole expérimental que celui décrit précédemment, mais j'ai cette fois-ci également joué sur la différence d'inténsité entre les bandes blanches et noires du motif visuel. Un contraste de 0 revient à présenter un motif uni, et donc à stimuler le poisson vestibulairement, et un contraste de 1 revient à avoir des bandes avec la différence d'intensité maximale. Deux hypothèses ont été testées dans cette partie. D'abord, dans le cas d'une stimulation multisensorielle conflictuelle, est-ce que l'augmentation du contraste pouvait permettre au poisson de passer d'un état vestibulaire, où le réflexe vestibulo-oculaire est dominant à un état visuel, où le réflexe optocinétique est dominant. Ensuite, dans le cas d'une stimulation multisensorielle cohérente, est-ce que

l'augmentation du contraste conduisait à une augmentation logarithmique de la réponse comportementale, en adéquation avec des expériences de la littérature ayant été réalisées avec le stimulus visuel uniquement.

En conflit, je n'ai pas obervé de changement de comportement entre un contraste de 0 et un contraste de 1. C'est un résultat qui fait sens, puisque dans mon travail précédent, je n'avais pas observé de différence majeure entre les réponses vestibulaire et conflictuelle. En regardant les données neuronales, on a pu comprendre que cela était dû au fait que les neurones visuels n'étaient pas du tout stimulés, puisque le motif visuel était immobile.

En cohérent, j'ai pu observer une augmentation logarithmique de la réponse comportementale quand le contraste augmentait de manière linéaire, correspondant aux résultats de la littérature pour une stimulation visuelle unimodale. Les réponses des neurones répondants au stimulus visuel étaient également log-correlées au contraste.

Cette étude nous a montré qu'une augmentation de contraste lors d'une situation de faible contraste avait plus d'impact sur la réponse comportementale que lors d'une situation de fort contraste dans un environnement multisensoriel. Ce résultat est intéressant puisqu'il permet de voir qu'un individu peut évaluer rapidement si un stimulus fait sens, avec un bout d'information limité venant d'un deuxième stimulus cohérent. Il aurait été également intéressant de développer la même expérience avec deux stimuli multisensoriels en opposition, pour constater quel comportement le poisson zèbre aurait adopté.

Dans le dernier chapitre de ma thèse, je me suis intéressé à l'apprentissage, et aux effet d'un environnement multisensoriel sur celui-ci. Il a été montré que le poisson rouge adulte pouvait modifier son réflexe vestibulo-oculaire lorsque les stimuli vestibulaire et visuel n'étaient pas cohérents, et j'ai voulu reproduire cette expérience sur des larves de poisson zèbre. Le protocole expériemental consistait en une alternance de phases d'entraînement multisensoriel et de phases de test vestibulaire. La congruence entre les deux modalités augmentait au fil de l'expérience, passant de 1 (cohérent) à 2 (amplifié) au bout des 25 minutes de l'expérience. L'évolution de la rotation des yeux lors des phases de test nous donnait une bonne indication sur l'influence de l'entraînement sur le comportement des animaux. J'ai voulu consécutivement regarder si nous pouvions bien observer ce changement de comportement, puis si ce changement était lié à l'action du cervelet, élément nécessaire dans le cerveau pour l'apprentissage moteur. J'ai finalement étudié l'impact de

l'environnement multisensoriel et du laser d'imagerie sur la réponse.

Sur 29 poissons ayant subi l'expérience décrite ci-dessus, 40% d'entre eux, appelés les apprenants, ont montré une adaptation durable, avec un gain comportemental augmentant de plus de 100% entre le premier et le dernier test vestibulaire. Par ailleurs, 45% des poissons, les semi-apprenants, ont montré une augmentation de gain au cours des 8 premières minutes de l'expérience, avant que celui-ci ne retourne au niveau du gain initial. Au total, cela a donc fait 85% des poissons qui ont montré un comportement d'apprentissage dans cet environnement multisensoriel.

J'ai par la suite ablaté les cellules de Purkinje de 24 poissons et lancé les mêmes expériences sur ces poissons. Les cellules de Purkinje sont une composante essentielle du cervelet et en représentent une des trois couches nécessaire à l'apprentissage moteur. Ces poissons ablatés ont présenté des statistiques d'apprentissage similaire aux poissons possédant toujours leurs cellules de Purkinje, avec 46% des poissons dans la catégorie apprenant, et 29% des poissons dans la catégorie semi-apprenant. Ceci nous a montré que le cervelet ne semblait pas jouer de rôle dans l'apprentissage observé.

J'ai ensuite voulu confirmer que l'environnement multisensoriel, avec une congruence augmentant au fil de l'expérience était bien la raison de cette augmentation de gain comportemental. J'ai donc adapté le protocole en remplaçant d'une part ces périodes d'entraînement par un stimulus cohérent, puis d'autre part par un stimulus vestibulaire. A ma surprise, les statistiques d'apprentissage étaient toujours similaires aux statistiques dans des conditions de base. Pour le protocole avec une congruence constante, 44% des poissons étaient dans la catégorie apprenant, et 38% dans la catégorie semi-apprenant. Pour le protocole avec un stimulus vestibulaire à la place de l'entraînement multisensoriel, 40% des poissons étaient dans la catégorie apprenant, et 33% dans la catégorie semi-apprenant. Ces informations nous ont donné l'indication que l'environnement multisensoriel n'était pas la raison de l'adaptation du réflexe vestibulo-oculaire.

J'ai finalement testé l'hypothèse que c'était le laser qui influençait l'adaptation. En effet, dans les premières expériences d'apprentissage que j'avais faites, le laser permettant d'imager le cerveau était actif, puisque j'avais enregistré le cerveau des poissons étudiés au début et à la fin du protocole. J'avais par la suite laissé le laser allumé, pour que les conditions des expériences soient les même lors des contrôles réalisés. Dans ce dernier protocole expérimental, j'ai donc éteint le laser, pour tester son influence sur l'adaptation.

Dans cette nouvelle configuration, les statistiques d'apprentissage étaient différentes: 18% des poissons était dans la catégorie apprenant, et 23% dans la catégorie semi-apprenant, soit seulement 45% des poissons montrant un comportement d'adaptation.

Après analyse de ces données, il semble que ce n'était pas l'environnement multisensoriel qui influençait l'apprentissage, contrairement aux expériences faites sur des poissons rouges que j'essayais de reproduire. Par ailleurs, le cervelet ne semblait également pas avoir d'influence sur l'augmentation du gain du réflexe vestibulo-oculaire, alors que c'était une des conclusions de l'étude sur les poissons rouges. Il semble que c'était le laser, et lui seul, qui était à l'origine de cette augmentation. Plusieurs hypothèses permettent d'expliquer l'implication du laser dans l'évolution comportementale observée. Il est possible que le laser ait déclenché un stress dans les poissons, et il a été montré que le stress déclenche des comportements erratiques. Dans notre cas néanmoins, le comportement semblait plus consistant qu'erratique. Il est également possible que le laser stimulait une région neuromodulatoire du cerveau, qui a pu changer le comportement de l'animal. Ma dernière hypothèse est que la lumière du laser touchait des photorécepteurs localisés dans le cerveau profond des larves de poisson zèbre, et déclenchait un état extrême de réveil, qui pourrait être à l'origine de l'apprentissage observé.

Mots clés: intégration multisensorielle · cerveau · neurones · comportement · poisson zèbre · microscopie à nappe de lumière · vestibulaire · visuel · super-additif · adaptation

Remerciements

Tout d'abord je voudrais remercier Volker Bormuth, qui a dirigé cette thèse et m'a accompagné et aidé du début à la fin. De sa confiance à ses conseils, en passant par ce que je pense être des nuits blanches passées pour relire et corriger ce manuscrit, je ne serais jamais arrivé à bon port sans lui.

J'aimerais également remercier Geoffrey Migault, dont le travail sur le microscope rotatif m'a permis de réaliser le mien sur l'intégration multisensorielle. Armé de patience, il a su m'expliquer en détail comment réaliser des expériences, et ce n'était probablement pas une mince affaire.

Je remercie Marcus Ghosh et Georges Debrégeas d'avoir supporté mes présentations à rallonge à l'heure de la sieste, et d'avoir su m'aiguiller alors que la digestion devait se faire lourde.

Un grand merci à Malika Pierrat, qui a rendu mes tâches administratives d'une simplicité rare, et dont les conversations m'ont permis de me soustraire à mes poissons l'espace d'un instant (ou de plusieurs).

Merci à la plateforme aquatique de l'IBPS, sans qui ce travail n'aurait tout simplement pas pu voir le jour.

Merci à toute l'équipe zebrafish d'avoir mis une ambiance géniale dans le labo, et d'avoir trouvé la détermination d'installer un canapé dans le bureau, après que nous en avions longuement rêvé. Merci à tout le labo LJP, dans lequel j'ai passé de superbes années.

Finalement, merci à Clara, à ma famille et aux fratés d'avoir fait semblant de s'intéresser à ma thèse pendant ces longues années. J'en profite pour répondre, dans le désordre, à quelques unes de leurs questions pour la postérité. Oui, mes poissons vont bien. Non je ne mange pas mes poissons après mes expériences. Non, je ne les ramène pas chez moi non plus. Non je ne travaille pas avec des crevettes, même si ç'aurait été très drôle. Et oui, promis, j'essaierai d'expliquer plus clairement ce que j'ai fait pendant cette thèse au moment de la soutenance (enfin j'espère).

Contents

List of Abbreviations

dpf: days post fertilization

fMRI: functional magnetic resonance imaging

GABA: gamma-aminobutyric acid

gad1b: glutamate decarboxylase 1b

GCaMP: green fluorescent protein - calmodulin- M-13 peptide

GECI: genetically encoded calcium indicators

HDF: hierarchical data format

hpf: hours post fertilization

KDE: kernel density estimation

NFA: normalized Fourier amplitude

nMLF: nucleus of the medial longitudinal fascicle

nIII: oculomotor nucleus

nIV: trochlear nucleus

OKR: optokinetic reflex

RMSE: root mean square error

RSS: sum of the square of the residuals

SNR: signal to noise ratio

UV: ultra violet

VOR: vestibulo occular reflex

I – Introduction

Moins sage que nos pères, je me sers et j'observe.
Élie Yaffa

I.1 Context and overview

I.1.1 Presentation

Humans and animals live in a multisensory world, and survive in it by interacting with their environment. There are five well known senses: vision, audition, touch, taste, and smell. Many more come to mind, although less widely known, such as pain, temperature, balance and movement perception, proprioception, and magnetic field perception. Unless taking part in a sensory deprivation experiment, all our experiences are multisensorial. We are constantly integrating sensory cues, and reacting to our surroundings with muscle movements, which allow us to behave differently in order to optimize our chances of survival [1].

In the brain, there is a convergence of information from different sensory modalities. Multisensory integration is the processing of all these sensory signals inside the brain, to have a coherent perceptual experience. Information need to be combined such that the resulting information is more informative and less noisy than each individual modality alone. Multisensory integration is necessary to our survival for numerous reasons:

- It allows for an error reduction in tasks [2], and decision making improvement [3].
- It leads to a faster response time [4], and more precise motor outputs [5].
- It helps to resolve conflicts in tasks involving multiple modalities [6].
- It makes learning better, because multisensory conditions are closer to natural perception [7].
- It allows for cross-sensory calibration during development [8] [9] (when one modality is missing, the development of the other modalities is impacted).

The continuous stream of information from outside our body needs to be processed so that the representation we make of what is happening around us is the closest to reality. The brain needs to sort these signals, and to reduce the noise in them, that originates from the nature of the signals or the way neurons process them [10]. As a matter of fact, there are around 100 billions neurons in an adult human brain, with an estimated 1 000 000 billions connections to link them. These numbers are so high it is hard to comprehend

the machinery the brain is. But multisensory integration of these continuous signals is in fact used in a major part of the cognitive functions [11] and has an influence on cerebral plasticity [12], which is at the center of learning processes.

I.1.2 Modeling multisensory tasks, and brain recording techniques

Psychophysical models have been developed to understand behaviour in multisensory tasks. Specifically, the Bayesian observer frame work has been successfully used to describe multisensory behavioural responses. This probabilistic approach takes into account the uncertainty associated with sensory information and the prior probabilities of encountering specific signals [13]. In this frame work, modalities are generally weighted based on an inverse estimate of their noise [14] [15]. Bayesian inference models suggest that, in addition to maximization of information and reliability from sensory cues, there is an interpretation based on prior knowledge [10]. Theoretical and computational models have been introduced to explore how the brain could implement such probabilistic models using neuronal population activity. However, extensive neuronal recordings are still needed to validate these models. Currently, our understanding of multisensory processing relies mainly on observations at the single-neuron level.

Interestingly, multisensory integration happens at various scales in the brain. Using electrophysiology, it has been shown that single neurons could detect multisensory inputs, through super-additivy [16], which means the response of the neuron is superior to the sum of the responses for each unisensory stimulus. These super-additive neurons could play a role in enhancing or amplifying multisensory information, which is a helpful process in a noisy environment. During an experiment, out of 40 neurons recorded in the cat superior colliculus, a multisensory center of the brain, 33% of them were super-additive, whereas 60% were additive (possibly encoding the presence or absence of a particular sensory feature), and 7% sub-additive (possibly helping filter out irrelevant or redundant sensory information) [17] (figure I.1). Up until recently, recordings at the scale of single neurons were limited to tens of neurons. As a result, psychophysical models lack extensive neuronal recordings necessary to evaluate their physiological relevance, and studies are typically conducted on single neurons in specific brain regions [13] [18]. However, the development of Neuropixel probes in recent years has allowed for recording up to 10,000 neurons in mice brains [19] with promising potential for research. But these probes only

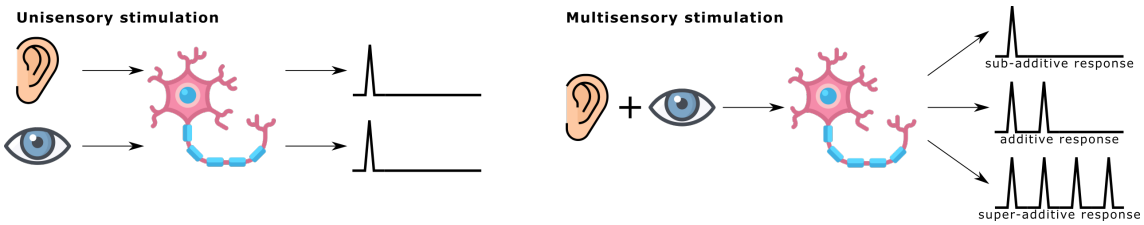

Figure I.1: Example of different multisensory responses for one neuron.

capture signals from neurons in close proximity to the 1 cm long probe, representing a limited number of neurons per brain region and still only a small fraction of the enormous amount of 70 million neurons in a mouse brain (and 100 billion in an adult human brain!).

On the other hand, at a larger scale using fMRI, it has also been shown that some regions we thought were uni-modal in the cortex are actually multi-modal [20]. For example, the auditory cortex is stimulated even in the absence of auditory sensory cues when we read lips [21] (figure I.2). A large number of multisensory regions has been identified in the brain, all receiving information from different sensory areas [22]. The problem with brain-wide imaging is that recorded voxels are not single cells (an fMRI voxel is 1 mm^3 and contains 100,000 neurons), and it is therfore not possible to have single neuron resolution in fMRI [23]. This sets a trade-off between single-cell recordings, and whole-brain imaging.

New developments in light-sheet imaging techniques and genetically encoded calcium indicators (GECI) have made possible a whole-brain recording of a vertebrate, at several brains per second, at cellular resolution [24] [25] (figure I.3). Due to its transparency, the vertebrate whose brain was successfully recorded was the larval zebrafish, at six days post fertilization. Larval zebrafish possess other advantages for light-sheet imaging, such as small and compact brains of around 100,000 neurons. With a neuron diameter of around $10\mu m$, the whole brain has a length of around $0.1mm$, compared to the $10cm$ of the human brain. This animal model can also be genetically modified to express genetically encoded calcium indicators, which emit fluorescence when bound to calcium ions, thus acting as a proxy to visualize neuronal activities. In addition to this, the simplicity of the larval zebrafish body makes possible a large description of its behaviour by a large community around the globe. It is the relationship between behaviour and neuronal activity that enables to describe properly neural circuits, and fully understand sub parts of the brain [26].

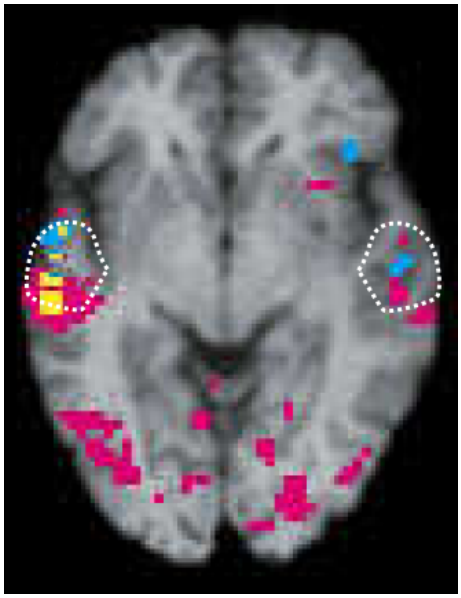

Figure I.2: Parts of the brain active during auditory and visual stimulations, recorded using fMRI, by Calvert *et al.* [21]. Regions in blue are activated during auditory speech perception, in purple are regions activated during silent lip reading, and in yellow are regions activated by both auditory speech and silent lip reading. The dotted white line indicates where the auditory cortex is.

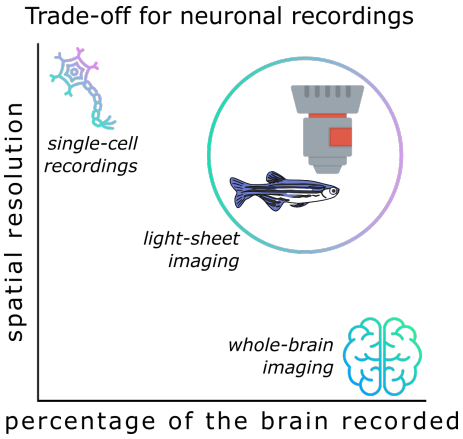

Figure I.3: Trade-off between single-cell recordings, whole-brain imaging, and light-sheet imaging.

I.1.3 Chosing modalities to study

To study multisensory integration, we need to simplify the very complicated multisensory process, and focus on at least two sensory modalities that make sense together. Visual and auditory systems have been widely analyzed in zebrafish. It would make sense to pick them to study multisensory integration, but the auditory circuit is not fully developped in larval zebrafish, and audio is detected through an organ of the vestibular system: the saccule [27].

Although the auditory system is not on the table, the visual system is a good candidate. It has been studied on zebrafish [28], rats [29], primates [30] and humans [31]. It is also conserved in vertebrates and even in flies [32], and the zebrafish visual system is used to study ocular diseases in humans [33]. In addition, at 5 dpf, zebrafish have a functional typical vertebrate retina [34], and the optokinetic response (OKR, consists in following the movement of the entire visual field with the eyes) is functional as soon as 3 dpf in zebrafish [35] [36].

The vestibular system, used to stabilize gaze [37] and body [38], is the second solid candidate to study multisensory integration. First of all, it is closely related to the visual system: in monkeys, a lot of neurons in the vestibular nuclei also respond to visual stimuli [39]. Moreover, the vestibular system is at the center of the vestibulo-ocular reflex (VOR), which is the eyes compensation during a movement, to keep a fixed visual image on the retina [40]. In terms of multisensory integration, the vestibular system does not have its own region in the cerebrum for monkeys and humans, in opposition to visual and auditory system [41], and therefore can be thought of as a multisensory modality. This system is functional as soon as 3 days post fertilization [42], and is well conserved across vertebrates [43] [44]. Finally, it is possible to image the brain while providing a vestibular stimulus, using a rotating light-sheet microscope [45].

I.2 From neurons to nervous system

Study of the mind and brain dates back millennia. Although the Greek philosopher Aristotle (384-322 BC) believed our spirit originated from our heart, Greek physician Hippocrates (460-377 BC) speculated the brain was at the center of our thinking and emotions. Galen (129-216) used dissections studies to discover cerebral ventricles, and

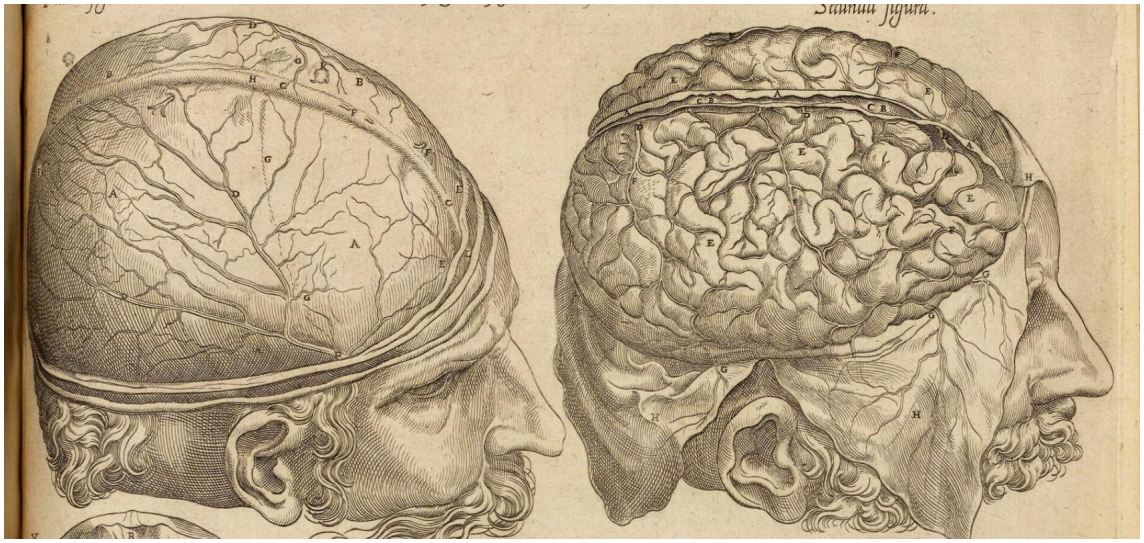

Figure I.4: Hand drawing of brain anatomy, by Vesalius in 1543.

inferred the nerves were pipes, allowing information transfers from all of the body organs to the brain. Vesalius (1514-1564) pointed out errors of Antiquity scientists, and published in 1543 *De humani corporis fabrica*, a book of anatomical drawings, including detailed drawings of the human brain (figure I.4). Since Galen, the dominant theory was that the three ventricles in the brain were at the center of senses, cognition and memory; it is Thomas Willis (1621-1675) who understood thoughts originated from cerebellar cortex convolutions. Santiago Ramon y Cajal (1852-1934) made a huge step in neuroscience, demonstrating neurons, i.e. brain cells, are independent, the same way other cells in the body are (figure I.5). Korbinian Brodmann (1868-1918) described the first cortical map of the human brain, and thanks to the development of *in vivo* imaging, we are nowadays able to have more precise maps of the brain from living subjects [46].

Centuries of anatomical and physiological studies have allowed us to have a good understanding of how the brain and the whole nervous system drive our lives. We will present here how neurons, synapses and brain circuits work.

I.2.1 Neurons

The neuron is the building block of the nervous system. It is a cell, and therefore possesses the same organelles as any cell in the body, such as a nucleus and mitochondria. The particularity of the neuron is that it has a membrane potential, and can depolarize along

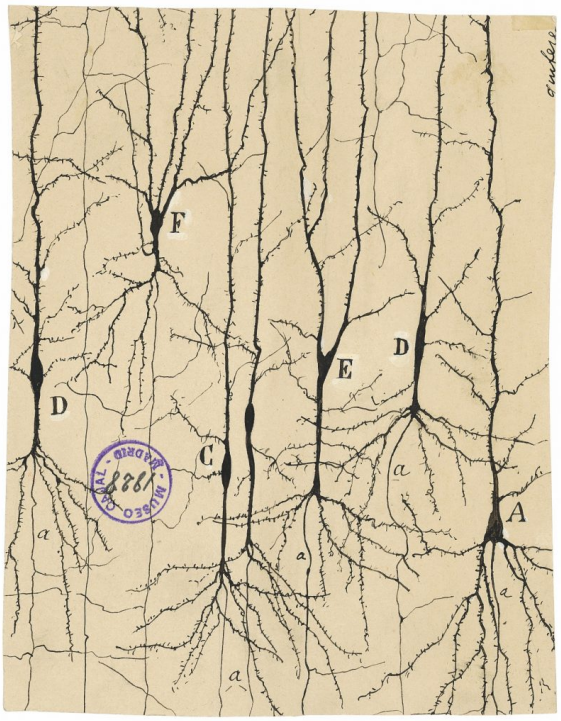

Figure I.5: Hand drawing of pyramidal neurons from the cortex, by Ramon y Cajal [47].

its ramifications, leading to an electrical current, called an action potential. This electrical current allows information to travel from the inputs of a neuron (the dendrites, around 7,000 per neuron), to its output (the axon). Myelin sheaths surround neurons axons, and allow electrical signal to travel faster. They are formed by glial cells, another type of cells found in the brain, with approximately three times more glial cells than neurons. Neurons widely vary in the central nervous system: as an example, in the cerebellum, granule cells have 3 to 4 dendrites, whereas Purkinje cells have up to 200,000 dendrites [48] (figure I.6).

An action potential appears when membrane potential exceeds a threshold value. Sodium ion channels open, and sodium ions enter the cell, provoking a local depolarization. This triggers a cell reaction along a dendrite or an axon. As the time constant of potassium ion channels is greater than sodium ion channels, they open later, and drive potassium ions in, leading to a repolarization. There is a refractory period after this event, during which sodium/potassium pumps move sodium ions out, and potassium ions in (figure I.7).

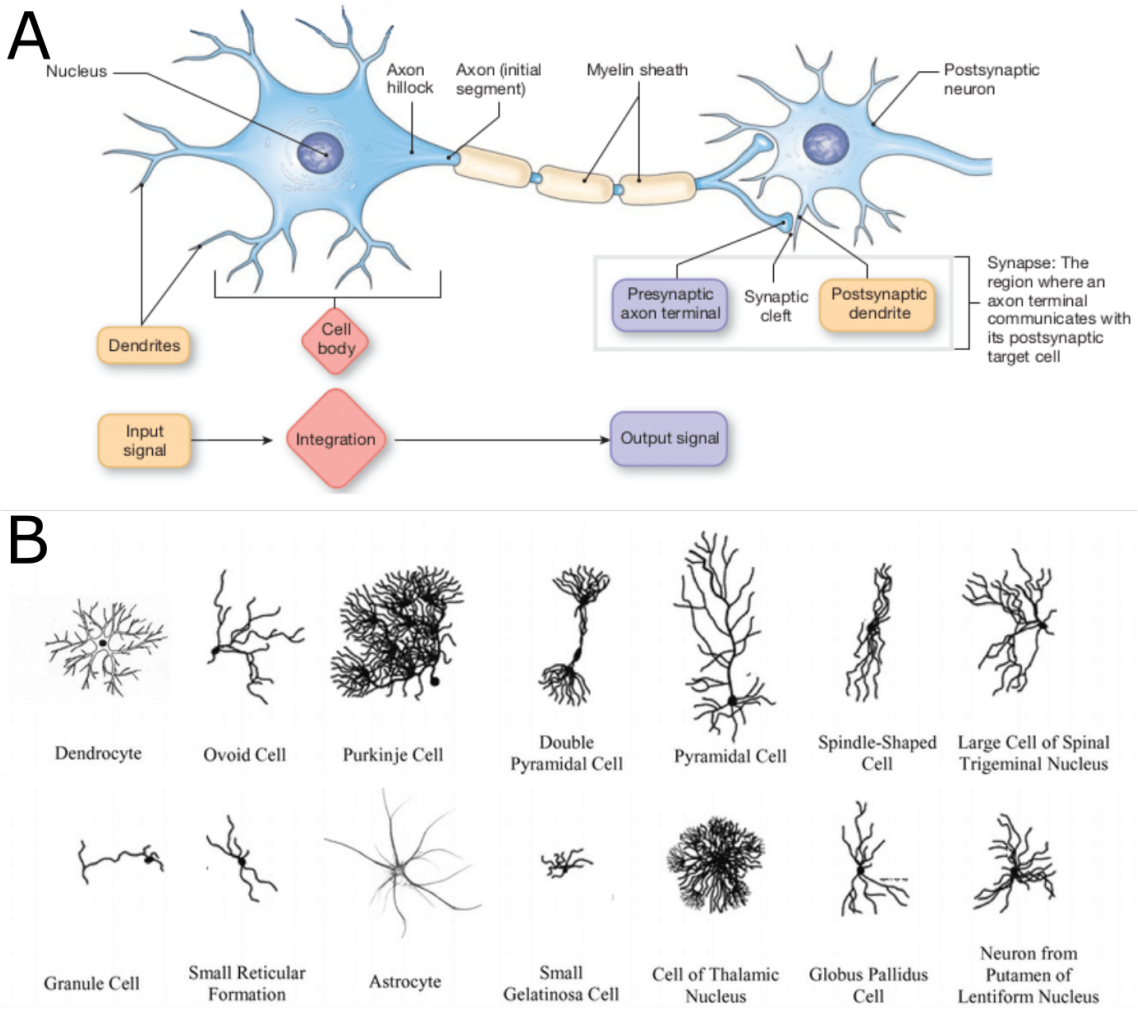

Figure I.6: **A**: Representation of a neuron, from Cook *et al.* [49]. **B**: Different types of neurons in the central nervous system [50], adapted from Ramon y Cajal drawing.

I.2.2 Synapses

Action potentials drive information from one end to the other of a neuron, but the transmission of this information between one neuron to the next is carried out by synapses. Synapses can either be electrical or chemical. In electrical synapses, there is a cytoplasmic continuity between pre and post-synaptic neurons, and the electrical current is continuous between the two neurons. In chemical synapses, the action potential leads to the release of neurotransmitters at the synapse from the pre-synaptic neuron. This neurotransmitter activates receptors in the post-synaptic neuron, and sodium ions flow into it (figure I.8). The type of neurotransmitter varies between synapses: in excitatory synapses, the most

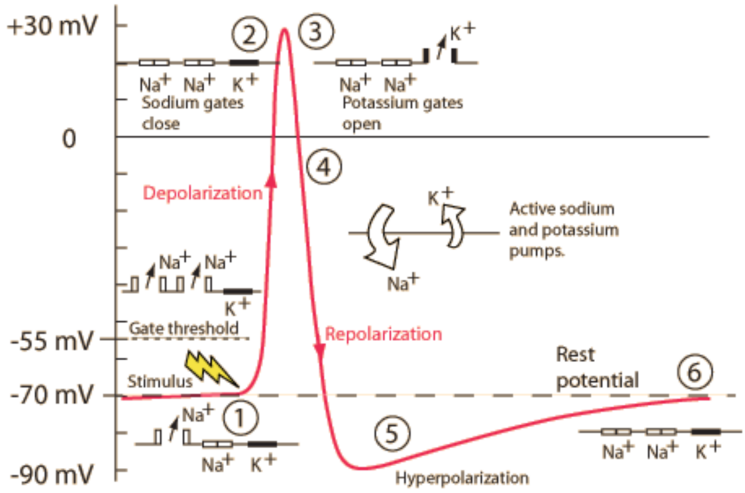

Figure I.7: Description of an action potential based on membrane potential and ion channels openings. Figure from https://neurofeedbackalliance.org

common neurotransmitter is glutamate, whereas in inhibitory synapses, it is GABA. Many other neurotransmitters exist, famous ones being acetylcholine, dopamine and serotonin. Excitatory and inhibitory inputs are integrated in the post-synaptic cell, and lead to a new action potential, if the electrical threshold is reached.

The strength of a synapse is related to the amount of neurotransmitters releases, and is not fixed in time. A constant synchronous firing between two neurons connected through a synapse leads to long-term potentiation, which is the strengthening of the synapse [51]: synapses are at the center of learning and adaptation.

I.2.3 Brain organization

The brain comprises a large amount of neurons, connected through synapses, and organized geographically and functionally. For example, a nucleus is a cluster of neurons in the central nervous system, whose neurons usually have similar connections and functions.

There are three main areas in the brain: the forebrain (prosencephalon), midbrain (mesencephalon), and hindbrain (rhombencephalon). The forebrain itself is made from the telencephalon and the diencephalon. In addition to the brain, the spinal cord is the second part of the central nervous system. It transmits motor commands, with nerve signals, from the motor cortex to the muscles, and sensory information, with afferent fibers, from the body to the sensory cortex.

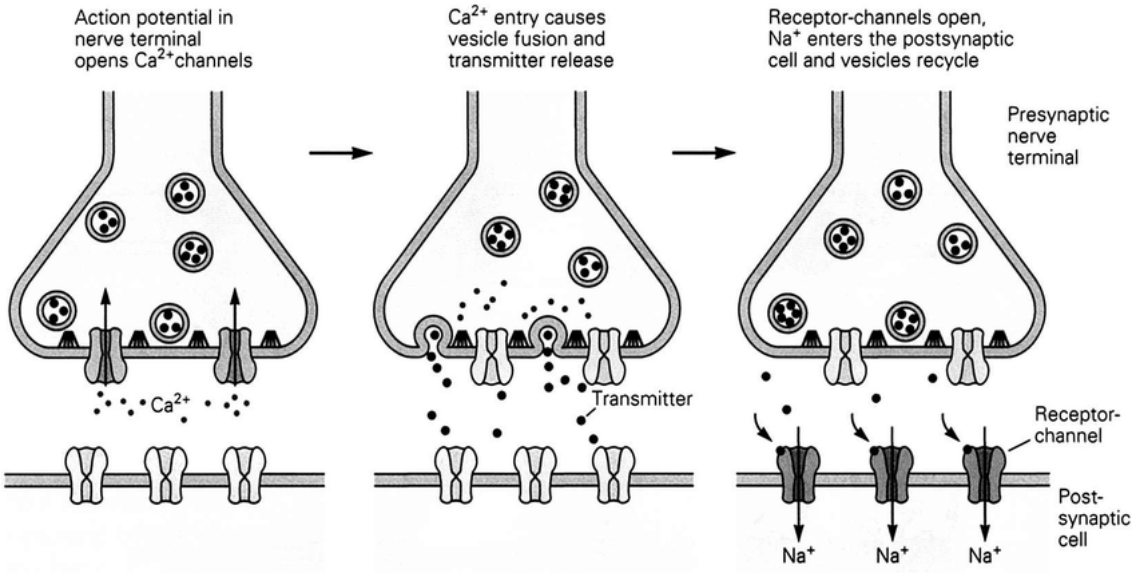

Figure I.8: Chemical synapse between two neurons mechanism, from Behnke *et al.* [52].

Some regions in the brain are worth mentioning (see figure I.9):

- In the telencephalon:
  - The cerebral cortex (attention, perception, awareness, cognition, thoughts, memory, language, consciousness).
  - The hippocampus (memory [53]).
  - The basal ganglia (movement planning, cognitive behaviour, saccadic eye movement [54]).
  - The olfactory bulb (olfaction).
- In the diencephalon:
  - The thalamus (relay for sensory and motor signals to cortex [55], cognition [56]).
  - The hypothalamus (metabolic control, thermoregulation, wake-sleep cycles, reproduction [57]).
  - The pretectum (pupillary light reflex [58], optokinetic reflex [59], somatosensory information mediator [60]).
- In the mesencephalon:

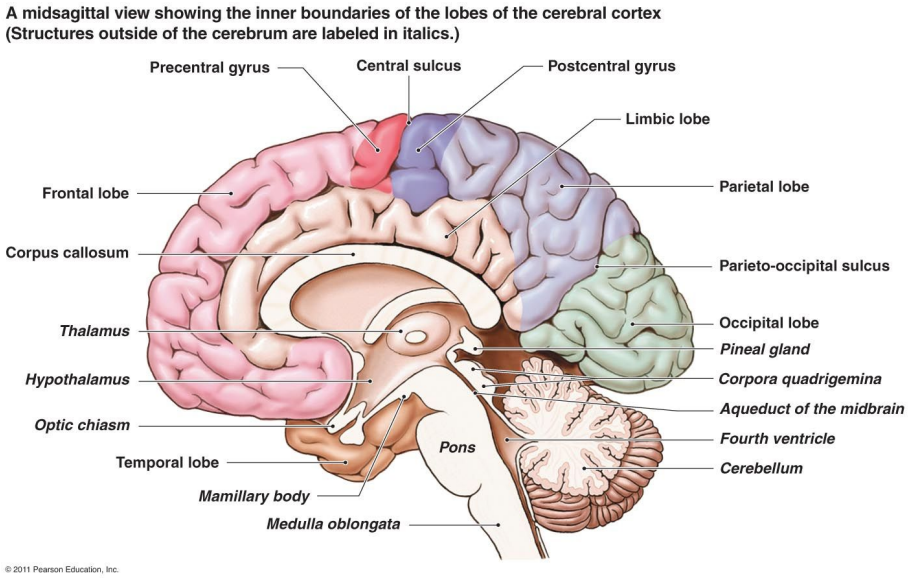

Figure I.9: Different regions of the human brain. Figure from https://mapp.mgh.harvard.edu

  - The tectum (spatial sensory integration [61]).
  - The tegmentum (autonomic functions [62], reward control [63], control of posture [64]).
  - The cerebral acqueduct (mediates circulation of the cerebrospinal fluid, as part of the ventricular system).

- In the rhombencephalon:
  - The pons (autonomous functions such as respiration [65] and sleep [66]).
  - The cerebellum (motor control and learning [67], cognitive processing and emotional control [68]).
  - The medulla oblongata (involuntary functions such as vomiting and sneezing, and autonomous functions of breathing, heart rate and blood pressure [69]).

I.3 Zebrafish as a model

The zebrafish (*Danio rerio*) is a fish originally found in India, and living in fresh water (figure I.10). George Streisinger started experimenting on this animal in 1972, and found

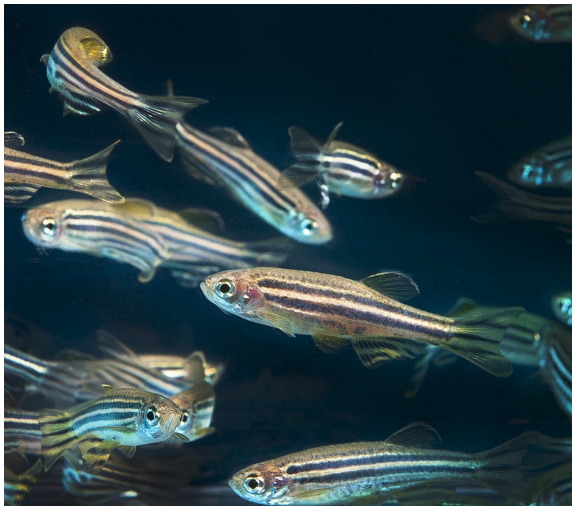

Figure I.10: Adult zebrafish swimming. Photo by Lynn Ketchum, taken at Oregon State University.

it a good model because of three reasons: the zebrafish lays a lot of eggs, it is transparent during larval development, and it can easily be genetically modified. In 2001, the contribution of zebrafish to the study of vertebrate development over the 1990's was already underlined [70], and it has since then been confirmed that zebrafish is vastly used in all the fields of biological and medical research [71]. In addition to neuroscience, zebrafish is used to study cardiovascular development [72] and diseases [73], immunology [74], and drug discovery [75] and development [76], amongst other fields.

Due to its small brain size (around 100,000 neurons), zebrafish is a very interesting model to understand brain circuits [77] (figure I.11). Moreover, its body is simple, and thus allows for a thorough description of its behaviour, and a possibility to link it to the neural circuits responsible for it [26]. A wide range of behaviours and their associated neuronal circuitry in the zebrafish has been studied so far, such as optokinetic response [78] [79], optomotor response [80], phototaxis [81], movement detection [82] and hunting behaviour [83], thermotaxis [84], auditory response [85], olfactory response [86], and vestibular behaviour [45].

Zebrafish development is very fast: larvae hatch between 48 and 72 hours post fertilization (figure I.12), and swim at 5 dpf [89]. At 30 dpf, the animals are not considered larvae any more, but juveniles. As zebrafish can be genetically modified with ease, genetic tools were developed, and allowed for the creation of a wide range of mutants. The nacre

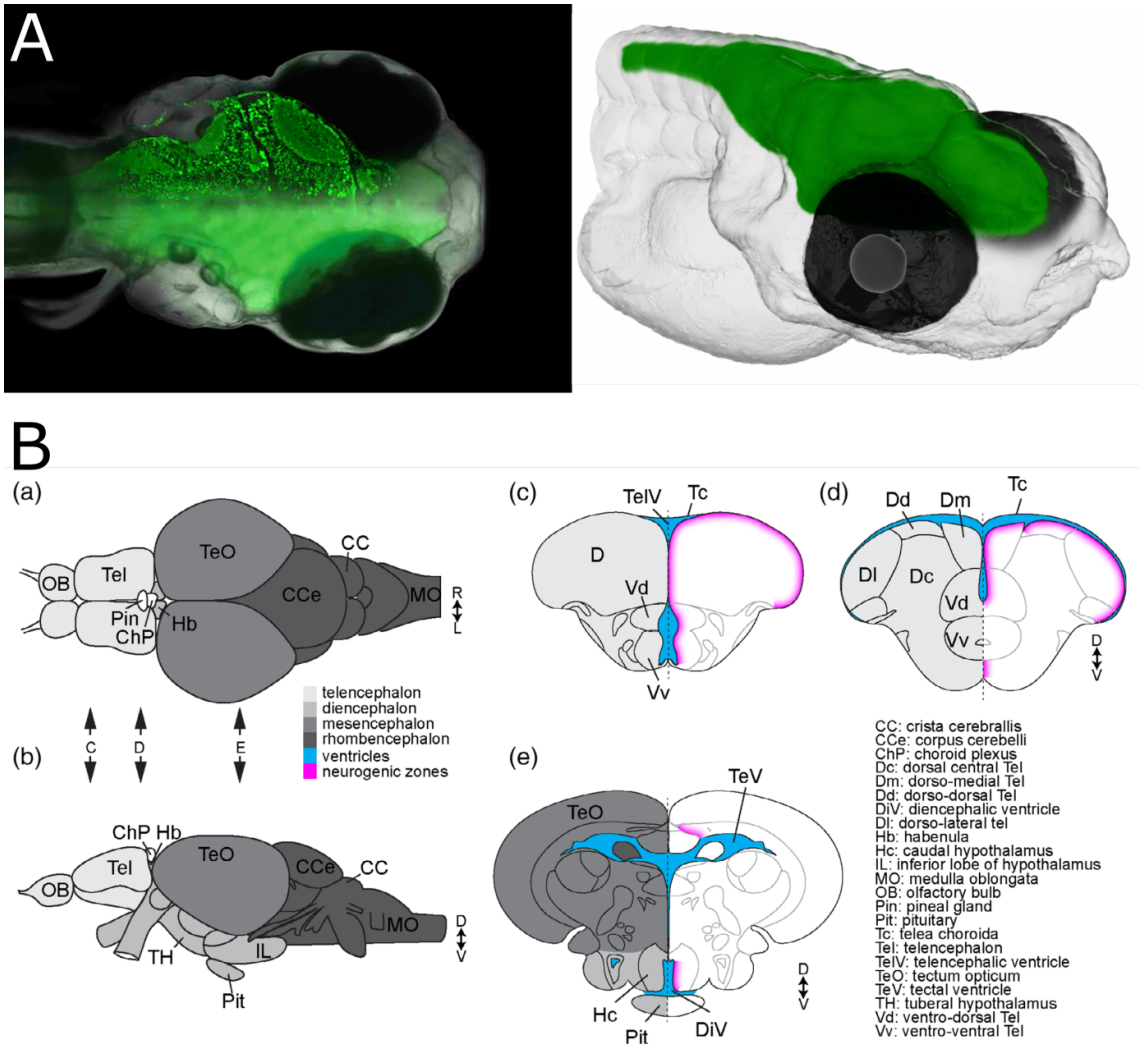

Figure I.11: **A**: Larval zebrafish and its brain in green, adapted from https://braintour.harvard.edu and [87]. **B**: Different regions of the zebrafish brain, from Jurisch *et al.* [88]

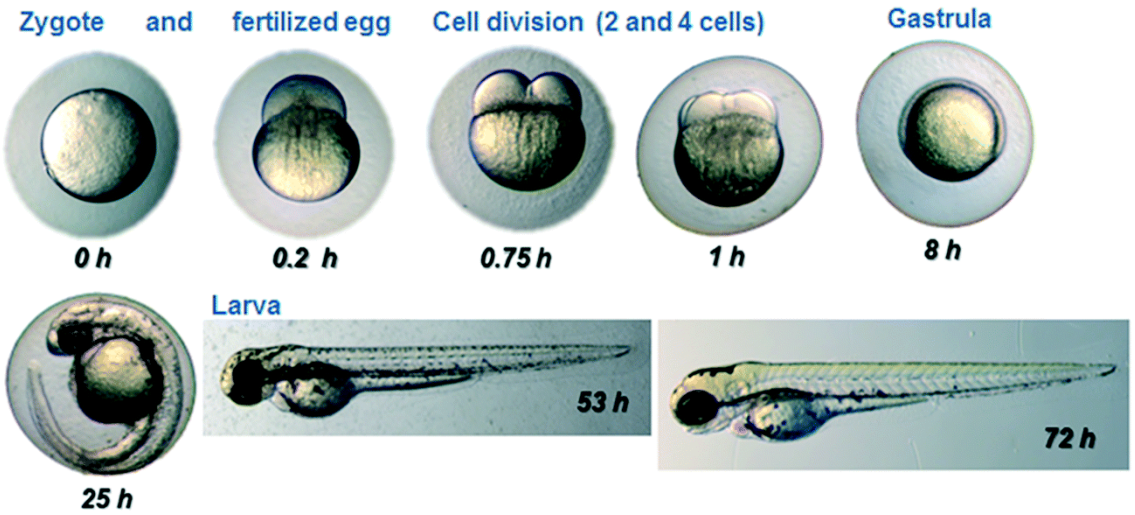

Figure I.12: Zebrafish development, from Cambero *et al.* [93]

[90] is one of them (figure I.13): due to its impaired melanin production, the nacre mutant is more transparent than the wild type, and makes it even easier to access the brain by optical microscopy. Another very interesting genetic modification in the neuroscience field is the GCaMP probe [91], which becomes fluorescent when bound to Ca^{2+} (calcium ions help transmit the electrical signal in neurons, and them entering the cell at the synapses is the trigger for neurotransmitters; they are also involved in genes transcription). GCaMP can be expressed in the whole brain or in subparts of the brain, making it possible to monitor neuronal activity of thousands of neurons at the same time with imaging techniques [92] [24].

I.4 Light-sheet imaging to record the brain

Electrophysiolgy was first developped by Hubel in 1956. The problem with this technique is that is it invasive, can only record neurons in proximity to the probe, does not reveal cellular identity, and cannot be used in small brains. As detecting calcium variation during action potential is non invasive in larval zebrafish [94], and intracellular concentration of calcium ions increases by a factor of 10 to 100 when there is an electrical current in the neuron [95], it is no surprise GECI are so widely used nowadays in neuroscience. Amongst GECI, GCaMP are the most widely used indicators *in vivo* [91], and have outperformed other calcium indicators, after several improvements [96]. In GCaMP, a green fluorescent

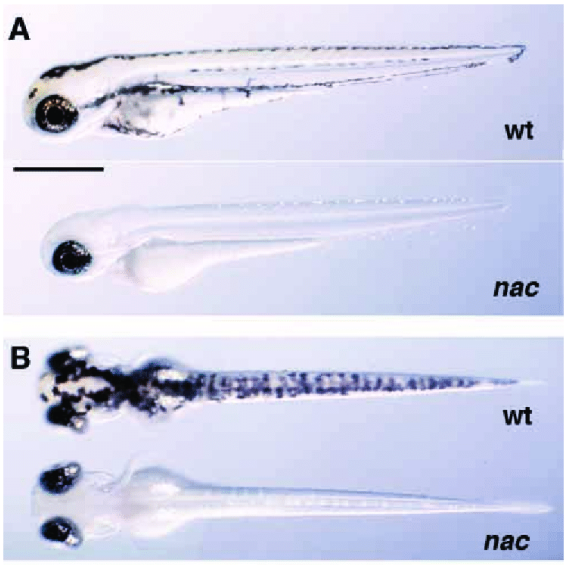

Figure I.13: Comparison between wild type (wt) and nacre (nac) zebrafish from the side (A) and top (B), adapted from Lister *et al.* [90]

protein emits light when stimulated by a 480 nm wavelength light.

The development of imaging devices has thrived in the last decades. A notable discovery is confocal microscopy by Marvin Minsky in 1961: the use of two pinholes blocked scattered and out-of-focus fluorescence light, and allowed Minsky to observe a Golgi apparatus with a greater resolution [97]. In 1995, this confocal imaging technology was used to record motor neurons in larval zebrafish, with neurons labeled with calcium indicators [98]. Many more imaging technologies have been developed since then [99].

The technology we use in this thesis is light-sheet imaging. A rotating mirror creates a light-sheet from a laser beam, and illuminates a whole plan of a sample. The light-sheet being in the focal plan of an objective lens, the fluorescence can be observed (figure I.14). Light-sheet imaging is well suited to image deep within transparent tissues or organisms, and photobleaching and phototoxicity is reduced compared to confocal and multiphoton imaging, because tissues are only exposed to the thin plane of light [100] from which fluorescence is collected. Light-sheet imaging has a performance that is often superior to traditional imaging methods [101], and is well suited to image large systems with high spatiotemporal resolutions over long scales of time [102]. In particular, it is well-suited to record a zebrafish whole brain [24] [92]. Let us note that two-photon microscopy [103] is also a widely used technique for functional imaging. Its main problem is that the frequency

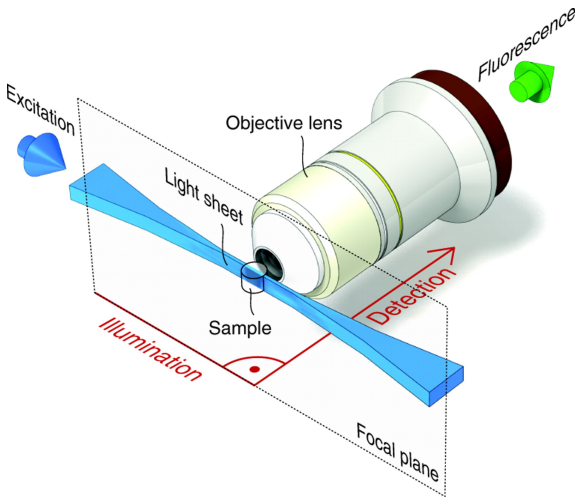

Figure I.14: Light-sheet microscopy explained, from Huisken *et al.* [104]

of acquisition is lower than light-sheet imaging, because the final image is built pixel by pixel.

The recording of a zebrafish brain volume through whole-brain imaging outputs a stack of images (see figure I.15). From these images, we extract the neurons coordinates. These coordinates are displayed in the left panel of figure I.16. Using a non linear transformation, we can project these coordinates on a reference brain [105], which provides us with a set of brain regions associated to each coordinate. These reference coordinates are displayed in the right panel of figure I.16. Neuron activity over time is extracted from sequentially

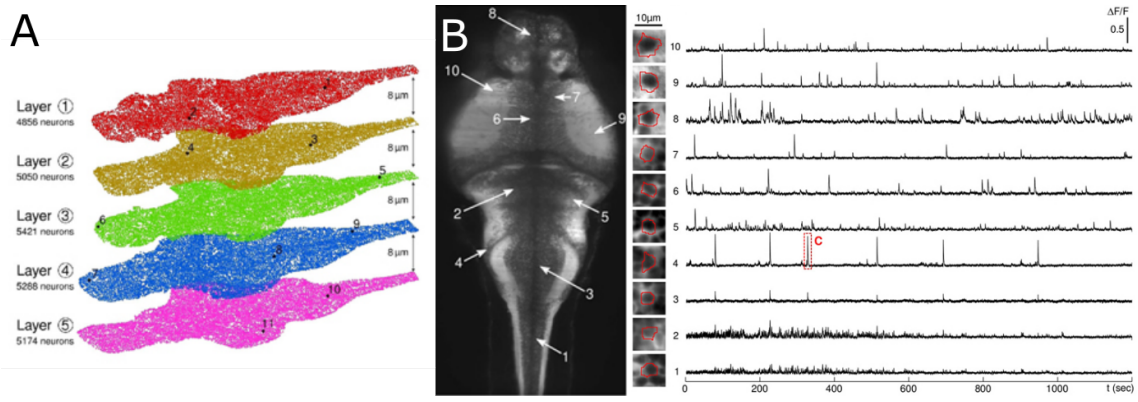

Figure I.15: **A**: Figure of different layers imaged with a light-sheet in a zebrafish brain. **B**: One layer of the zebrafish brain, with specific neurons and their activity. Adapted from Panier *et al.* [24]

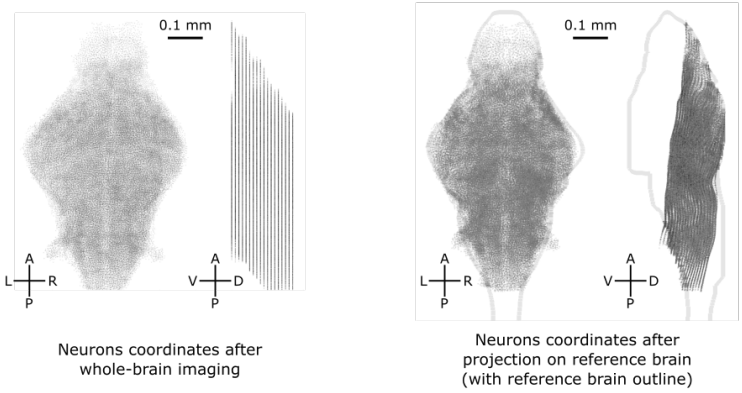

Figure I.16: Left panel is neurons coordinates as segmented from light-sheet images, for one fish. Right panel is neurons coordinates after projection in the reference brain, with reference brain outline in light grey.

recorded brain scans after motion correction. Because in calcium imaging the fluorescence is not the same across neurons, this raw signal of activity is not used, and instead we compute the $\Delta F/F = (raw\_signal - baseline)/(baseline - background)$ signal. The baseline subtraction enables us to center the fluorescence, while the difference between baseline and image background normalizes the neuron's activity. In this work, it is this ΔF/F we will refer to, when we speak about a neuron's activity.

I.5 The vestibular system

The vestibular system is a system of the inner ear, and a specificity of the vertebrates [106]. It allows for a sense of balance, and a coordination of movement with balance, as being able to maintain posture is vital for animals [107]. It is interesting to note that in a multi-sensory task, humans and monkeys tend to over-weight vestibular information over visual information [18]. The first detailed description of the vestibular organs was done by Du Verney in 1610, and the first functional study of the vestibular system done by Eswald in 1892 [108].

The vestibular system is made of two distinct parts: the semicircular canals, in charge of detecting angular accelerations, and the otolith organs, in charge of detecting linear accelerations and gravity in the horizontal and vertical plans [109] (figure I.17). These organs then project to the vestibular nuclei, which in turn project to the spinal cord, extraocular neurons, contralateral vestibular nuclei, and the cerebellum [110].

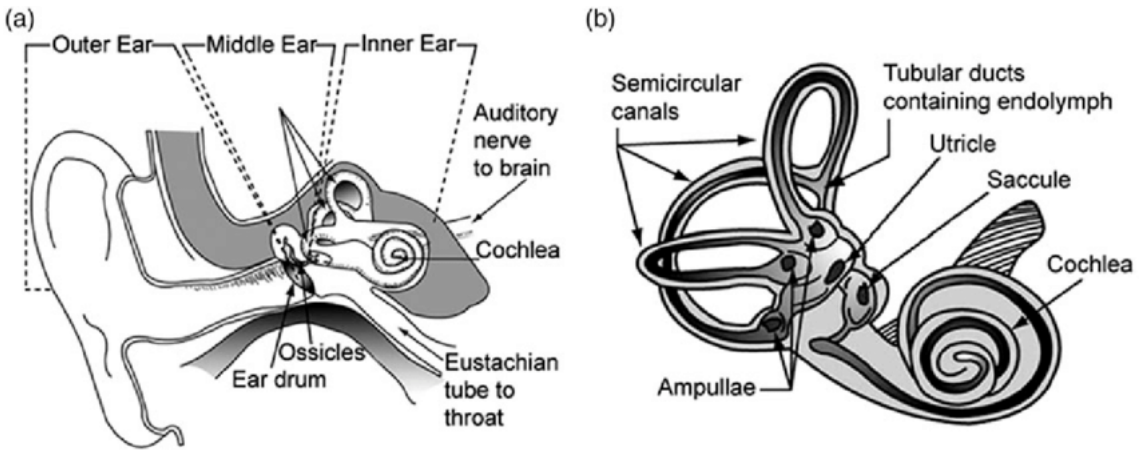

Figure I.17: **A**: Location of the vestibular apparatus with relation to the hear. **B**: Vestibular organ, with linear acceleration detectors (utricle and saccule), and angular acceleration detectors (the semicircular canals). Figure from Howard *et al.* [111].

I.5.1 From sensory input to neuronal signal

Acceleration detection is done with particular cells, called hair cells [112], present in the semicircular canals and otoliths (figure I.18). They convert mechanical movement to electrochemical activity, a process called mechanotransduction [113]. The movement of hair cells' stereocilium causes more or less neurotransmitters release at the synapse, depending on the direction of movement.

There are three semicircular canals, orthogonally oriented: anterior, horizontal and posterior, detecting angular accelerations around the three axes. This detection is done through a hair cell structure called crista, inside a widening of the semicircular canals called ampulla. The crista detects the inertia of the endolymph fluid when a head movement occurs.

There are two otoliths organs: utricle and saccule. The saccule detects vibrations in the vertical direction at relative high frequency and can thus also detect vibrations in the range of auditory frequencies. Though mammals and birds have the cochlear organ to detect sounds, fish and amphibians do not possess it, and use the saccule to detect vibrations in the auditory range [114]. Contrary to the saccule, the utricle has a sole vestibular purpose. In otoliths, hair cells are arranged in a patch called the macula. The difference of movement between the otolithic membrane (due to attached calcium carbonate crystals) and the macula, due to a density difference, allows to detect linear

accelerations. The macula is horizontal for the utricle, and vertical for the saccule.

The number of vestibular nuclei is four on the two sides of the brain. The superior and medial vestibular nuclei get inputs predominantly from the semicircular canals, but also from otolith organs. The lateral vestibular nucleus gets inputs from both semicircular canals and otolith organs. The descending vestibular nucleus gets inputs predominantly from the otolith organs [115].

I.5.2 The vestibular system in zebrafish

The zebrafish possesses the three semicircular canals, that start to form at 42 hpf, up until 5 dpf [117]. Nevertheless, the canals only start working when larvae are 35 dpf [118]. Two otoliths with hair cells are observable by 24 hpf [117], and both the utricle and saccule are functional at 72 hpf in larval zebrafish [42] [119] (figure I.19).

The vestibular system is involved in two different reflexes in vertebrates, and in particular in larval zebrafish: the vestibulo-ocular reflex, and the vestibulospinal reflex. The vestibulospinal reflex is the correction of posture with relation to gravity [120]. We will discuss in more details the vestibulo-ocular reflex just below.

I.5.3 The vestibulo-ocular reflex

The vestibulo-ocular reflex is the stabilization of the retinal slip (i.e. position of an image on the retina) during a head motion, with compensatory eye movement [106]. It is well preserved across species, in particular between human [41] and zebrafish [37], and pitch axis VOR is functional at 3 dpf in larval zebrafish [42]. Larval zebrafish also have a roll axis VOR response at 6 dpf [45]. However, their yawn axis VOR maturates only at one month [123]. The eyes correction, or VOR gain, for humans in the dark is up to 0.9 with head rotation frequency between 0.025 and $4Hz$ [124], and around 0.24 for larval zebrafish around pitch axis [37].

The utricles only play a minor role in VOR in monkeys [125], but with the absence of functional semicircular canals in larval zebrafish, they are responsible for VOR: ablating utricles results in no correction [37]. Interestingly, *Xenopus* tadpoles, which have no semicircular canals either, have adapted their way of swimming so that their head movements can be detected by the utricles, and stabilize their vision [126]. The three-neuron arc handles VOR in zebrafish larvae, with utricles projecting to tangential nuclei, projecting

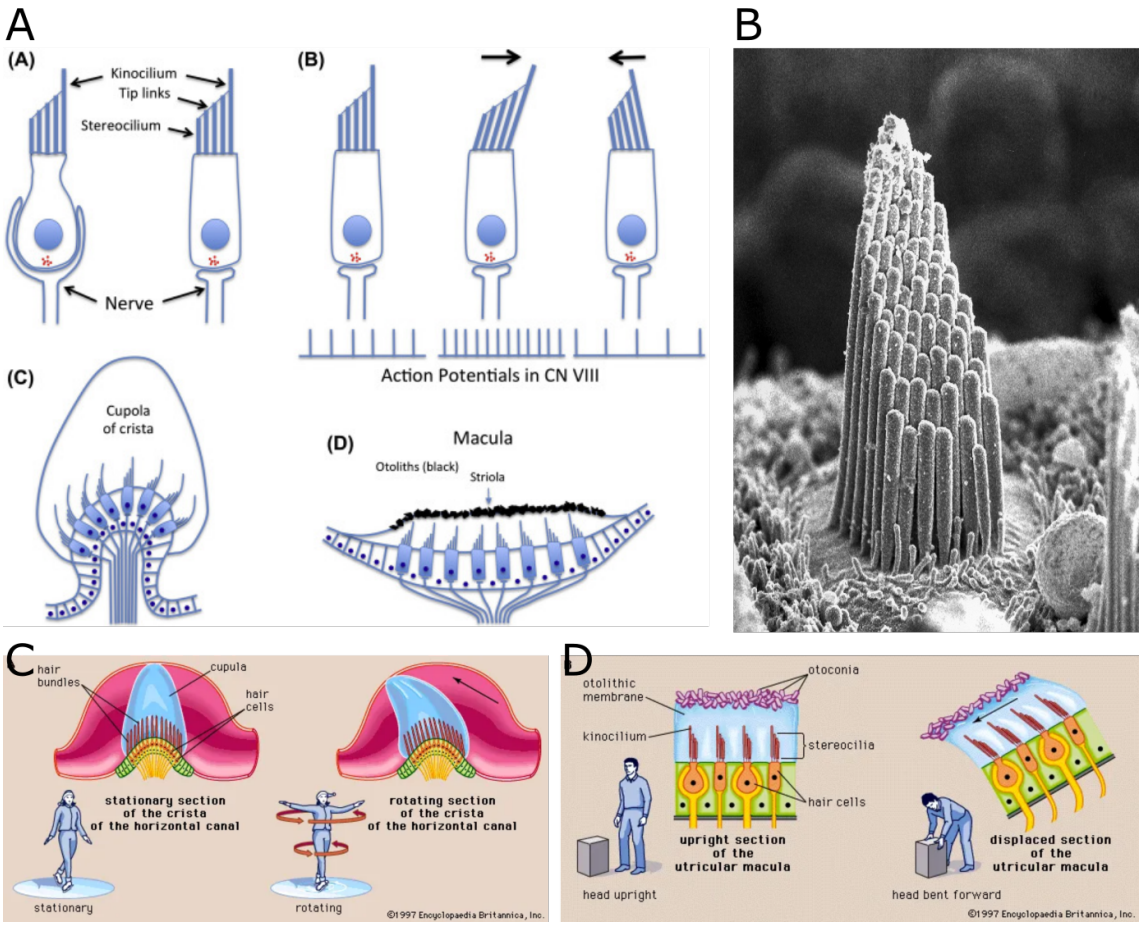

Figure I.18: **A**: (A) two types of hair cells, (B) effect of deflection on action potentials, (C) cristae structure, inside a semicircular canal, (D) macula structure, inside utricule and saccule. Figure from Swenson *et al.* [116]. **B**: Picture of a hair cell from the inner ear by Dr. David Furness. **C**: Effect of a movement on a semicircular canal, from https://www.britannica.com. **D**: Effect of a movement on a utricule or saccule, from https://www.britannica.com.

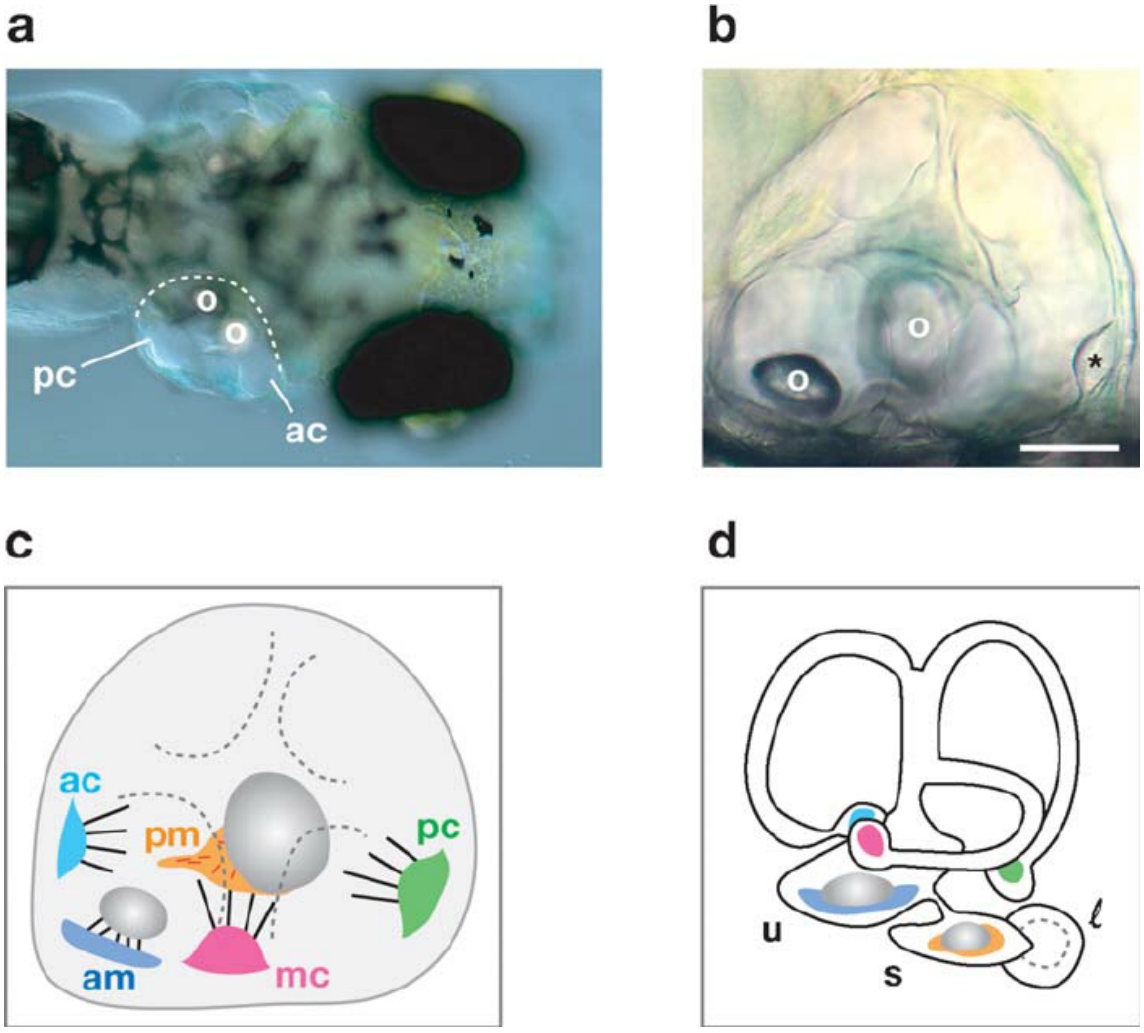

Figure I.19: **A**: Photo of a 5 dpf larval zebrafish. Anterior canal (ac), posterior canal (pc), and otoliths (o) are shown . **B**: Lateral close-up, asterisk is the neuroepithelium within the posterior canal. **C**: Representation of larval zebrafish ear (ac: anterior canal, pc: posterior canal, mc: medial canal, am: anterior macula or otolith, pm: posterior macula or otolith). **D**: Representation of adult zebrafish ear (u: utricle, s: saccule, l: lagena, the hearing organ, similar to a rudimentary cochlea). Figure from Nicolson *et al.* [121].

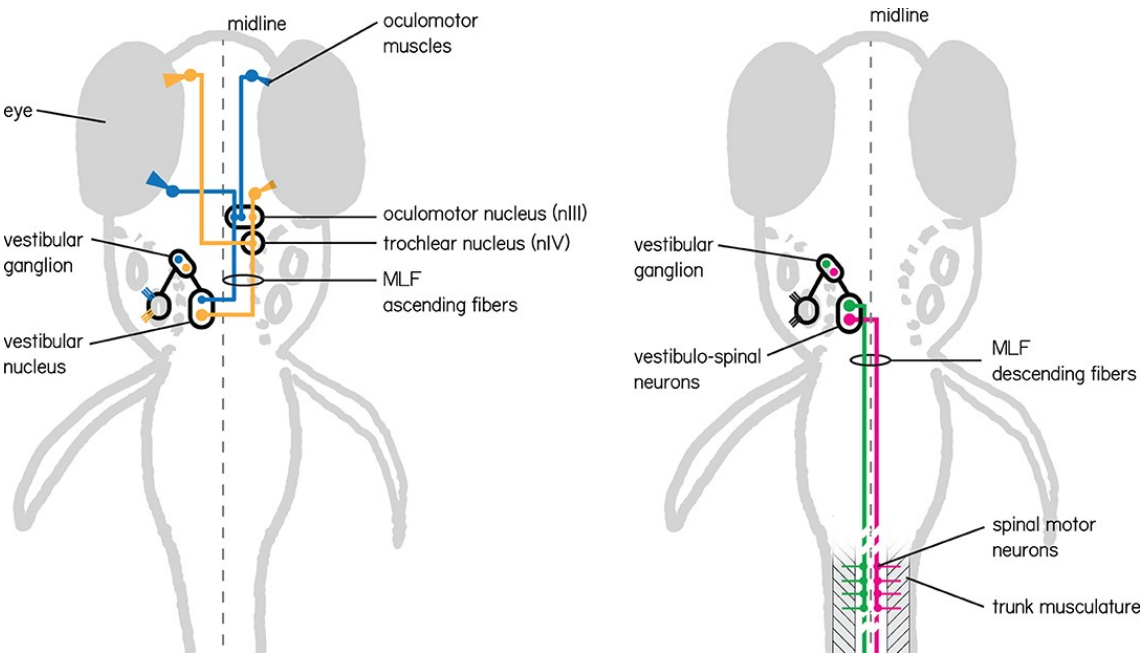

Figure I.20: Left panel is the vestibulo-ocular reflex circuit, and right panel is the vestibulospinal reflex circuit. Figure from Auer *et al.* [122]

in turn contralaterally to oculomotor nucleus [37] [44] [127] (figure I.20).

I.6 The visual system

Vision has been studied more than other sensory modalities [**?**], and the visual input dominates perception [128]. Because of the presence of light on Earth, eyes have become the premier sensory outposts of the brain, and, as a matter of fact, 96 % of animals possess a complex optical system [129]. In the second century, Galen used the work of anatomists to describe many components of the eye. Ibn Al-Haitham described the eye in more details, and studied the effect of light on vision in the XI^{th} century [130], and it was ultimately Kepler who discovered in 1604 how the image was formed and inverted on the retina [131]. Franz Joseph Gall suggested the visual cortex was a subpart of the cortex in 1810 [132], and Hermann Munk located the primary visual cortex in the occipital lobe of the brain in 1881 [133].

The visual system comprises the eyes, and the nerves and tracks projecting the information from the sensory organ to the visual cortex. Eyes are an optical system, transforming light to brain signal, after projection of it on the retina. Fibers of the retina become the

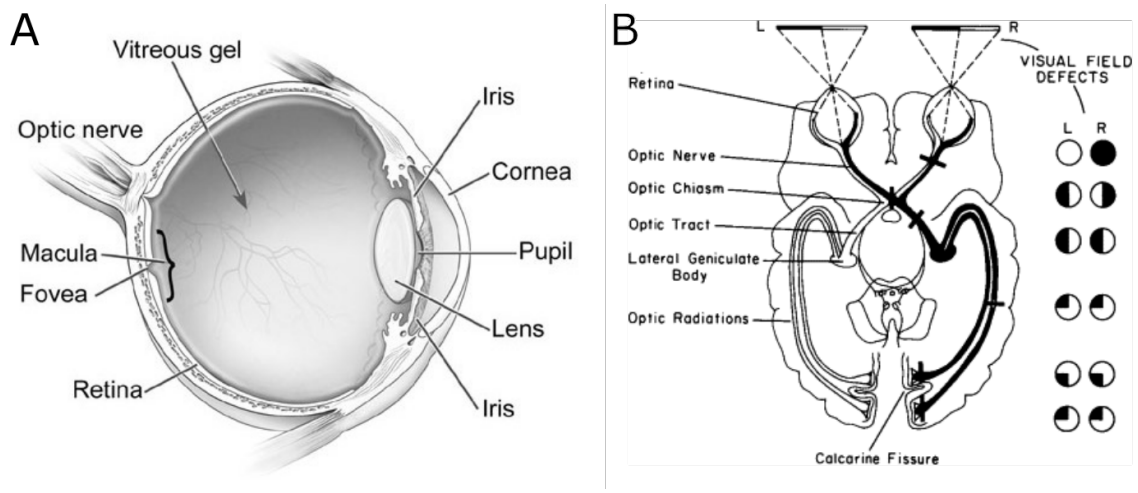

Figure I.21: **A**: Structure of the human eye. The retina transforms light into neuronal signal. Figure from https://www.alberta-retina.com. **B**: Optic track from the eyes to the visual cortex, from Love *et al.* [134].

optic nerves, and meet at the optic chiasm. At the optic chiasm, optic nerves from nasal part of the retina cross the brain to join optic nerves from temporal retina of the other eye. The new optic tracks join structures called lateral geniculate nuclei, and optic radiations then project to the visual cortex [134] [135] (figure I.21). The visual cortex then projects to 18 different areas in the brain [136], including to higher visual cortical areas, to the thalamus, and to subcortical areas like the superior colliculus, striatum, or the brainstem nuclei [137].

I.6.1 From sensory input to neuronal signal

Light detection is done in the retina, where the epithelium is lined with two types of photoreceptors: rods and cones. Rods are sensitive to blue/green wave length, and cones to red, green, or blue, depending on whether they are long-wave, middle-wave, or short-wave cones, respectively [138]. In addition to colour sensitivity difference, rods are more sensitive to light in dim conditions, whereas cones are sensitive only to bright light. This is the reason we do not see colours at night. Photons are absorbed by visual pigments, which consist of a retinal bound to a protein called opsin [139] (the pigment is called rhodopsin in rods). This leads to the closing of calcium ion channels, to the hyperpolarization of the photoreceptor, and to the end of glutamate (excitatory neurotransmitter) transmission at the synapse [140]. Photoreceptors are non-spiking neurons with a significant time constant

[141].

Signal processing is then done in the retina, organized with five different layers. The first layer is the outer nuclear layer, with the photoreceptors. The second layer is the outer plexiform layer, and consists of horizontal cells, which allow for contrast enhancement and colour oponency through photoreceptors inhibitory feedback [142]. The third layer is the inner nuclear layer, with bipolar cells, which contribute to the receptive field properties of the ganglion cells. The fourth layer is the inner plexiform layer, and is made of amacrine cells, which are thought to contribute to the generation of transient responses in ganglion cells [143]. The fifth layer is the ganglion cell layer [144], which project optic fibers to the brain (figure I.22).

I.6.2 The visual system in zebrafish

Zebrafish retina is very similar to that of humans, with the difference that they possess five photoreceptors instead of four [146], allowing them to see UV lights [147]. The layered retinal organisation is visible at 60 hpf, and well developped at 72 hpf [146] (figure I.23). In terms of vision, larval zebrafish can detect a decrease in light intensity at 68 hpf, and movement at 73 hpf [35]

Retinal ganglion cells project contralaterally to the pretectum, the thalamus, and the optic tectum [148], and in particular, direction-selective retinal ganglion cells project to ten different retinal arborization fields in the optic tectum [80]. Neurons in the pretectum are symmetrical, strongly direction sensitive [149], and binocular, in opposition to the monocular neurons of the arborization fields [80]. Interestingly, dorsal neurons of the pretectum can integrate visual information over time [150]. When showing zebrafish visual stimuli, neuronal activity is also spotted in the anterior hindbrain, and in premotor processing regions of the hindbrain. Oculomotor regions are stimulated, such as dorsally and ventrally located extraocular motor neurons [149]. Tail motor regions are also stimulated, such as anterior rhombencephalic turning regions (responsible for swim direction, but also for correlation of swim direction over time [151]), ventromedial spinal projection neurons [80], and nucleus of the medial longitudinal fasciculus (in charge of postural control for tail orientation [152]) [149] (figure I.24).

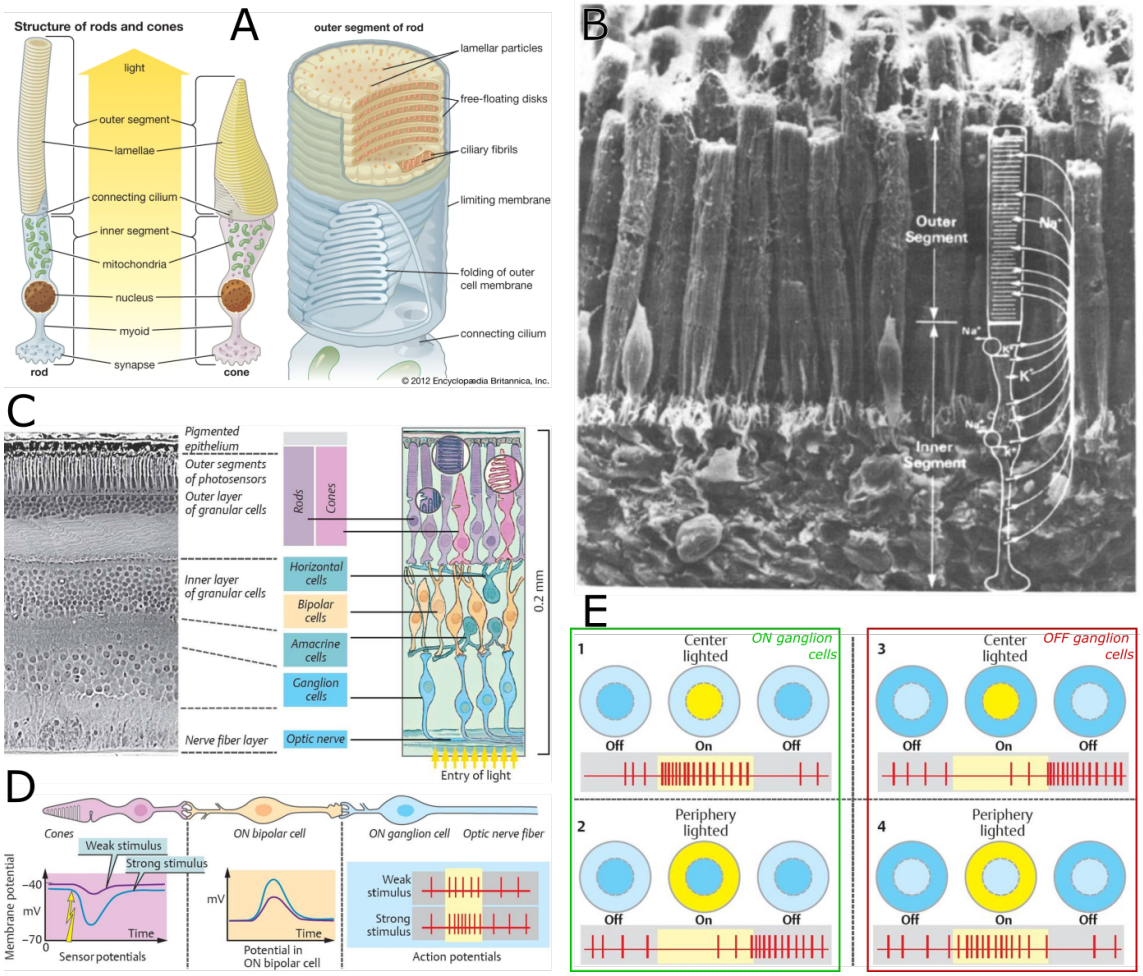

Figure I.22: **A**: Structure of photoreceptors, from https://www.britannica.com. **B**: Photoreceptors of the retina under microscope, from Pugh *et al.* [145]. **C**: Structure of the retina, from https://doctorlib.info. **D**: Influence of light on different cells of the retina, from https://doctorlib.info. **E**: Receptive fields of ON and OFF ganglion cells, from https://doctorlib.info.

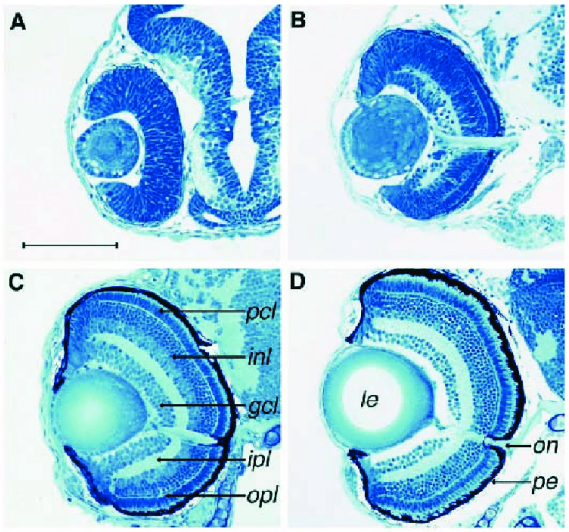

Figure I.23: Transverse section of development of wild-type zebrafish eye (ventral is down, scalebar is $100\mu m$). **A**: At 36 hpf, retinal cells do not form layers. **B**: At 60 hpf, the 5 layers of the retina are visible. **C**: At 72 hpf, retinal stratification is well developed (gcl: ganglion cell layer, inl: inner nuclear layer, ipl: inner plexiform layer, opl: outer plexiform layer, pcl: photoreceptor cell layer). **D**: At 5 dpf, cones can be told apart from rods in outer nuclear layer (le: lens, on: optic nerve, pe: pigmented epithelium). Figure from Malicki *et al.* [146].

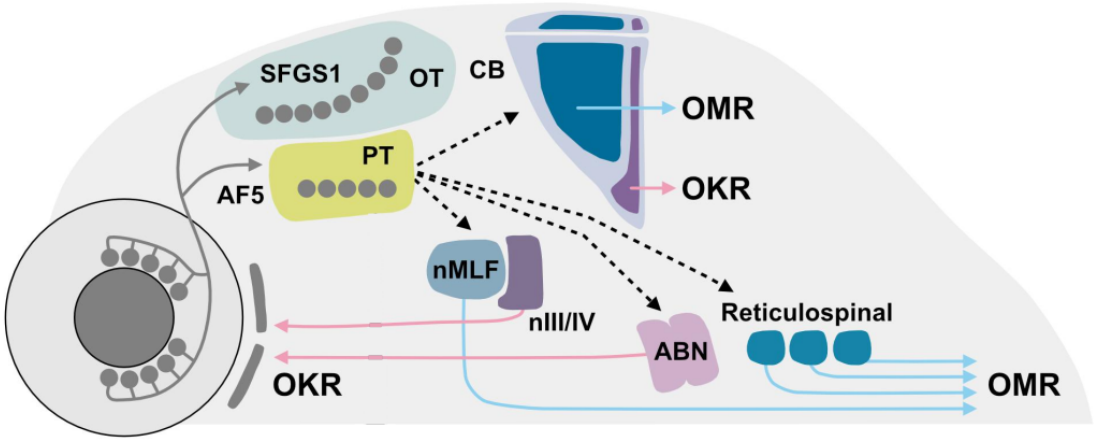

Figure I.24: Optic flow processing circuits in the zebrafish brain. SFGS: stratum fibrosum et griseum superficiale (sublayer of the optic tectum), OT: optic tectum, CB: cerebellum, AF: arborization field, PT: pretectum, OMR: optomotor response, OKR: optokinetic reflex, nMLF: nucleus of the medial longitudinal fascicle, nIII: oculomotor nucleus, nIV: trochlear nucleus, ABN: abducens nucleus. Adapted from Matsuda *et al.* [153].

I.6.3 The optokinetic reflex

The optokinetic reflex stabilizes the visual image on the retina, and allows for high resolution vision [154]; it is widely preserved across animals [155]. At 73 hpf, zebrafish begin to have a response to moving patterns around their yaw axis, and at 80 hpf, virtually all the fish respond to these patterns [35]. OKR improves steadily between 73 and 96 hpf, and OKR gain of 96 hpf fish is 0.9, comparable to adult performances [36]. If the moving pattern consists of stripes, the relationship between stripes contrast and gain is logarithmic, and saturates at very high contrasts, which means maximum gain is reached at very high contrasts [79].

During optokinetic reflex in zebrafish, neuronal responses are highly stereotypical across fish, except for scattered neurons in the stratum periventriculare of the optic tectum [156]. The pretectum is sufficient and necessary for OKR [149], and sends a signal to motor neurons in charge of the extraocular muscles [155]. The optic tectum is not involved in the reflex circuit, and ablating it only has a slight influence on OKR gain [79]. The cerebellum is not directly involved in the reflex but receives sensory and motor inputs related to the OKR through mossy fibers. The pretectum also projects OKR-related information to the inferior olive, reaching the cerebellum through climbing fibers [156].

I.7 Multisensory integration

We constantly integrate multisensory information coming from our sensors. For example, our body ownership feeling is due to the integration of visual, tactile, and proprioceptive information in the brain [157]. Multisensory integration allows us to interact with the world, but also to change: when we learn something, it is more effective if the training we undergo involves more than one sensory modality, because our default interaction with the world is multisensorial [7].

In this section we will focus on the multisensory aspect of the brain, and on models that have been developped to understand it.

I.7.1 Anatomy of multisensory integration

There are many multisensory convergence areas in the brain, including the superior colliculus, basal ganglia, the cerebellum [158] and motor regions (such as the nucleus of the

medial longitudinal fasciculus in zebrafish [159]), as well as the parietal, frontal [160], and prefrontal cortex [20], the latter being usually associated to complex cognitive operations [161], such as causal inference in the case of multisensory problems [162]. In addition, most, if not all, of the neuronal processes in the neocortex are multisensorial [163]. As a matter of fact, multisensory perception is not a localized process, but is rather the integration of many multisensory operations happening in multiple areas of the brain [164]. Interestingly, some of what we think are unisensory regions are not so unisensory after all: the auditory cortex is stimulated when we read lips for instance [21]. The open question is whether the areas we thought were unisensory are intrinsically multisensory, whether multisensory areas are adjacent to unisensory centers (like the medial superior temporal area, located in monkeys extrastriate visual cortex [18]), or whether multisensory regions of the brain project feedbacks to these centers [20] [165].

The superior colliculus is a particularly interesting multisensory area of the brain. Called tectum in non mammal animals, it overlaps sensory maps from different modalities [166], with visual inputs in the upper layers, other sensory convergence areas in intermediate layers, and motor areas in the deepest layers [61]. When stimuli are time and space coherent, there is a response enhancement in the tectum output neurons, while other areas are inhibited [167]. The tectum receives inputs from many regions of the brain, including the thalamus and hypothalamus, the cerebellum, the raphe (responsible in zebrafish for initiation and maintenance of sleep [168], and short term motor learning [169]), the torus semicircularis (part of the auditory pathway in zebrafish [170]), the nucleus isthmi (active during hunting behaviours [171] in zebrafish), and the contralateral tectum. These inputs are though to carry information from different types of modalities [61].

In order for multisensory integration to be effective, the brain needs to be able to compute correlations between stimuli, and compare them across time. It also needs to deal effectively with conflicting multisensory situations [172]. Species have developed neuronal strategies to act (preferentially as fast as possible) when undergoing conflicting multisensory stimulations. For example, in such a situation between auditory and visual stimulations, mice tend to favour auditory cue (although preference to visual cue can be induced with training). This is due to the fact that neurons in the auditory cortex project massively to inhibitory interneurons in the posterior parietal cortex, silencing projections from the visual cortex [6] [173].

I.7.2 A model for multisensory integration: divisive normalization

There are many ways to integrate multisensory information [174], and many models to explain non-linear operations in the brain [175]. In particular, the brain has canonical neural computations, i.e. defined operations happening everywhere. Some of them are exponentiation (a thresholding operation), linear filtering (a weighted sum by linear receptive fields), and divisive normalization, a computation in which a neuron's response is divided by a pool of neurons average [176]. In divisive normalization, the response to a multimodal stimulus is not the sum of the responses to unimodal stimuli, but rather the average [177]. This model explains well neurons activities in fruit flies antenna lobe (equivalent to olfactory bulb in vertebrates), in the retina [178], and in the visual cortex and auditory nerves [179]. More broadly, divisive normalization is well suited for multisensory integration models [180].

I.7.3 Super-addivity during multisensory integration

Neuronal response to multisensory stimulation can be enhanced when the stimuli come from the same location (spatial rule), when they happen at the same time (temporal rule), or when one of them is weak (inverse effectiveness rule) [166]. This enhancement is called super-additivity: it is when the number of spikes a neuron generates when responding to a multisensory stimulation is higher than the sum of spikes for unisensory stimulations. The usual response of multisensory neurons is linear, and super and sub-additivity are more rarely observed at population level [181]. Divisive normalization can properly model inverse effectiveness, and super and sub-additive neurons responses [180].

Although multisensory processes in the brain do not only rely on super-additivity [182], super-additive neurons have been widely used to identify multisensory regions in brain imaging [183]. The reality is that basic summation model explains a lot of bi-modal combinations in the superior colliculus. As super-additivity occurs, as we said, when one of the two stimuli has a weak influence on neural response, it might be due to near threshold signals from the weak stimulus [17]. As a matter of fact, while the number of spikes seems super-additive when one of the stimuli causes a weak response, the voltage current related to each stimulus is integrated linearly [184]. So super-additivity may simply be due to the intrinsic non-linearity of action potential triggering.

I.8 Learning and adaptation

Learning and adaptation allow us to evolve as individuals and integrate new skills that will make us more suited to survive.

In this section we will see the different learning processes there are, from the synapse level to the cerebellum scale.

I.8.1 Plasticity at the scale of the synapses

The amplitude of the synaptic response after trains of action potentials is not constant in time. This property allows for plasticity to happen at the synapse level.

In short-term plasticity, after a certain time, the synapses recover their initial strength [185]. Facilitation is a form of short-term plasticity, and consists in the increase of synaptic response (and therefore the increase of post-synaptic neuronal response), when stimuli are very close in time [186]. Facilitation occurs at the millisecond timescale, but other short-term enhancement mechanism can happen at longer timescales, such as augmentation, in seconds, and post-tetanic potentiation, in minutes [187]. Facilitation, augmentation, and post-tetanic potentiation are all due to an increased concentration of calcium ions in the pre-synaptic neuron, because of the elevated frequency of incoming action potentials, leading to a greater release of neurotransmitters. It is also possible that the elevated frequency of incoming action potentials leads to a depletion of the vesicles containing neurotransmitters in the pre-synaptic neuron, in which case we speak of short-term depression [188].

On the other hand, long-term plasticity has been shown to last for up to 16 weeks [189]. Repeated stimulations of the pre-synaptic neuron have a long-term effect on the activity of the post-synaptic neuron in excitatory synapses [190]. Experiments done on pyramidal neurons of the rat hippocampus have shown that the frequency of pre-synaptic stimulation has a key role in synaptic plasticity [191]. A repeated pre-synaptic stimulations at a high frequency (100 Hz) results in a sustained increased post-synaptic activity, called long-term potentiation [192]. In opposition, with a pre-synaptic stimulation at low frequency (1 Hz), there is a decreased post-synaptic activity, called long-term depression [193]. Long-term potentiation and depression can be observed between two neurons in which the post-synaptic neuron fires shortly after or before the pre-synaptic one, respec-

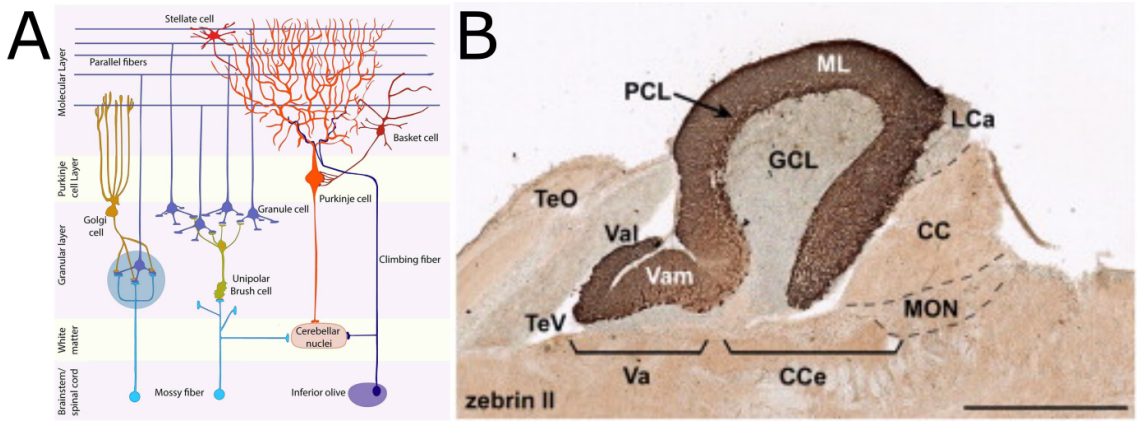

Figure I.25: **A**: Neuronal organization of the cerebellum. Figure from Consalez *et al.* [198]. **B**: Layered organization of the adult zebrafish cerebellum. Sagital section, anterior to the left. ML: molecular layer, PCL: Purkinje cell layer, LCa: lobus caudalis cerebelli, GCL: granule cell layer, TeO, optic tectum, Val: lateral division of the valvula cerebelli, CC: crista cerebellaris, Vam: medial division of valvula cerebelli, TeV: tectal ventricle, MON: medial octavolateralis nucleus, Va: valvula cerebelli, CCe: corpus cerebelli. Figure from Bae *et al.* [199].

tively, a phenomenon called spike timing dependant plasticity [194]. We can also talk about habituation (sometimes referred to as adaptation), during which the response to the same stimulus presented multiple times decreases in intensity [195]. At a neuronal level, habituation is due to calcium channels opening during action potentials, and calcium entering the cell, resulting in a cell current decrease, and a form of self-inhibition from the neuron [196]. It is amusing to note that the reason we are able to see is because our eyes constantly do micro-movements, to not have the constant same image projected on the neurons of the retina, which continually habituate [197].

I.8.2 Mechanisms of motor learning

The anatomy of the cerebellum, responsible for motor learning is highly conserved across vertebrates [200]. In humans, although it represents only 10 % of the total brain volume, it contains more than 50 % of the total number of neurons in the brain [**?**], making it a very complex system. The cerebellum is organized in three layers: the granule cell layer, the Purkinje cell layer, and the molecular layer (figure I.25).

The granule cell layer is composed of granule cells, getting sensory feedbacks from their mossy fibers inputs [201]. The Purkinje cell layer is made of Purkinje cells; a single

one of them can receive signals from 200,000 granule cells [48]. Purkinje cells also receive signals from the inferior olive, through climbing fibers. One cell is connected to a single climbing fiber, divided into around 500 synapses [202]. The inferior olive sends a strong [203] error signals to the Purkinje cells and therefore contributes to timing and learning operations [204]. The climbing fibers signals originating from the inferior olive can also represent harmful consequences of a movement, or wrong movement executions [201]. The molecular layer is composed of Purkinje cells dendrites, climbing fibers, and axons of the granule cells, in the form of parallel fibers. At the end of the circuit, the deep cerebellar nuclei are the only cerebellar outputs [205], and project to cortical and subcortical areas of the brain [206]. In particular, three (dentate, emboliform, and globose; the two latter are fused into the interposed nucleus in humans) of the four deep cerebellar nuclei (the three plus the fastigii) project to the motor cortex and are involved in voluntary limb movements [207].

Motor learning takes place in the cerebellum because of long-term depression [208]. It happens specifically when a granule cell, through a parallel fiber, fires repeatedly at a Purkinje cell synapse, while one climbing fibre fires synchronously at the same location [201]. Many models exist to describe how this local depression explains cerebellar motor learning [209], and Marr's theory, published in 1969, is still relevant nowadays [210]. It hypothesises that after long-term plasticity has occured in Purkinje cells, they have correlated context from the parallel fibers to error from the climbing fibers. After the learning, the context alone is enough to accurately predict a motor output [211].

I.8.3 Learning and adaptation experiments in fish

Many adaptation experiments have been performed on fish, and zebrafish in particular, in which the cerebellum is confirmed the be an important part of motor learning.

Adaptation seems to begin at three weeks for zebrafish, in situations in which they need to make a decision based on visual pattern associated electro-shocks [212]. In larval zebrafish though, Purkinje cells have been depicted as prediction error signal encoders during a periodical stimulus [213], and their ablation prevents the fish from adapting in long timescales [214]. The inferior olive has been shown to make possible short-term learning through compensatory changes in motor output [92]. In goldfish, removing the cerebellum after VOR adaptation does not result in a change of behaviour, but the absence

of cerebellum prevents VOR adaptation [215]. The adaptation to an artificial change in VOR gain for these goldfish, happens in six hours, with significant improvements after thirty minutes. [216].

In zebrafish, it is interesting to note that regions of the brain other than the cerebellum can trigger short-term learning. Glial cells accumulate evidence that a motor output results in no actual action on the environment. When glial cells activities are high enough, zebrafish switch to a passive state [217]. The dorsal raphe nucleus as well is involved in short-term motor learning, through an increased average activity [169]. As the raphe nuclei account for 85 % of all the serotonergic neurons in the brain [218], this raphe mediated short term learning can be thought of as neuromodulation, a situation in which a restricted group of neurons influences multiple neurons through the release of a specific neurotransmitter.

I.9 Summary and aim of this work

We have seen that the combination of vestibular and visual stimulations was interesting in terms of multisensory integration, and have explained how the vestibular and visual circuits work. We have gone through notions of neuroscience, and through how the zebrafish is a good model to study neuronal circuits of the brain. We have seen that technologies, and in particular light-sheet imaging, allow us to image the entirety of a zebrafish brain. Finally, we have covered theory and state of the art about multisensory integration, and learning.

Our main question is the following: what is going on inside the head of a zebrafish during a multisensory stimulation, at whole-brain scale, with single-cell resolution?

This work will tackle the following consecutive questions on multisensory integration.

We will first visualize multisensory neuronal data, with the hypothesis that if we overlap brain recordings from different types of stimuli, we will observe areas of the brain that will be responsive to several of them. This analysis is not focused on single-cell resolution, but with rather define global multimodal regions in the brain.

We will then study the multisensory integration of vestibular and visual information, at single-cell resolution, and hope to find multisensory neurons inside the brain of larval

zebrafish, which we will try to link to the behaviour under multisensory stimulation.

We will then study the influence of visual contrast on behavioural and neuronal responses, when coupled with vestibular stimulation. In particular, Rinner *et al.* have shown that the evolution of behavioural response was logarithmically correlated to the contrast [79]; we will test this hypothesis when vestibular stimulation is added.

Finally, the last hypothesis we will be testing is: is it possible to induce learning in larval zebrafish in a mismatching multisensory environment?

This work's new approach is the combination of vestibular and visual stimulations, along with behaviour analysis, and whole-brain imaging. Our setup allows for eye tracking and light-sheet microscopy, while the animal model is rotated and presented with moving gratings at the same time. All in all, we aim at providing an exhaustive analysis of behavioural and neuronal responses to the combination of vestibular and visual modalities, that will allow us to go beyond the state of the art shown in this introduction.

II – Visualizing multisensory brain data

II.1 Introduction

Humans live in a multisensory environment. We can interact with our surrounding because we have information on it. We can see what is in front of us, hear noises around us, smell, taste, and touch objects. We have information on whether it is too hot or too cold, and we can feel pain. Migrating birds can even feel the Earth magnetic field in order to orientate themselves. Although we might survive using only one of these senses, the combination of them allows us to have a more precise, robust and complete perception of our environment. Trying to stand on one leg with the eyes closed is a good indication on the importance of visual information along with inner ear balance. The perturbing experience when trying to watch a movie with the wrong subtitles is another indication on how important coherence between auditory and visual information is.

In order to understand how we can thrive in a multisensory environment, we need to look at how multisensory data is processed inside the brain. A stimulation, whatever it is - as long as it is perceivable -, will provoke a surge of activity in certain brain regions. Studying these brain regions for different kinds of stimulations can provide interesting insight on how the brain actually works to sort out the signals, and have a robust motor output.

In the first part of my thesis, I will present this first approach taken on multisensory integration: finding multimodal regions inside the brain.

The zebrafish team at the Jean Perrin lab works on different parts of the fish behaviour: mechanotaxis (response to movement), phototaxis (response to light), thermotaxis (response to temperature), chemotaxis (reponse to chemicals). This allowed me to access loads of datasets on these different modalities, from the works of Geoffrey Migault [219], Guillaume Le Goc [220], and Raphael Olive [221]. The classic way to tackle a neurobehaviour project is to study a behaviour, and then record neuron's activity, trying to link the neuronal recordings to the behaviour.

The first part of this work was finding a metric to compute how the neurons signals are linked to the simulations. I then built a program to visualize the data, with many options to optimize the interface. Using this program, in the end, I was able to look inside

the brain, and find interesting areas as to where multisensory integration could be taking place.

II.2 Results

II.2.1 Datasets presentation

a) Methods summary

Having access to multiple datasets from multiple experiments, the first objective was to understand the data. Once I had, I needed to find a good metric to be able to say which neurons were the most responsive. For each fish whose brain activity was recorded, I had information on between 10,000 and 100,000 neurons, scattered all across the central nervous system. Information on these neurons, as well as their coordinates was conveniently stored in HDF5 files.

In the HDF5 files, there was a lot of information from different experimental protocols. I explain here the different protocols one after the other. I then go through different methods to analyze the neurons responses, and weight the pros and cons of each of them.

In this part, I aim at explaining the data I was manipulating, and discuss a good way to say if a neuron was responsive or not. This first analysis provided me with a unique response value for each neuron of each dataset, and helped me compare the datasets.

b) Explanation of the different protocols of the study

In each HDF5 file, there were different data recordings for an experimental protocol, done on one fish. Here, I explain these protocols.

Along with the neurons coordinates, HDF5 files contained information about the experimental protocol stimulus. Experimental protocols are displayed in figure II.1, with their associated stimulus time traces. I studied 38 HDF5 files in total, split as follow:

- Vestibular stimulations (11 of them) were obtained using a rotating microscope. The light-sheet, and objective were mounted on the setup, and allowed for a stable

recording during the rotational movement. Motor rotation could either be sinusoidal ($10°$ amplitude at $0.2Hz$, during 10 minutes with GCaMP6s sensor) or step like ($15°$, $20°$, and $25°$ amplitude with a velocity of $60°/s$ and a step length of 10 s, during 10 minutes with GCaMP6s sensor).

- Visual stimulation (1 in total) was obtained by projecting a striped pattern on a bent screen below the fish. Movement of the projected stripes was sinusoidal ($10°$ amplitude at $0.2Hz$, during 10 minutes with GCaMP6s sensor).
- Auditory stimulations (3 of them) were obtained with a speaker positioned below the fish, providing a periodic acoustic pulse (sound frequency of $750Hz$ between $121 - 161dB$ every 10 s, during 30 minutes with GCaMP6f sensor).
- Finally, thermotaxis stimulations, with either hot (9 of them) or cold (14 of them) water were obtained with a water dispenser, delivering the water at random times during the experiment (20 hot or cold water flows of $24 - 30°$ or $11 - 21°$, separated by $10 - 30$ s, during around 8 minutes).

Having information on the stimuli, along with neurons signals, it was time to find a way to tell whether a neuron was responsive to a stimulation.

c) How to link the neurons signals to stimuli

I needed to find a good way to link the different neurons to the stimuli. In order to do this, I went through different analysis strategies.

First of all, I needed to take into account the fluorescence dynamics. Neurons do not light up instantaneously as they emit action potentials, nor do they stop instantaneously as their activity stops. There is a time constant when fluorescence rises, and another when it decays. In the lab, we were able to approximate this rise and decay with a simple decaying exponential kernel, with a time constant of $2.6s$. The first step was therefore to convolve all the stimuli signals with this exponential kernel. What the convolved signals looked like after an additional step of normalization is shown in figure II.2.

The type of stimulus varied, depending on which modality was analyzed. As I gathered datasets and did not do these experiments myself, I could not define the same type of stimulus for all the modalities. This added an additional difficulty to the data analysis.

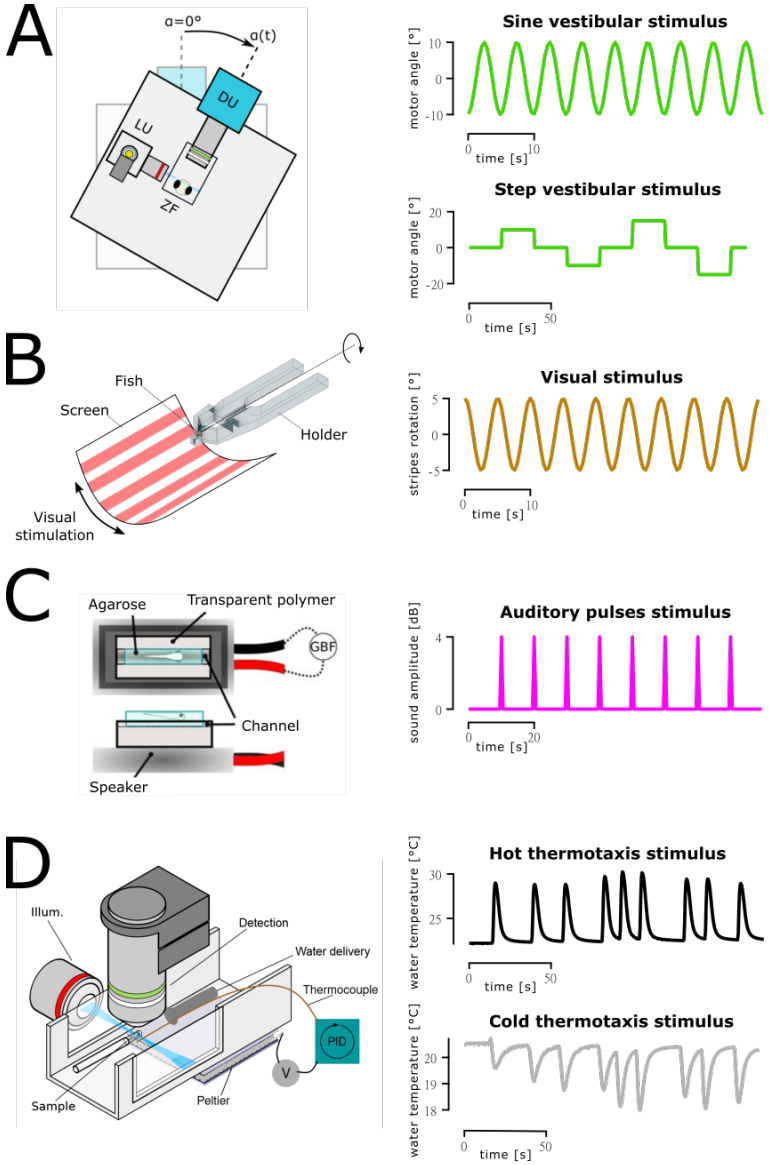

Figure II.1: Experimental protocols on left panels, with associated stimulus traces on right panels. **A**: vestibular experiments from [219], **B**: visual experiment from [219], **C**: auditory experiments from [221], **D**: thermotaxis experiments from [220].

My goal was to be able to say whether a neuron was responsive to a stimulus, and I did it by analyzing their ΔF/F signals. A few handpicked neurons' ΔF/Fs are plotted in figure II.3. Following are ways I tried to link a neuron's ΔF/F signal to the processed stimulus signal.

- When looking at auditory and thermotaxis stimulations, the first possible way to analyze neurons' responses was subtracting neurons' activities before and after the pulse. If the pulse was occuring at time t, $neuron\_activity = \sum_{i=t}^{t+n-1} \Delta F/F_i - \sum_{i=t-n}^{t-1} \Delta F/F_i$, with n the number of points considered before and after the pulse. The problem with this formula was that it was not easily applicable to sine signals, and I therefore discarded it.

- An interesting way to analyze the data was with Fourier analysis. But as thermotaxis experiments were random pulses, it was not relevant.

- Correlation was a quick and easy way to determine whether a neuron was responsive to the stimulus. Taking the stimulus array $stim$ and the ΔF/F of a neuron, $corr = \frac{cov(stim,\Delta F/F)}{\sigma_{stim} \cdot \sigma_{\Delta F/F}}$, cov being the covariance, and σ the standard deviation. Correlation gives an indication on whether two signals vary the same way, the opposite way, or not together a all. It was interesting, but for the auditory pulses, accoustic sounds lasted for a few time steps, and could be missed by the analysis.

- Linear regression was a good way to study the relationship between a stimulus and a neuron's response. A high regression coefficient meant the neuron's ΔF/F was similar to the stimulus, and very active. The problem was that it was possible to have responsive neurons with low responses, and these neurons could be easily detected using Fourier transform for instance. To that extent, the F-statistic came in handy. In a linear or multilinear regression, this statistic provides a value determining whether the fit is better than a trivial one, with only a constant regressor. Said differently, it tests the hypothesis stating that all coefficients of the regression are 0, except for the coefficient associated to the constant regressor, which is the average of the signal. F-statistic is very interesting, because a neuron with a low response, but very responsive to the stimulus is detected with it.

There was no perfect way to analyze neural data, and all of the strategies suggested above had their pros and cons. Although I spent a lot of time using correlations to study

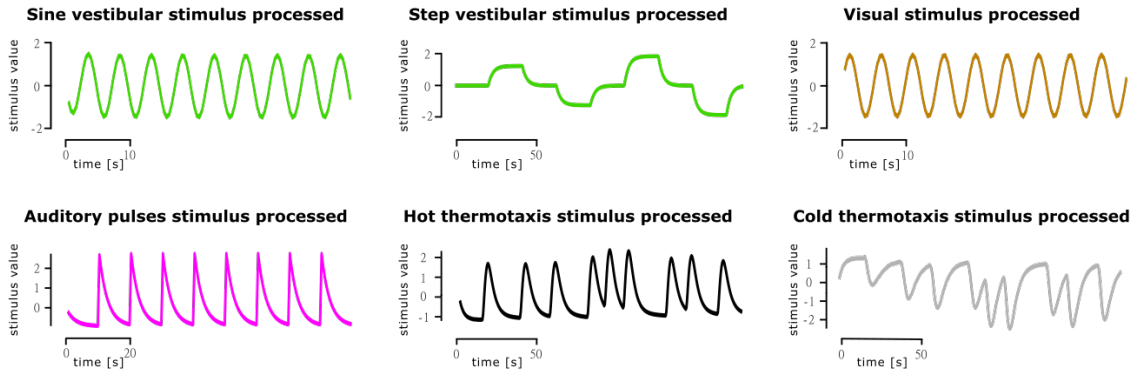

Figure II.2: Stimulus signals after being convoluted with an exponential kernel (to account for fluorescence dynamics), and normalized.

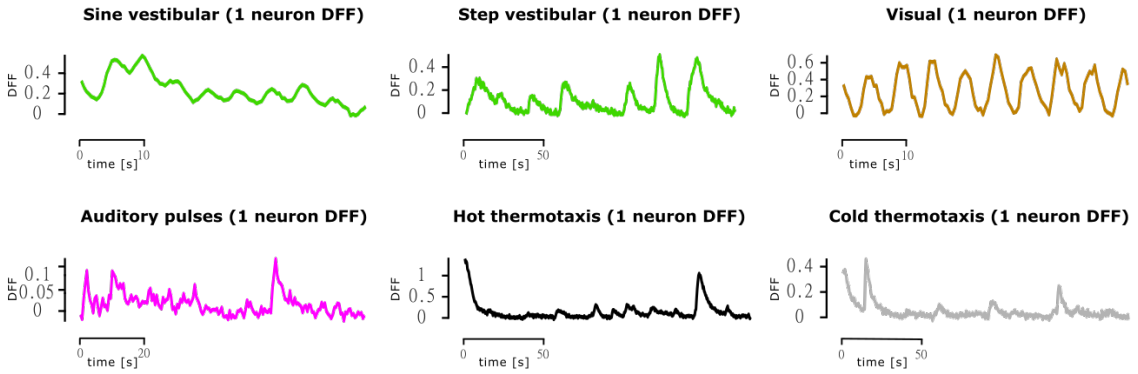

Figure II.3: ΔF/Fs corresponding to the stimuli times, for different handpicked neurons. We looked for neurons which displayed at least a small response to the stimulations.

the ΔF/Fs, the F-statistic approach was the one that provided the best results. It was therefore with this F-statistic that I analyzed the responsiveness of neurons to stimuli. Precise computation of F-statistic is provided in annex VIII.1.

II.2.2 Building a program that easily allows to visualize data

a) Methods summary

My goal was to be able to visualize in a common reference frame the data recorded in different animals, in an simple and informative way.

In order to do that, I defined a grid, the size of the reference brain. This way, each neuron, with a particular set of coordinates in this reference brain, was going to be as-

sociated to the closest grid point. The grid increment was the distance between two grid points, and could be define arbitrarily. I set this increment to be $5\mu m$, which is the average neuron radius. As we discussed above, each neuron had a metric, the F-statistic. For each fish, I therefore had a set of F-statistics associated to grid points. The grid allowed to compare the 38 experiments I had, since the space of comparison was common to all the fish. In this part, I will go through the Matlab program I made to visualize the data.

b) Visualizing the most responsive neurons

I needed to display the most responsive neurons, and find regions in the fish brain where most responsive neurons of different modalities overlapped.

The program allowed to pick two datasets from the list of 38, based on the stimuli I wanted to compare. I could then either set a threshold for the F-statistic, or display a certain number of neurons with the highest F-statistic (figure II.4). It was possible to manipulate the grid using a set of controls that allowed me to rotate the visualization, zoom in, or select a reference plane (horizontal, coronal or saggital) on which to project the grid points on. The selected datasets were coloured green and magenta, and the grid points most responsive to both modalities were in black. Size of the grid points could be changed.

Next, I implemented a function to visualize isovalues for one dataset F-statistics with a user defined threshold for the isovalue (figure II.5).

Using this program, I was able to visualize the areas in the brain that were the most responsive to a certain type of stimulation, along with the F-statistics isovalues. The program made it possible to reveal potentially multisensory areas in the brain. In the following, I will discuss further interesting functionalities of this program.

c) Other interesting options of the program

The program made it possible to display most responsive neurons for two different selected datasets, and F-statistic isovalues for one of the two datasets. Here, we are going to go through the other options available.

Figure II.4: Program interface to display most responsive areas. The top 1,000 most responsive grid points, approximately, are displayed in the transverse plan, in green for a vestibular dataset, and magenta for a visual dataset. Black dots are overlapping green and magenta grid points.

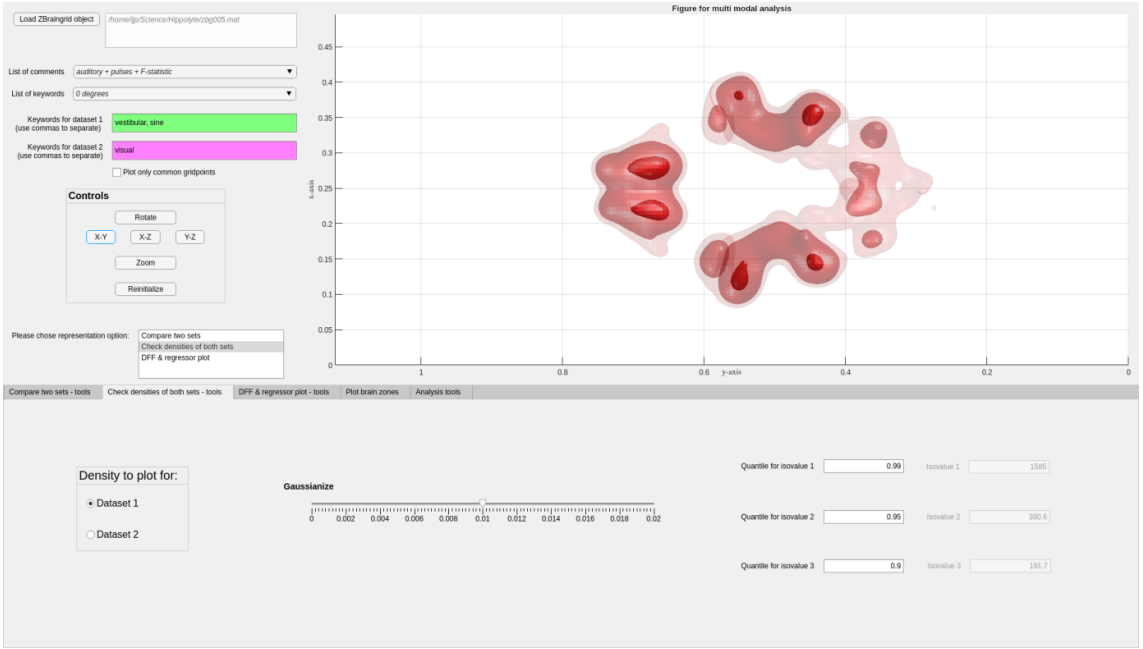

Figure II.5: Program interface to display F-statistics isovalues. Represented are the isovalues for a vestibular dataset.

Further optional functionalities were organized in different tabs on the graphical user interface.

One of the tabs was dedicated to visualizing the neuronal response over time related to a single user defined grid point. (figure II.6). The user could then select two datasets, which could be different from the datasets displayed, and visualize the $\Delta F/Fs$ of this grid point for the two selected fish, alongside with the stimuli. This grid point's brain region was also shown. This guaranteed an easy access to specific regions' $\Delta F/Fs$.

Another tab allowed to overlap chosen brain regions over the current plot (figure II.7). Multiple regions could be selected, as well as the whole brain. Along with the 3D plot of the regions, it was possible to have a projection of these regions onto one of the three main plans.

The last tab gave three options to save parts of the selected data for further analysis (figure II.8). The first one allowed to save the index of the points that were the closest to the selected grid point in the $\Delta F/F$ tab. The second one allowed to save average response to stimuli within a certain radius, around the grid point selected in the $\Delta F/F$ tab. The last one allowed to save the index of the plotted neurons.

These options allow the user to navigate through the data, and save them for a later analysis.

II.2.3 Finding multimodal areas

a) Methods summary

My goal in this part was to examine the neuronal activity in the fish brain in response to various sensory stimulation and to identify specific regions where neurons responsive to different modalities intermingle.

The first step was to average all the fish brains for a given modality. As we will see, there are different ways to do so, each coming with interesting approaches and limitations. The second step was to display the most responsive grid points for each of the modalities together, and find grid points which intersect. I did this using the program explained above.

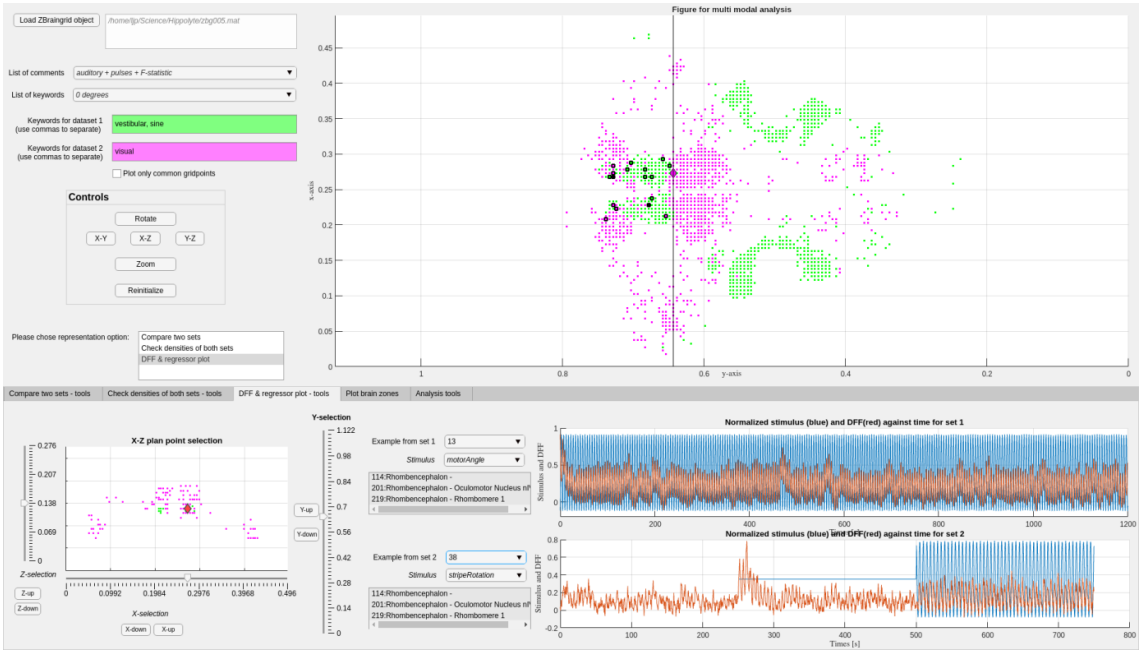

Figure II.6: Program interface to visual $\Delta F/Fs$ at a selected grid point. Here, the grid point selected seems to respond to both vestibular and visual stimulations.

Figure II.7: Program interface to plot brain regions along with data.

Figure II.8: Program interface for analysis tools.

This work's goal was to answer the following question: are there clusters in the brain that integrate information from different sensory modalities?

b) How to average neurons in the grid

Averaging the recorded neuronal activity across datasets for a given type of stimulation was the first step towards identifying multisensory areas.

Let us consider a particular grid point, for which we want to average the F-statistics from different datasets. Two methods come to mind.

The first one is summing all F-statistics, taking a value of 0 for a dataset if no neuron from this dataset is associated to the grid point; then dividing by the total number of datasets. This method is interesting in the way that it smooths the data: if there is only one dataset with a neuron associated to a particular grid point, but with a very high F-statistic, then the averaged value of this grid point will be much lower, and this provides the information that we do not have enough data to actually label this grid point responsive.

The second method is summing only the F-statistics of datasets with at least one

neuron associated to the grid point, then dividing by the number of datasets involved. This method is also interesting in the way that the absence of data is not penalised with a lower averaged F-statistic.

The problem with the first method, is that a highly responsive grid point might in fact not be that responsive, and "beat" more interesting grid points. For instance, say we have 10 datasets, and two different grid points. A first grid point has the following associated F-satistics: $(5, 5, 5, 5, 5, 5, 5, 5, 5, 5)$. A second grid point has $(15, \_, \_, 15, \_, \_, \_, \_, 15, \_)$, where "_" indicates the absence of neurons in the grid point voxel for that dataset. Using the first method, average F-statistics for grid points 1 and 2 are respectively 5 and 4.5, even if grid point 2 looks more promising. Second method solves this problem, with average F-statistics of 5 and 15. Second averaging method is not perfect though: we might detect an outlier at some point for a particular fish. I performed both analysis, so both methods are for the reader to compare. Nevertheless, it is good to keep in mind that the way I averaged the signals to have the grid point averaged response in figures II.9, II.10 and II.11 corresponds to second method. Simply put, the averaged signal is the mean of existing responses. Results for first averaging methods can be found in annex VIII.2.

Now that I had picked an averaging method, I had an F-statistic average for each modality, and could therefore try and find multisensory regions.

c) Multimodal areas in the brain

I started by visualizing F-statistic isovalues in figure II.9. Clear clusters emerged from these most responsive brain areas.

I then plotted the 2.5% most responsive grid points from the averaged datasets, in figure II.10, with a more detailed plan by plan plot in figure II.11. Some of the clusters did overlap, in specific regions of the brain. The three main clusters were:

- One anterior to the oculo-motor neurons,
- One in the cerebellum,
- One in the dorsal hindbrain, which is a potential motor-neurons area.

When picking individual multimodal grid points, I could display the average response for each neuron associated to this grid point, and check this response was correlated to the

stimulus.

This analysis allowed to identify three locations in the brain where neurons from different experiments responded to the stimulations, making them multimodal regions.

II.3 Discussion

In this chapter, we were able to look into the data, and determine an interesting metric, the F-statistic, to analyze the neurons' signals, and link them to the stimuli. Next step was to compare all the fish and stimuli through a visual interface, to try later to identify a potential multimodal region in the brain.

We coded a program that facilitated data browsing. Through the use of the F-statistic metric, displaying most responsive areas in the brain to a stimulus was possible, along with finding the regions associated to these areas. It was even possible to visualize the ΔF/Fs associated to a picked grid point.

Given 38 datasets, and 5 modalities, we were able to look inside the brain of the larval zebrafish, and identify regions where neurons responding to several modalities intermingled. These regions were located anteriorly to the oculo-motor regions, in the cerebellum, and in the dorsal hindbrain.

Although we could infer these regions include multisensory neurons, we could not know for sure, as our data was scattered across several fish. As a matter of fact, if we compare two experiments, they were performed on two different fish. A common response area provides an indication on the region being multimodal, but we do not know for sure this region's neurons would have been responsive to both modalities in the same fish. An easy fix to this limitation would be to do multisensory experiments on fish, and record their neuronal activity. This way, we would be able to actually see the individual neurons firing in response to both stimuli. This is the work presented in the next chapter of this thesis.

The strength of this work is the high number of datasets, and the wide range of modalities studied. The visualizing tool makes it convenient to navigate the data, and one can easily download it to include their own data. This makes comparison with new data quick and effective. We took a voxel size of $5\mu m$, but it is very easy to increase this value

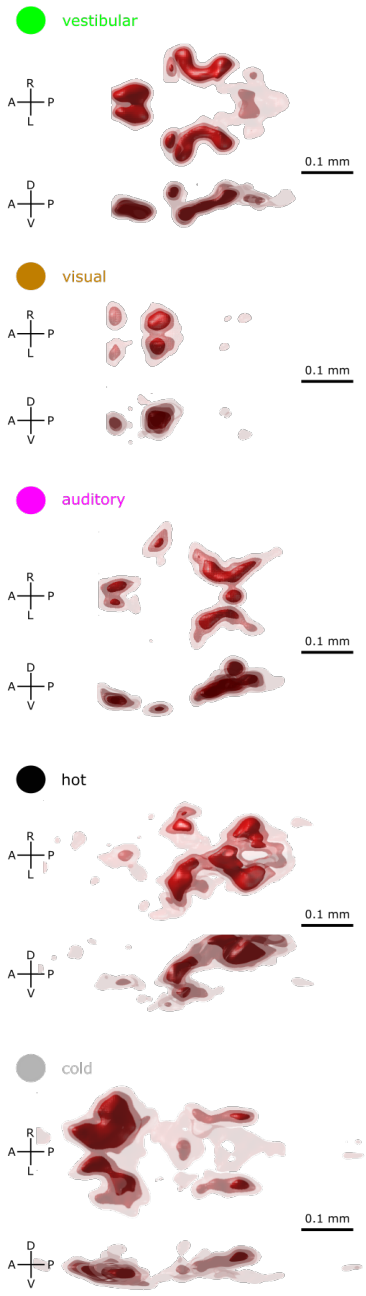

Figure II.9: F-statistic isovalues. Scarlet red corresponds to top 2.5% F-statistic, intermediary red to 5% and light red to 10%.

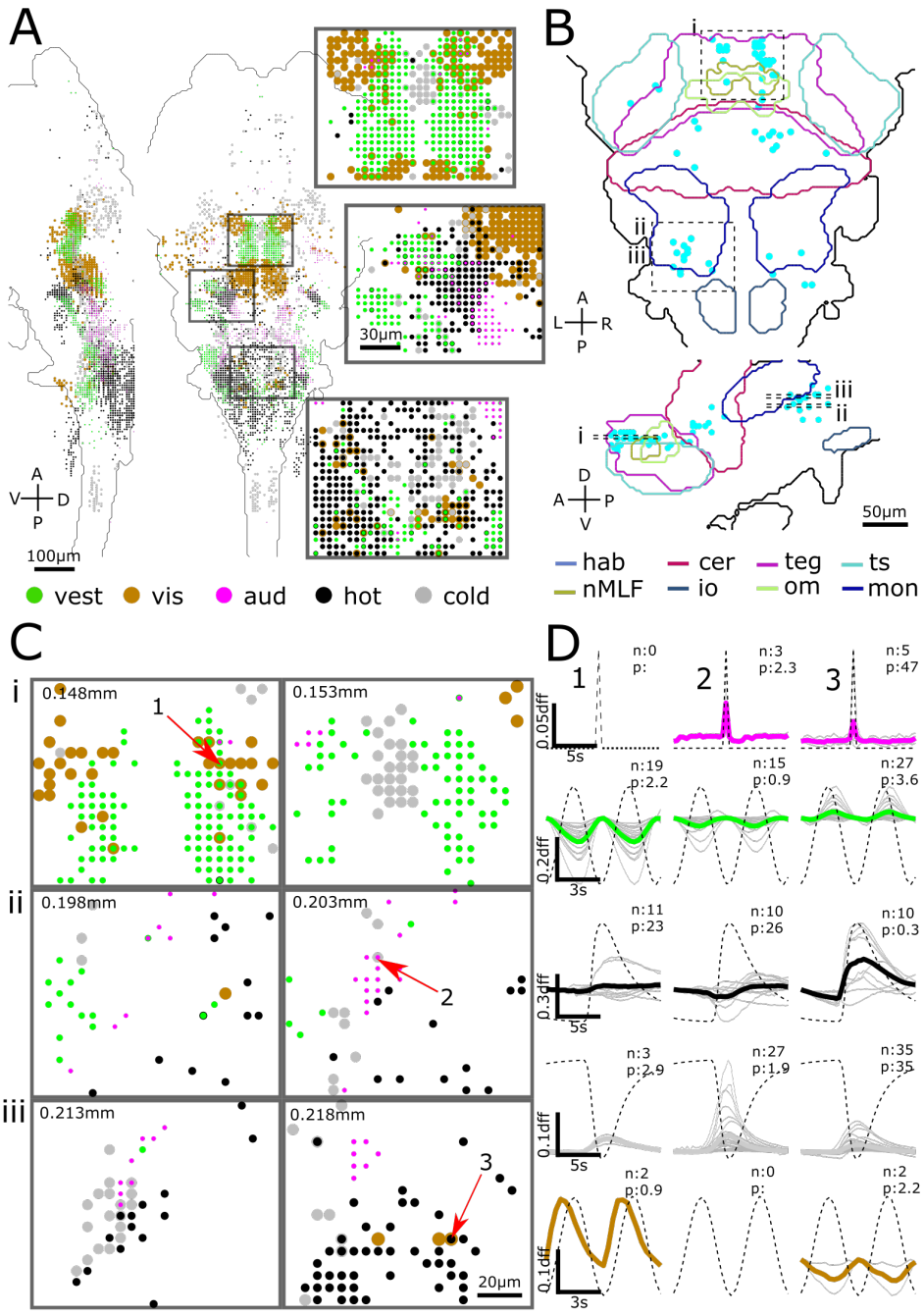

Figure II.10: Representation of the 2.5% most responsive grid points, based on the average of the F-statistic per grid point over all recorded animals. **A**: Projection of most responsive grid points in midsagittal plane and frontal plane with details on the right. **B**: Grid points responding to more than one modality in light blue, projections on frontal and midsagittal planes. Important brain areas contours are specified (hab: habenula, cer: cerebellum, teg: tegmentum, ts: torus semicircularis, nMLF: nucleus of the medial longitudinal fasciculus, io: inferior olive, om: oculomotor nucleus, mon: medial octavolateral nucleus). **C**: Details for specific planes. **D**: Averaged answer to stimuli for neurons associated to grid points selected in **C**. n is the total number of neurons whose signals were averaged and p is the percentage of grid points with a higher F-statistic.

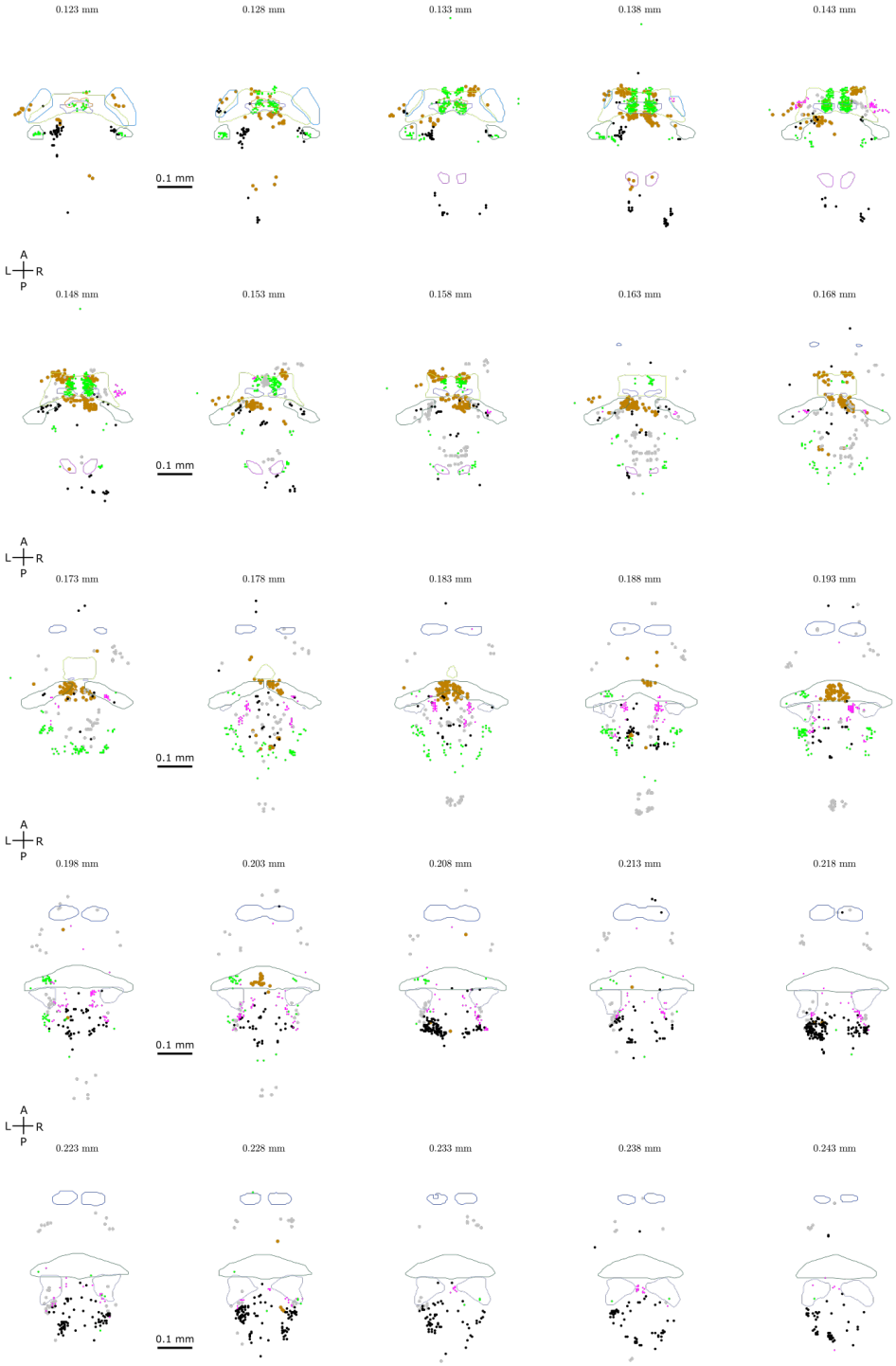

Figure II.11: Detail of each frontal plan for 2.5% most responsive grid points, for each modality. Vestibular is in green, visual in brown, auditory in purple, hot in black, and cold in grey.

in order to look for wider areas in the brain, with a reference size bigger than a neuron's radius.

III – Integration of multisensory information

III.1 Introduction

Multisensory integration is thought to be important for animals and human beings to survive. The sensory information is integrated in the brain in order to form a robust perception of the environment. It is this perception that allows us to interact with that environment in the best way possible. A good example of how multisensory integration works is trying to understand someone speaking with their hand or a mask over their mouth: it is not as effective as when we see the lips and combine this visual information with the auditory information. Understanding how this information is processed and combined in the brain leads to a better understanding of how animals and humans respond to the many stimuli from the world around them.

Multisensory integration in the brain has been thouroughly investigated. It is believed nowadays that most of the brain processes multisensory information, and that unisensory areas of the brain are more the exception than the standard [165]. Some regions of the brain are highly multisensorial, such as the superior colliculus / tectum [184], the cerbellum [222], motor related areas [159], as well as the parietal, frontal [160], and prefrontal cortex [20]. Multimodal neurons have been widely identified because of a particularity they can have: super-additivity [183]. We speak of super-additivity when the number of spikes a neuron generates in response to a multimodal stimulus is higher than the sum of the spikes it generates in response to each unimodal stimulation alone.

In larval zebrafish, our animal model, research shows that deep layers of the tectum can integrate multisensory inputs, along with being responsible for motor commands [61]. Granule cells of the cerebellum have also been identified to be a multimodal part of the brain, responding to flashes of light, moving gratings, and electric shocks [158].

The study of vestibular-visual integration provides an interesting model system to study multisensory integration in larval zebrafish. Both sensory pathways are well developed at the larval stage where whole-brain functional imaging is possible. Eyes motions can be monitored conveniently by video tracking because of the large eyes. Both sensory systems are direction sensitive and evoke directed behavioural eye responses that are not discrete but continuous.

Vestibular-visual integration is central to self-motion estimation. When a fish is naturally roll-tilted in space in a clockwise direction along its rostro-caudal body axis, e.g. due to turbulent water flow, its visual environment moves counter-clockwise relative to the fish. The vestibular and the visual system both provide a separate stream of sensory information to the brain signaling amplitude and direction of the body's roll-tilt: (i) The vestibular system in the inner ear detects the gravitational acceleration and reports the angular change in orientation relative to the gravitational field. (ii) The visual system detects the motion of the entire visual environment relative to the fish. The fish can estimate that only self-motion must have caused the observed visual flow based on the prior that its visible environment is static in space. Both the vestibular and the visual sensory streams of information are integrated in the brain to drive eyes movements to stabilize gaze in space, and to execute tail movements to stabilize posture against the external perturbation.

To our knowledge, no previous work has been done on combining vestibular and visual stimuli while doing whole-brain imaging in larval zebrafish.

The visual system of the zebrafish has been investigated in detail [149] [156] [80], leading to the identification of precise brain areas involved in the process of the visual information. Similarly, the vestibular system has been studied using a rotating light-sheet microscope [45], which has also uncovered brain regions associated to inner ear stimulation.

Our study focuses on the combination of these stimulations. How does the fish respond to the two stimuli presented together? Can we expect to find multisensory neurons, i.e. neurons activated by both vestibular and visual stimuli? Where would these neurons be, and how would they integrate this information? Those are the questions we aim to answer here.

In order to study multisensory integration, we presented the fish with a range of combinations between rostro-caudal rotations (vestibular pattern), and horizontally moving stripes (visual pattern).

We began the study analyzing the behaviour of the fish by looking at its eyes. Our results show that a conflicting combination leads to a vestibular capture, i.e. a behaviour similar to a unisensory vestibular stimulation. When presented to a coherent stimulation though, the response is higher than the sum of the responses to both unisensory modalities,

showing a super-additivity phenomenon.

We then looked into the brain of paralyzed animals using light-sheet imaging, presented with the same stimulations. We found that the number of multisensory neurons and their locations is stereotypical across a wide panel of fish.

Finally, we fitted different models to describe the activity of these neurons. A linear model, adding the responses of the two unisensory stimuli is sufficient to accurately describe the multisensory activity. We used this model to identify super-additive neurons that could be responsible for the behaviour we observed.

III.2 Methods

III.2.1 The experimental setup and sample preparation

Under natural conditions, vestibular and visual information are correlated, and if well calibrated the perception of self-motion along the two pathways is coherent. However, under experimental conditions, both sensations can be disentangled to create conflicting conditions of different degrees that are useful to probe the system's response to various multisensory scenarios. To decorrelate vestibular and visual input, we mounted a fish in a sample chamber of a rotating microsocope filled with embryonic medium E3. The fish was hold by its trunk in a gel of agarose. For the behavioural experiments, agarose was removed around the eyes to allow for free movement. Rotating the microscope roll-tilted the fish around its rostro-caudal axis and thus stimulated the vestibular system. Evoked eye movements were recorded with a camera. A curved screen was mounted on the microscope beneath the fish. On the screen we projected moving red gratings with a video projector, to fully control the visual environment and to decorrelate it movement from the vestibular stimulation. In addition, the microscope was equipped with a light-sheet forming unit and a fluorescence detection unit to perform brain-wide functional calcium imaging of evoked neural activity. Figure III.1 describes the setup. Ideally, the screen should have covered 360° of the fish's visual field. Here we only covered the lower hemisphere to maintain access to the fish's brain from above for the neuronal recordings.

We studied the multisensory responses at the behavioural and neuronal level in transgenic Tg(elavl3:H2B-GCaMP6f) [**?**] zebrafish larvae of age between 5–8 days post fertilization (dpf) carrying the nacre mutation making them more transparent. For the neural

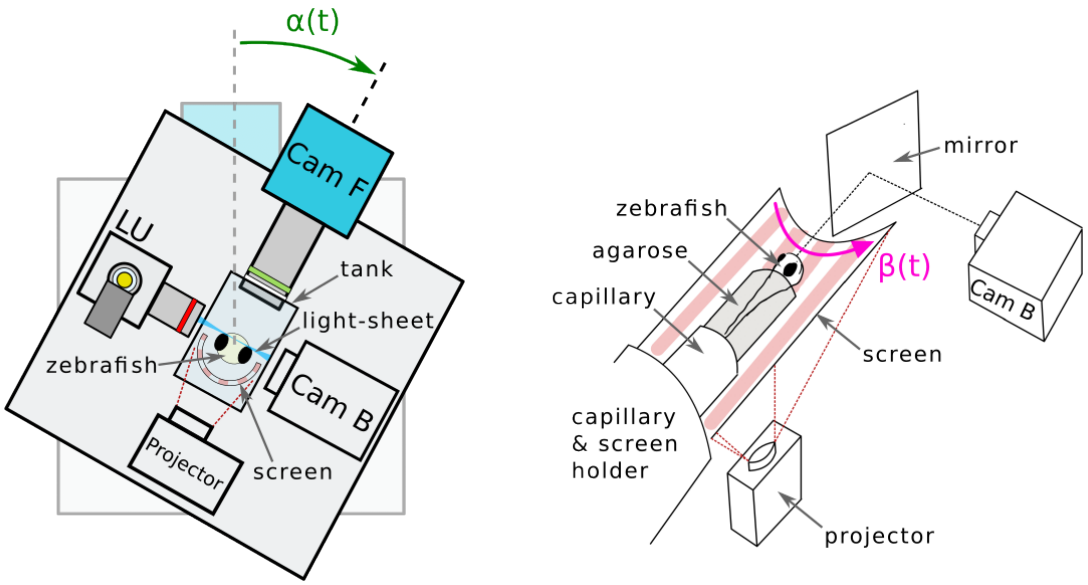

Figure III.1: Experimental setup description. Left panel shows light-sheet imaging along with vestibular stimulation setup. Right panel shows visual stimulation setup. LU: light-sheet unit, Cam F: camera for fluorescence detection, Cam B: camera for behaviour recording.

experiments, the fish were paralyzed before being mounted in agarose by bathing them for 2–5 min in a solution of 1 mg/mL α-bungarotoxin (Thermofisher Scientific) in E3 medium. We then transferred them into pure E3 medium and waited for ≈30 min to insure absence of motor activity and normal heart beating. We paralyzed the fish to prevented movement artifacts in the neuronal recordings due to eye movements and to simplify the interpretation of the experiments. The retina is stimulated by movements of the visual environment relative to the eye. We controlled in our open-loop experiments only the movement of the visual environment relative to the fish, which however equals the movement relative to the eyes when fish are paralyzed and eyes do not move.

The light-sheet laser power was set so that the behaviour elicited with laser was similar to the behaviour without laser. Annex VIII.3 presents the observed behaviours under different laser powers.

III.2.2 The experimental stimulation protocol

The angular motion of the fish body relative to its dorsal-up posture was denoted $\alpha_{vest}(t)$ and counted as positive in the clockwise direction. The angular movement of the visual

pattern on the screen was denoted $\beta_{vis}(t)$ and counted as positive in the same direction. With this system we created four different sensory scenarios defined by the congruence, c, of the visual information about self-motion relative to the vestibular one, $c = -\beta_{vis}/\alpha_{vest}$ (see figure III.2).

1. **Coherence, c = 1:** When the fish was roll-tilted clockwise, the visual pattern moved counter-clockwise on the screen with equal absolute amplitude $\beta vis = -\alpha_{vest}$. This configuration restored the natural sensory condition in which the visual information about body roll-tilt was congruent with the vestibular information.

2. **Conflict, c = 0:** A static image was projected on the screen (so $\beta_{vis} = 0$), which rotated with the fish so that the visual environment did not move relative to it. This is known in the literature as a head-attached object and was designed to create a conflict in the self-motion perception along the two sensory pathways, with a vestibular perception of motion versus a visual perception of no motion.

3. **Opposition, c = -1:** Both the roll-tilt motion of the fish and the motion of the visual pattern on the screen moved in the same direction and with equal absolute amplitudes, $\beta_{vis} = \alpha_{vest}$. The visual and the vestibular system signalled self-motion with equal absolute amplitudes but in opposite directions.

4. **Enhancement, c = 2:** When the fish was roll-tilted clockwise, the visual pattern moved counter-clockwise on the screen with twice the absolute amplitude $\beta_{vis} = -2 \cdot \alpha_{vest}$. The visual information signaled self-motion in the same direction as the vestibular system, but at twice the amplitude.

A positive congruence means that the visual stimulus signals self-motion in the same direction as the vestibular stimulus and a negative congruence means that the visual stimulus signals self-motion in the opposite direction.

Each fish was presented with unisensory stimuli, and with a set of multisensory stimuli defined by different congruence levels. The unisensory vestibular stimulus was created by replacing the projected grating with a homogeneous grey image of the same total luminance as the grating. In all sensory scenarios, the vestibular and visual stimuli were driven sinusoidally at a frequency of $f_{stim} = 0.2$Hz for 30s corresponding to 6 stimulation periods. The relative phase shift between the two stimuli in the multisensory periods was

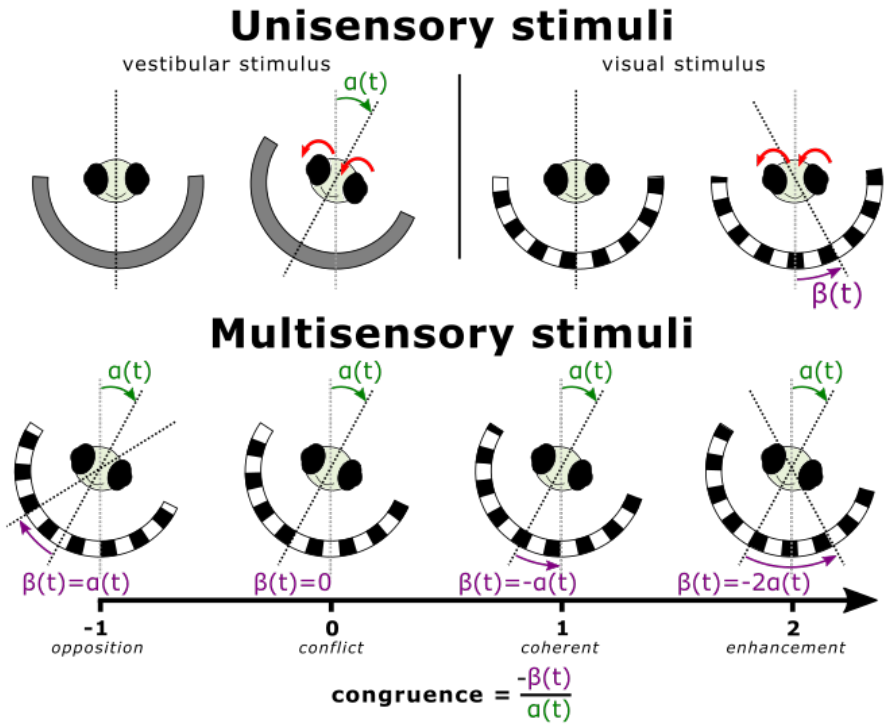

Figure III.2: The experimental protocol. Top: Schematics of the different uni- and multisensory stimulations applied to the fish. The vestibulo-ocular reflex is elicited when the fish is physically roll-tilted in space, while the opto-kinetic reflex is elicited by a moving grating with a video projector on on a screen fixed in the referential of fish. Roll-tilting the fish and showing him at the same time a moving grating created a multisensory stimulation scenario characterized by its congruence value, which we defined as minus the ratio between the visual and the vestibular stimulation amplitudes.

set to zero. Only the sign and absolute value of the amplitudes of the two sinusoidal waveforms were varied to create the congruence levels.

For the behavioural experiments, the sequence of sensory scenarios was (see figure III.3): vestibular at 30 and 15°, visual at -15, -30, and -60°, again a vestibular stimulation scenario at 30°, followed by multisensory scenarios at visual congruences of -1, 0, 1, 2 at 30° vestibular stimulation, again a unisensory vestibular stimulation of 15°, followed by multisensory scenarios at visual congruences of -1, 0, 1, 2 at 15° vestibular stimulation. In all multisensory scenarios the vestibular stimulus was always combined with the corresponding visual stimulation amplitudes to create the congruence levels. Between every sensory scenario we paused the stimulation for 10s. The total length of the protocol was 600s.

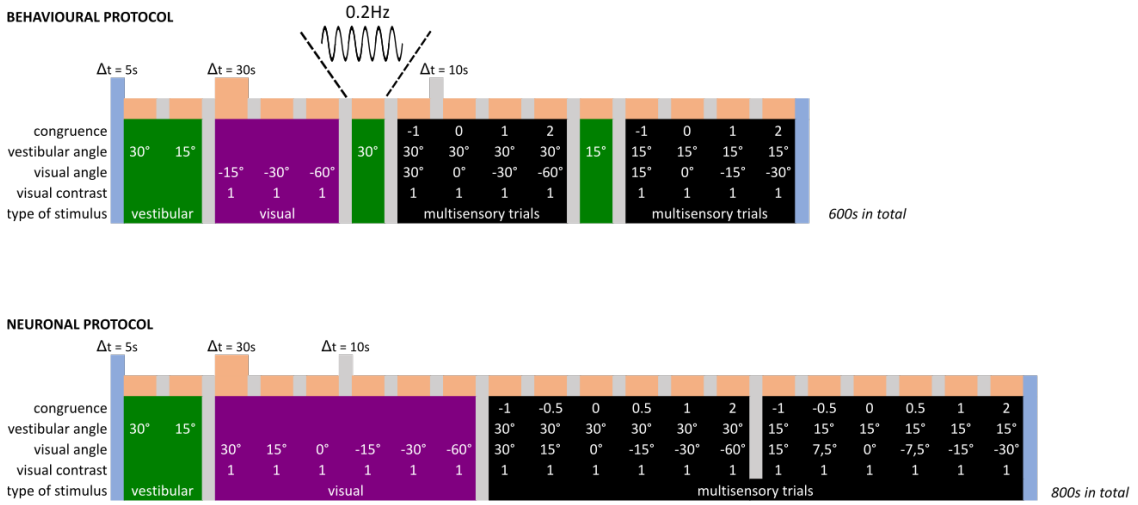

Figure III.3: Description of the experimental protocols for behavioural and neuronal experiments, showing the applied sequences of sensory scenarios for the behavioural and the neural recordings. Gray and blue parts indicate time intervals where the stimulation was paused.

For the imaging experiments, the sequence of sensory scenarios was (see figure III.3): vestibular at 30 and 15°, visual at 30, 15, 0, -15, -30, and -60°, multisensory at visual congruence of -1, -0.5, 0, 0.5, 1, 2 at 30° and then at 15° vestibular stimulation with the corresponding visual stimulation amplitudes. Between every sensory scenario we paused the stimulation for 10s but continued to image the brain with the light-sheet microscope. The total length of the protocol was 800s.

III.2.3 Data analysis

For the behavioural investigations, eye movements were video tracked at a rate of 25Hz. The recorded images were averaged offline by calculating the median over the stimulation cycles. We determined the eye angle in the averaged images by placing four landmarks on the eye from which we formed two intersecting segments. Using the segments orientation, we determined the angular change of the eyes rotation between the maximum and minimum of the stimulation cycle. The angular change of the eye was defined as the average of the measurements obtained with the two segments, for the two eyes (figure III.4).

For the neuronal analysis, we automatically identified all neurons in the recorded fluorescence images (for details on my developed algorithm see the annex VIII.4). For every

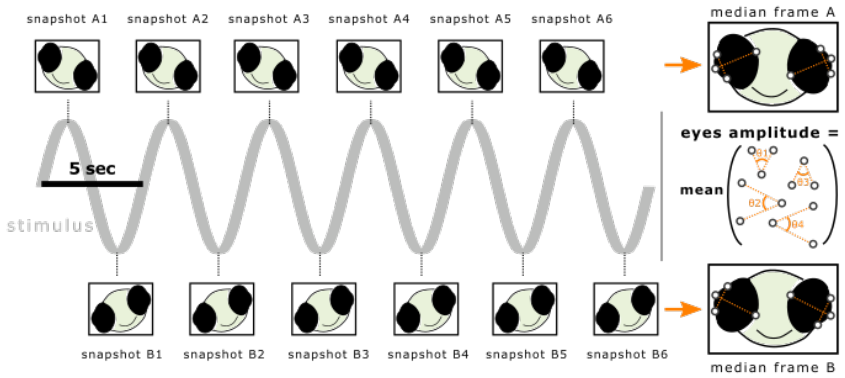

Figure III.4: For different unisensory, and multisensory stimulations, we recorded for 30 seconds. Stimulations were sinusoidal, with a 5 seconds period. Snapshots were taken on sine extrema and averaged. Eye tracking was done manually, placing 8 markers on the eyes, at specific pupil locations. We built 4 segments with these 8 markers. The segments angle average between two extrema was the eyes amplitude.

detected neuron, we estimated the relative variations of the fluorescence intensity, $\Delta F/F$, with respect to the baseline signal as $\Delta F/F$ = (F(t) - baseline)/(baseline - background). The background was estimated from the average intensity of pixels outside the brain and the baseline fluorescence signal was estimated for each neuron by a running 10 th percentile estimation of the fluorescence time signal in a sliding window of 50 s.

For further analysis, we either calculated, per neuron, the normalized Fourier amplitude, NFA, of the response, R, at the stimulation frequency of 0.2 Hz as NFA = $\tilde{R}(f_s) - \tilde{n}(f_s)/\tilde{n}(f_s)$. The noise was estimated at the stimulation frequency, $\tilde{n}(f_s)$, as the mean amplitude over a frequency window encompassing 20 points to the left and right of the peak, with windows starting three points from the peak. The NFA can be related to the signal-to-noise ratio commonly used in signal processing, $\text{SNR} = \text{R}(f_s)^2 / \sum_{i,i\neq 0,i\neq idx_{fs}} \tilde{n}_i^2 = a \cdot \text{NFA}^2$, with $a = 0.022$ in our case, where the value of a depends on the number of samples (see annex VIII.5 for more details).

We also calculated for every sensory scenario the trail average response over the six stimulation cycles. By linear regression, we quantified then how well the multisensory responses could be predicted by different linear and non-linear combinations of these average responses.

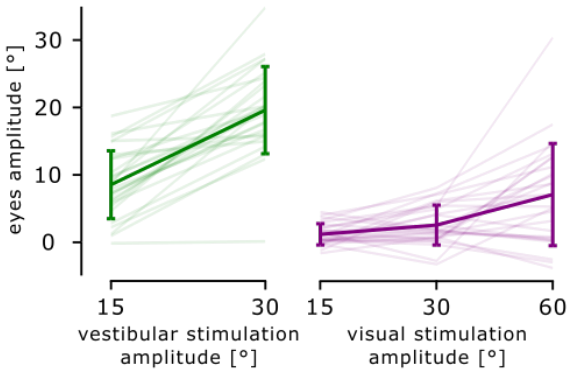

Figure III.5: Eyes amplitude to 15° and 30° vestibular stimulation on the left, to 15°, 30° and 60° visual stimulation on the right (n = 27).

III.3 Results

III.3.1 Behavioural responses under multisensory stimulations

The unimodal vestibular roll-tilt stimuli of 15° and 30° in amplitude evoked compensatory eye movements of on average 8.70± 0.95° and 19.5 ± 1.21° (mean ± SEM, N = 27) respectively (figure III.5). The response thus increased quasi-linearly with the stimulus and counteracted the body roll. A linear regression to the data defined a gain of the VOR response of 0.63 ± 0.06 which was smaller than one.

Unimodal visual stimulation of 15° elicited only very weak eye movements of 1.14± 0.32° (mean ± SEM, N = 27) along the roll axis via the rotational OKR. For larger stimulus amplitudes of 30° and 60° the behavioural response increased to 2.52± 0.57° and 7.2± 7.8° respectively (figure III.5). A linear regression of the data points gave an average response gain of 0.11 ± 0.01. This low rotational OKR gain was surprising to us, especially when compared to published OKR responses in the yaw axis, where high response gains have been observed. We hypothesised that projecting the moving visual environment onto a cylinder completely surrounding the fish, rather than onto the lower half of the cylinder, might enhance the response. However, this was not the case (data not shown). We concluded that a rotational OKR is functional along the roll-tilt axis in larval zebrafish, but only with a weak response gain. The visual response might be suppressed by the vestibular system that does not signal motion under this condition.

Next, we analyzed the eyes responses to the combined vestibular-visual stimulation

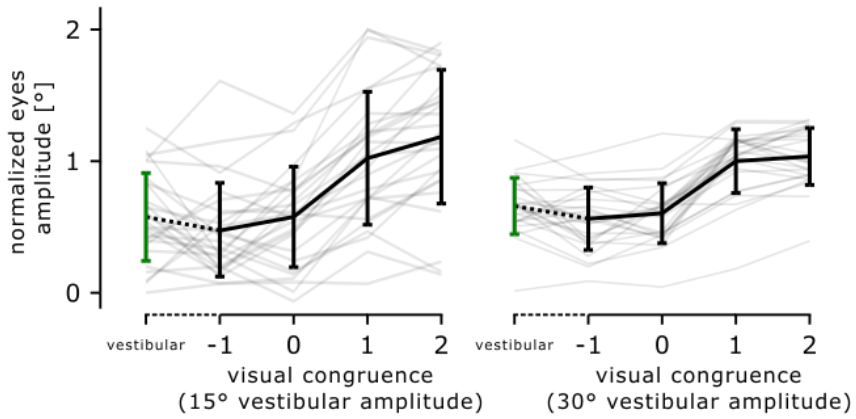

Figure III.6: Comparison between eyes amplitude (normalized by vestibular stimulation angle) for different multisensory congruences. Vestibular response is displayed for comparison. We compared vestibular response to coherent response (congruence = 1), using a t-test. For 15°, p-value = 7.89E-07, for 30°, p-value = 2.32E-10 (n = 27).

scenarios for the congruence levels (-1,0,1,2). We normalized all eye responses by the amplitude of the vestibular component of the stimulus, which describes the induced body roll-tilt. We made this choice to investigate how well the fish can estimate its body roll angle using vestibular and visual information, where we use the eye response as read out of this estimate. The results are shown in figure III.6. For a congruence level of 1 (coherent sensory information), we found that the normalized multimodal response had a value of 1.02 ± 0.50 (1.00 ± 0.24) at a body roll-tilt of 15° (30°), which was significantly different from the unimodal vestibular response at this stimulation amplitude (p = 7.89E-07 (p = 2.32E-10)), and also significantly larger compared to the sum of the visual and vestibular unimodal responses (p = 2.56E-05 (p = 2.80E-07))(figure III.7). For the congruence level 2 (enhancement) the normalized response was further increased. For a congruence levels of -1 and 0 (opposition or conflict), we found that the normalized multimodal response was only slightly reduced compared to the vestibular-only reference.

In summary, the unimodal vestibular response was much stronger compared to the very weak visual response but still had a gain less then one. Neither one could alone drive compensatory eye movements large enough to compensate body rotations and thus to stabilize gaze in space. Under multisensory conditions, visual and vestibular responses were non-linearly integrated with a strong effect when the sensory channels provided a coherent sensation of the body roll. In this condition, they synergistically worked together

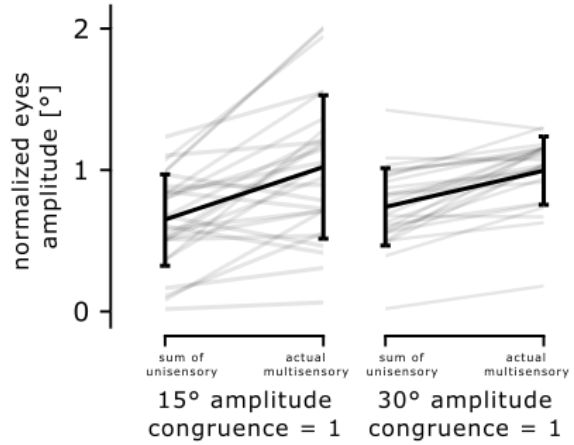

Figure III.7: Normalized eyes amplitude comparison between sum of unisensory responses and actual multisensory response for congruence = 1. We compare those using a t-test. For 15°, p-value = 2.56E-05, for 30°, p-value = 2.80E-07 (n = 27). Multisensory response is super-additive.

to reach a normalized response gain of average value 1, required for good gaze stabilization. The visual stimulus had thus a strong impact and the multimodal response was a super-additive combination of the unimodal responses. In contrast, when the visual information signaled a conflicting body rotation direction, it was almost ignored and the vestibular response dominated.

III.3.2 Neuronal response to multisensory stimuli

We submitted N=16 paralyzed fish to the sequence of sensory scenarios described in III.3, and recorded simultaneously the evoked neural brain activity.

a) Identification of multisensory neurons via Fourier analysis

We are presenting here our analysis of the unimodal vestibular and visual sensory scenarios with 30° stimulation amplitude respectively. To estimate the response strength to the stimuli, we calculated for each neuron the normalized Fourier amplitude (NFA) at the stimulation frequency (see Methods III.2.3 and VIII.5 for details). Figure III.8 shows for a selected fish how the NFA values are distributed and correlated to each other.

We labeled neurons as vestibular (visual) responsive when their normalized Fourier amplitude was larger than a cutoff value that varied between 5.13 and 7.74, with an average of 6.32 (4.60 and 8.05, average: 6.02), depending on the fish, in response to the

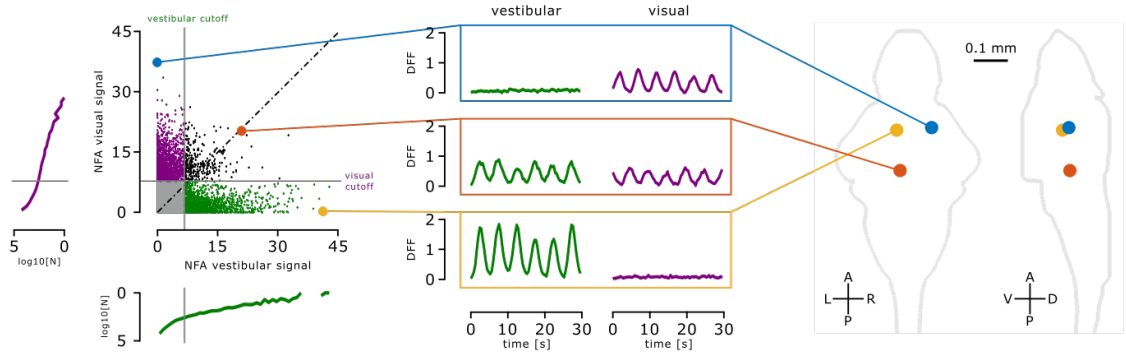

Figure III.8: Left panel: neurons NFA for vestibular and visual stimulati, for one fish. Distribution of neurons is also provided, on a logarithmic scale, with cutoff values. In green are the vestibular neurons, in magenta are the visual neurons, and in black are the multisensory neurons for this fish. Blue, orange and yellow points are the best visual, multisensory and vestibular neurons respectively. Central panel: best neurons responses to vestibular and visual stimulations. Right panel: best neurons location in the brain.

vestibular (visual) stimulus. This threshold corresponded to a SNR of between 0.57 and 1.29, with an average of 0.86 (0.46 and 1.40, average: 0.78) and was defined as three times the standard deviation of a Gaussian fit to the distributions (see annex VIII.6 for a detailed plot on one fish). All other neurons where labeled as unresponsive to the stimuli. Neurons that where above threshold for both stimuli where labeled multisensory. The neural response and anatomical location of the neurons with the strongest responses in the three conditions are shown in figure III.8 for a selected fish.

We applied this analysis to all N=16 fish (figures III.9 and III.10). The distributions of the NFAs for the two stimuli were comparable across fish. We counted per fish in average 32077 ± 5364 neurons in total with 944 ± 474 vestibular neurons ($2.94\% \pm 1.41$), 1530 ± 398 visual neurons ($4.80\% \pm 1.03$), and 103 ± 92 multisensory neurons ($0.31\% \pm 0.26$). The identified neurons where stereotypically organized in the brain (figure III.11). From the 1648 multisensory neurons found across the 16 fish, 742 neurons where located in the rhombomere 1 (46.38%), 307 in the tegmentum (19.19%), 224 in the Gad1b cluster 2 (14.00%), 125 in the cerebellum (7.81%), 51 in the posterior pretectum (3.19%), 24 in the pallium (1.50%), 4 in the habenula (0.25%), 85 additional in the posterior hindbrain (except from rhombomere 1) between rhombomere 2 and 7 (1.06% and 4.25%), and 128 (7.75%) were found in cranial motor neuron nuclei.

The highest spatial density of multisensory neurons was found in the tectum and in

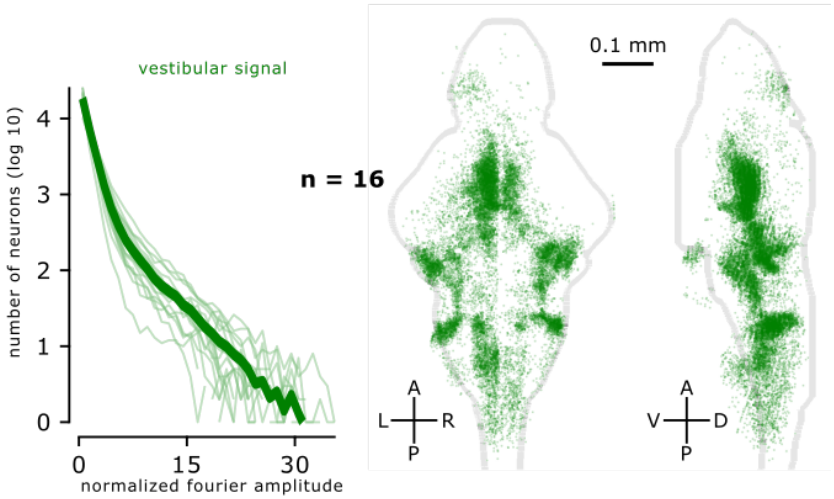

Figure III.9: Left panel: distribution of neurons for different NFA, for vestibular stimulation, with logarithmic scale, across 16 fish. Right panel: most responsive neurons for vestibular stimulation (944 ± 474, n = 16).

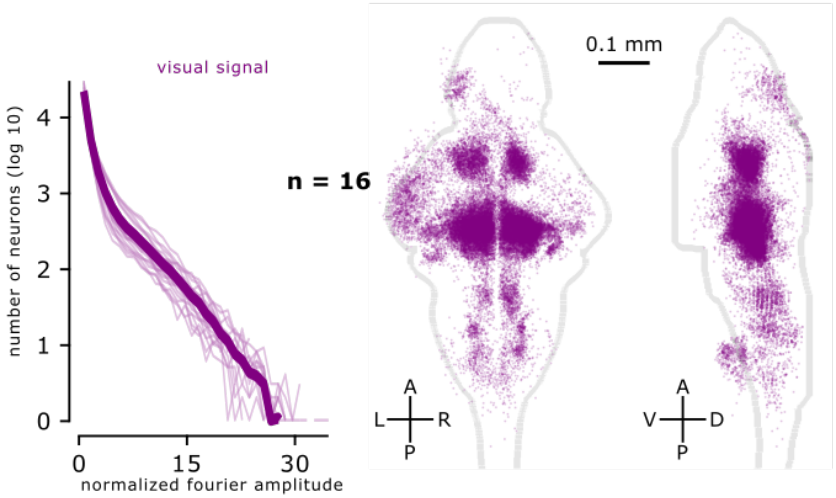

Figure III.10: Left panel: distribution of neurons for different NFA, for visual stimulation, with logarithmic scale, across 16 fish. Right panel: most responsive neurons for visual stimulation (1530 ± 398, n = 16).

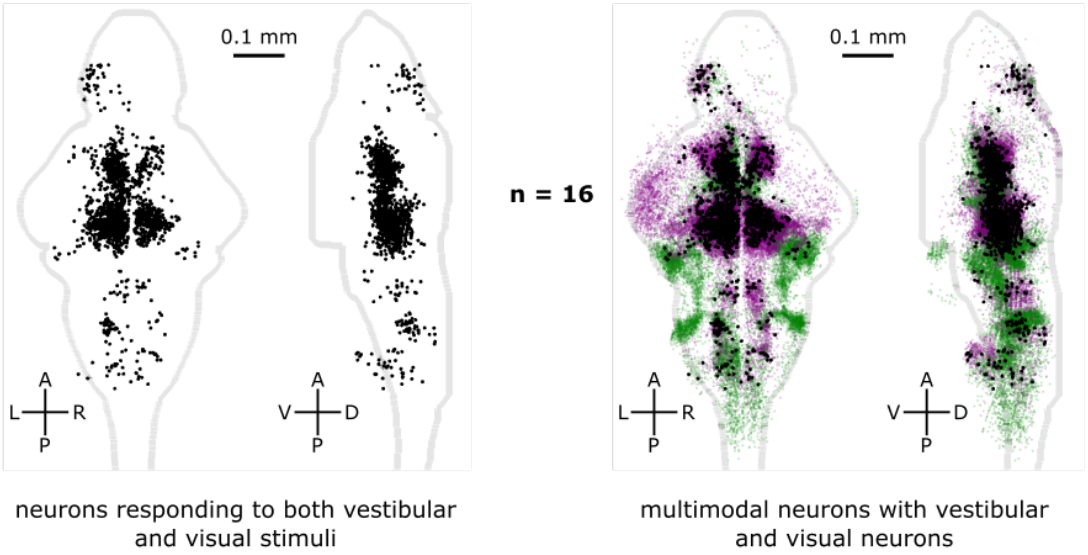

Figure III.11: Left panel: neurons most responsive to both vestibular and visual stimulations (103 ± 92, n = 16). Right panel: same neurons, overlapped with most responsive vestibular and visual neurons.

rhombomere 1 with a characteristic three dimensional organization of four clusters. We determined the 3D hull of this density distribution (figure III.12) by kernel density estimation (details in annex VIII.7) after duplication of every multisensory neuron location to the mirror symmetric location in the other brain hemisphere. We will refer to this region in the following as the multisensory region. Figure III.13 shows how this multisensory region overlaps with different brain regions defined in the ZBrain atlas of the larval zebrafish brain [105]. The amount of overlap of selected brain areas with this multisensory region are:

- 78.1%, 65.8%, and 100% for the nuclear medial longitudinal fascicle (nMLF), and the oculomotor nuclei nIII and nIV, respectively,
- 25.8% for the tegmentum, involved in gaze stabilization and postural control, among other functions,
- 7.5% for the cerebellum, responsible for motor control,
- 16.1% for the thalamus, which is a relay for sensory information,
- 17.2% for the pretectum, which is involved in visual processing,

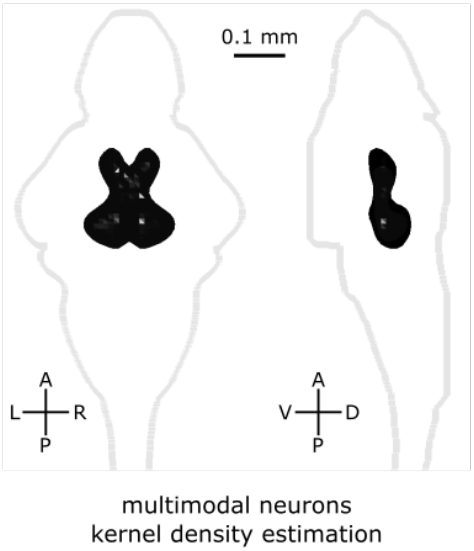

Figure III.12: Kernel density estimation of multisensory area, after multisensory neurons were mirrored around left/right plan.

- 23.0% for the superior part of the raphe nucleus, a major serotonergic center of the brain,
- 85.6% for three different gad1b inhibitory clusters,
- only less than 1% for the tectum stratum periventriculare, the zebrafish's homologous region to the superior colliculus, which is described as a highly multisensory brain region in higher vertebrates.

A more detailed plot, layer by layer is shown in the annex VIII.8.

Figure III.14 shows the projections of neurons that have their cell somata located in the multisensory region, given by Kunst *et al.* [223]. We observe projections to the hindbrain, projections to an area near the eyes, projections to the cerebellum, and finally projections to the contralateral multisensory area. Note that not all neurons in this region are multisensory, and we cannot claim that the drawn projections are from multisensory neurons.

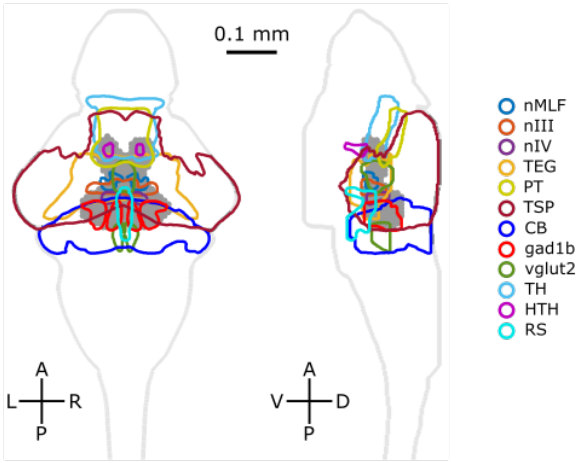

Figure III.13: Regions from ZBrain atlas overlapping with multisensory area (shaded grey). ZBrain atlas regions are from Randlett *et al.* [105]. nMLF: nucleus of the medial longitudinal fascicle, nIII: oculomotor nucleus, nIV: trochlear nucleus, TEG: tegmentum, PT: pretectum, TSP: tectum stratum periventriculare, CB: cerebellum, gad1b: gad1b inhibitory clusters, vglut2: vglut2 cluster 1, TH: thalamus, HTH: hypothalamus 6.7FRhcrtR-Gal4 cluster, RS: raphe superior.

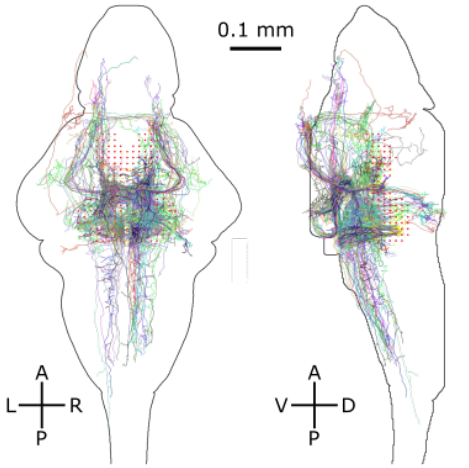

Figure III.14: Projection of neurons whose cell bodies are in multisensory area (dotted red). Projection data is from Kunst *et al.* [223]

b) Prediction of multisensory response with combination of unisensory responses

Here, we analyzed the data recorded during the entire sequence of sensory scenarios. Our aim was to test what linear or non-linear combination of the measured unimodal responses best predicted the neurons response during the multisensory scenarios.

For every multisensory scenario, we formed the vestibular ($\mathrm{DFF}_{vestibular}$) and visual ($\mathrm{DFF}_{visual}$) regressors from the responses to the unimodal stimulations that corresponded to the vestibular and visual stimuli used to create the corresponding congruence level; e.g., for the fit to the congruence level of 1 that was created with a base vestibular stimulus amplitude of 30°, we formed the vestibular regressor from the response to the vestibular stimulus of 30° in amplitude, and the visual regressor from the response to the visual stimulus of −30 in amplitude (see figure III.2). For each regressor, we then subtracted the mean and calculated the trial average (averaged over the six stimulus periods).

The six tested models are displayed in figure III.15.

The vestibular, the visual and the sum model had no adjustable parameter. These parameter-free models tested how well the unimodal vestibular or visual regressor, or the sum of both regressors, predicted the response during the multisensory scenarios, respectively. With the simple linear model, we introduced the first free fit parameter, **w**. This model assumed that the multisensory response was proportional to the sum of the unimodal visual and vestibular responses with **w** being the proportionality constant. The linear model calculated the weighted sum of the unisensory regressors and allowed the independent scaling of the two regressors. The non-linear model was an extension of the linear model with an additional non-linear therm that was proportional to the product of both responses.

Neurons included in the analysis where those identified in the previous analysis, which responded at least to one of the two unimodal sensory stimuli (30° in amplitude). This corresponded to a total of $\mathrm{N}_{total} = 2372 \pm 552$ neurons per fish across the 16 fish ($7.43\% \pm 1.40$ of all recorded neurons) (see figure III.16). Note that we did not restrict our analysis to the neurons in the multisensory region, which we identified in the previous section, because we also wanted to include neurons that were unimodal, e.g. vestibular neurons that did not respond to visual stimuli but that showed modulated responses in the multisensory scenarios (see Figure III.19 for an example).

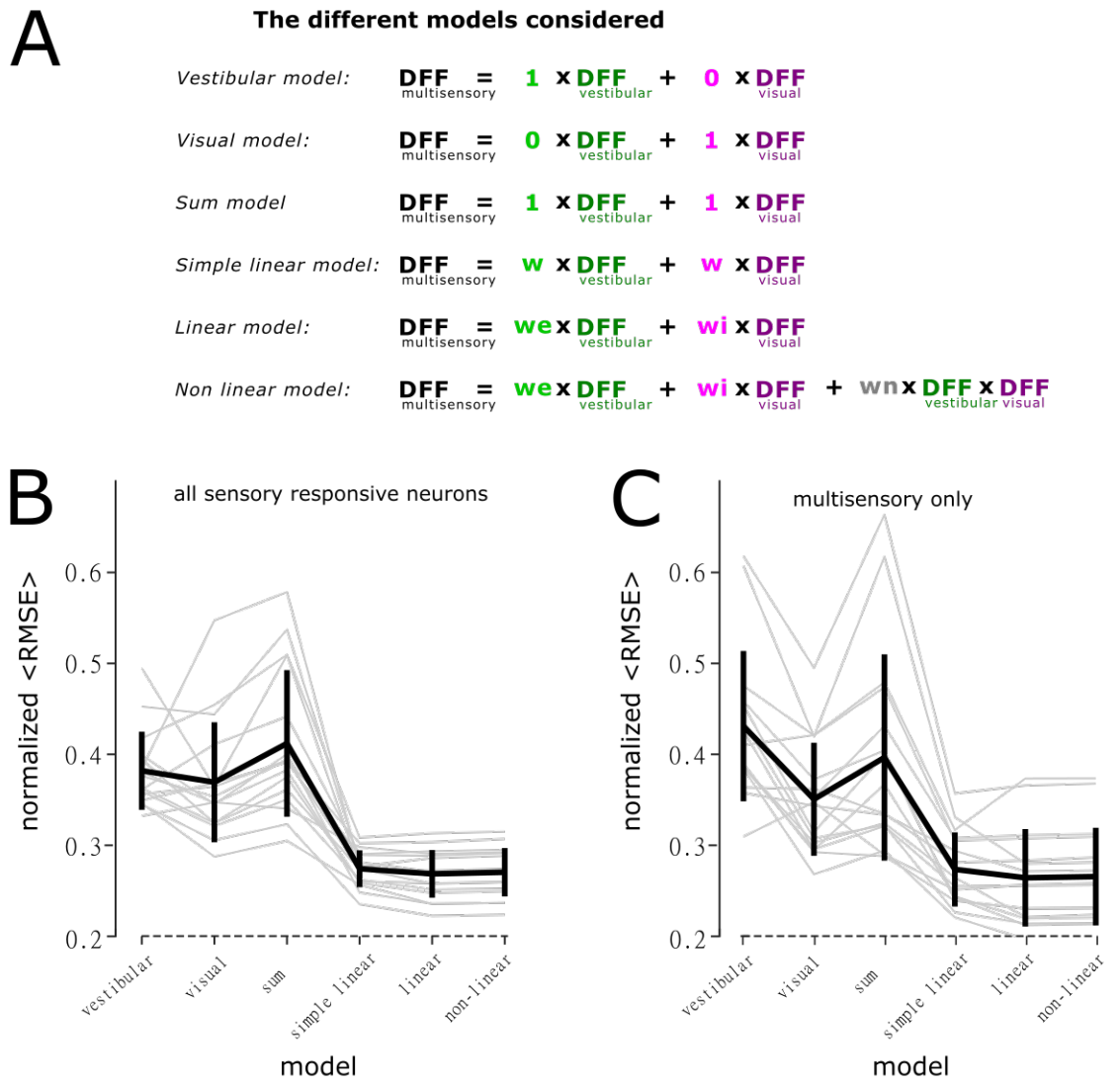

Figure III.15: **A**: The six models we considered for this analysis. Coefficients that are trained are w, we, wi, and wn. **B**: Average root mean square error after fitting the models for each fish to all neurons with a response to vestibular and/or visual stimuli. RMSE is computed for each multisensory modality for each neuron, and divided by the neuron's peak to peak $\Delta F/F$ amplitude. **C**: Same as B but here the model was fitted only on the multisensory neurons.

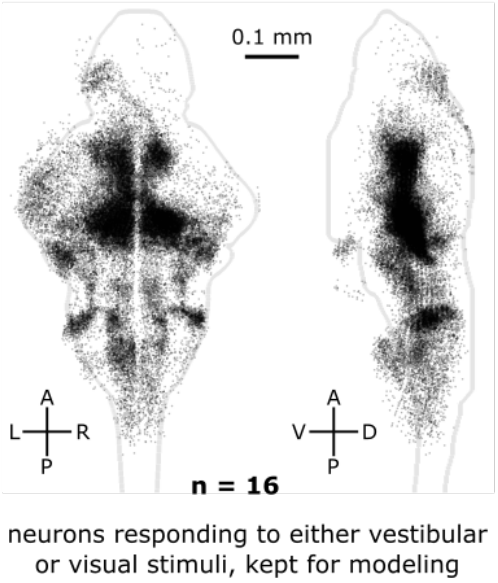

Figure III.16: Neurons responding to either vestibular or visual stimulus, kept for modeling.

We tested the prediction power of each model on the responses to the eight multisensory scenarios with the congruence levels -1, 0, 1, and 2. We used leave-one-out cross validation, which means that we performed a global fit for each model to the response of a neuron during seven multisensory scenarios, and then tested how well the model predicted the response to the one left out (test data). We calculated the root mean square error between the predicted and the actual response. We repeated this analysis for all possible eight permutations and averaged the resulting RMSE and saved this value as the parameter describing the prediction power of the fitted model for this neuron. We further averaged this RMSE over all neurons per fish and over all fish (see figure III.15).

After fitting the six models to our data, we obtained the following results. The overall mean RMSE was not significantly different when comparing the vestibular model (RMSE = 0.0512), the visual model (RMSE = 0.0462), and the sum model (RMSE = 0.0435). But, the simple linear model predicted the multisensory responses significantly better with an RMSE of 0.0332. The more complicated linear and non-linear models did not significantly improve prediction performance, with RMSE of 0.0322 and 0.0324 respectively. The RMSE increase between the last two models was due to cross validation.

The RMSE normalized by the value $max(\Delta F/F_{multisensory}) - min(\Delta F/F_{multisensory})$

was for each model 0.382, 0.369, 0.412, 0.274, 0.268, and 0.270, respectively.

We were surprised that the linear model did not predict significantly better the multisensory responses compared to the simple linear model. We next wondered whether this was because we included neurons that were not multisensory into the analysis. Interestingly, when restricting the analysis to the multisensory neurons that we detected in the previous section, the linear model still did not outperform the simple linear model (see figure III.15). Therefore, we only analyzed further the fit results from the simple linear model, which facilitated the analysis because we could concentrate on a single parameter.

Figure III.17 shows the distribution of the simple linear model coefficient $\mathbf{w}$, across all fish. The distribution was right-sided skewed with a maximum at about $\mathbf{w}$=0.6. For 65% of the neurons, $\mathbf{w}$ was between zero and 0.8, indicating that their multisensory response was less then the sum of the unisensory responses. We call them in the following sub-additive neurons. For 24% of neurons, the coefficient was $0.8 < \mathbf{w} < 1.2$. Their multisensory response was equal to the sum of the unisensory responses with a precision of ±20%. We call them additive neurons. And $10.30\% \pm 8.24$ of the neurons had a $\mathbf{w} > 1.2$, which means that their multisensory response was enhanced compared to the sum of the unisensory responses. We call them super-additive neurons. Only a small fraction (1%) of the neurons had a negative $\mathbf{w}$. Figure III.18 shows how these four classes of neurons are spatially distributed in the brain.

Figure III.19A displays example neurons with their neural activities and their anatomical locations in the brain for coefficient values $\mathbf{w} = [-1, 0, 0.55, 1, 6.75]$. Figure III.19B shows some additional example of specific response types:

1. First neuron is a vestibular neuron which does not appear to respond to visual stimuli, but whose multisensory response decreases as congruence increases.

2. Second neuron is a multisensory neuron whose multisensory response seems to depend far more on the visual than on the vestibular stimulus.

3. Third neuron is a multisensory neuron whose multisensory response seems to depend far more on the vestibular than on the visual stimulus.

4. Fourth neuron is a multisensory neuron whose multisensory response seems to depend on both modalities in an equal manner.

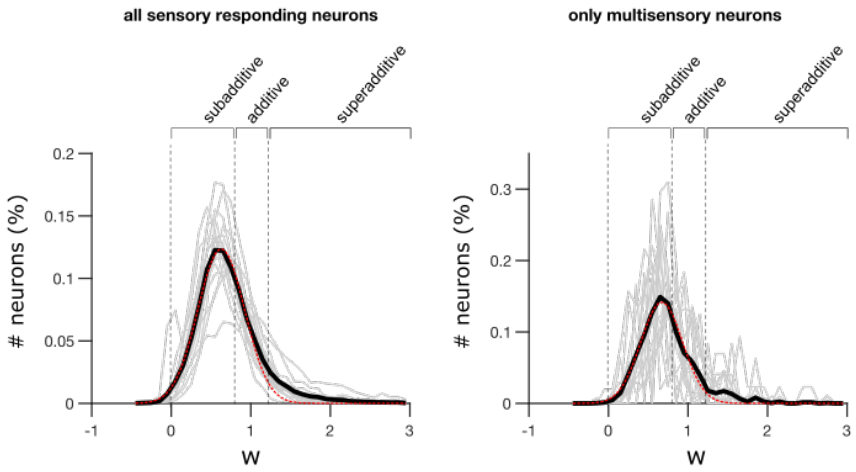

Figure III.17: Distribution of the simple linear model coefficient, **w**. The distributions for the individual fish are shown in gray, the average distribution over all neurons from the n=16 fish is shown in black, and a Gaussian fit to the central part of the distribution is shown in red. **A**: All sensory responding neurons were fitted, N = 37952 neurons. **B**: Only multisensory neurons were fitted, N = 1648 neurons.

5. Fifth neuron is a multisensory neuron, whose multisensory response appears to depend only on the visual stimulus.

In total we found 244 ± 174 super-additive neurons per fish that corresponded to $0.45\% \pm 0.29$ of all neurons in the brain. We were especially interested in these neurons because this super-additive response correlated with the observed super-additive behavioural response during the coherent multisensory scenario (c=1). Their spatial organization in the brain was sparse and dense. We determined the 3D hull of their density distribution (figure III.20). We used kernel density estimation (details in annex VIII.7) after we duplicated every neuron location to the mirror symmetric location in the other brain hemisphere. The identified region overlapped with several brain regions annotated in the ZBrain atlas (figure III.21). The regions we found are similar to those that overlapped with our identified multisensory region. The amount of overlap per brain region was:

- 84.4%, 64.5%, and 85.2% for the nuclear medial longitudinal fascicle (nMLF), and the oculomotor nuclei nIII and nIV, respectively,
- 23.0% for the tegmentum,
- 3.5% for the cerebellum,

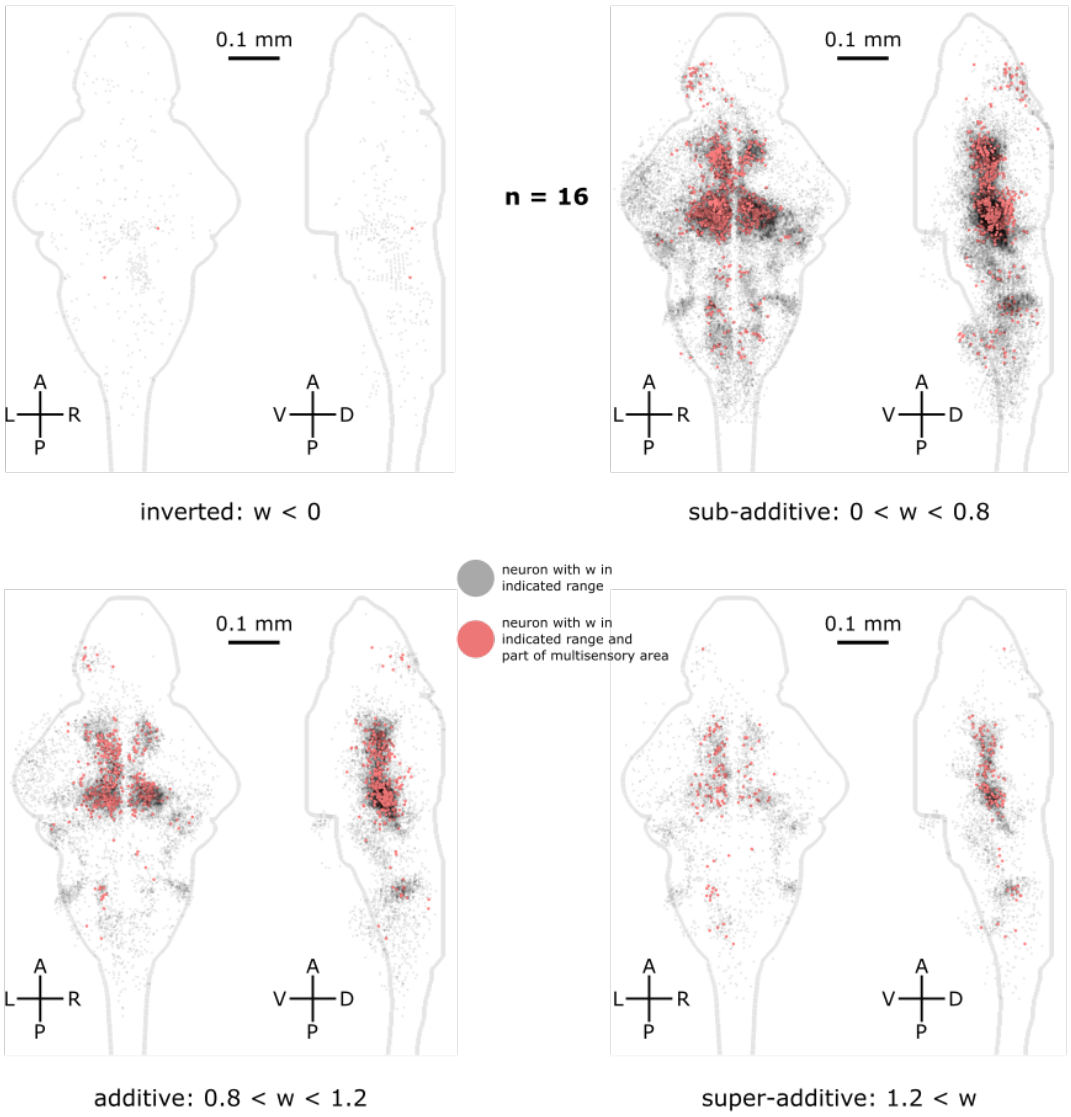

Figure III.18: Spatial distribution in the brain of the four classes of neurons we identified, based on their simple linear model coefficient, **w**. Neurons that are also part of the multisensory region identified earlier are showed in red.

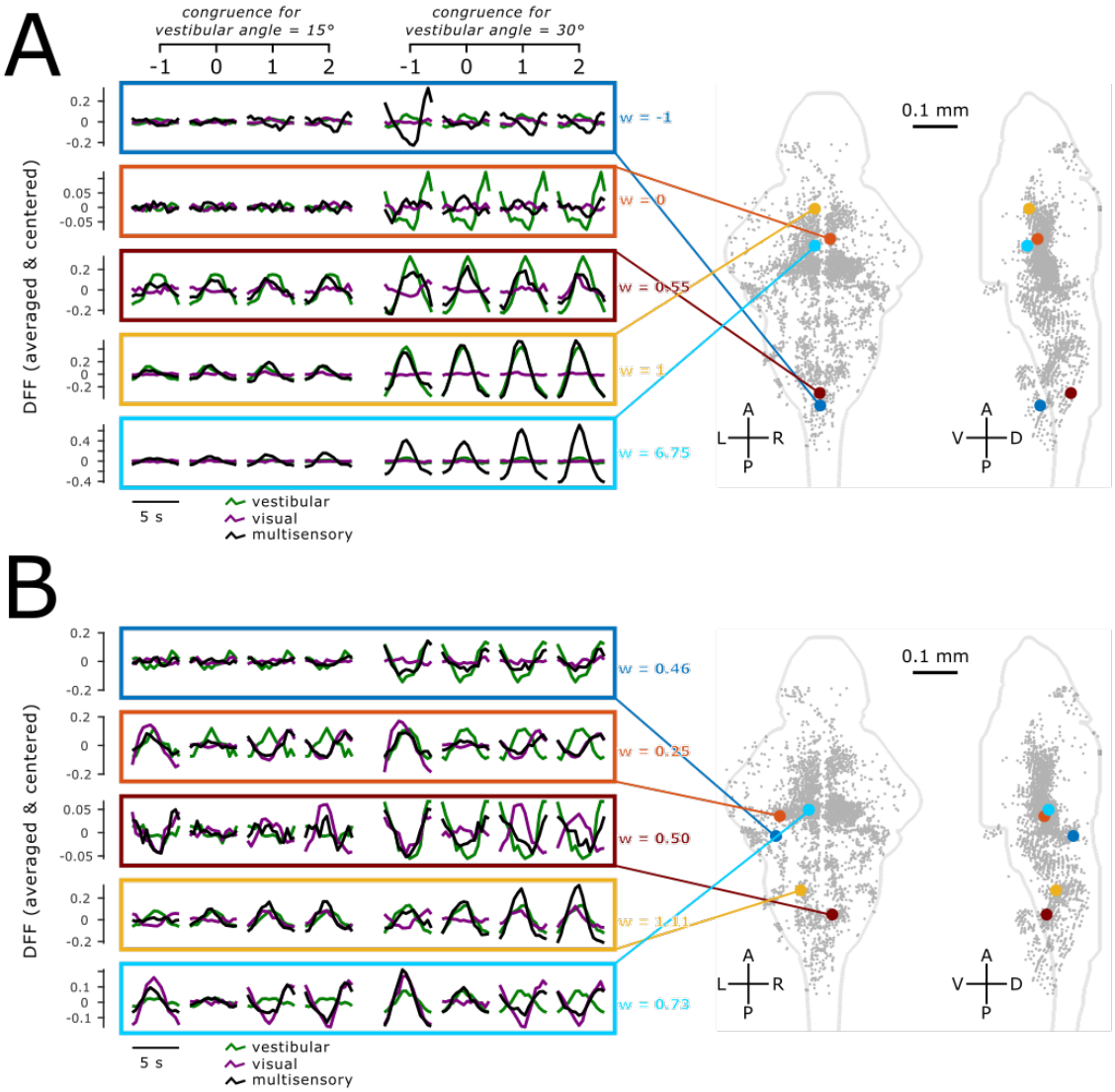

Figure III.19: **A**: Selected neurons, with $\mathbf{w} = [-1, 0, 0.55, 1, 6.75]$. **B**: Neurons with specific responses. Neuronal activities are shown in left panel, and location in the brain in right panel.

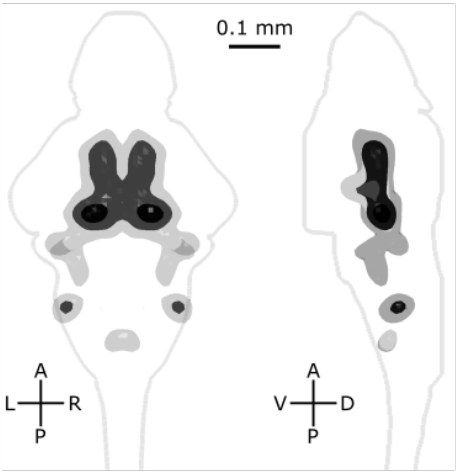

Figure III.20: Kernel density estimation of super-additive neurons, after super-additive neurons were mirrored around left/right plan.

- 12.2% for the thalamus,
- 8.1% for the pretectum,
- 2.5% for the superior part of the raphe nucleus,
- 50.9% for the gad1b inhibitory clusters,
- 53.7% for the multisensory region.

A more detailed plot, layer by layer is shown in annex VIII.8.

III.4 Discussion

In this chapter, we found that behavioural responses to vestibular and visual stimulations in larval zebrafish vary a lot. In the case of multisensory stimulations, the coherence of the two stimuli has a great influence on the behaviour: whereas there seems to be a vestibular capture phenomenon when there is no stimuli coherence, the response is much higher when there is. In addition, the actual response to coherent multisensory signals is higher than the sum of unisensory responses. This super-additivity behaviour suggests that the two stimuli are not simply summed in some neurons of the brain.

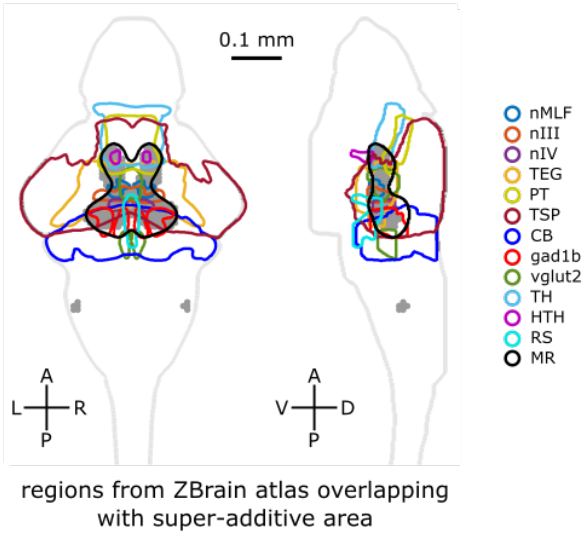

Figure III.21: Regions from ZBrain atlas overlapping with super-additive area (shaded grey). ZBrain atlas regions are from Randlett *et al.* [105]. nMLF: nucleus of the medial longitudinal fascicle, nIII: oculomotor nucleus, nIV: trochlear nucleus, TEG: tegmentum, PT: pretectum, TSP: tectum stratum periventriculare, CB: cerebellum, gad1b: gad1b inhibitory clusters, vglut2: vglut2 cluster 1, TH: thalamus, HTH: hypothalamus 6.7FRhcrtR-Gal4 cluster, RS: raphe superior, MR: multisensory region.

Analyzing brain data, we identified, in response to a vestibular stimulation, the vestibular nuclei, the cerebellar nuclei, and the motor neurons, described in the literature. Similarly, we identified, in response to a visual stimulation, scattered neurons in the visual tectum, the pretectum, the anterior hindbrain visual cluster, and to a certain extent the inferior olive, described in the literature. We found neurons responding to both vestibular and visual stimulation, and noticed their stereotypical location in the brain. This multisensory region widely overlaps with motor neurons and with some gad1b inhibitory clusters, and includes parts of the thalamus, the cerebellum, the tegmentum, and the raphe superior. It projects axons to contralateral regions of itself, to the cerebellum, to areas near the eyes, and to the hindbrain. It is interesting to note that although motor regions have most of their neurons in this multisensory area, they only represent 8% of it.

We then modeled neurons responding to either vestibular or visual stimulus. Modeling can help understand how the brain processes and integrates information from these inputs, and the underlying computations. We saw that a simplified linear model was enough to describe their responses to multisensory stimulations. We analyzed coefficients from a simple linear model, and uncovered neurons whose response to a multisensory stimulation

was higher than the sum of their responses to unisensory stimulations. These neurons were sterotypically located in the brain, more numerous than multisensory neurons, and overlapped with a bit more than half of the multisensory region. Most of the oculomotor neurons are part of this super-additive region, which could explain the behaviour described earlier. More generally, in the neurons kept for modeling, 65% were sub-additive, 24% additive, and 10% super-additive.

This work provides an extensive analysis on behavioural and neuronal responses of larval zebrafish when presented with a combination of vestibular and visual stimulations.

In the case of a coherent stimulation between the two stimuli, the brain combines the information from them and the resulting eye behaviour is adapted to the stimulation. Multisensory neurons are found in different regions of the brain, but one area has a particularly dense proportion of these neurons. This shows the global multimodal aspect of the brain, but still highlights that some regions are specifically dedicated to multisensory integration. The super-additive nature of some neurons in the brain, including half of the multisensory neurons shows that there exist neuronal computations to optimize motor outputs.

The limitations of this work include the fact that the fish were immobilized in agarose on the experimental aspect, and the fact that we did not have access to the neurons action potentials directly on the modelling aspect.

As fish could only move their heads, there was no possibility to track other balancing movement that fins or tail would have elicited. Being unable to swim freely, their behaviour could be different from what it is in a freely swimming environment. We add that not being in a familiar environment could also modify the fish actions. We have not found a way to free both the eyes and the tail with the rotating microscope we are currently using, along with having the same conditions of experiment, and enough stability. It is possible to imagine a fish holder that could allow for that manipulation. In terms of freely swimming fish, one could imagine to build a virtual reality device, able to rotate a small water tank around the 3 main axes, with visual patterns projected on its walls and ground. This setup would include cameras to track the fish, in order to rotate it around its rostro-caudal axis.

As for the modeling aspect, we have fitted a model on calcium imaging data, and the relationship between action potentials and fluorescence is non linear. The fact that super-additive neurons are all located in a stereotypical area could simply be a coincidence. Unfortunately, with the current imaging technologies available, we have not found a way to image the whole brain with action potential precision.

This study only focused on behavioural and neuronal responses elicited by vestibular and visual stimulation, and thus does not generalizes to other possible modalities.

Vestibular and visual stimulations are only two types of possible stimulations, among many others. We are missing tactile, auditory, olfactory, and gustatory stimuli, for example. We can wonder if these stimulations would elicit eyes rotation, and if so, if the coherence of these stimuli combined would have a similar effect on behaviour as vestibular and visual stimuli do. From a neuronal perspective, it would be interesting to study whether the multisensory region we uncovered is solely associated with vestibular and visual responses, or if other modalities are integrated in it as well.

To uncover the full multisensory aspect of the brain, one could imagine an experimental setup in which many additional modalities are tested, and do a global map of larval zebrafish response, with different types of multisensory combinations. This is a daunting task, and chances are multisensory integration will still be investigated two stimuli at a time in the nearby future.

IV – Influence of visual contrast on multisensory response

IV.1 Introduction

In the previous chapter, we created different multisensory stimulation scenarios characterized by the congruence of the visual stimulus relative to the vestibular stimulus. In this chapter, we investigated how the contrast of the visual pattern affected the behavioural and neural response. We focused on the conflict (congruence = 0) and the coherent (congruence = 1) multisensory scenarios.

When two sensory stimuli are strongly conflicting the inconsistency must be resolved by prioritizing one cue over the other. This process represents an elementary example of a decision-making mechanism. Our objective, was to understand the neuronal processes that drive these sudden transitions. A conflicting multisensory situation can be induced by continuously rotating the fish while delivering a visual pattern fixed with respect to the animal body. In this context, one of two competing behaviours may be elicited: in the optical state (OS), the vestibulo-ocular reflex is suppressed, and the gaze is stabilized onto the visual pattern; in the vestibular state (VS), the visual input is ignored, and vestibular-driven eyes movements maintain the gaze stable in space (see figure IV.1).

We hypothesized that such two states exist for zebrafish and that we might be able to induce a transition between the two states by continuously morphing the sensory inputs, controlling the contrast of the visual pattern. More precisely, starting from a VS state (no contrast in the visual image), we could continuously increase the contrast of the visual stimulus to increase the reliability of the visual cue. Such an experiment should reveal the existence of a flickering regime between the VS and the OS state when both stimuli are equally reliable. In this bi-stable regime, we would expect the velocity of eyes movements to stochastically oscillate between two discrete values. Such a regime would be an interesting model system to study neuronal circuits underlying decision making.

We will first see the results of the experiments that tested the existence of such a bi-stable state in a conflicting condition. I will then present a similar morphing experiment but with both stimuli presented in a coherent manner (congruence = 1). For this condition, I investigated if contrast modulated the response in a linear or non-linear manner.

In summary, we want to understand how visual contrast is used by the fish, when a visual stimulus is paired with a vestibular stimulus. We will study behaviour and brain-wide neural responses to answer this question and to investigate whether a flickering regime

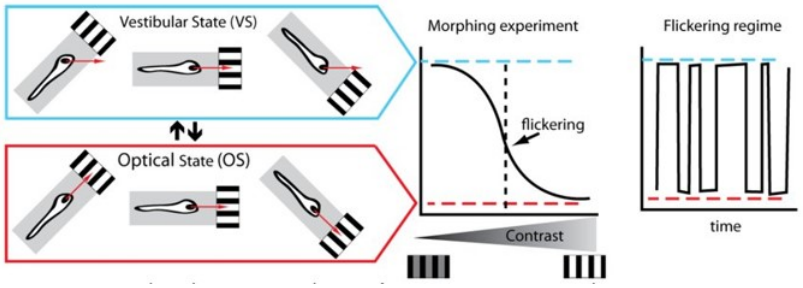

Figure IV.1: Hypothesized bi-stable dynamics under conflicting sensory inputs: vestibular state (blue) where gaze stays fixed in space (red arrow) following the vestibular input, and optical state (red) where gaze is locked onto the moving grating (red arrow). In a morphing experiment, the grating contrast is gradually increased, leading to a transition from the vestibular state to the optical state. In a theoretical flickering regime, when both stimuli are equally intense, the system exhibits stochastic transitions between the two states.

can be identified in a conflicting condition, and whether the multisensory response in a coherent condition is integrated linearly or non-linearly in in the multisensory response.

IV.1.1 Methods summary

We used the rotating light-sheet microscope described in the previous chapter (see figure III.1 and methods section III.2.1) to create the contrasting and the coherent multisensory scenarios. In short, the fish was roll-tilted around its anterior-posterior body axis by rotating the microscope. The screen, fixed on the microscope, rotated with the fish and the video-projector projected either a static (conflict) or a moving grating (coherent) onto the screen. For the experiments presented here, in addition, we modulated the contrast of the visual grating. At a contrast of 0% all the projected stripes had the same grey colour, producing a uniform grey image. At a contrast of 100% the stripes were black and white. For any contrast between 0% and 100% stripes were projected in two shades of grey, one darker than the other. For all contrast levels the total luminance was set equal. Note that we placed a red low pass filter on the video projector. From the grating, only the red component was projected on the screen. This was necessary to prevent interference of the projected visual stimulus with the neural calcium imaging of the green fluorescent GCaMP6f.

We submitted the fish to different sequences of uni and multisensory scenarios while varying the contrast of the projected visual grating. The sequences for the behavioural

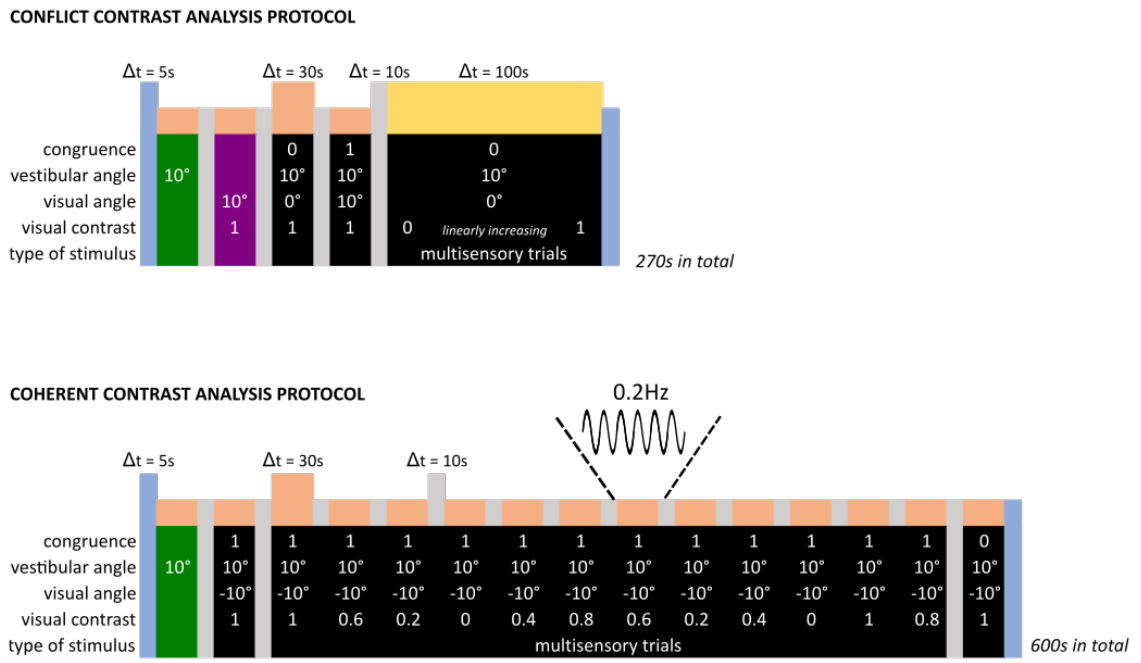

Figure IV.2: Description of the behavioural experimental protocols for conflict and coherent contrast analysis.

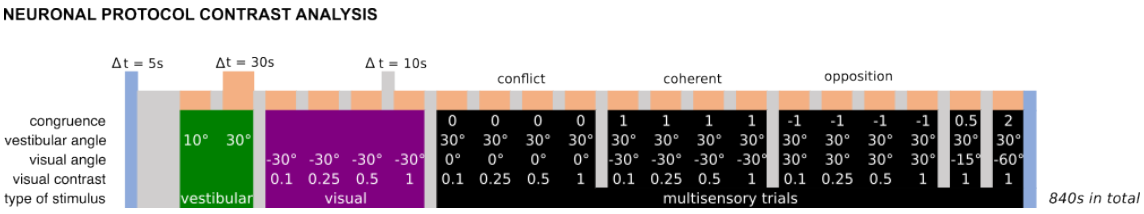

Figure IV.3: Description of the neuronal experimental protocols for conflict and coherent contrast analysis.

experiments are shown in figure IV.2 and for the neuronal recordings in figure IV.3.

For these contrast-increasing experiments, we had to ensure that our projector linearly rendered the luminance sent by the computer. As a matter of fact, a majority of the projectors on the market have a parameter called gamma that sets the smoothness of the transition from black to white in the projected images. The luminance of the output depends on the luminance of the input according to the power law $V_{out} = V_{in}^{\gamma}$. A value of gamma greater than 1 adapts the images to the perception of the human eye. We ensured that our projector's gamma parameter was set to 1, in order to maintain linearity in luminance, and therefore linearity in contrast, from the code to the visual projection.

As in the previous chapter, we used transgenic Tg(elavl3:H2B-GCaMP6f) [**?**] zebrafish larvae of age between 5–8 day post fertilization (dpf) carrying the nacre mutation making them more transparent.

For data analysis, we tracked eye movements and quantified the neural responses as described in the previous chapter (see the corresponding methods section III.2) with the following modifications. Here we applied the Fourier analysis per pixel and, in addition to the NFA, also extracted the phase of the response relative to the stimulus. This allowed us to plot phase maps of the brain response as hsv image stacks (hue = phase, saturation = 0, value = amplitude) as described in Migault et al. 2018 [45]. The color in the maps represented the phase of the response and the brightness the amplitude of the NFA at the stimulation frequency.

To average phase maps across different fish, we used the Computational Morphometry ToolKit CMTK (http://www.nitrc.org/ projects/cmtk/) to compute for every fish the morphing transformation from the average brain stack (anatomical stack) to the corresponding Elav3-h2B stack of the zBrain atlas [105]. To apply the transformation to the phase maps, we interpreted every pixel value as a complex number $z = Ae^{i\phi}$. We then transformed the real and the imaginary part of the corresponding phase maps independently, averaged the transformed real and imaginary parts for different fish and finally calculated from the average complex number amplitude and phase of the average phase map $< z >=< a > +i < b >=< A > *e^{i\phi}$.

IV.2 Results

IV.2.1 Visual contrast integration in multisensory behaviour

We analyzed the evoked eye movements of 12 fish in response to the conflicting multisensory scenario as the contrast of the projected visual pattern was linearly increased. No change in response was observed between contrast at 0% and contrast at 100% (figure IV.4). No correlation between contrast and behavioural response could be revealed.

We conclude that for all contrast levels, the visual pattern had no effect on the behavioural response. Consequently, we did not observe a flickering regime.

Having studied the response of fish in a conflicting environment, we focused on the

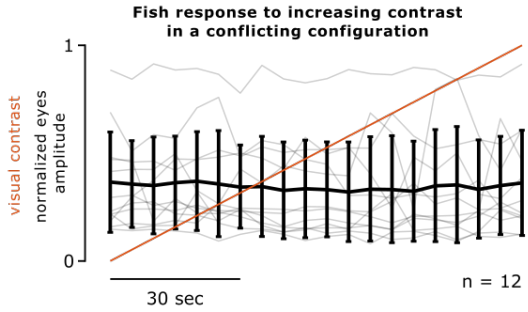

Figure IV.4: In the case of a conflicting multisensory stimulation (*congruence* = 0), there is no change in behaviour when the visual stimulus contrast increases from 0 to 100%. The eyes responses were normalized to the 10° amplitude of the vestibular stimulus.

response of fish in a coherent environment.

Figure IV.5 (left panel) shows the measured angular eye amplitudes in response to the coherent multisensory stimulation at different visual contrast levels. We created two consecutive sequences of six contrast levels with the values 0%, 20%, 40%, 60%, 80% and 100% chosen in a random order (see protocol displayed in figure IV.2). From the eyes responses recorded, we could already infer that contrast had an effect on the fish's response. Sorting the responses by contrast allowed us to plot the evolution of normalized eye amplitude against contrast for the 7 fish. The responses were normalized to the vestibular stimulation amplitude of 10°. Figure IV.5 (right panel) shows the mean response for 7 fish. The response increased sub-linearly with the contrast and was well fitted with a logarithmic function $a + b \cdot \log(contrast + c)$, where a = 0.7, b = 0.13 and c = 0.05.

IV.2.2 Visual contrast integration in multisensory neuronal responses

Next, we performed brain-wide calcium imaging experiments at the congruence levels 0, 1, and -1 corresponding to conflict, coherence, and opposition, respectively. The details of the experimental protocol are shown in figure IV.3. Note, that fish were paralyzed in these experiments and did not move their eyes in response to the stimulation to avoid motion artefacts due to eye movements.

Figure IV.6 shows phase maps for five increasing levels of visual contrast recorded at the congruence level c=0 (conflict), from 6 paralyzed fish. The phase map at $contrast = 100\%$ was exactly the same as the phase map at $contrast = 0\%$, the latter essentially correspond-

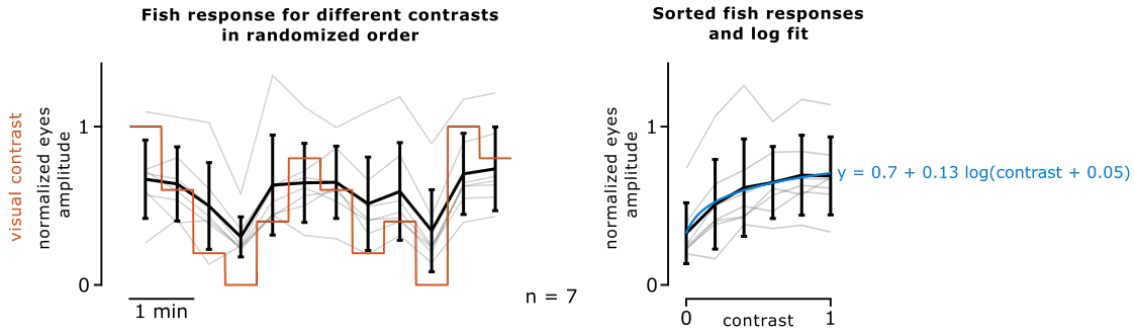

Figure IV.5: In the case of a coherent (*congruence* = 1) multisensory stimulation, the average fish response can be explained using a logarithmic function, with the parameters provided. The eyes responses were normalized to the 10° amplitude of the vestibular stimulus.

ing to a unisensory vestibular stimulus. The visual system was not activated. However, the absence of neural responses from visual brain areas in this experimental condition does not explain the absence of an effect of contrast in the behavioural experiments, because the eyes did not move during imaging, as the fish were paralyzed. In the behavioural experiments, the stimulus evoked compensatory eye movements, most likely driven by the vestibulo-ocular reflex with a non-negligible gain of about 0.5, corresponded to an amplitude of about 5°. Eyes movements relative to a static visual environment leaded to a retinal shift and must have stimulated the visual system during the behavioural protocol. A congruence level of -0.5 in the multisensory scenario could restore this sensory state in paralyzed fish. This means that the resulting visual flow on the retina moves in the opposite direction compared to the natural coherent stimulus condition. Consistent with this argument, we observed the emergence of visual brain areas with increasing contrast in phase maps calculated from recordings at congruence level -1 (opposition) (see figure IV.7). At present, we do not understand why this strong visually evoked neural activity in this condition does not suppress or at least attenuate the vestibular reflex in the behavioural experiments with imposed conflicting multisensory stimuli. We did not perform the recording at a congruence level of -0.5, however, we believe that even at this level of congruence, there will be strong visual responses in the phase maps.

Figure IV.8 shows phase maps for five increasing levels of visual contrast recorded at the congruence level c=1. At 0% contrast the phase map was equal to the vestibular only phase map. For increasing contrast levels, the neurons previously identified as visually

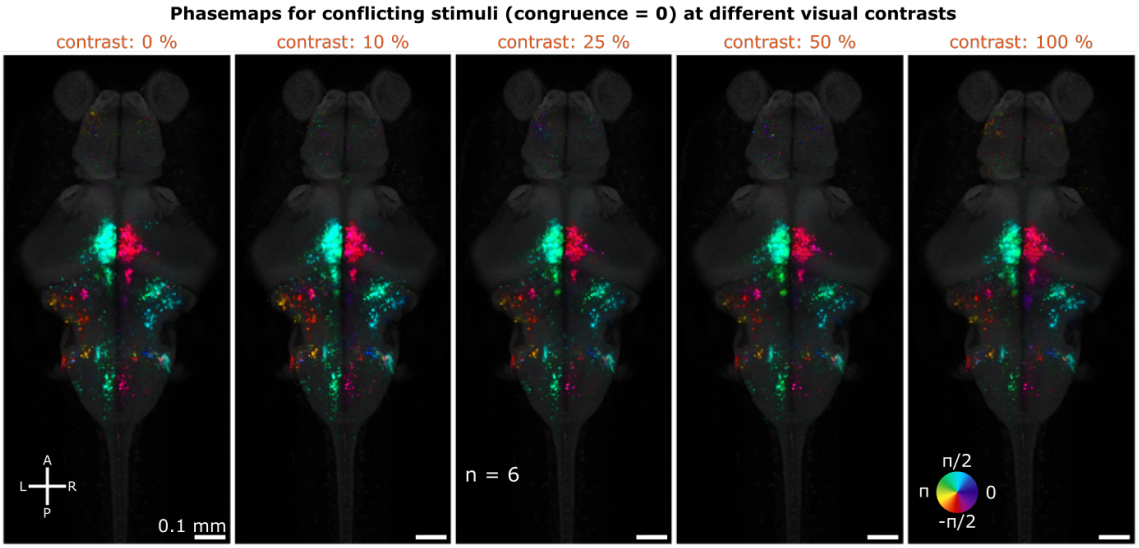

Figure IV.6: Averaged phase maps for conflicting multisensory stimuli (*congruence* $= 0$) with increasing contrast. There is no evidence that the stripes were detected by the fish. The phase maps are similar, with only the vestibular circuits active, whatever the contrast.

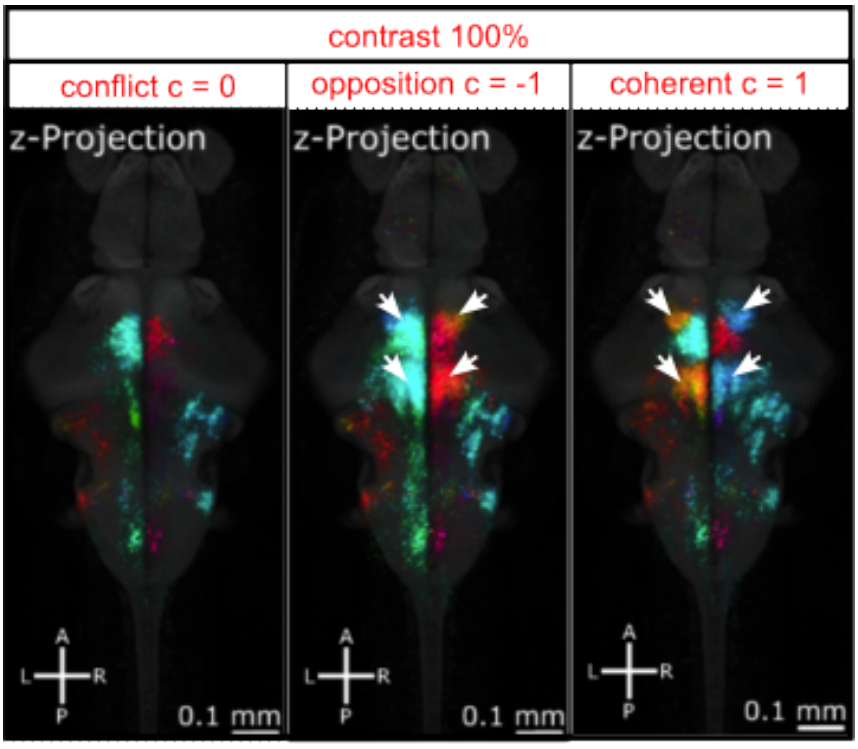

Figure IV.7: Averaged phase maps at 100% visual contrast for conflict, opposition, and coherent multisensory stimuli (*congruence* $= 0, -1, 1$). White arrows indicate areas responding to visual stimuli.

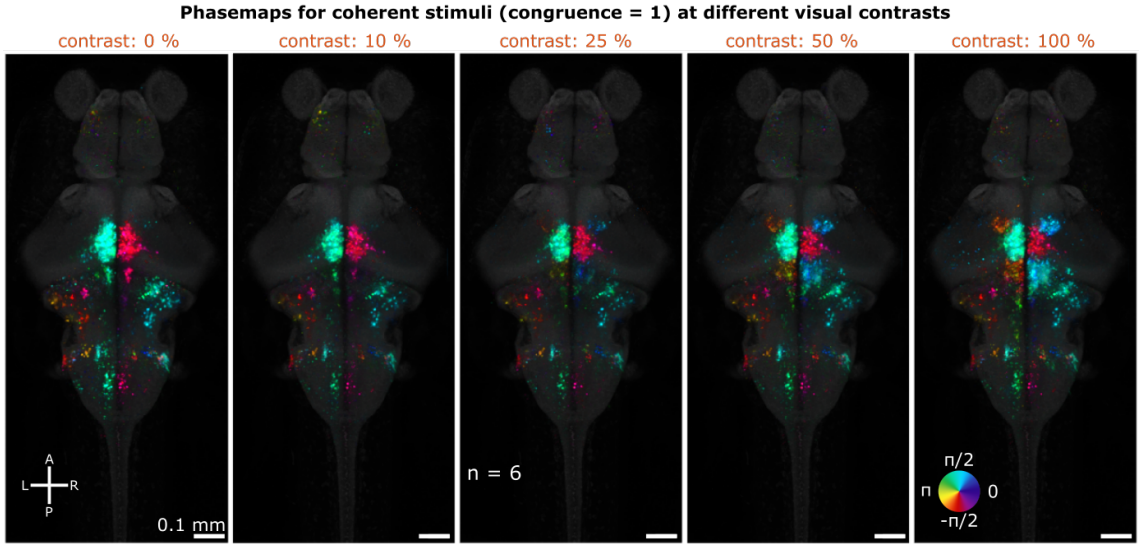

Figure IV.8: Averaged phase maps for coherent multisensory stimuli (*congruence* = 1) for four increasing levels of visual contrast. For increasing contrast the response amplitude of the visual pathway increased.

responsive lit up with increasing intensity for increasing contrast. The four characteristic visual clusters became more and more prominent in the phase maps as well as some neuronal responses in the optic tectum.

For more details, all phase maps recorded for the different congruence levels are available in the annexes in a layer-per-layer view (see annex VIII.9).

Next, we computed the neural responses at the single neuron level and identified all visually responsive neurons by Fourier analysis from the responses to the visual stimulation scenario (see figure IV.9A). We clustered the neuronal responses into eight functional clusters using k-means clustering. Interestingly, four of the clusters, overlapped with the four spatial clusters of the spatial organisation of the visual neurons in the brain. The other four clusters were found in the left tectum. The mean activities of the four main visual clusters had a similar logarithmic dependence on contrast as observed for the behavioural response and were modulated at the same frequency as the stimulus, which was set at 0.2Hz.

The response profiles in the optic tectum were more variable, with logarithmic responses, linear responses, and even a cluster with a step shaped response profile. In

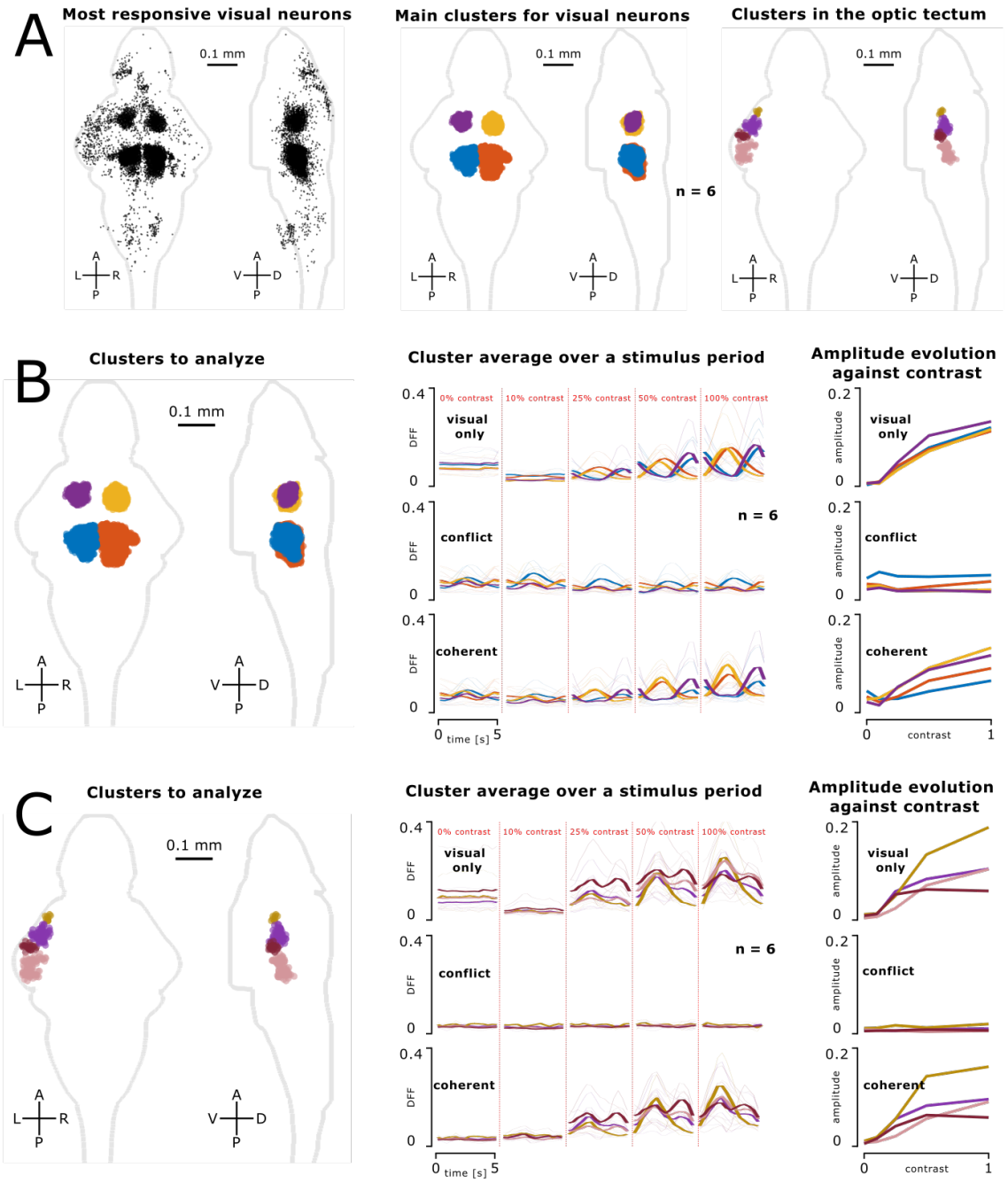

Figure IV.9: **A**: The left panel shows the most responsive neurons to visual stimulation. The middle panel shows the four main visual clusters that we identified for the analysis from the recording during the visual-only trials. The right panel is a clustered selection of neurons in the optic tectum. **B**: Average $\Delta F/F$ for neurons in the selected clusters, for visual, conflicting ($congruence = 0$), and coherent ($congruence = 1$) stimulati, at different contrasts. The right panel shows the amplitude evolution as a function of contrast. **C**: Average $\Delta F/F$ for neurons in the selected clusters, for visual, conflicting ($congruence = 0$), and coherent ($congruence = 1$) stimuli, at different contrasts. The right panel shows the amplitude evolution as a function of contrast.

addition to these observations, the clusters in the optic tectum responded at twice the stimulation frequency. The observed response profiles in the tectum were the same for visual-only and multisensory stimulation scenarios (data not shown).

Neuronal clusters in the optic tectum were not active during the conflicting stimuli, whereas they were when the visual stimulus alone was presented. The four main clusters for the visual response (which include the two parts of the pretectum) showed some response in the case of the conflicting stimulation, but this may be due to the fact that some neurons in this area were multisensory, as we saw in the previous chapter.

IV.3 Discussion

In this chapter, we studied contrast integration in fish behaviour and neuronal response.

When presented with a coherent stimulus, fish response was log shaped against contrast. The same shape was found in most of the visual neurons of the brain.

Rinner *et al.* [79] observed in larval zebrafish a similar logarithmic relation of the OKR in the yaw direction with increasing visual contrast levels, when only visual the stimulus was presented. It is interesting that in our case vestibular stimulation did not impair this logarithmic relation. Interestingly we found, that this was not the case anymore in a conflicting situation, in which the contrast had no influence on the behavioural response even at maximal contrast levels.

An interesting variation of the behavioural experiment, which we did not implement, would be to characterize how increasing contrast would attenuate the behavioural response in a multisensory congruence=-1 scenario (opposition). We noticed in the previous chapter that the behavioural response to an opposition stimulation (with contrast of 100%) elicited a response that was a bit lower than the vestibular response. We recorded the brain during such an experiment with paralyzed fish, but did not do the behavioural experiment. We expect to measure an attenuation in eyes rotation amplitude with increasing contrast, along with a logarithmic dependence.

The strength of our work is to be able to combine complex stimuli such that they mim-

ick the sensory environment encountered during natural situations, but also to decorrelate them, to test conflicting sensory situations.

It is interesting to note that the response to coherent stimuli is a logarithmic function of the visual contrast. From an evolutionary point of view, this allows an individual to quickly assess whether a stimulus makes sense, with a small amount of information from an additional stimulus. As a matter of fact, the strength of multisensory integration lies in the ability to maximize the reliability of the representation of the environment with the minimum amount of information available.

V – Learning in a multisensory environment

V.1 Introduction

Learning and adapting are at the center of life. Without these capabilities, a new born would virtually be unable to interact with its environment. It is through learning and adaptation that animals and humans develop the ability to eat, walk, and communicate with each other. Without the possibility to learn, societies would have never been able to thrive the way they did, as knowledge would not have been able to stream from an older to a new generation.

A learning process can occur naturally in one's life, by connecting a behaviour to an internal state (I ate this food, do I feel good?). It can also be supervised by a peer (I learned to read because someone taught me to). Understanding how we are able to learn, in all the forms learning takes, helps us understand how life works.

In order to understand how we can learn and therefore interact better and better with our environment, we need to look at how we can elicit a change in behaviour. As a matter of fact, a change in the environment can induce such a change in behaviour. In particular, in a multisensory environment, a mismatch between two sensory inputs is likely to make us adapt to this new situation.

Let us take the following example. Suppose you are playing darts, and you become good at the game, so you hit the target everytime. If you were to put on fresnel prism glasses, you would see your surroundings with a fixed angular shift. The target would appear at a different location than where it really is. If you threw darts at this target, you would miss it, as you are aiming at a mirage target. Nevertheless, given some time, you would learn how to internalize this new target representation, and aim straight at it, changing the way you throw your projectiles. In this mismatching multisensory environment, in which vision and proprioception do not match, you would adapt. Removing the glasses after the first training would result in you visualizing the actual target location. But because you learned how to throw darts in the altered situation, you would once again miss the target, and need to start another training period to finally regain your initial throwing skills (figure V.1). Such an experiment has been conducted with primates, and shows that when they wear spectacles that changes the visual gain in VOR, they are able to achieve up to 75% compensation [224].

In this last chapter of my thesis, I will present this example's approach on zebrafish: we will use a mismatching multisensory environment to try to induce learning in the animal, and charaterize this learning.

Pastor *et al.* have shown that it was possible to increase the VOR gain in adult goldfish using a mismatching multisensory environment, with a significant increase of response after only one hour [216] (figure V.2). They have also shown that the cerebellum was necessary for this motor learning process [215]. On the other hand, Ahrens *et al.* [92] have shown that adaptation could be made possible in larval zebrafish. Here, we will perform experiments similar to Pastor *et al.* on larval zebrafish, and verify whether a certain multisensory mismatch allows to elicit a learning behaviour in them.

The first part of this work is to show this adaptation behaviour. We will focus on one good fish, and then discuss the results of the experiment on a large number of fish. We will then study the influence of the cerebellum on adaptation, by ablating the zebrafish Purkinje cells, a part of the cerebellar circuit. Finally, we will analyze the influence of the type of stimulation, and the influence of the laser on adaptation.

V.2 Results

V.2.1 It is possible to induce adaptation in a multisensory environment

a) Methods summary

We wonder here whether we can induce adaptation through a multisensory environment in larval zebrafish as young as 5 to 8 days post-fertilization.

During one of my experiments, I did not set the correct visual amplitude in a multisensory stimulation. The congruence was higher than 1, although I wanted a coherent stimulation. This resulted in an increasing vestibular gain as fish underwent this pseudo-coherent stimuli. I decided to build an experiment to test whether this behaviour evolution could be reproducible.

The goal we want to achieve is increase a behavioural response to a unisensory stimulation, through a multisensory training. In order to do this, we are going to consecutively test vestibular response, and train using multisensory stimuli, with increasing congru-

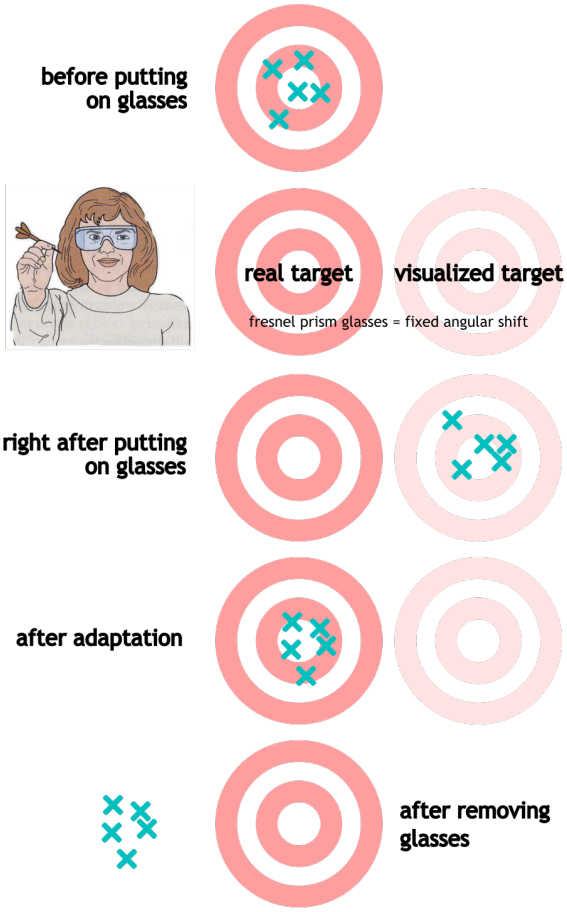

Figure V.1: When putting on fresnel prism glasses, the target appears with an angular shift, on the right of the actual target. When throwing darts at it, one will miss the actual target. After some training, it is possible to learn how to thrown in this mismatching multisensory environment. Upon removing the glasses, the target now appears exactly where it is supposed to be, but because of the former training, one will miss it again, and need to train again to hit it properly.

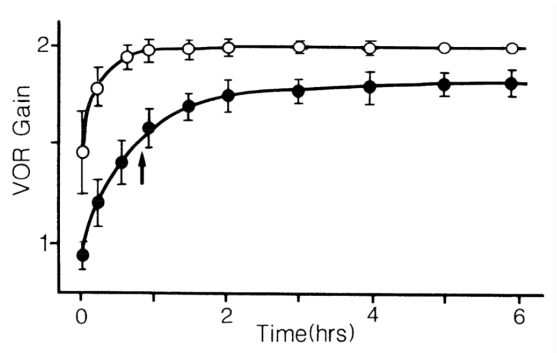

Figure V.2: Evolution of vestibulo-ocular reflex gain for adult goldfish during an adaptation experiment, in which the congruence between vestibular and visual stimulation is 1. Black dots are responses to vestibular stimulation, white dots are responses to multisensory stimulation. Figure from Pastor *et al.* [216].

ence, from 1 to 2 (figure V.3). The first vestibular stimulus sets the baseline, and after this baseline, we alternate sequences of $3min30sec$ of training, and $30sec$ of vestibular response testing. Exact protocol is described in figure V.4.

We are going to test this protocol on GCaMP fish in the first place, and see if we can obtain this increase in response we are looking for. Doing this on many fish will provide us with a good indication on the percentage of fish that can show a sustained change in behaviour.

We want to show that a change in behaviour is possible in a multisensory environment, and check whether this change is reproducible.

b) The eyes rotation almost doubles in a mismatching multisensory envionment

We need to show learning can be triggered with a mismatching multisensory experiment, as we described in this chapter's introduction.

Figure V.5 shows the evolution of eyes response during the experiment described above, for the first fish we tested. Yellow patches are training periods. Using tracking technique described in figure III.4, we extracted normalized eyes angles during training and vestibular testings. Orange horizontal lines show the level of congruence during training. Triangle markers are eyes angles in a multisensory situation, and circle markers are eyes angles in

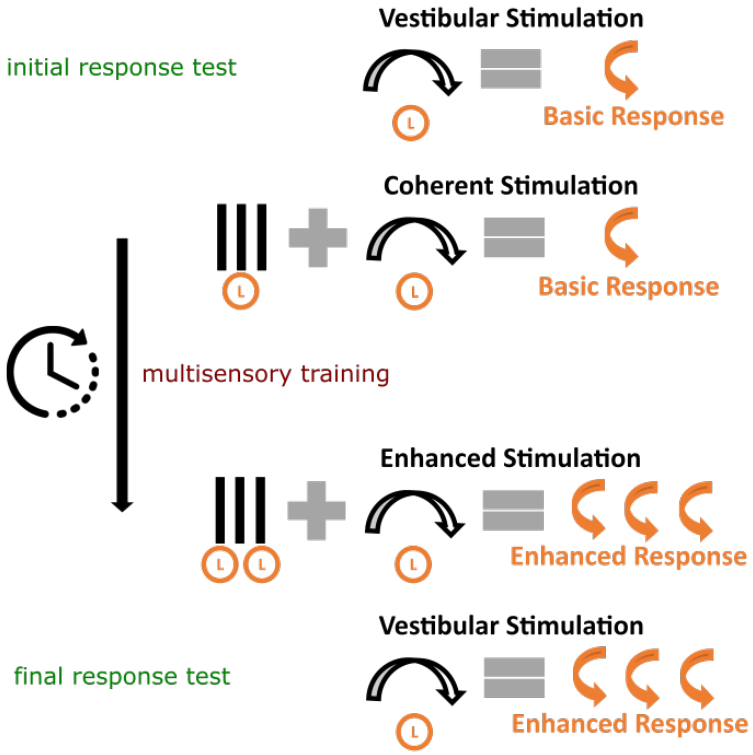

Figure V.3: The adaptation experiment consists in a vestibular response baseline, and then an alternation of multisensory training, with a congruence going from 1 (coherent), to 2 (enhancement), and vestibular testing.

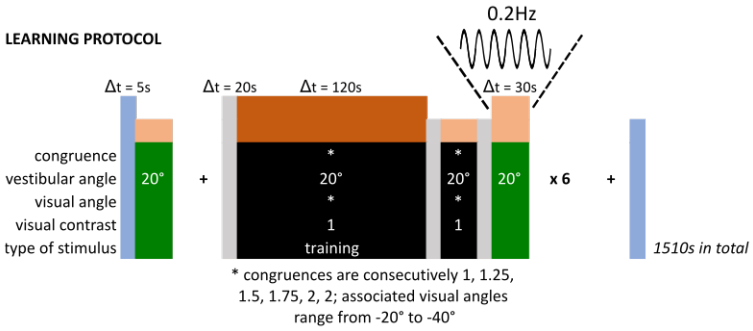

Figure V.4: Description of the learning experimental protocol.

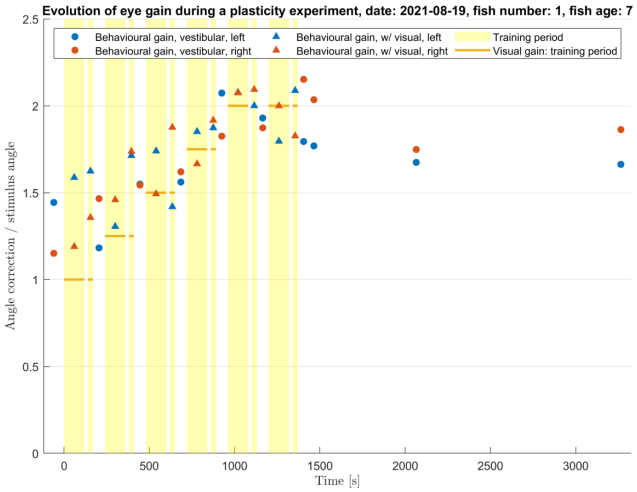

Figure V.5: Evolution of eyes response along learning experiment, for a fish showing a great change in behaviour. Yellow patches are training periods, and orange lines are the congruence between vestibular and visual stimuli. This fish displays a 53% increase in response to vestibular stimulus at the end of the experiment compared to the beginning.

a vestibular situation.

This fish had an initial vestibular response gain of 1.3, which corresponds to a 26° eyes response amplitude to a 20° stimulation amplitude. After 24 minutes of experiment, this vestibular response was 40°, which is way above the 20° vestibular stimulation provided, and a 53% increase from the initial response.

After the multisensory trainings, we left the fish with no stimulus, to see if this evolution in vestibular response would be maintained. After a bit less than one hour, response was still around 35°, which is a 35% increase from the initial response.

Note that light-sheet imaging, and therefore laser, was on during this experiment, as we recorded the brain at the beginning and at the end of it. Unfortunately, brain data were hardly usable, because of the eyes movements.

This fish shows us it is possible to elicit a change in behaviour in a mismatching multisensory experiment. Even after the trainings are over, response to vestibular stimulation is still much higher than the initial response. It is a clear display of adaptation.

c) Experiments on many fish show a sustain adaptation in many of them

We showed a great increase in behavioural response over the course of around 24 minutes, for one fish. Now let us perform the same experiment over a large number of fish, and see whether this type of behaviour is reproducible.

The experiment was done on 28 additional fish, and we show the results in figures V.6. What we display here is only the responses to vestibular stimulations. We do not show the responses to multisensory trainings, as what interests us is whether this training can influence the unisensory response gain.

Plotting the average vestibular response evolution during the course of the experiment, we notice an increase in the first 500 seconds, across the 29 fish. It is not exactly clear what happens after the beginning of the experiment, as some of the fish seem to keep increasing their response amplitude, whereas others do not.

To have a better understanding of what is going on, we cluster the fish into three categories (figure V.7):

- The learners, with a sustained response amplitude increase along the whole experiment. 12 out of the 29 fish, or 41% of them are learners. Normalized eyes amplitude is 0.48 initially, 0.80 after two trainings (+67% after 480 seconds), and 1.02 after six trainings (+113% after 1440 seconds).
- The half learners, with an increase in response amplitude at the beginning of the experiment, followed by a decrease for the rest of it, in a bell-shape evolution. 13 out of the 29 fish, or 45% of them are half learners. Normalized eyes amplitude is 0.60 initially, 0.92 after two trainings (+53% after 480 seconds), and 0.42 after six trainings (−30% after 1440 seconds).
- The non learners, with no significant evolution in response amplitude. 4 out of the 29 fish, or 14% of them are non learners. Normalized eyes amplitude is 0.32 initially, 0.33 after two trainings (+3% after 480 seconds), and 0.43 after six trainings (+34% after 1440 seconds).

In these experiments, as for the fish presented above, laser was on to record the brain at the beginning and at the end of the protocol.

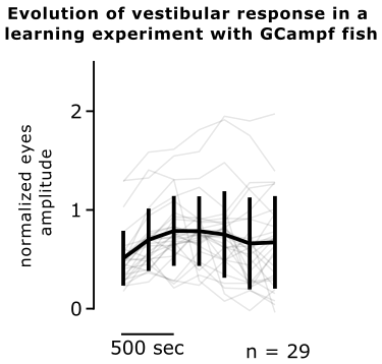

Figure V.6: Evolution of normalized eyes angle for 29 fish, during the learning experiment.

Out of the 29 fish we studied, 41% showed a sustained increase of eyes response. An additional 45% showed an initial increase, followed by a decrease in eyes response. This data show that almost 50% of the fish we studied displayed a long-term learning behaviour, and that more than 85% of them had a change in behaviour, in this multisensory stimulation.

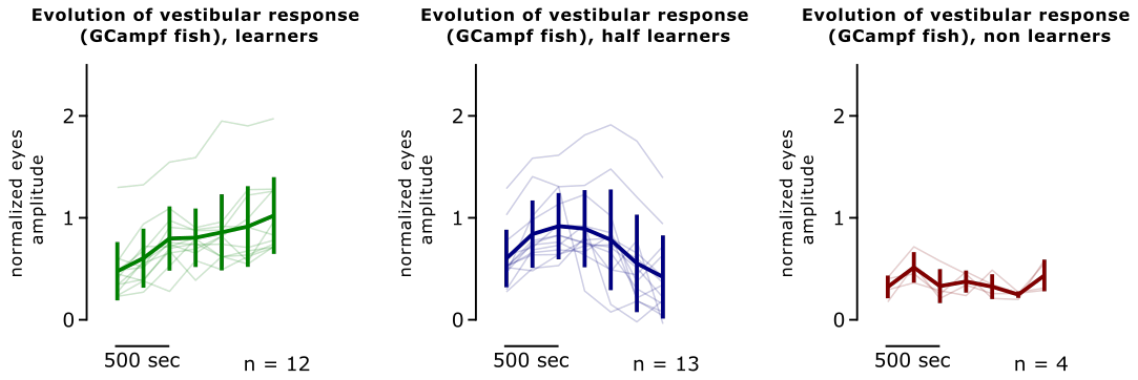

Figure V.7: Evolution of normalized eyes angle for 29 GCaMP fish, with laser on, during the learning experiment. The fish are sorted in different categories, upon how they performed behavioural adaptation. Left panel shows learners, i.e. fish whose eyes response is increasing during the whole experiment. Central panel shows half learners, i.e. fish whose eyes response is increasing at the beginning of the experiment, before decreasing, giving this bell-shape curve. Right panel shows non learners, i.e. fish whose response does not change during the protocol.

V.2.2 Purkinje cells ablation has no effect on adaptation

a) Methods summary

It seems like in the experiments we perform, the evolution of vestibular gain is due to some sort of motor learning. We now ask the question whether the cerebellum is involved in this process.

In order to test this hypothesis, we are going to do the same training experiment on fish whose Purkinje cells can be ablated. We will first perform the experiments on non-ablated fish, and compare the results to ablated fish, according to the protocol described in Markov *et al.* [214].

This straightforward protocol will provide us with valuable information on the involvement of the cerebellum in the adaptation we observe.

b) Behaviour of PC-Ntr fish is similar to behaviour of GCaMP fish

In this part and in the later parts, we are switching from GCaMP fish, to PC-Ntr fish. It is possible to remove the Purkinje cells of these fish, and therefore check whether the cerebellum is involved in the adaptation we observe. We first wonder if the PC-Ntr fish behaviour is similar to GCaMP fish behaviour.

The proportion of learners, half learners and non learners in PC-Ntr is as follow (figure V.8):

- Learners: 11 out of the 24 fish, or 46%. Normalized eyes amplitude is 0.36 initially, 0.77 after two trainings (+114% after 480 seconds), and 0.98 after six trainings (+172% after 1440 seconds).
- Half learners: 7 out of the 24 fish, or 29%. Normalized eyes amplitude is 0.34 initially, 0.77 after two trainings (+126% after 480 seconds), 0.48 and after six trainings (+41% after 1440 seconds).
- Non learners: 6 out of the 24 fish, or 25%. Normalized eyes amplitude is 0.86 initially, 0.82 after two trainings (−5% after 480 seconds), and 0.67 after six trainings (−22%

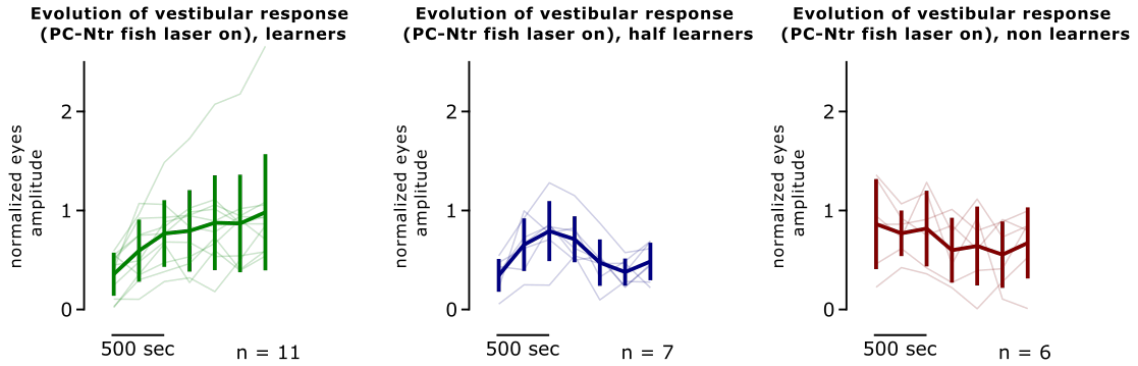

Figure V.8: Evolution of normalized eyes angle for 24 PC-Ntr fish, with laser on, during the learning experiment. The fish are sorted in different categories, upon how they performed behavioural adaptation. Left panel shows learners, i.e. fish whose eyes response is increasing during the whole experiment. Central panel shows half learners, i.e. fish whose eyes response is increasing at the beginning of the experiment, before decreasing, giving this bell-shape curve. Right panel shows non learners, i.e. fish whose response does not change during the protocol.

after 1440 seconds).

A Kolmogorov-Smirnov test (testing the hypothesis that two sets of samples come from the same distribution) between GCaMP and PC-Ntr proportions returns a p-value of 0.976.

In order to compare even better, we take another statistic: the maximum normalized vestibular gain during the experiment. For GCaMP fish, 0% of the fish have a maximum normalized vestibular gain below 0.5, 50% between 0.5 and 1, 40% between 1 and 1.5, and 10% above 1.5. For PC-Ntr fish, 0% of the fish have a maximum normalized vestibular gain below 0.5, 46% between 0.5 and 1, 50% between 1 and 1.5, and 4% above 1.5. A Kolmogorov-Smirnov test for these two distributions returns a p-value of 0.997.

We show the proportions and maximum normalized vestibular gain for GCaMP and PC-Ntr in figure V.9.

We still observe adaptation in PC-Ntr fish, with a similar proportion that GCaMP fish. The maximum normalized vestibular gain is also similar between these two groups. This data tells us the behaviour of GCaMP and PC-Ntr fish is similar.

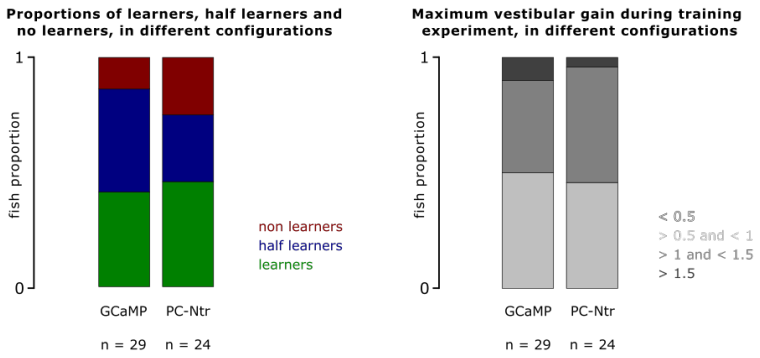

Figure V.9: Comparison between GCaMP and PC-Ntr fish. Left panel: proportions of learners, half learners and non learners. Right panel: maximum normalized vestibular gain.

c) We still observe adaptation after ablation of the Purkinje cells

We need to show whether non-ablated and ablated fish have a different behaviour in our learning experiment.

We first checked that the ablating protocol was working fine. Figure V.10 shows picture of PC-Ntr fish before and after ablation, highlighting Purkinje cells in red. Purkinje cells are present before ablation at 5 dpf, and right after a night in metronidazole at 6 dpf. At the time of the experiment, at 7 dpf, and later at 8 dpf, the fluorescence of the cells is close to nothing, telling us they were successfully ablated.

We compare the general evolution of vestibular gain between non-ablated and ablated fish in figure V.11. Going into more detail, the proportion of learners, half learners and non learners in Purkinje cells ablated PC-Ntr is as follow (figure V.12):

- Learners: 12 out of the 26 fish, or 46%. Normalized eyes amplitude is 0.35 initially, 0.57 after two trainings (+63% after 480 seconds), and 0.96 after six trainings (+174% after 1440 seconds).

- Half learners: 4 out of the 26 fish, or 15%. Normalized eyes amplitude is 0.66 initially, 1.27 after two trainings (+92% after 480 seconds), 0.49 and after six trainings (−26% after 1440 seconds).

- Non learners: 10 out of the 26 fish, or 39%. Normalized eyes amplitude is 0.75 initially, 0.61 after two trainings (−19% after 480 seconds), and 0.57 after six trainings

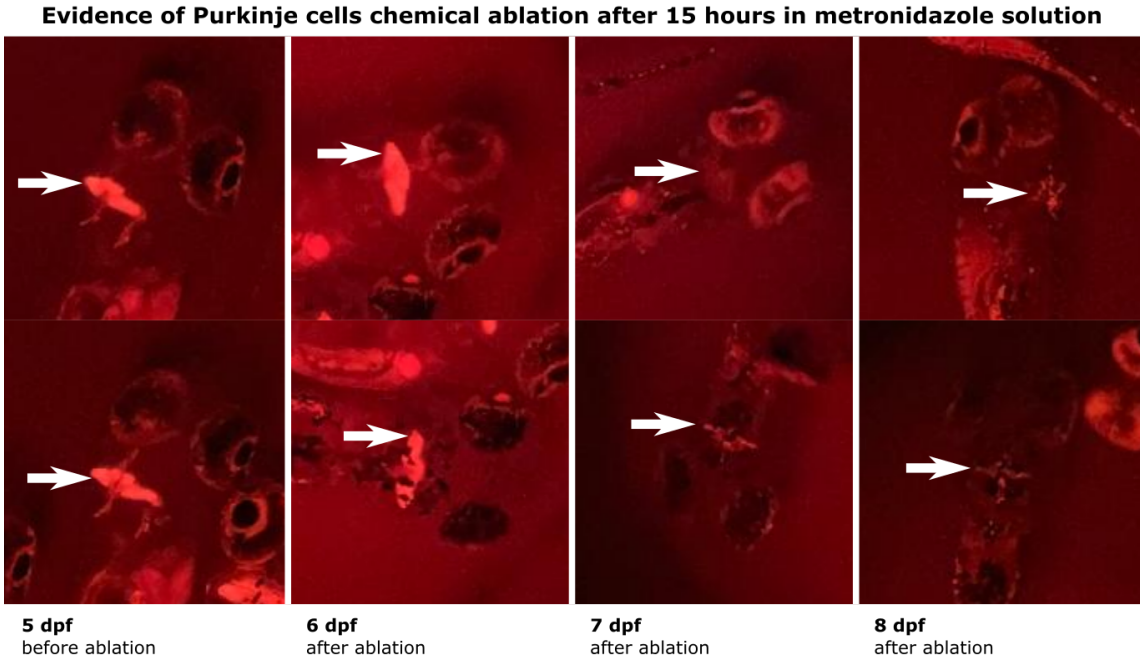

Figure V.10: Evidence of Purkinje cells ablation.

(−24% after 1440 seconds).

A Kolmogorov-Smirnov test for these proportions, between non-ablated and ablated PC-Ntr fish, returns a p-value of 0.976.

Let us now analyze maximum normalized vestibular gain during the experiment. For non-ablated fish, 0% of the fish have a maximum normalized vestibular gain below 0.5, 46% between 0.5 and 1, 50% between 1 and 1.5, and 4% above 1.5. For ablated fish, 0% of the fish have a maximum normalized vestibular gain below 0.5, 35% between 0.5 and 1, 54% between 1 and 1.5, and 11% above 1.5. A Kolmogorov-Smirnov test for these two distributions returns a p-value of 0.997.

We show the proportions and maximum normalized vestibular gain for non-ablated and ablated in figure V.13.

From this data, it does not seem like the ablation of Purkinje cells has an impact on adaptation.

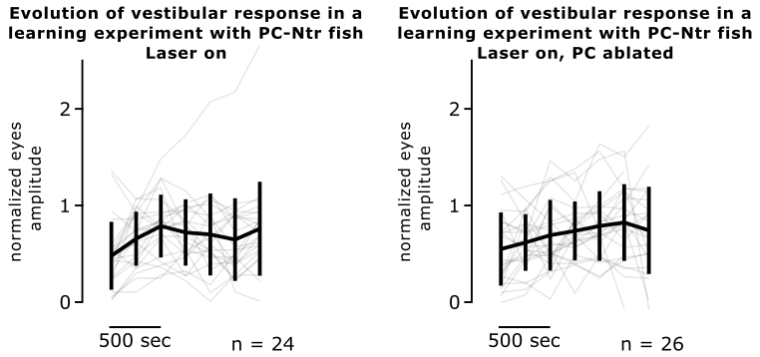

Figure V.11: Evolution of normalized eyes amplitude during learning experiments. Left panel is PC-Ntr fish, and right panel is PC-Ntr fish with chemically ablated Purkinje cells.

V.2.3 Adaptation does not see to be linked to the multisensory environment

a) Methods summary

From our initial experiment, we inferred the adaptation observed was due to the mismatching multisensory environment the fish were in. Is this really the case?

Here we will do different controls to confirm or refute the hypothesis that the adaptation is due to the multisensory environment. The two controls we are going to do consist

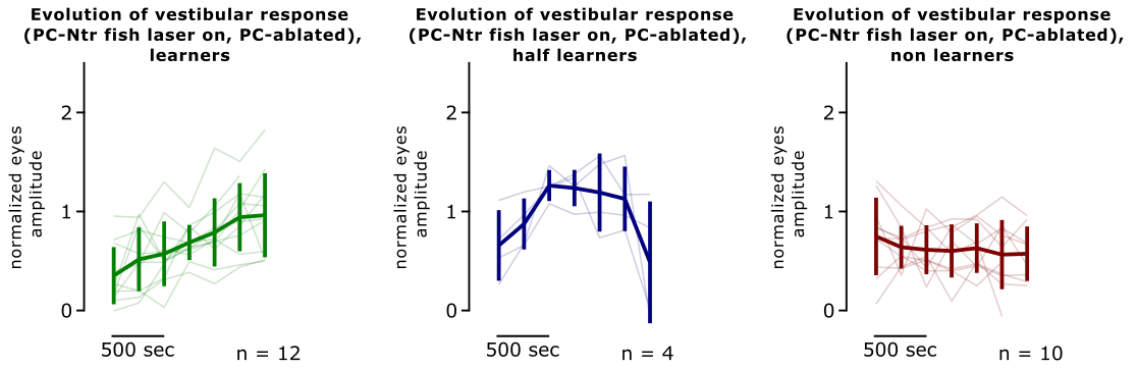

Figure V.12: Evolution of normalized eyes angle for 26 PC-Ntr fish, with laser on, during the learning experiment. Purkinje cells of the fish were ablated using metronidazole. The fish are sorted in different categories, upon how they performed behavioural adaptation. Left panel shows learners, i.e. fish whose eyes response is increasing during the whole experiment. Central panel shows half learners, i.e. fish whose eyes response is increasing at the beginning of the experiment, before decreasing, giving this bell-shape curve. Right panel shows non learners, i.e. fish whose response does not change during the protocol.

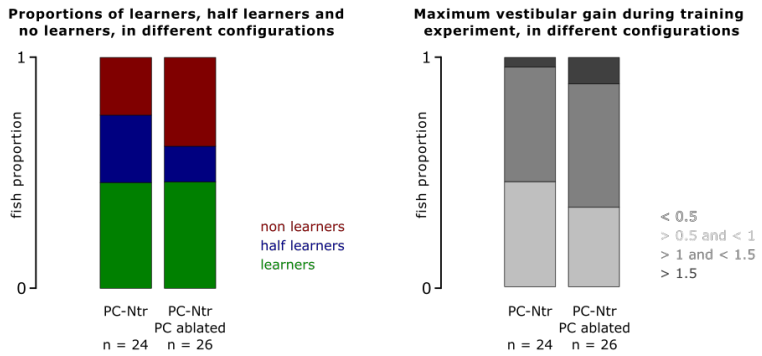

Figure V.13: Comparison between non-ablated and Purkinje cells ablated fish. Left panel: proportions of learners, half learners and non learners. Right panel: maximum normalized vestibular gain.

in changing the training period configuration. In the first control, we are going to test whether the increasing congruence between vestibular and visual stimuli has an influence on behaviour. We are going to display a visual pattern with a fixed congruence of 1 (coherent stimulation), from the beginning to the end of the experiment ("coherent training"). In the second control, we are going to test whether the visual has an influence on behaviour. In this case, the training periods are going to be a simple vestibular stimulation, so there will be no multisensory environment ("vestibular training").

With these controls, we aim to answer the following question: is the combination of vestibular and visual stimuli necessary for adaptation, or is there something else behind this vestibular gain increase we observe?

b) Coherent training leads to the same adaptation as mismatch training

In this "coherent training" control, we need to show whether increasing congruence has an influence on increasing vestibular gain along the experiment.

We compare the general evolution of vestibular gain between normal training and "coherent training" in left and middle panels of figure V.14. Going into more detail, the proportion of learners, half learners and non learners for "coherent training" is as follow (figure V.15):

- Learners: 7 out of the 16 fish, or 44%. Normalized eyes amplitude is 0.33 initially,

0.72 after two trainings (+118% after 480 seconds), and 0.97 after six trainings (+194% after 1440 seconds).

- Half learners: 6 out of the 16 fish, or 38%. Normalized eyes amplitude is 0.41 initially, 0.63 after two trainings (+54% after 480 seconds), 0.37 and after six trainings (−10% after 1440 seconds).

- Non learners: 3 out of the 16 fish, or 18%. Normalized eyes amplitude is 0.36 initially, 0.65 after two trainings (+81% after 480 seconds), and 0.41 after six trainings (+14% after 1440 seconds).

A Kolmogorov-Smirnov test for these proportions, between normal training and "coherent training", returns a p-value of 0.976.

Let us now analyze maximum normalized vestibular gain during the experiment. For normal training, 0% of the fish have a maximum normalized vestibular gain below 0.5, 46% between 0.5 and 1, 50% between 1 and 1.5, and 4% above 1.5. For "coherent training", 0% of the fish have a maximum normalized vestibular gain below 0.5, 66% between 0.5 and 1, 27% between 1 and 1.5, and 7% above 1.5. A Kolmogorov-Smirnov test for these two distributions returns a p-value of 0.997.

We show the proportions and maximum normalized vestibular gain for normal training and "coherent training" in figure V.17.

From this data, it does not seem like the increasing congruence has an impact on adaptation.

c) Vestibular stimulation in place of training leads to the same adaptation as mismatch training

In this "vestibular training" control, we need to show whether the multisensory environment has an influence on increasing vestibular gain along the experiment.

We compare the general evolution of vestibular gain between normal training and "vestibular training" in left and right panels of figure V.14. Going into more detail, the proportion of learners, half learners and non learners for "vestibular training" is as follow (figure V.16):

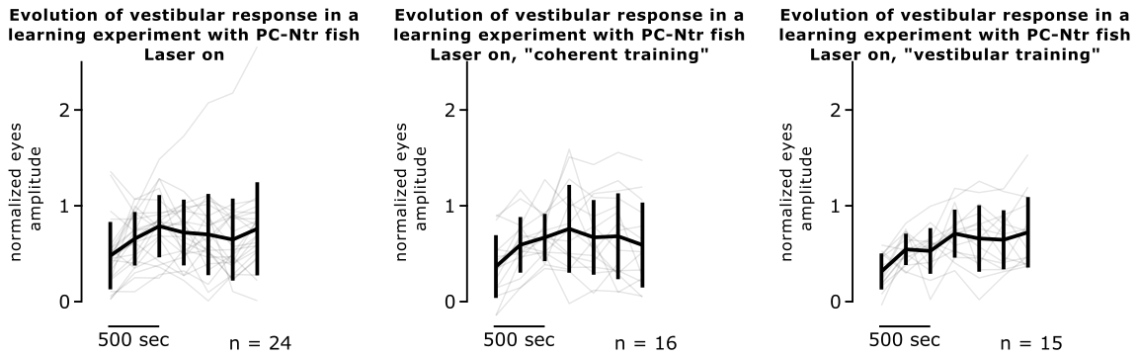

Figure V.14: Evolution of normalized eyes amplitude during learning experiments. Left panel is fish trained with increasing congruence in multisensory environment, middle panel is fish trained with a fixed congruence of 1 in a multisensory environment ("coherent training"), and right panel is fish trained only with vestibular stimulation, with no visual input ("vestibular training").

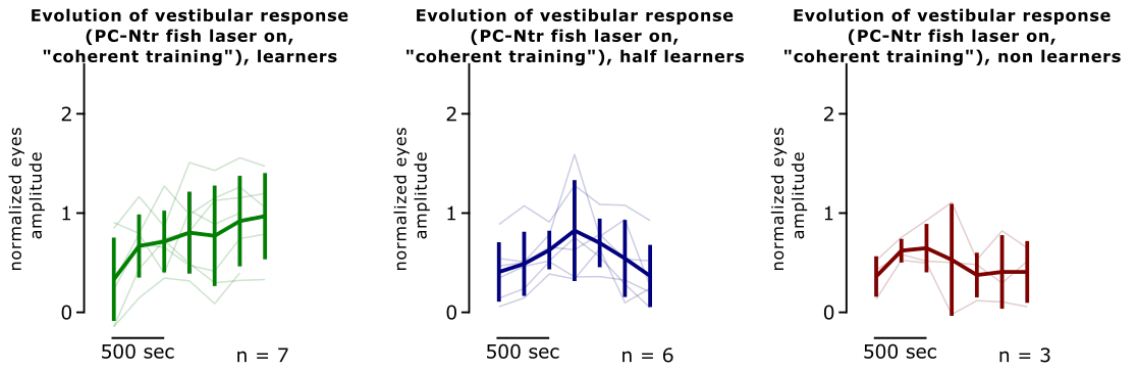

Figure V.15: Evolution of normalized eyes angle for 16 PC-Ntr fish, with laser on, during the learning experiment. Fish are trained with a fixed congruence of 1 in a multisensory environment ("coherent training"). The fish are sorted in different categories, upon how they performed behavioural adaptation. Left panel shows learners, i.e. fish whose eyes response is increasing during the whole experiment. Central panel shows half learners, i.e. fish whose eyes response is increasing at the beginning of the experiment, before decreasing, giving this bell-shape curve. Right panel shows non learners, i.e. fish whose response does not change during the protocol.

- Learners: 6 out of the 15 fish, or 40%. Normalized eyes amplitude is 0.25 initially, 0.68 after two trainings (+172% after 480 seconds), and 1.02 after six trainings (+308% after 1440 seconds).

- Half learners: 5 out of the 15 fish, or 33%. Normalized eyes amplitude is 0.34 initially, 0.55 after two trainings (+62% after 480 seconds), 0.39 and after six trainings (+15% after 1440 seconds).

- Non learners: 4 out of the 15 fish, or 27%. Normalized eyes amplitude is 0.38 initially, 0.28 after two trainings (−26% after 480 seconds), and 0.69 after six trainings (+82% after 1440 seconds).

A Kolmogorov-Smirnov test for these proportions, between normal training and "vestibular training", returns a p-value of 0.976.

Let us now analyze maximum normalized vestibular gain during the experiment. For normal training, 0% of the fish have a maximum normalized vestibular gain below 0.5, 46% between 0.5 and 1, 50% between 1 and 1.5, and 4% above 1.5. For "vestibular training", 0% of the fish have a maximum normalized vestibular gain below 0.5, 50% between 0.5 and 1, 38% between 1 and 1.5, and 12% above 1.5. A Kolmogorov-Smirnov test for these two distributions returns a p-value of 0.997.

We show the proportions and maximum normalized vestibular gain for normal training and "vestibular training" in figure V.17.

From this data, it does not seem like the multisensory environment has an impact on adaptation.

V.2.4 Adaptation seems to depend on the laser

a) Methods summary

The adaptation does not seem to depend on the multisensory environment. The last question we ask is whether this adaptation depends on the laser.

As we specified earlier in this chapter, light-sheet laser was on during all the experiments we described above. This was originally the case because we wanted to record the

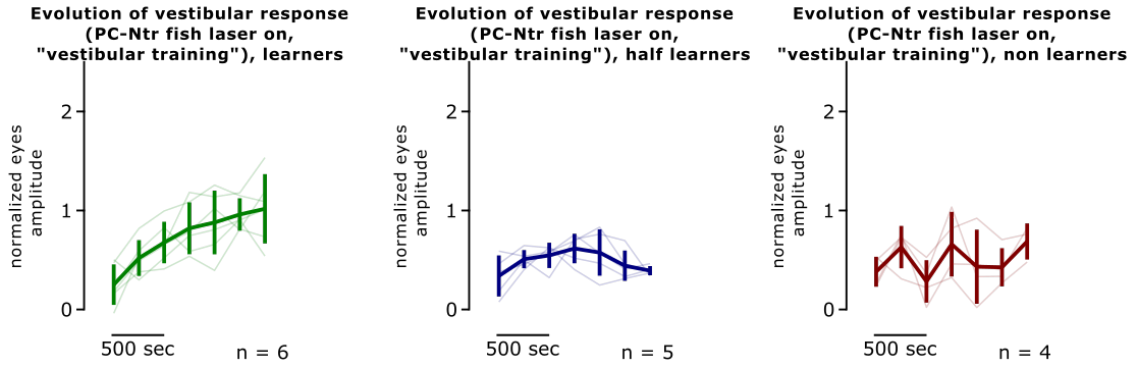

Figure V.16: Evolution of normalized eyes angle for 15 PC-Ntr fish, with laser on, during the learning experiment. Fish are trained only with vestibular stimulation, with no visual input ("vestibular training"). The fish are sorted in different categories, upon how they performed behavioural adaptation. Left panel shows learners, i.e. fish whose eyes response is increasing during the whole experiment. Central panel shows half learners, i.e. fish whose eyes response is increasing at the beginning of the experiment, before decreasing, giving this bell-shape curve. Right panel shows non learners, i.e. fish whose response does not change during the protocol.

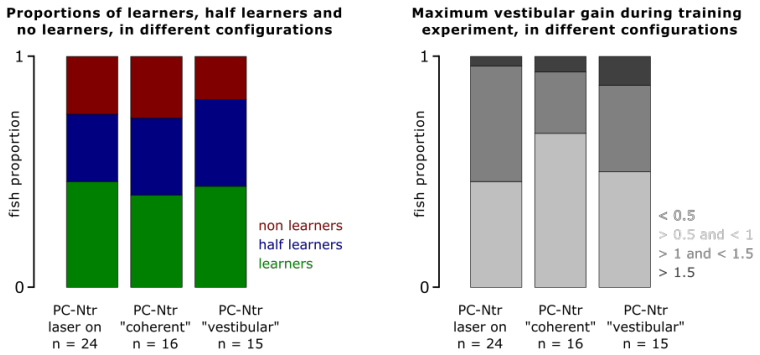

Figure V.17: Comparison between regular training with increasing congruence, "coherent training", and "vestibular training". Left panel: proportions of learners, half learners and non learners. Right panel: maximum normalized vestibular gain.

fish brain at the beginning and at the end of the experiment. We kept the laser after the initial period, because we wanted the protocol to be unchanged. In this last series of experiments, we are comparing the behaviour with and without laser.

The answer we seek is whether the adaptation we observe is due to the laser, or whether it has another cause.

b) Light-sheet laser has an influence on adaptation

Here, we compare the responses with laser to responses without laser, to analyze whether the laser has an influence on increasing vestibular gain along the experiment.

We compare the general evolution of vestibular gain between laser on and laser off configurations in figure V.18. Going into more detail, the proportion of learners, half learners and non learners for laser off is as follow (figure V.19):

- Learners: 3 out of the 17 fish, or 18%. Normalized eyes amplitude is -0.05 initially, 0.10 after two trainings (+300% after 480 seconds), and 0.32 after six trainings (+740% after 1440 seconds). Negative value is due to hand tracking error.
- Half learners: 4 out of the 17 fish, or 23%. Normalized eyes amplitude is 0.18 initially, 0.53 after two trainings (+194% after 480 seconds), and 0.06 after six trainings (-67% after 1440 seconds).
- Non learners: 10 out of the 17 fish, or 59%. Normalized eyes amplitude is 0.02 initially, 0.10 after two trainings (+400% after 480 seconds), and 0.16 after six trainings (+700% after 1440 seconds). The very high increase is simply due to the fact the the initial response is really low. A response of 3.2° at the end of the experiment, for a stimulation of 20° makes us conclude the fish does not really respond to the stimulation.

A Kolmogorov-Smirnov test for these proportions, between laser on and laser off, returns a p-value of 0.320.

Let us now analyze maximum normalized vestibular gain during the experiment. For laser on configuration, 0% of the fish have a maximum normalized vestibular gain below 0.5, 46% between 0.5 and 1, 50% between 1 and 1.5, and 4% above 1.5. For laser off

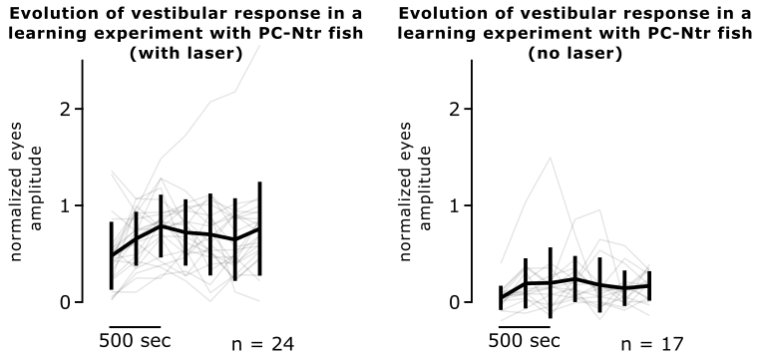

Figure V.18: Evolution of normalized eyes amplitude during learning experiments. Light-sheet laser is on for left panel, and is off for right panel.

configuration, 28% of the fish have a maximum normalized vestibular gain below 0.5, 44% between 0.5 and 1, 28% between 1 and 1.5, and 0% above 1.5. A Kolmogorov-Smirnov test for these two distributions returns a p-value of 0.534.

We show the proportions and maximum normalized vestibular gain for laser on and laser off configurations in figure V.20.

From this data, it does seem like the laser has an impact on adaptation.

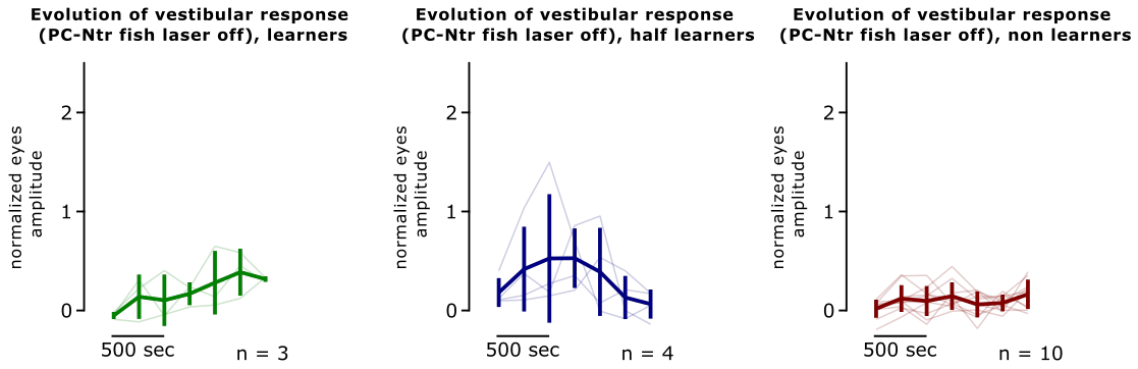

Figure V.19: Evolution of normalized eyes angle for 17 PC-Ntr fish, with laser off, during the learning experiment. The fish are sorted in different categories, upon how they performed behavioural adaptation. Left panel shows learners, i.e. fish whose eyes response is increasing during the whole experiment. Central panel shows half learners, i.e. fish whose eyes response is increasing at the beginning of the experiment, before decreasing, giving this bell-shape curve. Right panel shows non learners, i.e. fish whose response does not change during the protocol.

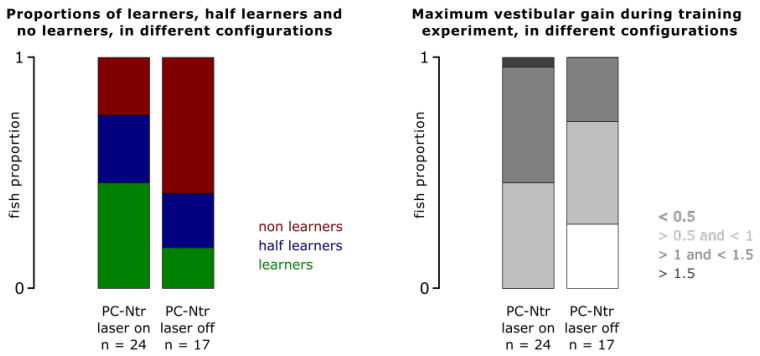

Figure V.20: Comparison between laser on and laser off configurations. Left panel: proportions of learners, half learners and non learners. Right panel: maximum normalized vestibular gain.

V.3 Discussion

In this chapter, we found fish could radically change their behavioural response. We started by noticing a VOR gain evolution for one fish, from 26° to 40°, for a 20° vestibular stimulation. This represented a positive evolution of 53 % along the 24 minutes of the experiment alternating training and test periods, with an increasing visual congruence during training phases. We hypothesized this behaviour was reproducible, and tested the same experiment on 28 additional fish. More than 40% of them demonstrated a sustained increase in response.

At this point, we thought this change in behaviour might be due to cerebellar motor learning, and submitted Purkinje cells ablated fish to the same experiment. Fish were successfully ablated with metronidazole at 4 dpf. In both control and ablated fish, 46 % of them demonstrated sustained increase in response. Additional statistical tests gave us the indication that the ablation of these important cells of the cerebellum had no influence on VOR gain change.

In order to be sure that this evolution was due to the mismatching multisensory environment, we then performed control experiments. To our surprise, the increasing visual congruence seemed to have no effect on sustained increase (44 % of the fish), and removing visual information led to the same proportion of adapting fish (40 % of them). Shutting the laser on the other hand provided a much lower amount of sustained adaptation, with only 18 % of the fish showing this behaviour.

The influence the laser has on this increase in behavioural response could be explained in different ways. Following is a non exhaustive list of hypotheses.

It is possible that the animals are stressed by the laser, and stress has been shown to provoke erratic behaviour in zebrafish [225]. What we observe though, is a behaviour that seems more consistent than erratic, with an elevated number of fish increasing their VOR response along the experiment.

Another hypothesis is that the laser amplifies eyes rotation. Beppi *et al.* [226] [227] have shown that the startle reflex habituation was modified when flashes of light above a certain intensity were provided. In these experiments, light intensity had a positive impact on total distance travelled by the fish. It is possible that the laser has a similar influence on their VOR response, with no other influence from their visual environment.

The laser could also be stimulating a neuromodulatory area of the brain, releasing neurotransmitters that in turn increase the VOR response. The dorsal raphe nucleus for instance has been shown to be involved in short-term motor learning [169], possibly through the release of serotonin. Maybe the raphe is stimulated by high intensity laser, or another region of the brain involved in such processes.

Our last hypothesis is that the laser stimulates deep brain photoreceptors of the animal. Because larval zebrafish are mostly transparent between 5 and 8 dpf, the laser can easily enter the fish central nervous systems, and trigger a reaction that is hard to predict. We have known for a while that deep brain photoreceptors exist in non mammalian vertebrates [228], and they have been shown to be scattered across the zerbafish brain [229]; enucleated zebrafish even have light-seeking behaviour [230]. With this information in mind, the increase in VOR response could therefore be due to a state of extreme wakeness in the fish, with highly stimulated deep brain photoreceptors.

Initially, as we thought the mismatching multisensory environment had an influence on response, we were excited to test the limits of this learning context. We hypothesized that the increment in visual congruence could have an impact on response. This could have been the reason for the half learner behaviour observed during the experiment, with fish increasing their response, before they stopped responding. We hypothesized that the visual flow perceived by the animals could trigger a give-up behaviour, and that an incremental learning, instead of an "all-in" learning could produce different proportions of

learners. We though of computing fish response during an initial vestibular recording, and starting from this initial gain, instead of systematically starting with a training congruence of 1, to further test whether the behavioural distance to goal had an influence on learning success.

The greatest limitation of this chapter is that we did not have time to perform experiments at intermediate laser powers. As we explain in more detail in annex VIII.3, laser power does have an influence on whether the fish integrates visual information. At low laser power, it seems the fish is able to perceive visual information, as the behavioural response to multisensory stimulations is different from responses to vestibular and visual stimuli. We even observe super-additivity when stimuli are coherent. At higher laser power, there is no evidence that visual information is involved in fish behaviour. It is possible that an amount of fish between 16 % (no laser) and 46 % (laser on) could have been learners at intermediate laser power.

The strength of this study is the identification of a simple protocol that triggers learning in larval zebrafish as young as 5 to 8 dpf. Using this protocol, it could be possible to record the brain of the animals, and have a whole-brain information of the learning mechanisms, provided that the larvae are more stable in agarose. We have not been able to explain precisely the reasons why a high power laser has such an effect on VOR evolution, but research on learning and adaptation certainly has a bright future, with a protocol that allows recording brain wide neuronal activity during the learning period. Such population recordings also in specific cell types would be very informative and such experiments are currently not possible in other model systems.

VI – Contribution to submitted article

During my thesis, I contributed as second author to an article written by Natalia Beiza-Canelo, and recently submitted, *Magnetic actuation of otoliths allows behavioral and brain-wide neuronal exploration of vestibulo-motor processing in larval zebrafish.* This article is provided in chapter IX.

In the experiments described in the previous chapters, the vestibular system was stimulated by physically rotating the fish around its rostro-caudal body axis. The problem with these rotations is that they make it technically difficult to simultaneously perform large-scale neuronal recordings using light-sheet microscopy, or circuit interrogation using optogenetic tools. My host lab overcame this challenge for functional imaging by developing a rotating ultra-stable miniturized light-sheet microscope [45], which I successfully used in my thesis. But it is even more challenging to add optogenetics or electrophysiology to this rotating system in addition to the light-sheet microscope.

For her article, Natalia developed a new way to stimulate the inner ear of the fish without having to rotate the animal in space. A ferrofluid was injected into the animal's vestibular system, resulting in magnetic nanoparticles covering their utricular otoliths. Moving a magnet in close proximity to the fish was then sufficient to elicit a vestibular response, just like a normal body rotation. The advantage of the method is that it is compatible with all standard optical and electrophysiological methods used in neuroscience.

The behaviour of the injected fish to this fictive magnetic stimulation was similar to the response when fish were physically rotated, and the same vestibular neuronal clusters were revealed in the brain. This new technique opens the door to new multisensory protocols, including vestibular stimulation on short time scales, e.g., mimicking in immobilized fish the vestibular feedback they receive when swimming freely.

For this article, I did the control experiments on rotated fish. I measured with the rotating light-sheet microscope the average behavioural response to a physiological vestibular stimulation in 39 fish, and I recorded the evoked neuronal activity from 8 fish and computed an average phase map revealing the vestibular clusters of the brain for comparison.

VII – Conclusion and perspectives

Sur le plus haut trône du monde, on n'est jamais assis que sur son boule.
Élie Yaffa, inspiré par Michel Eyquem De Montaigne

VII.1 Summary

Multisensory integration is happening at every second of our lives, and this thesis aimed at clarifying some behavioural and neuronal aspects of this process. Many regions in the brain have already been identified to be multisensorial, and modern day technologies such as light-sheet imaging, in combination with innovating animal models such as the genetically altered zebrafish allow us to look underneath the skull and understand better how multisensory stimuli are combined from a neuronal perspective.

We started by explaining the data gathered in the lab after years of research. We discussed ways to link neuronal signals to experimental stimulations, and showed a tool allowing to efficiently visualize responsive areas inside the brain. We compared responses to different stimuli, and identified multimodal areas near motor regions, in the cerebellum, and in the dorsal hindbrain of the fish. This initial work was a good first step into multisensory integration, but the fact that the experiments were not done on the same fish was definitely a limit, since we could not tell whether the neurons just intermingled in the multimodal regions, or if they were multisensory themselves.

So we then built an experiment in which the fish underwent two kinds of stimulations, to actually identify multisensory neurons. This work focused on the vestibular and visual systems, because they are well conserved across species, and functional in larval zebrafish. From a behavioural perspective, we found that responses to vestibular, visual, and multisensory stimulations were widely variable, and that the coherence of these stimuli would elicit super-additive behaviours. Diving in the brain of the animals, we were able to identify a multisensory cluster that was very consistent across fish. Neurons responses could be modeled linearly, and another cluster of super-additive neurons was discovered, bridging the gap with the behaviour observed. This super-additive area largely overlapped with the multisensory area discovered. Although these two regions included a large percentage of the oculomotor neurons of the brain, these motor regions only made up for less than 10% of the total number of multisensory and super-additive neurons. This provided the information that other neurons in the brain process multisensory signals.

We next focused on visual integration in a multisensory environment, through contrast influence. In a conflicting multisensory environment situation, we did not see an influence of contrast on response, but in a coherent one the fish response had a logarithmic relationship to contrast, confirming unisensory observations of the literature. Neuronal responses in the brain associated to visual stimulation also showed this logarithmic dependence to contrast.

In the last chapter, we took a different turn. A wrong setting in an experiment led me to observe a great increase in behavioural response in a mismatching multisensory environment. This chapter aimed at digging into this exciting new observation, and finding out if this increase was provoked by these multisensory conditions. Contrary to what we initially thought, the multisensory nature of the fish environment did not seem to be the reason of the observation we made. The laser on the other hand, or rather the absence of it, led to no adaptation. It was unclear to us why this was, and we raised a few hypotheses about how the laser could change the behaviour of the fish, through stress, neuromodulation, or deep brain photoreceptors stimulation.

VII.2 Future perspectives

Future perspectives of this thesis would include developing a new protocol that allows to envisage more than two sensory stimulations. It could be possible to use auditory cues, or skin taps, and see if the multisensory neurons we observe in this work are also responsive to these stimuli. The magnetic nanoparticles and the associated vestibular protocol used by Natalia in her article could help build a more compact setup, and include the new stimuli more easily.

The adaptation protocol we described raises exciting new questions on learning in fish as young as 5 dpf. We did not have time to push the experiment further and investigate in detail reasons why the behavioural gain increases so much, but at the moment it is hard to believe this increase is random. Being able to understand how behaviour is modulated the way we observed could provide interesting insights as to how young animals adapt their behaviour to survive.

In order to further study multisensory circuits, we could ablate the identified multisensory region or super-additive region. Recording the behaviour of the animals would then give insights on the underlying neuronal computations. Moreover, we could establish the exact neuronal circuit responsible for behaviour by recording behaviour and neuronal activity at the same time. I tried it for some experiments, but had a lot of artefacts from eyes movements, and the data was not usable. We could also label specific neurons with appropriate zebrafish lines. Finally, we could study connections numerically (a first approach was done in figure III.14). In the end, the multisensory area could definitely modulate lots of different areas in the brain, and deserve to be studied in more detail.

VIII – Technical annexes

VIII.1 F-statistic analysis

To compute the F-statistic, we do two linear regressions. The first one is a degenerate linear regression, with only one regressor, corresponding to a column of ones (with one regressor, the first parameter is $p1 = 1$). In the second linear regression, we put the additional regressors we want (suppose for instance we have 4 new regressors, $p2 = 5$). The first degree of freedom for the F-statistic is the number of additional regressors for the second linear regression $p2 - p1$. The second degree of freedom is the number of points our vectors have (n). We then compute the sum of the square of the residuals for the two models, and obtain $RSS1$ for the degenerate model, and $RSS2$ for our test model. The F-statistic is given by the following formula:

$$F_{stat} = \frac{\frac{RSS1 - RSS2}{p2 - p1}}{\frac{RSS2}{n - p2}}$$

VIII.2 Multisensory atlas, other averaging method

As mentioned in the second chapter, we chose an averaging method, because it did not penalize the lack of neuron at a particular grid point. In figures VIII.1, VIII.2, and VIII.3, we show the results for the alternative averaging method, in which the lack of neurons at a grid point results in an F-statistic of 0 for this grid point.

VIII.3 Influence of laser on behaviour

The first behaviour experiments we did with laser at high power ($24mW$ before lightsheet creation) showed different results from no laser experiments. This may be due to the laser hitting the left eye, blinding the fish, blocking vision of moving gratings. In order to have the same behaviour with and without laser, so that the neuronal data make sense, we lowered the laser power, and compared the results. With laser at $10mW$ before lightsheet creation, the behaviours are comparable (figure VIII.4), and in order to confirm it, we analyzed response to multisensory stimulation and super-additivity.

Comparing response to vestibular and to coherent stimulation gives a good idea on whether visual stimulation is correctly perceived. We performed a t-test on the difference between vestibular and coherent responses for laser off and laser on at $10mW$, and the

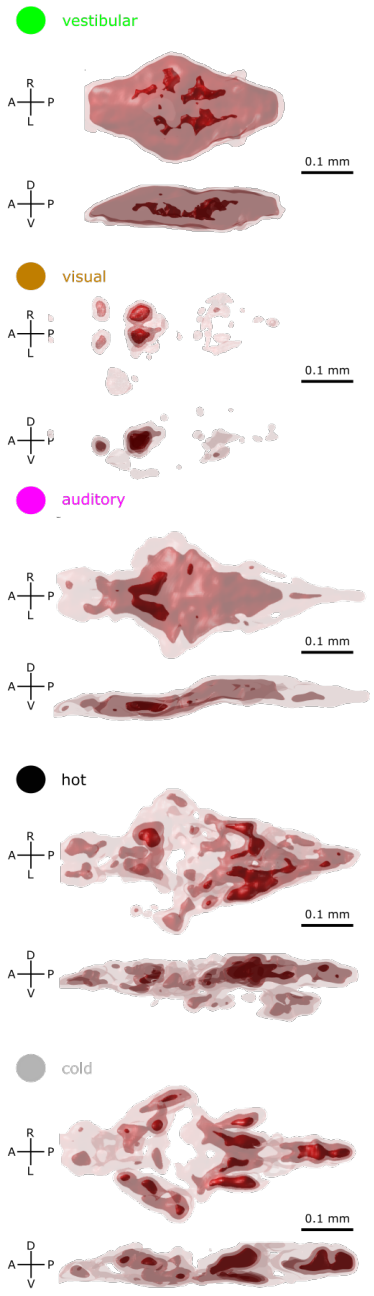

Figure VIII.1: F-statistic isovalues. Scarlet red corresponds to top 2.5% F-statistic, intermediary red to 5% and light red to 10%.

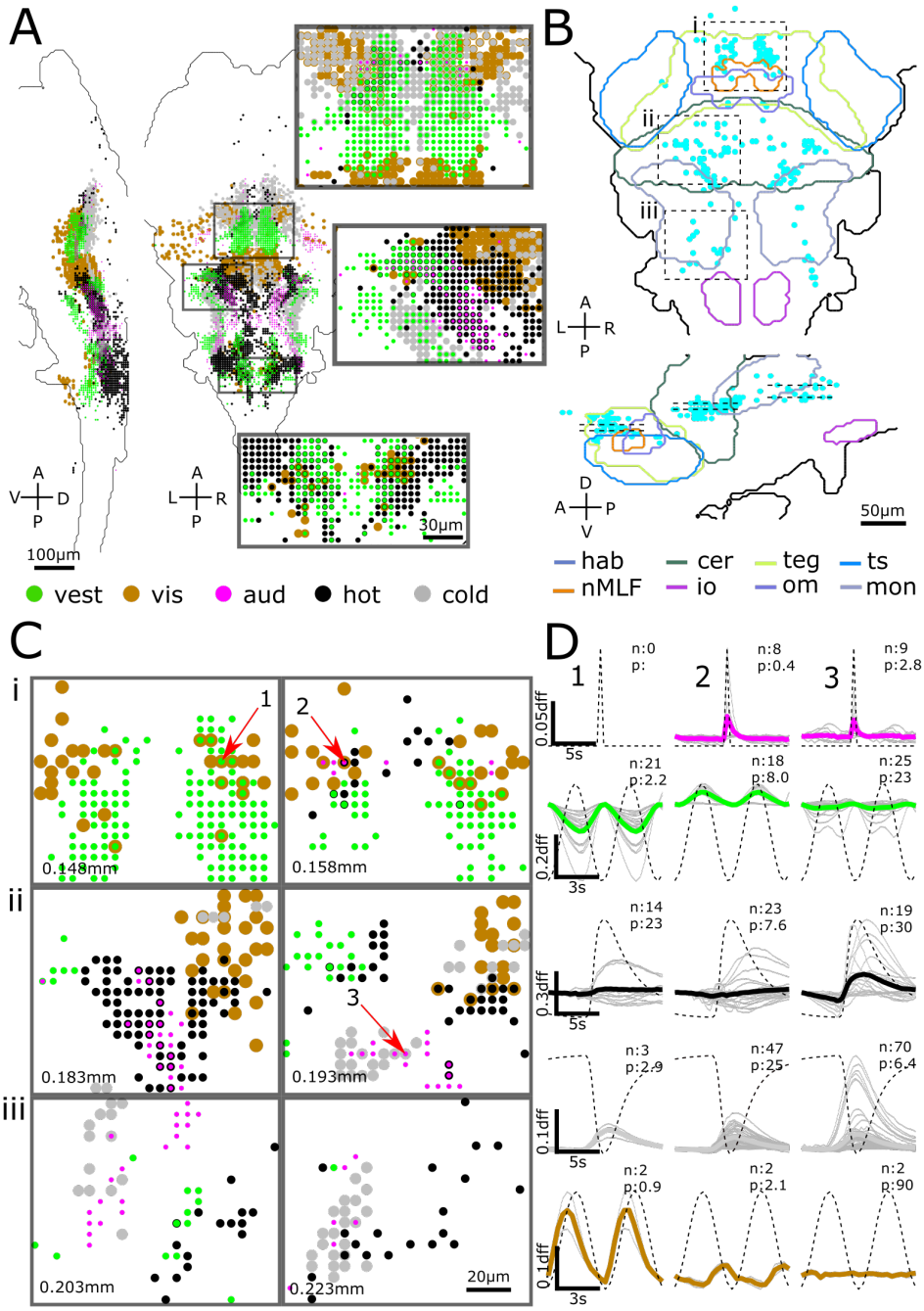

Figure VIII.2: Representation of the 2.5% most responsive grid points, using F-statistic. (A) Projection of most responsive grid points in midsagittal plane and frontal plane with details on the right. (B) Grid points responding to more than one modality in light blue, projections on frontal and midsagittal planes. Important brain areas contours are specified (hab: habenula, cer: cerebellum, teg: tegmentum, ts: torus semicircularis, nMLF: nucleus of the medial longitudinal fasciculus, io: inferior olive, om: oculomotor nucleus, mon: medial octavolateral nucleus). (C) Details for specific planes. (D) Averaged answer to stimuli for neurons associated to grid points selected in (C). n is the total number of neurons whose signals were averaged and p is the proportion of grid points with a higher F-statistic.

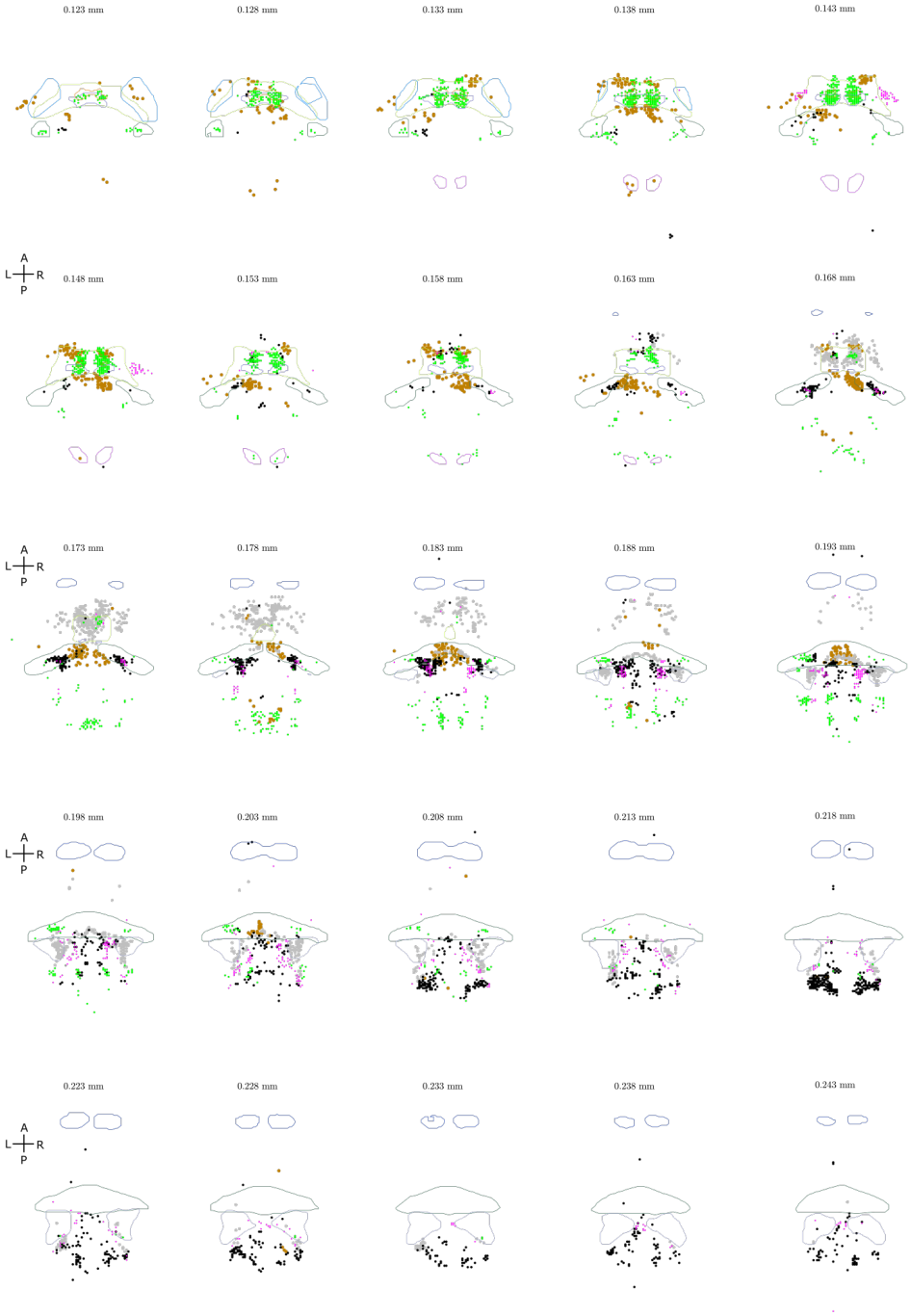

Figure VIII.3: Detail of each frontal plan for 2.5% most responsive grid points, for each modality. Vestibular is in green, visual in brown, auditory in purple, hot in black, and cold in grey.

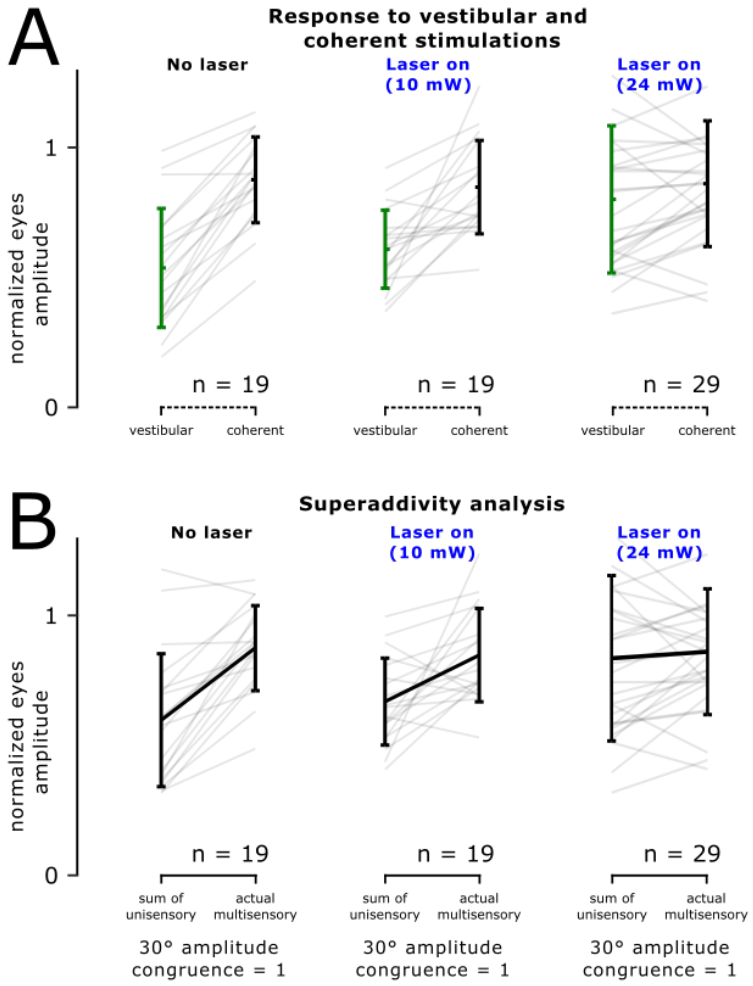

Figure VIII.4: Influence of laser power on response. Laser power is before light-sheet creation.

p-values were respectively p = 2.68E-08 and p = 1.26E-04 (it was p = 3.69E-02 for laser on at $24mW$). We also checked for super-additivity, which is an interesting behaviour we wanted analyzed in the neuronal data, by comparing the sum of unisensory responses, and the actual multisensory response. A t-test on the difference for laser off and laser on at $10mW$ gave respective p-values of p = 5.57E-06 and p = 4.49E-03 (it was 0.46 for laser on at $24mW$).

Although the p-values are never the same for multisensory comparison and super-additivity check, values for laser at $10mW$ are significant enough to believe we have the same kind of behaviour with and without low power laser, with just a slight influence of it on response.

VIII.4 Neuron localization

Here I describe a program I did that improved neurons detection from whole-brain imaging data.

We want to identify neurons on a layer of the brain. Previously to this analysis, we have created a mask to contour the brain and not the whole image. Here are the different steps of the segmentation algorithm:

- We create a gaussian filter, approximately the size of a neuron.
- We create a new mask for the image, removing pixels below a certain value, to remove some of the background.
- We perform a linear regression of the gaussian filter on each pixel of the image to segment. This returns a coefficient, and an F-statistic (which tells us how that regression performs compared to a degenerate regression).
- We then take the F-statistic matrix for each pixel, and apply a new mask: the linear regression coefficients higher than a certain value.
- We convolve this new matrix with the initial gaussian filter.
- We perform a new linear regression on that convolved matrix, with the gaussian filter. We only keep the regression coefficient this time.
- From that matrix of coefficient, each pixel with a value higher than all its neighbours is going to be considered a neuron center.
- Every center is assigned a fixed shape, a circle of 6 µm. Every pixel inside of that circle is taken as part of the neuron.

When the parameters for the background and the coefficient for the first linear regression are properly defined, this algorithm allows to finely identify the neurons on a layer of the brain. It seems more effective than the algorithm formerly used in the lab, the watershed algorithm (figure VIII.5): as a matter of fact, it detects more precisely locations where there is no neuron. Its limitation is that if several neurons are very close to each other, it will only detect one of them, so the amount of neurons detected is going to be lower than the actual number of neurons.

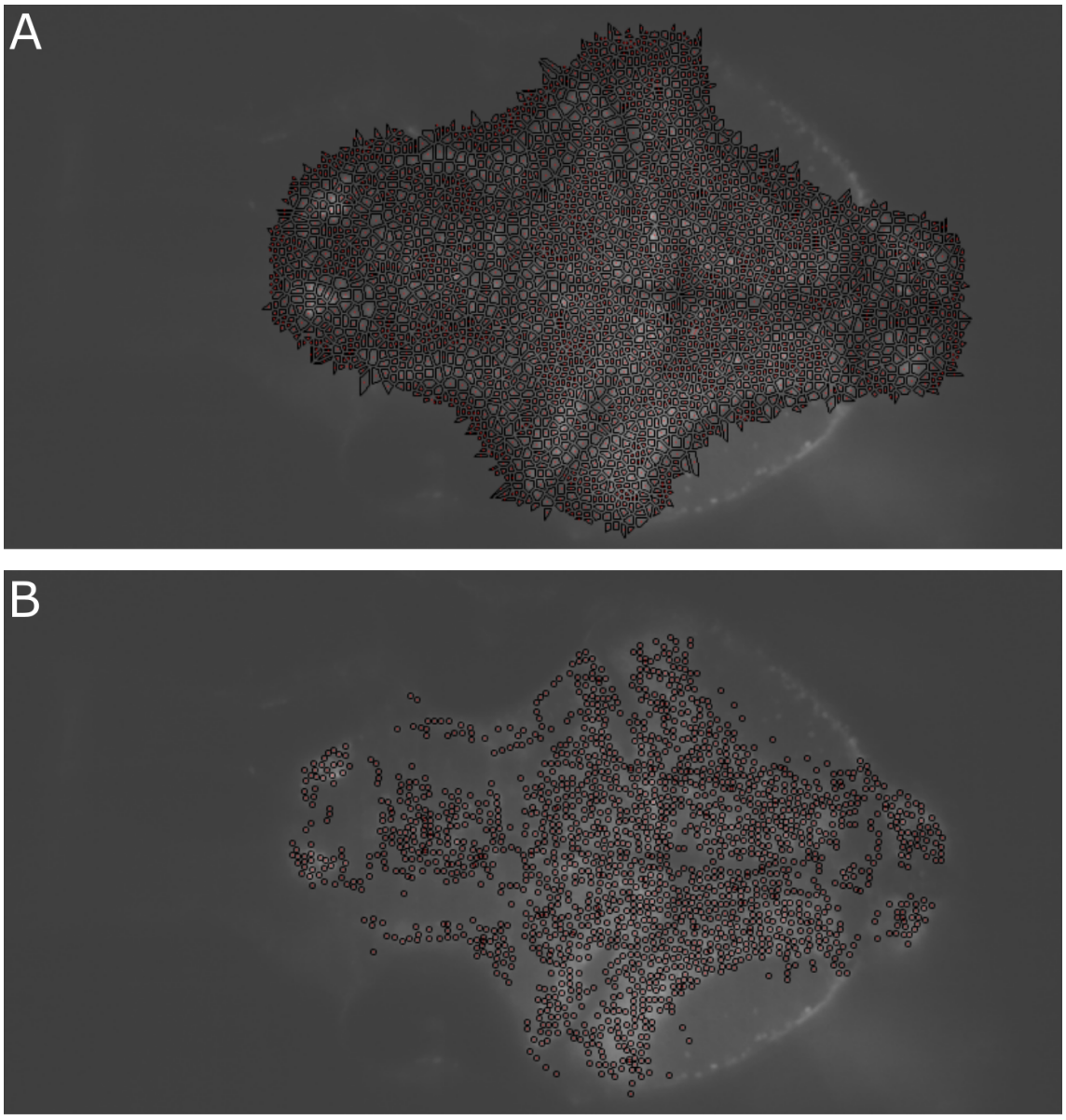

Figure VIII.5: Layer of whole-brain recording for one fish, with identified neurons. **A**: Watershed algorithm. **B**: Algorithm I developed.

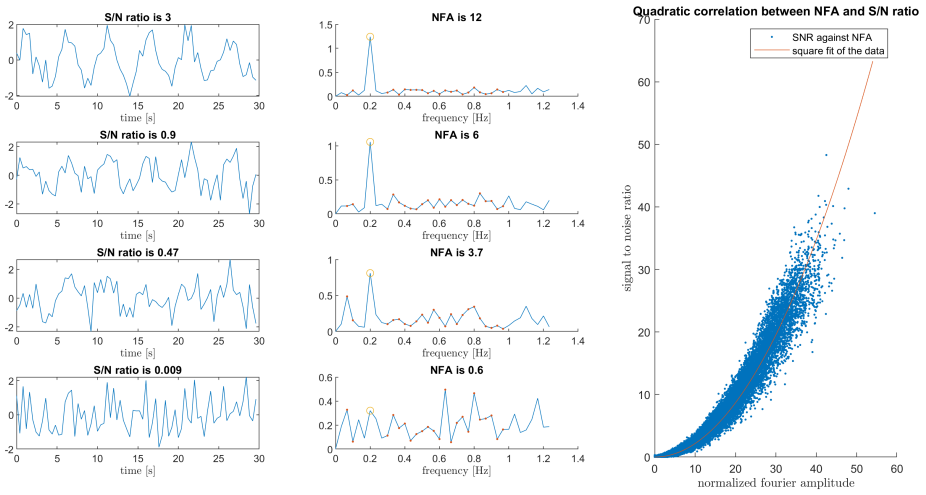

Figure VIII.6: Comparison between signal to noise ratio and normalized Fourier amplitude for sine signals with different noise levels. Left colum shows actual signal, middle column shows amplitudes in the frequency space (yellow dot is the frequency of interest, red dots are frequencies used for normalizing window), and right plot shows relationship between normalized Fourier amplitude and signal to noise ratio for 50,000 signals.

VIII.5 Normalized Fourier Amplitude

To compute the normalized Fourier amplitude, we first compute the discrete Fourier transform for our signal. We then take the amplitude associated to the frequency of stimulation, A. We then define a window around this frequency, without taking the amplitudes around our reference frequency, nor the 0 frequency into account. We compute the average amplitude associated to this frequency window, n. We then normalize A to obtain the normalized Fourier amplitude, using the following formula: $NFA = \frac{A-n}{n}$. If this value is below 0, we set it to 0.

Figure VIII.6 shows signal to noise ratios and normalized Fourier amplitudes for generated sine signals with different noise levels. The relationship between the signal to noise ratio ($SNR = \frac{E(signal^2)}{E(noise^2)}$) and the normalized Fourier amplitude can be described with the following polynomial equation: $SNR = 0.0216 \cdot NFA^2$. This shows us that the normalized Fourier amplitude depends only on the square root of the signal to noise ratio at a certain frequency.

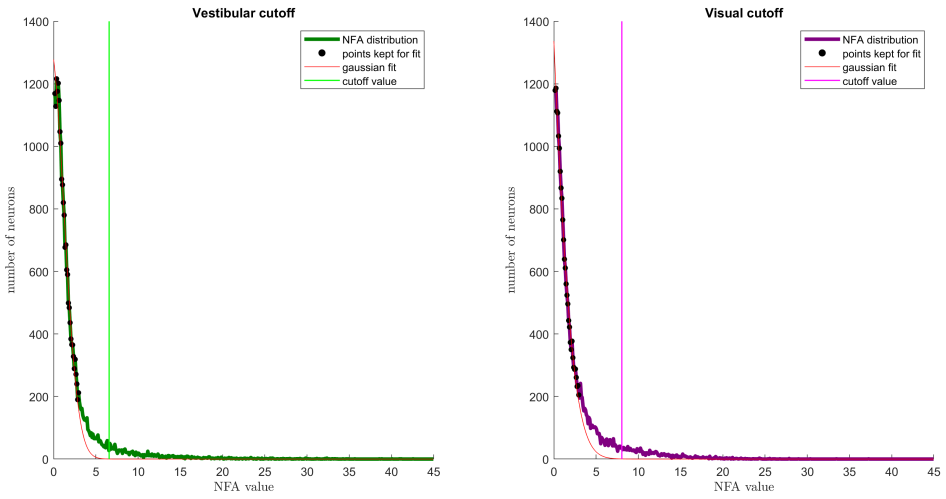

Figure VIII.7: NFA distributions, first 30 points used to fit gaussian, and associated cutoff values for vestibular on left panel, and visual on right panel, for one fish.

VIII.6 Cutoffs in NFA distributions

In order to define which neurons are responsive to either vestibular or visual signal, we set a threshold value. We do that by fitting a gaussian on the first 30 points of the NFA distribution. The cutoff value is then set to be 3 standard deviations from the mean of this gaussian, corresponding to the observed tail (figure VIII.7).

VIII.7 Kernel density estimation

A kernel density estimations (KDE) allows to estimate the probability density function of a random variable based on kernels, according to the following formula:

$$KDE(x) = \frac{1}{n \cdot h} \Sigma_{i=1}^{n} K(\frac{x - x_i}{h})$$

In this formula, n is the number of points considered, h is the bandwidth (a smoothing parameter), and K is the kernel. In my case, x_i are 3D coordinates vectors of points of interest, x is the 3D coordinates vector of the point whose KDE needs to be estimated, and the kernel is a multivariate gaussian distribution. The bandwidth is $12.8\mu m$, which roughly corresponds to one neuron and a half.

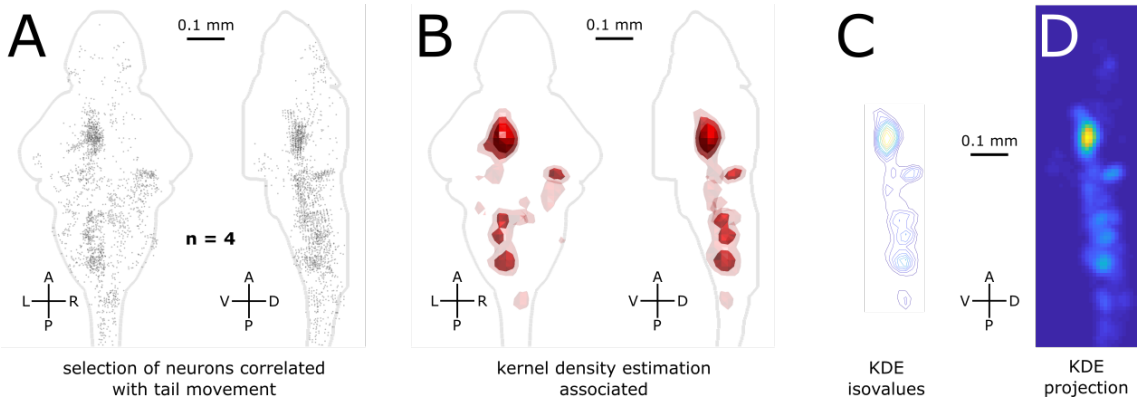

Figure VIII.8: **A**: Selection of neurons across four fish, correlated with tail movement. **B**: KDE associated to neurons displayed in **A**. **C**: KDE isovalues in the YZ plan. **D**: KDE values projection on the YZ plan.

I designed a Matlab class allowing to manipulate KDEs in a practical manner. This class makes it easy to add new coordinates, and plot the density estimation in different ways: 3D or 2D isovalues, and KDE values projection (figure VIII.8).

VIII.8 Details on multisensory and super-additive regions

In figure III.13 we show regions overlapping with multisensory area. Figure VIII.9 shows this overlap layer by layer. Similarly, figure VIII.10 shows the overlap layer by layer for figure III.21.

VIII.9 Neuronal phasemaps for multisensory integration

Figures VIII.11, VIII.12, VIII.13, VIII.14, VIII.15, VIII.16, and VIII.17 are the detailed phasemaps for different stimulations. Phasemaps are shown layer by layer, and the last picture is a projection on the transverse plane. Some brain regions are plotted as well. Average phasemaps are computed out of 16 fish.

VIII.10 Eyes hand tracking error

Figure III.4 explains how eyes tracking is handmade. In order to measure how reliable this method is, we tracked 30 images twice, and computed the 30 tracking errors (figure

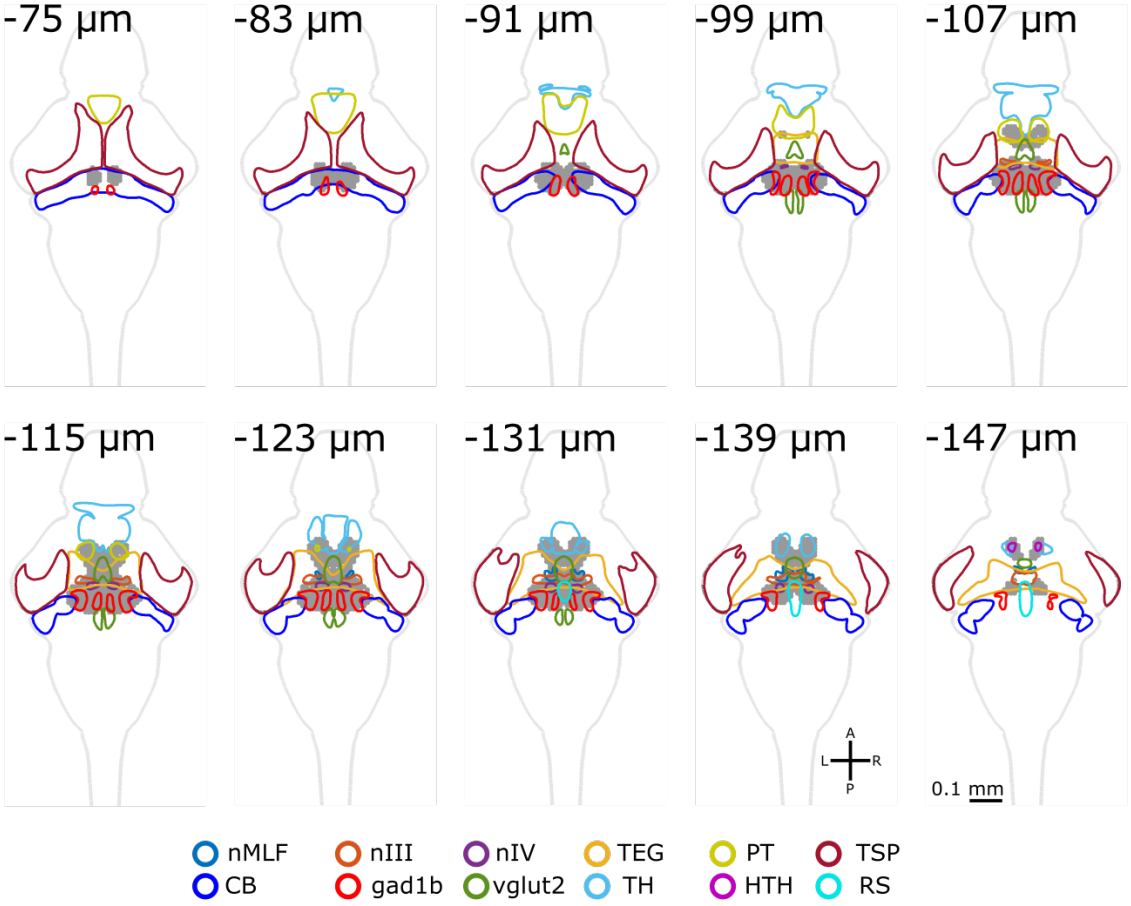

Figure VIII.9: Regions from ZBrain atlas overlapping with multisensory area (shaded grey), layer by layer. ZBrain atlas regions are from Randlett *et al.* [105]. nMLF: nucleus of the medial longitudinal fascicle, nIII: oculomotor nucleus, nIV: trochlear nucleus, TEG: tegmentum, PT: pretectum, TSP: tectum stratum periventriculare, CB: cerebellum, gad1b: gad1b inhibitory clusters, vglut2: vglut2 cluster 1, TH: thalamus, HTH: hypothalamus 6.7FRhcrtR-Gal4 cluster, RS: raphe superior.

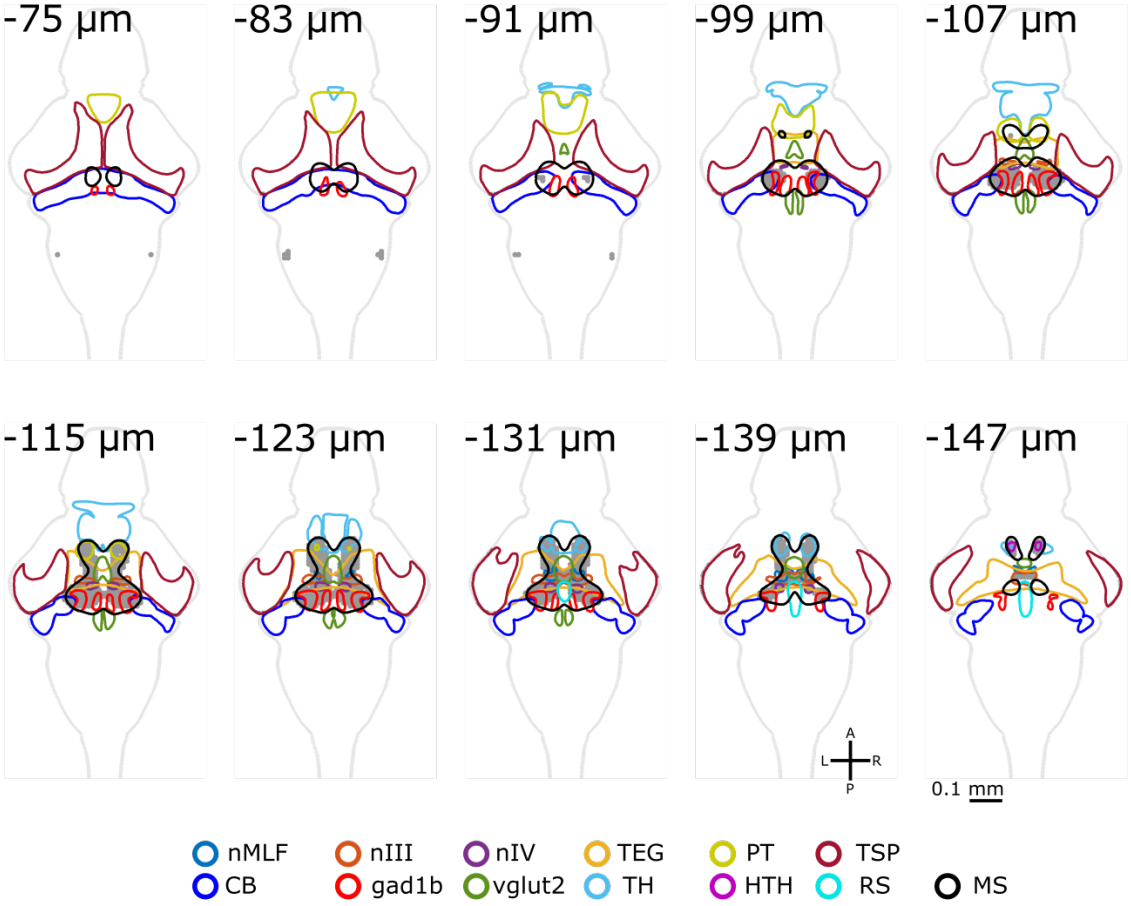

Figure VIII.10: Regions from ZBrain atlas overlapping with super-additive area (shaded grey), layer by layer. ZBrain atlas regions are from Randlett *et al.* [105]. nMLF: nucleus of the medial longitudinal fascicle, nIII: oculomotor nucleus, nIV: trochlear nucleus, TEG: tegmentum, PT: pretectum, TSP: tectum stratum periventriculare, CB: cerebellum, gad1b: gad1b inhibitory clusters, vglut2: vglut2 cluster 1, TH: thalamus, HTH: hypothalamus 6.7FRhcrtR-Gal4 cluster, RS: raphe superior, MR: multisensory region.

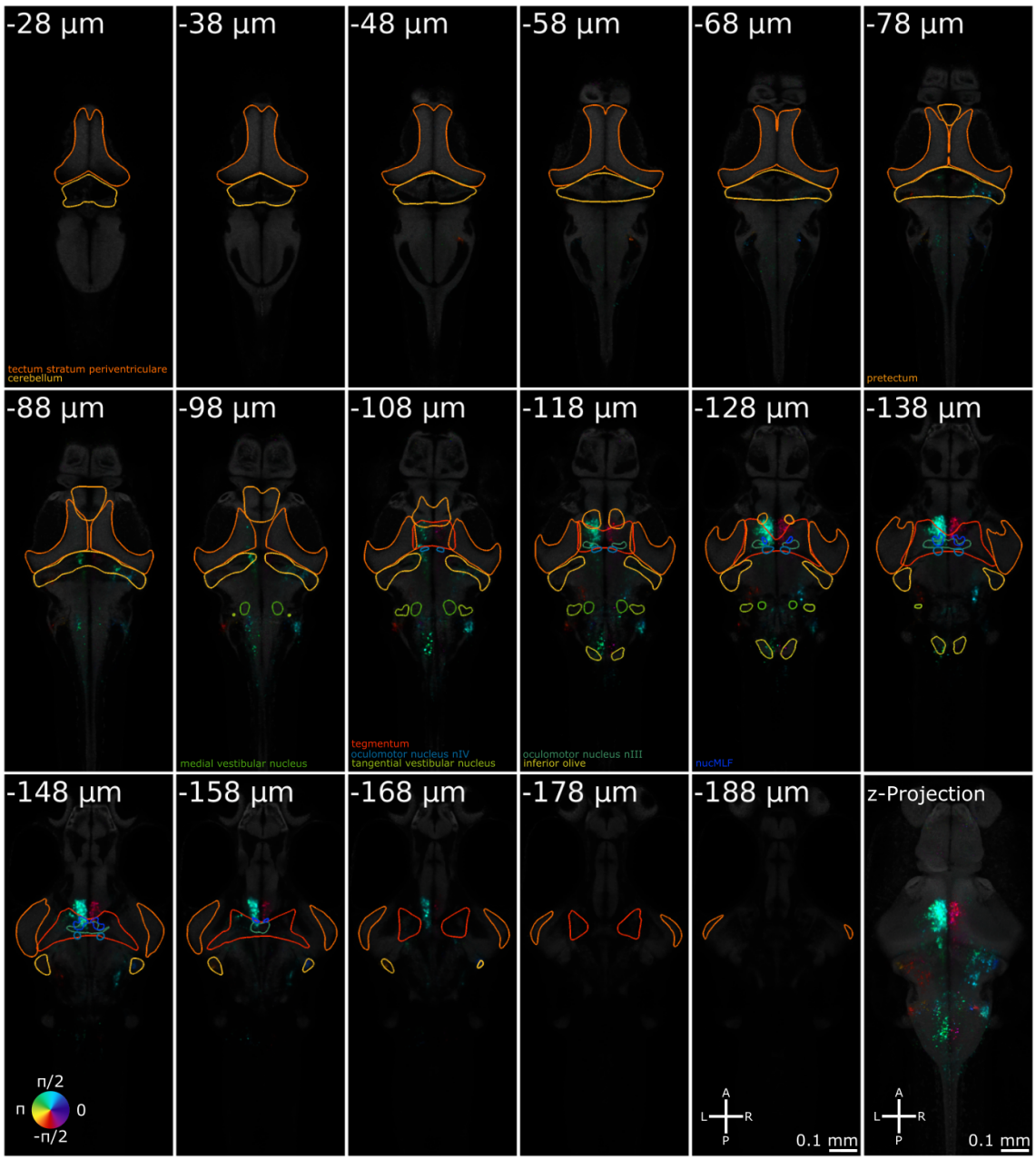

Figure VIII.11: Vestibular phasemap.

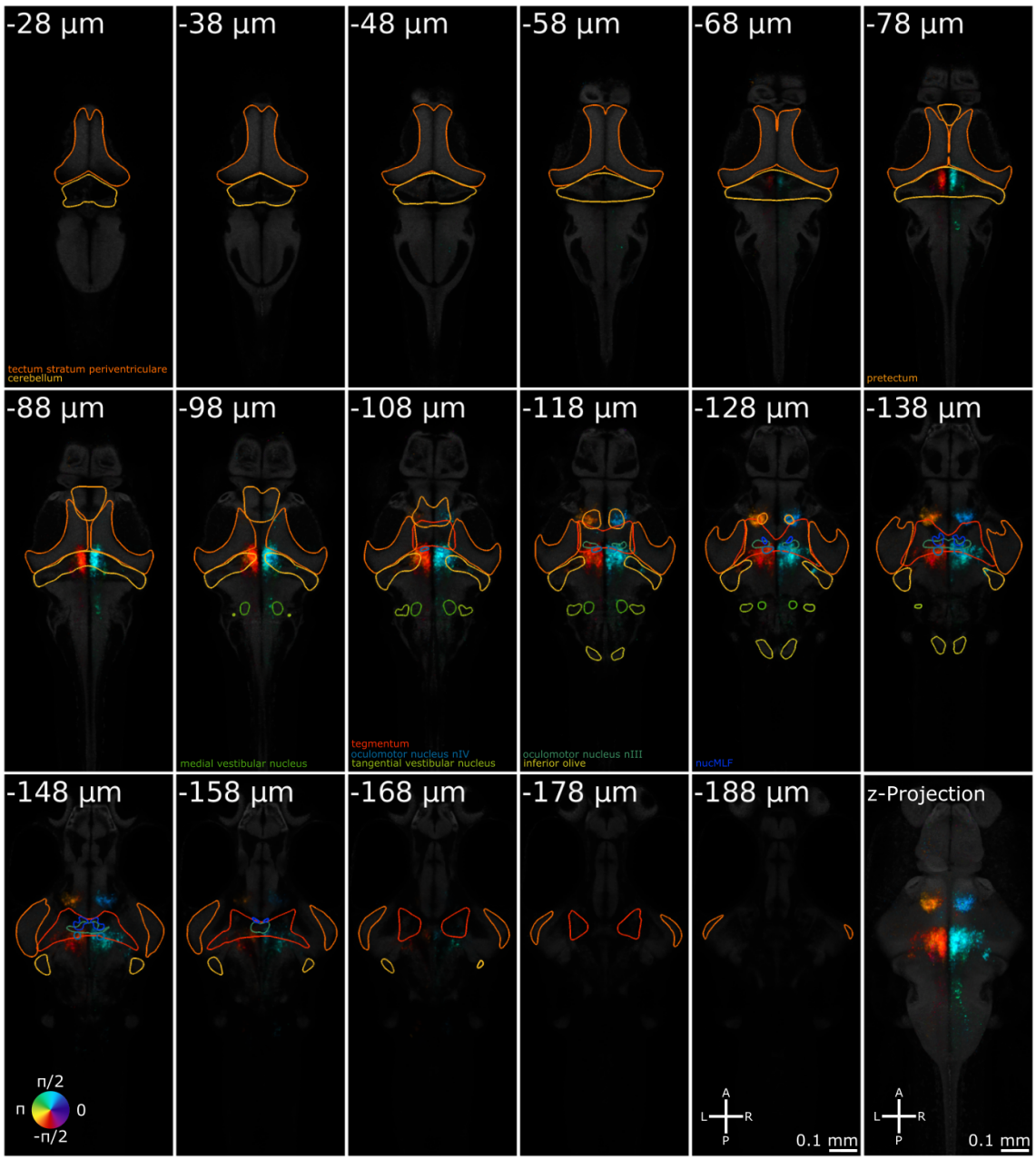

Figure VIII.12: Visual phasemap with a phase of 0.

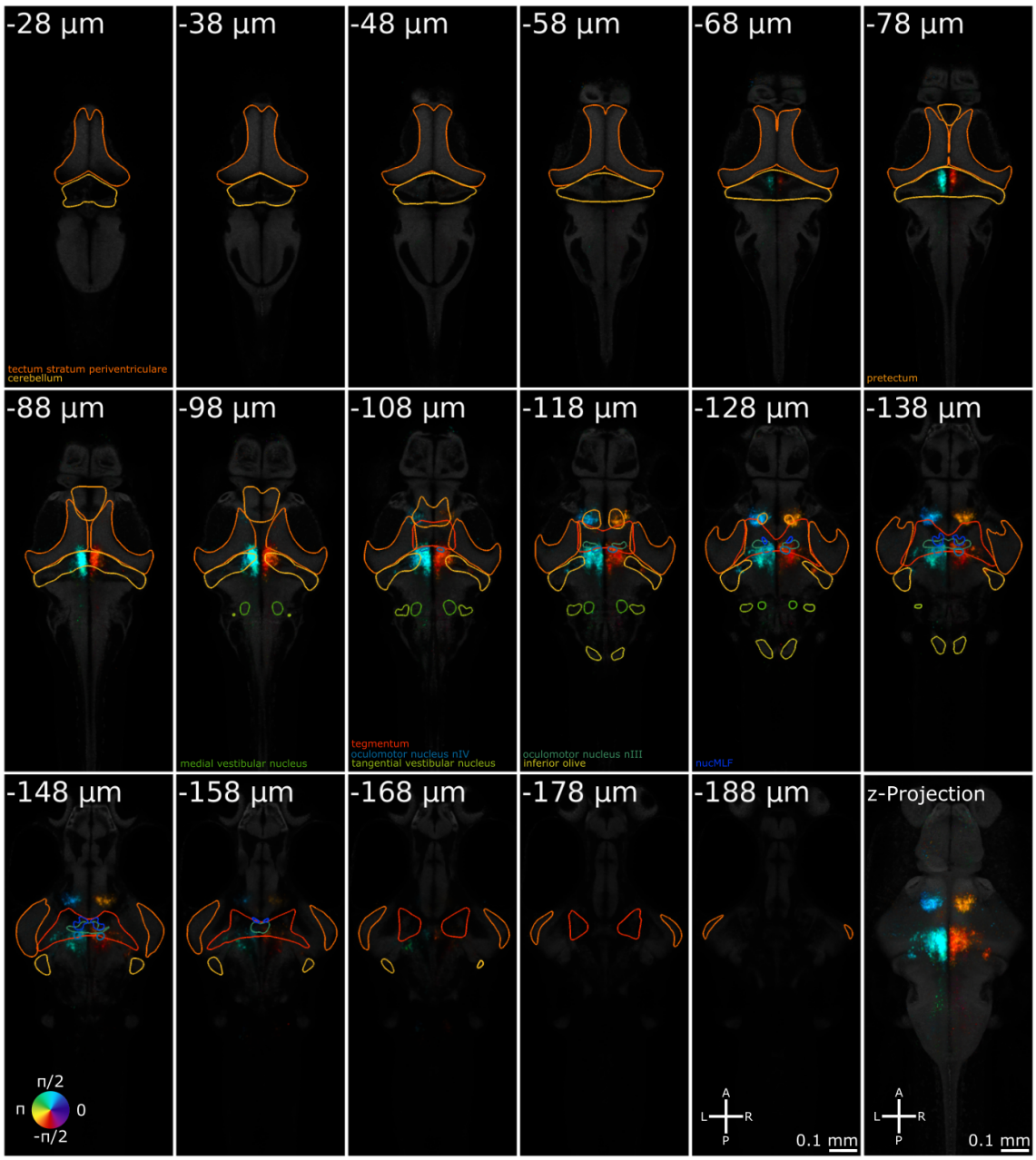

Figure VIII.13: Visual phasemap with phase of π.

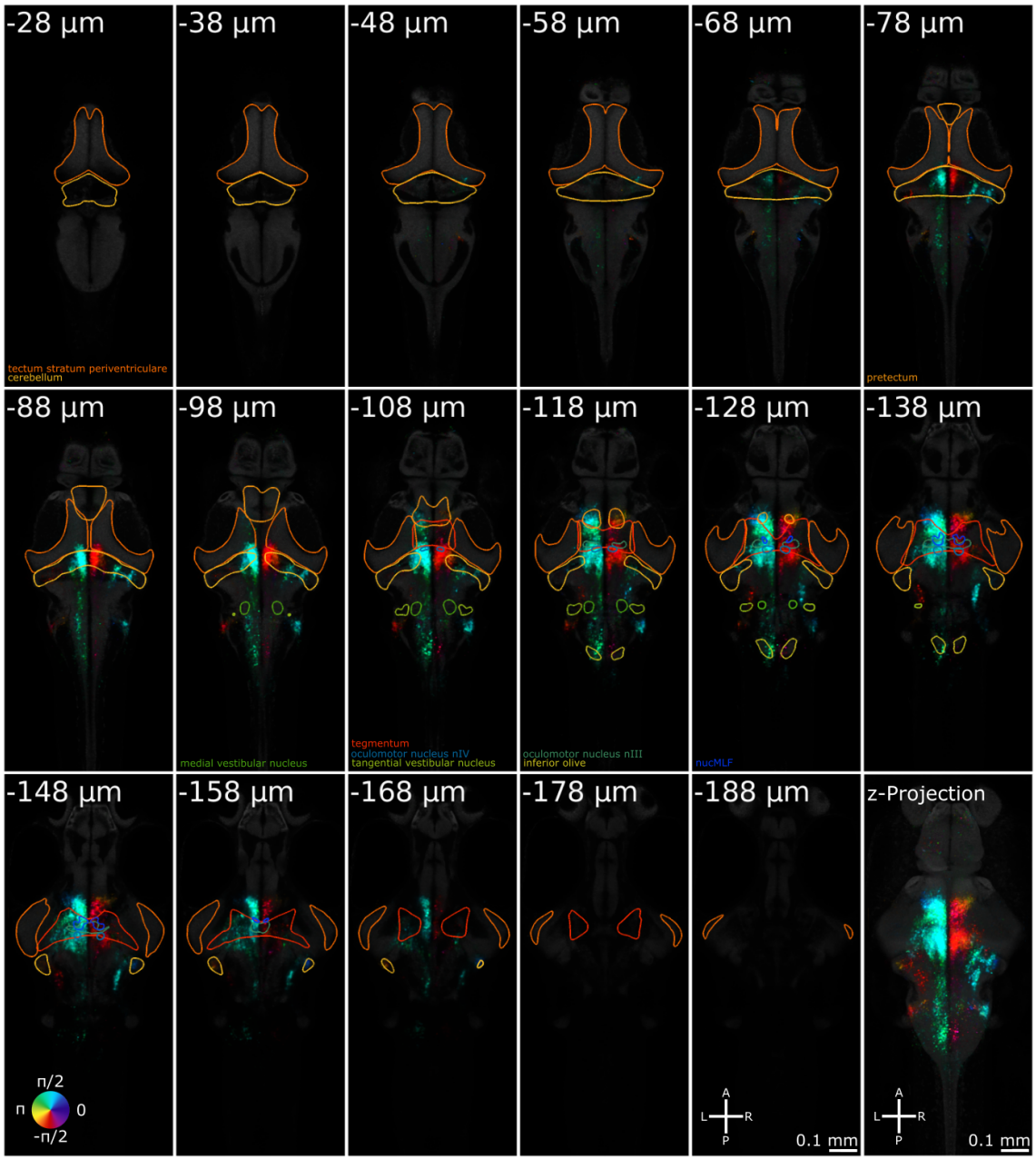

Figure VIII.14: Opposition phasemap (*congruence* = −1).

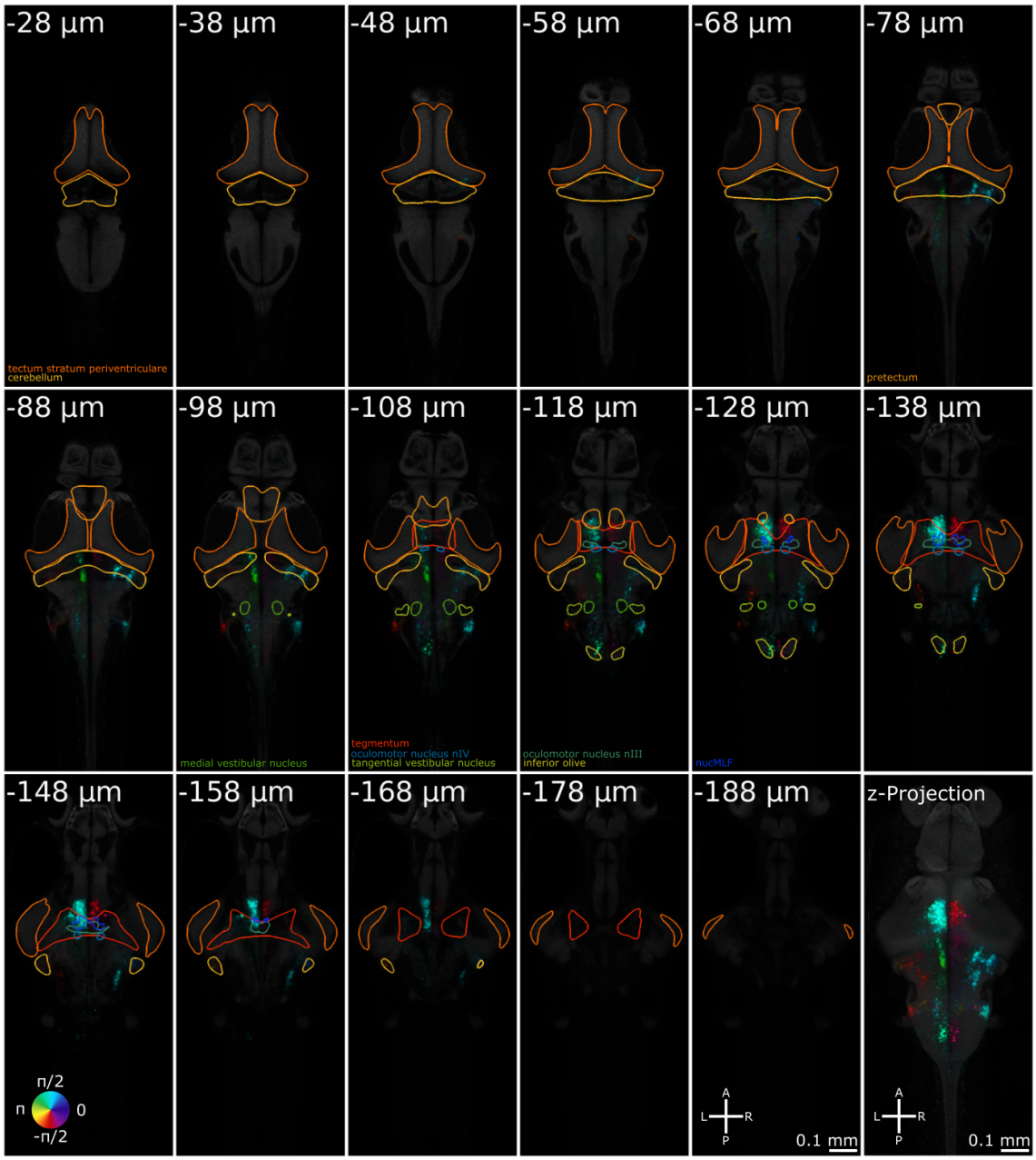

Figure VIII.15: Conflict phasemap (*congruence* = 0).

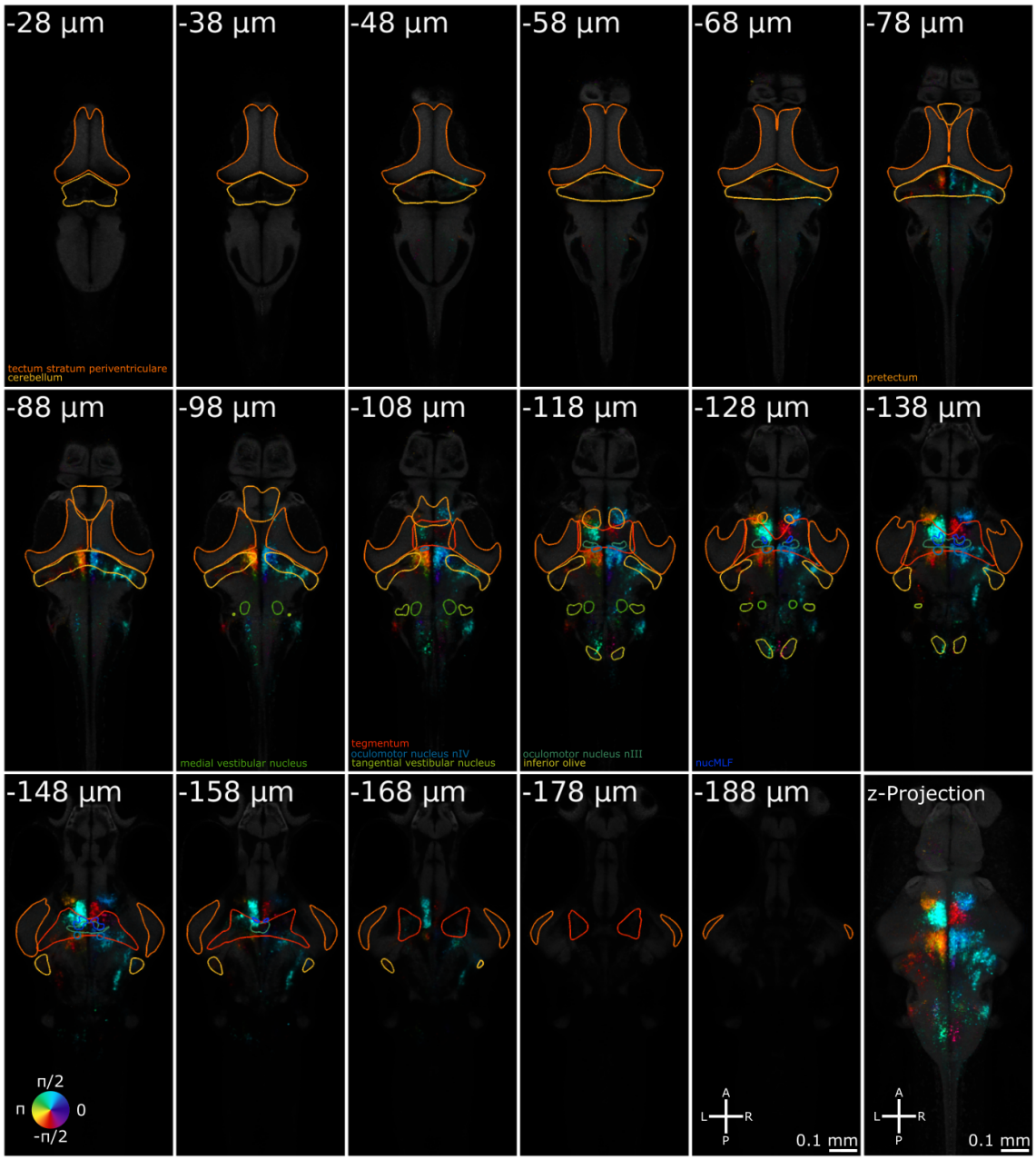

Figure VIII.16: Coherent phasemap (*congruence* = 1).

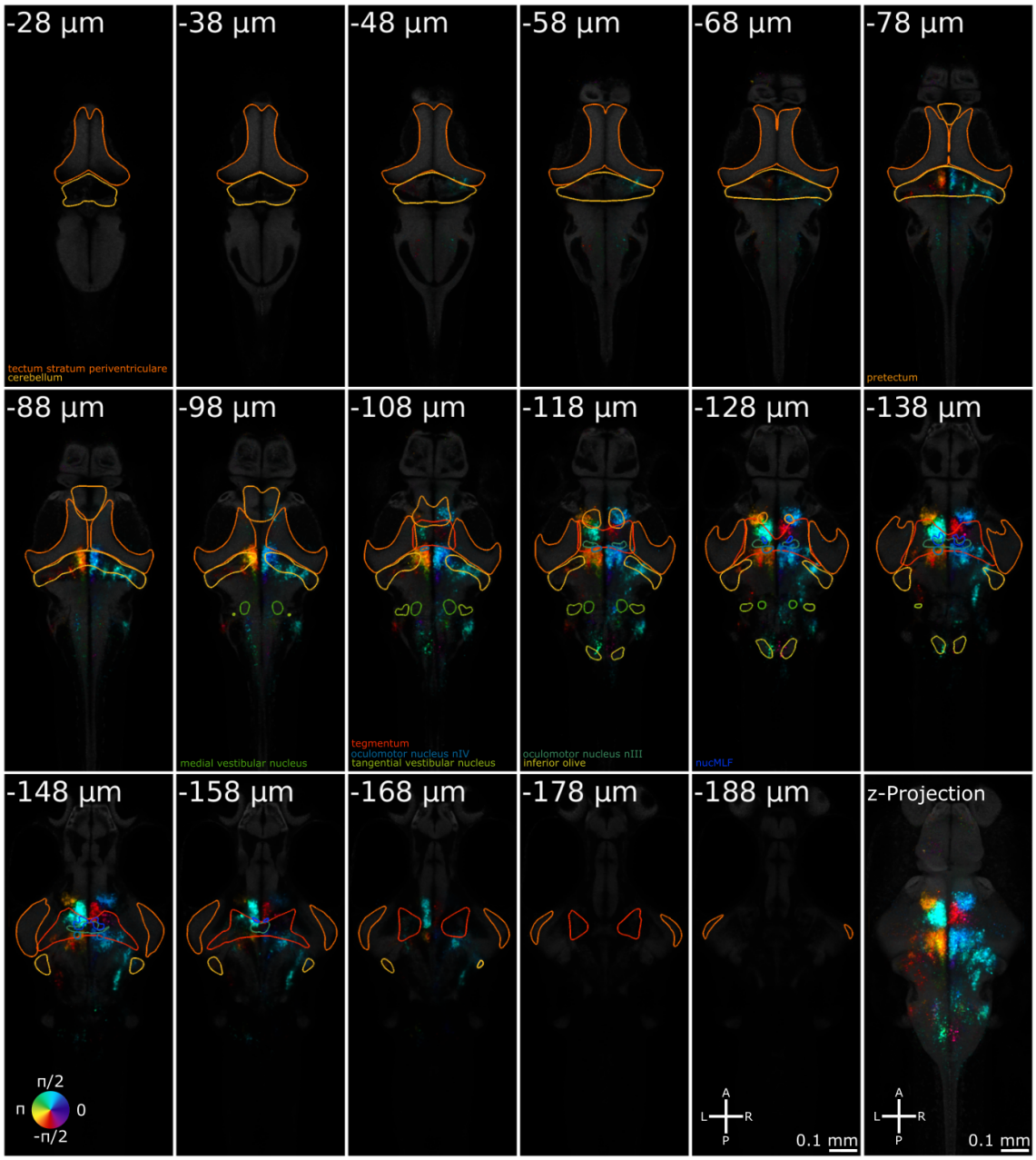

Figure VIII.17: Amplification phasemap (*congruence* = 2).

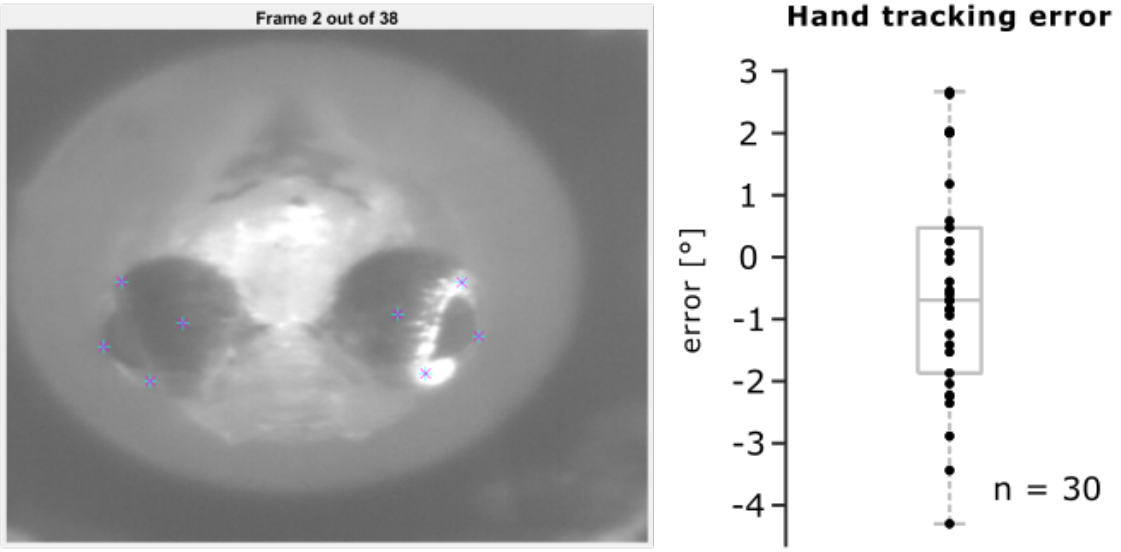

Figure VIII.18: Left panel shows an example of hand tracking on an average frame, with 8 points clicked at particular locations of fish left and right eyes. Right panel is the angle error between one frame tracked twice, for 30 frames.

VIII.18). The images were taken randomly from all the datasets available, to provided a large sample of fish. Hand tracking provides a low error, with most of the error angles being lower than 2°. The maximum error angle is 4.5°.

VIII.11 Tail tracking

I designed an algorithm to track the tail at the beginning of my thesis. The problem with the algorithm we used at the time, which fitted an ellipse on the fish tail, was that it detected non existing movements. The algorithm I did was inspired by the algorithm developped by Stih *et al.*, Stytra [231]. It first located the fish body, and then divided the tail into segments. To find a new segment, a pixels center of mass was computed in a nearby region, and the new segment would go from the initial point through the center of mass, with the provided segment length. Assembly of these segments would provide a solid indication on the tail curvature (figure VIII.19).

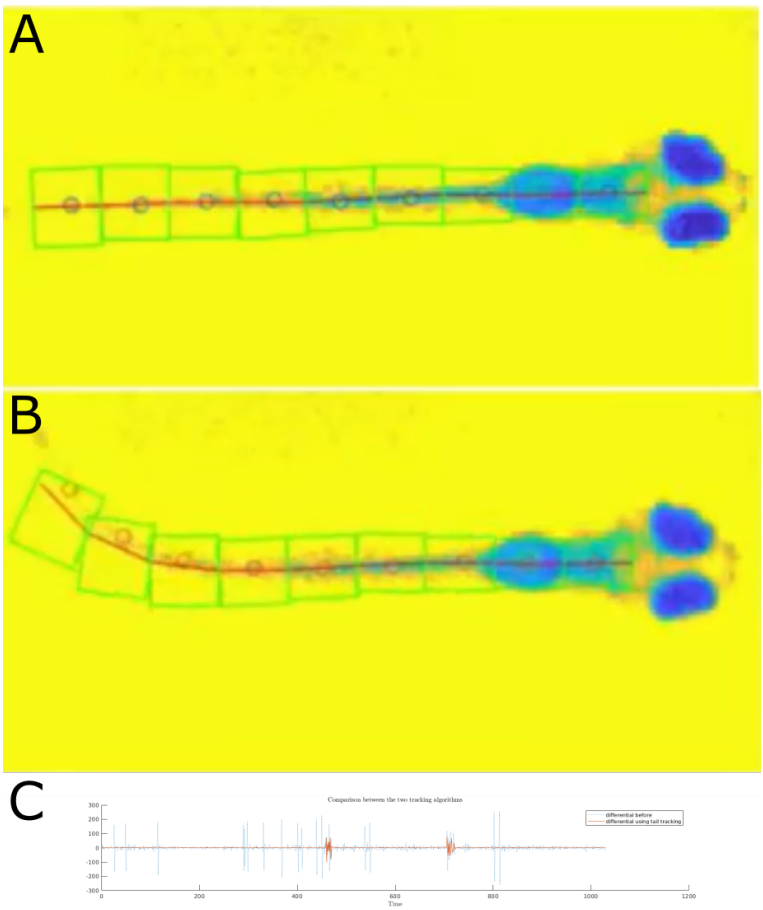

Figure VIII.19: **A**: Tail tracking in red on a fish at rest. **B**: Tail tracking in red on a fish moving its tail. **C**: Comparison between ellipse algorithm used before in blue (showing non existing movements), and tail tracking algorithm I developped in orange.

IX – Submitted article

Magnetic actuation of otoliths allows behavioral and brain-wide neuronal exploration of vestibulo-motor processing in larval zebrafish

Natalia Beiza-Canelo[1] **Hippolyte Moulle**[1] **Thomas Pujol**[1,2] **Thomas Panier**[1,3]

Geoffrey Migault[1] **Guillaume Le Goc**[1] **Pierre Tapie**[1] **Nicolas Desprat**[4] **Hans Straka**[5]

Georges Debrégeas[1]

Volker Bormuth[1,*]

[1] Sorbonne Université, CNRS, Institut de Biologie Paris-Seine (IBPS),
Laboratoire Jean Perrin (LJP), Paris, France.
[2] IBENS, Département de Biologie, Ecole Normale Supérieure, CNRS, Inserm,
PSL Research University, Paris, France.
[3] Sorbonne Université, CNRS, Institut de Biologie Paris-Seine (IBPS),
Plateforme d'Imagerie, Paris, France.
[4] Laboratoire de Physique de l'École normale supérieure, ENS,
Université PSL, CNRS, Sorbonne Université, Université Paris Cité, F-75005 Paris, France
Paris Diderot University, 10 rue Alice Domon et Leonie Duquet, 75013, Paris, France
[5] Faculty of Biology,
Ludwig-Maximilians-University Munich, Grosshadernerstr. 2, 82152 Planegg, Germany

[*] Corresponding : volker.bormuth@sorbonne-universite.fr

April 13, 2022

Monday 29th April, 2024, 17:39 version

Abstract

The vestibular system in the inner ear plays a central role in sensorimotor control by informing the brain about the orientation and linear acceleration of the head. However, most neurophysiological experiments are performed using head-fixed configurations depriving animals of vestibular inputs. To overcome this limitation, we decorated the utricular otolith of the vestibular system with paramagnetic nanoparticles. This procedure effectively endowed the animal with magneto-sensitive capacities: applied magnetic field gradients induced forces on the otoliths resulting in robust behavioral responses comparable to that evoked by rotating the animal by up to 20°. We recorded the whole-brain neuronal response to this fictive vestibular stimulation using light-sheet functional imaging. Experiments performed in unilaterally injected fish revealed the activation of a commissural inhibition between the brain hemispheres. This magnetic-based stimulation technique opens new perspectives to functionally dissect the neural circuits underlying vestibular processing and to develop multisensory virtual environments including vestibular feedback.

***K*eywords** zebrafish · vestibular system · ferrofluid · magnetic actuation · zebrafish · whole-brain imaging · light-sheet microscopy

1 Introduction

The vestibular system continuously informs the brain about self motion and body orientation within the gravitational field. The vestibular apparatus is located in the inner ear and comprises several organs that report on the various components of the acceleration forces. Rotational acceleration of the head induces an endolymph flow in the semicircular canals, which is detected by mechanosensitive structures called cupulae, respectively. Translational acceleration, as well as gravitational forces, act on two otolithic structures overlaying on the utricular and saccular epithelia, and whose motion is transduced by mechanosensitive hair cells to which they are coupled.

Neuronal signals encoding the head orientation and movement are relayed to neuronal circuits that drive compensatory movements in order to stabilize gaze and posture. Vestibular information is first processed in the brainstem vestibular nucleus and the cerebellum, which receive direct vestibular afferent input. Information is further distributed to oculomotor, skeletomotor, and autonomous motor systems, and in mammals, also via the thalamus to cortical systems [1]. At the various stages of signal processing, vestibular information is integrated with non-vestibular sources of self-motion information such as visual, somatosensory and proprioceptive inputs as well as locomotor efference copies [2].

In spite of the central role played by the vestibular system in sensorimotor tasks, most neuronal recordings are currently performed in animals deprived of any vestibular signals, i.e., under head- or body-fixed stationary conditions. This is due to the inherent challenge of combining neural recordings and natural vestibular stimulation as the latter necessitates to rotate or translate the animal's head in space, and is thus incompatible with head-fixed recording configurations required for most functional calcium imaging techniques.

Our knowledge on the vestibular system thus essentially derives from electrophysiological experiments in which the spike activity of a small number of neurons is sequentially monitored using implanted electrodes.

As vestibular processing is widely distributed across the brain, zebrafish constitutes a promising model animal to study the neuronal substrate of this highly conserved sensory system. The small size and transparency of the larval zebrafish brain indeed offers the unique opportunity to record cell-resolved brain-wide neuronal activity using light-sheet based calcium imaging [3, 4, 5, 6]. With the exception of the semicircular canals, which are still immature in young larvae [7], the vestibular system is mostly functional in larval zebrafish as early as 6 days post-fertilization [8], an age at which whole-brain imaging is routinely performed. This is evidenced by the capacity of the larvae to efficiently stabilize their posture and gaze in response to body rotation, via vestibulo-ocular and vestibulo-spinal reflexes [8, 4, 9, 10, 11].

Two experimental methods to provide controlled vestibular stimulation, while performing functional whole-brain imaging, were recently introduced. In the work from Migault *et al.* [4], we solved the problem by co-rotating the fish and the (miniaturized) light-sheet microscope, thus keeping the imaging volume unchanged during the stimulation. Favre-Bulle et al.[9, 5] generated a fictive vestibular stimulus using optical tweezers to displace the utricular otolith. Although these two approaches enable simultaneous neural recording, they both involve demanding optical developments that may hamper their broad diffusion among groups employing neurophysiological methods. Furthermore, the accessible stimulation range, in terms of maximal acceleration that they can emulate, is limited.

Here we present an alternative approach based on the magnetic actuation of the otoliths after surface coating by ferromagnetic nanoparticles. These superparamagnetic iron oxide nanoparticles are available in the form of colloïdal solutions called ferrofluids [12]. Although they do not carry a permanent magnetic moment, these particles acquire a magnetization in an externally applied magnetic field and can be manipulated by magnetic field gradients. Their magnetic susceptibility is several orders of magnitude larger than biological tissues [13], allowing the application of large forces. Biocompatible ferrofluids have been used to study mechanical properties inside living tissues *in vivo* [14, 15, 16, 17, 18] and functionalized nanoparticles have allowed targeting cellular components such as DNA and proteins with high specificity [19, 20] or to deliver drugs into compartments that are difficult to access as e.g., the inner ear [13].

Magnetic actuation offers several advantages over optical tweezers in the context of biological systems. First, biological tissues are fully transparent to magnetic fields. Forces can thus be exerted in a controlled way deep within the specimen regardless of its optical transparency. Second, magnetic fields do not induce heating, and, with the exception of magnetoreceptive species [21], most animals are insensitive to this physical parameter. Thus, besides the injection itself, this technique is physiologically non-invasive even for extremely large magnetic intensity.

Here we show that the injection of ferrofluid into the otic vesicle of larval zebrafish allows controlled magnetic forces to be exerted on the otolith, mimicking naturally occurring gravitational and acceleration forces. This fictive vestibular stimulation elicits strong and robust compensatory eye and tail movements, comparable to those evoked by roll or tilt motion of the animal over large angles. We simultaneously recorded the brain-wide neuronal activity evoked by this fictive vestibular stimulation using functional light-sheet microscopy. By

injecting the ferrofluid into a single ear we disentangled the contribution of each utricle to the brain-wide neuronal response, which is not possible under natural conditions when rotating the animal [4]. This constitutes the first use of a ferrofluid to stimulate a sensory system *in vivo*. The method is inexpensive, easy to implement and compatible with most neurophysiological recording methods such as optogenetics or electrophysiology.

2 Results

After ferrofluid injection into the otic vesicle, vestibular-driven behaviors can be evoked through magnetic stimulation

We injected a custom-made ferrofluid [22] into both inner ears of zebrafish larvae 5 days after fertilization (dpf). The ferrofluid consisted of 11 nm in diameter iron oxide (γ-Fe_2O_3) particles with citric acid surface functionalization to make them stable in water (pH 7, see Methods). After the injection, the otic vesicle maintained its shape and the ferrofluid was visible as a red-orange tinge (Figure 1A). The otolith itself, once dissected out and washed, also displayed a slight orange coloration, indicating that some of the injected ferrofluid particles had permanently bound to the otolith. The otolith was thus magnetized, as could be confirmed by approaching a permanent magnet to its proximity. The otolith immediately moved towards the magnet as shown in the Supplementary Figure S1.

Next, we tested whether this nanoparticle coating of the otolith could yield magnetic forces *in vivo* on the otolith comparable to the gravitational force that acts on it when the head/body is rolled or tilted in space (Figure 1B). To do so, we examined the behavioral response (compensatory eye and tail movements) that were induced through magnetic actuation. We thus immobilized a bilaterally injected fish in a drop of 2% low melting point agarose on a thin glass slide and removed the agarose around the eyes and tail to allow free movements (Figure 1C). The specimen was placed in a chamber filled with the embryonic medium E3. A front and a side camera were used to monitor the eyes and tail movements evoked by the in-plane movement of a small permanent neodymium magnet positioned beneath the fish.

We observed two distinct responses depending on the orientation of the movement with respect to the body axis. When the magnet was moved along the medio-lateral axis, the eyes rolled and the tail bent in a direction opposite to the magnet (Movie 4 Part I). Such movements are characteristic of responses elicited by a roll motion of the animal (i.e., a rotation along its longitudinal axis) via vestibulo-ocular and vestibulo-spinal reflexes [4, 8]. In this case, the magnetic force acted laterally on the otolith, as does the gravitational force during a roll motion. When the magnet was moved along the antero-posterior axis, the eyes rotated along the tilt axis and discrete swim bouts were triggered. Here the response to the magnetic stimulation was in line with compensatory eye movements and tail kinematics elicited upon tilting the fish [8] (see Movie 4 Part II).

To quantify these responses, we imposed controlled sinusoidal displacements to the magnet using a two-axis motorized stage either along the lateral axis (fictive roll stimulus) or along the antero-posterior axis (fictive tilt stimulus). We used a frequency of 0.5 Hz and an amplitude of 2.5 mm corresponding to the radius of the magnet (see the following section describing the numerical simulations for an estimation of the corresponding magnetic force). Typical behavioral responses of such recordings are shown in the Movie 4. We found the

behavioral response to be strong in 80 % of the tested fish, which confirmed the robustness of the method. Importantly, the observed vestibular behaviors were reproducible and stable over time with only small variability over 150 stimulus repetitions in the same fish (Figure 1D). From the averaged cyclic ocular rotation signal, we extracted an angular range of $\alpha = 13.2° \pm 7.4°$ (mean ± standard deviation) during simulated roll motion and $\beta = 8° \pm 4.3°$ for simulated tilt motion (Figure 1). Interestingly, the behavioral responses were stronger for lower concentrations of injected ferrofluid (Figure 1E).

These values can be compared to those obtained during natural vestibular stimulation in which the animal is actually rolled or tilted in space. As an illustration, we show in Figure 1E the angular range ($\alpha = 14.1° \pm 5.8°$ (mean ± standard deviation) of eye rotation measured in larvae exposed to a sinusoidal roll motion of ±15°. One may notice that both the mean and the standard deviation are comparable in both experiments, indicating that the large variability across specimen is not specific to the fictive ferromagnetic stimulation. From the roll motion-evoked responses, we calculated a gain of the roll vestibulo-ocular response in darkness of $g_{roll} = 0.5 \pm 0.2$ and for the ocular motor tilt response a gain of $g_{tilt} = 0.3$ is reported [8]. From this calibration, we thus estimated that the fictive magnetic vestibular roll and tilt stimuli corresponded to a peak-to-peak stimulus of $\alpha/g_{roll} \approx \pm 14° \pm 27°$ (mean ± std) and $\beta/g_{tilt} \approx \pm 7° \pm 4°$ (mean ± std), respectively.

Ferrofluid injection into the inner ear does nor impair vestibular function.

Hair cells in the vestibular system are sensitive to mechanical and chemical stress, which can lead to cell death, thus impairing sensory function [23]. We assessed possible damage induced by either the injection procedure or by the ferrofluid itself using a simple behavioral assay. Fish use their vestibular system to keep their dorsal side-up posture stable during swimming. Therefore, uncorrected rolling along the rostro-caudal body axis during a swim bout can be used as an indication of vestibular dysfunction [24, 25, 26] (Figure 2A). We quantified the outcome of this procedure by calculating a roll ratio, i.e., the proportion of roll events over a total of 5 swimming events after a mechanically evoked startle response [27] (see Methods). The roll ratio was measured at 2, 24 and 48 hours after the injection had been performed at 5 dpf.

Control (non-injected) fish had a mean roll ratio of 0.44 ± 0.36 (mean ± std, N = 10) at 5 dpf (Figure 2B). Although the vestibulo-ocular reflex is fully established at 5 dpf [8], vestibular-driven postural control is still being refined between 5 to 7 dpf as evidenced by the decrease of the roll ratio during this period. As a second (negative) control, we performed a similar assay on larvae injected bilaterally with the calcium chelator BAPTA (5 mM), which disassociates hair cell tip-links and disrupts the mechano-electrical transduction [28]. Two hours after the injection, the roll ratio was close to one (mean roll ratio: 0.93 ± 0.11, see Movie 4), indicative of an almost complete loss of vestibular-driven postural control. Tip links have been shown to regenerate in 8 to 24 hours [29]. Hence, 48 h after BAPTA injection, the roll ratio of the larvae were significantly lowered and not significantly different anymore to control fish, reflecting a progressive recovery of posture control by tip link regeneration.

Next, we performed similar tests on buffer- and ferrofluid-injected fish, in order to disentangle the effect of the injection procedure from the ferrofluid itself on the vestibular system. Two hours after injection, the roll ratio (0.51 ± 0.31 and 0.65 ± 0.21, respectively) for both conditions were not significantly different from that of control fish (Tukey test $p > 0.1$). This remained so at 24 h and 48 h post injection. Finally, we injected

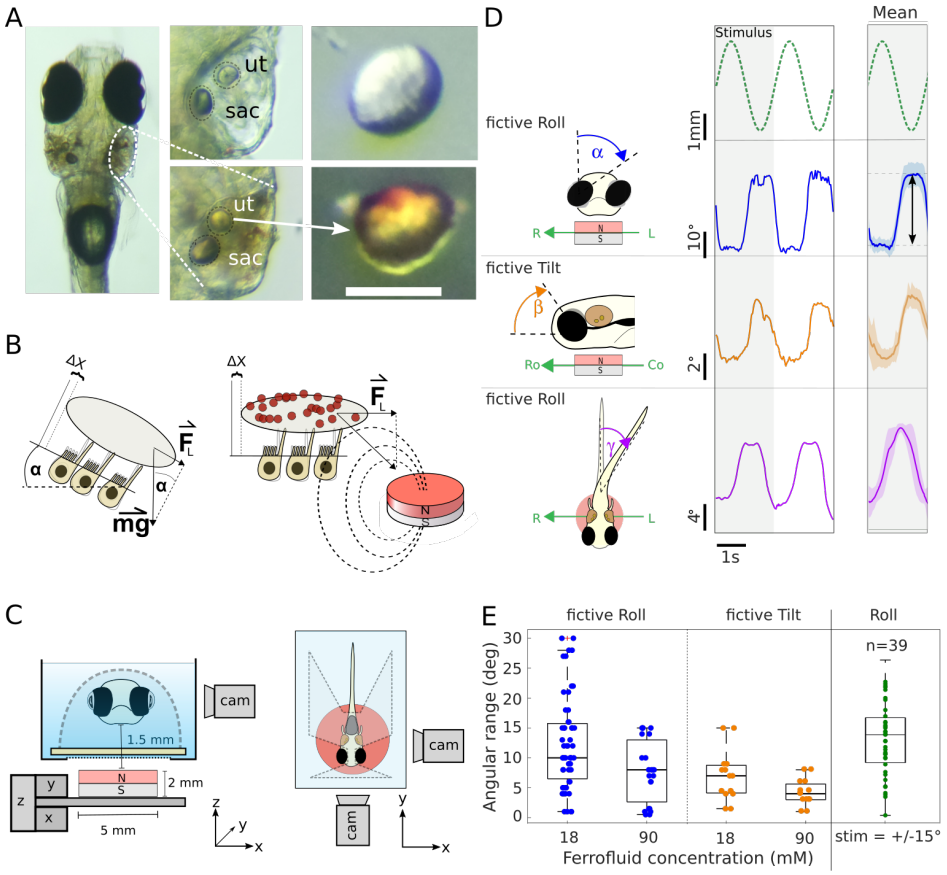

Figure 1: Magnetic actuation of the otoliths after surface coating by ferromagnetic nanoparticles. **A** Top view of a 5 dpf zebrafish larva after bilateral intra-otic ferrofluid injection. Middle column: Zoom onto the otic vesicle with injected ferrofluid (bottom) and before injection (top). The otoliths of the utricle, ut, and of the saccule, sac, are visible. Right: Bright-field image of an utricular otolith dissected from a control fish (top) and from a fish after ferrofluid injection (bottom). Attached iron nanoparticles appear in red-orange. Scale bar = 50 μm. **B** The diagram on the left illustrates the lateral force experienced by an otolith when the head is rotated relative to the gravitational field, $F_L = g \cdot sin(\alpha)$ (top). The right side illustrates an otolith covered with nanoparticles that exert a lateral force onto the otolith when placed in a magnetic field gradient. **C** Left: Diagram of the setup in front view. An x,y-motorized stage and a manual z-stage (black) move the magnet (red) under the head-tethered fish, mounted in agarose (outlined by a dashed line). Right: Top view of the setup illustrating the front and side cameras (cam) for eye motion tracking. The magnet center is aligned with the center of mass of the fish inner ears (not drawn to scale). **D** Evoked eye and tail movements in response to the magnet motion along different directions in a sinusoidal manner beneath a fish injected with 18 mM ferrofluid solution. Left column shows the two first cycles of a 150 repetition trial and right columns shows the average trial response and standard deviation. **E** Angular range of evoked eye rotation angles (peak-to-peak, see arrow in 1D) in response to fictive roll and tilt stimuli plotted for two concentrations of ferrofluid bilaterally injected into the inner ears ($N_{roll,18mM}$=24, $N_{roll,90mM}$=11, N_{tilt} = 9 for both concentrations).

DiASP that fluorescently labels functional hair cells as it diffuses through the mechanotransduction channels if mechanotransduction is functional. Hair cells became clearly labeled after the injection (see inset Figure 2B). Thus, neither the injection procedure itself nor the ferrofluid seem to significantly affect the function of the vestibular organs.

Finally, we examined the kinematics of free swimming behavior in ferrofluid-injected fish compared to uninjected control larvae. We found that inter-bout interval and turn angle distributions were not significantly different from control fish, while the average displacement per swim bout was only marginally increased (Figure S2 and Movie 4). The various tests confirmed that the ferrofluid injection procedure has a very limited impact on the functionality of the vestibular system and on the locomotor behavior.

Numerical simulations of the magnetic force exerted onto the magnetized otolith.

To evaluate the impact of magnetic forces on the nanoparticle-covered otolith and its dependency on the magnet position relative to the larva, we resorted to numerical simulations (Figure 3A). This approach revealed the existence of a range of magnet positions within which the force exerted onto the magnetized particle varies linearly with the radial distance to the center of the magnet. The force is maximal when the particle is located above the edge of the magnet beyond which it decreases and eventually vanishes. The maximal lateral force and the extent of the linear regime increases with magnet diameter, while the maximal force decayed as z^{-4} as expected for a magnetic dipole, where z is the vertical distance to the magnet. These results suggest that the magnet should be placed as close as possible beneath the fish and that horizontal displacements should remain smaller than the radius of the magnet. Under these conditions, the force-displacement relationship is expected to be linear.

To estimate the maximum force that can be imposed onto the otolith, we measured the velocity in water of an isolated otolith (obtained after dissection of an injected larva) submitted to a comparable magnetic field as in the *in vivo* experiment. Taking into account the otolith diameter, that controls the drag force, we obtained an estimated force of $\sim 1\,\mathrm{nN}$. We can then compare this value to the gravitational forces exerted on the otolith *in vivo* when the head is tilted in space. The utricular otolith in fish is a calcium carbonate (aragonite) crystal with a density of $2.83\,\mathrm{g.cm^{-3}}$ and a diameter of $\sim 55\,\mu m$ at the age of 6 dpf [9]. From these values, we estimated that under natural conditions, the maximal gravitational force experienced by the utricular otolith is $\sim 1.6\,\mathrm{nN}$ when the fish is rolled 90°. The magnetic and gravitational forces acting on the otolith are thus in the same range, which *a posteriori* explains the capacity to drive large vestibular-like behavioral responses as detailed above.

Our simulations can also be used to evaluate the number of nanoparticles attached to the otolith. A single particle experiences $\sim 0.007\,\mathrm{fN}$ of lateral force when placed at the edge of a 5 mm in diameter magnet positioned 2 mm beneath the particle. Therefore, approximately $1.4{\cdot}10^8$ particles are required to produce a total of 1 nN force. This corresponds to a ~ 1 monolayer of particles bound to the otolith. This fine coating represents only 0.2 ‰ of the mass of the otolith and is thus unlikely to interfere with the vestibular function, in agreement with our observations.

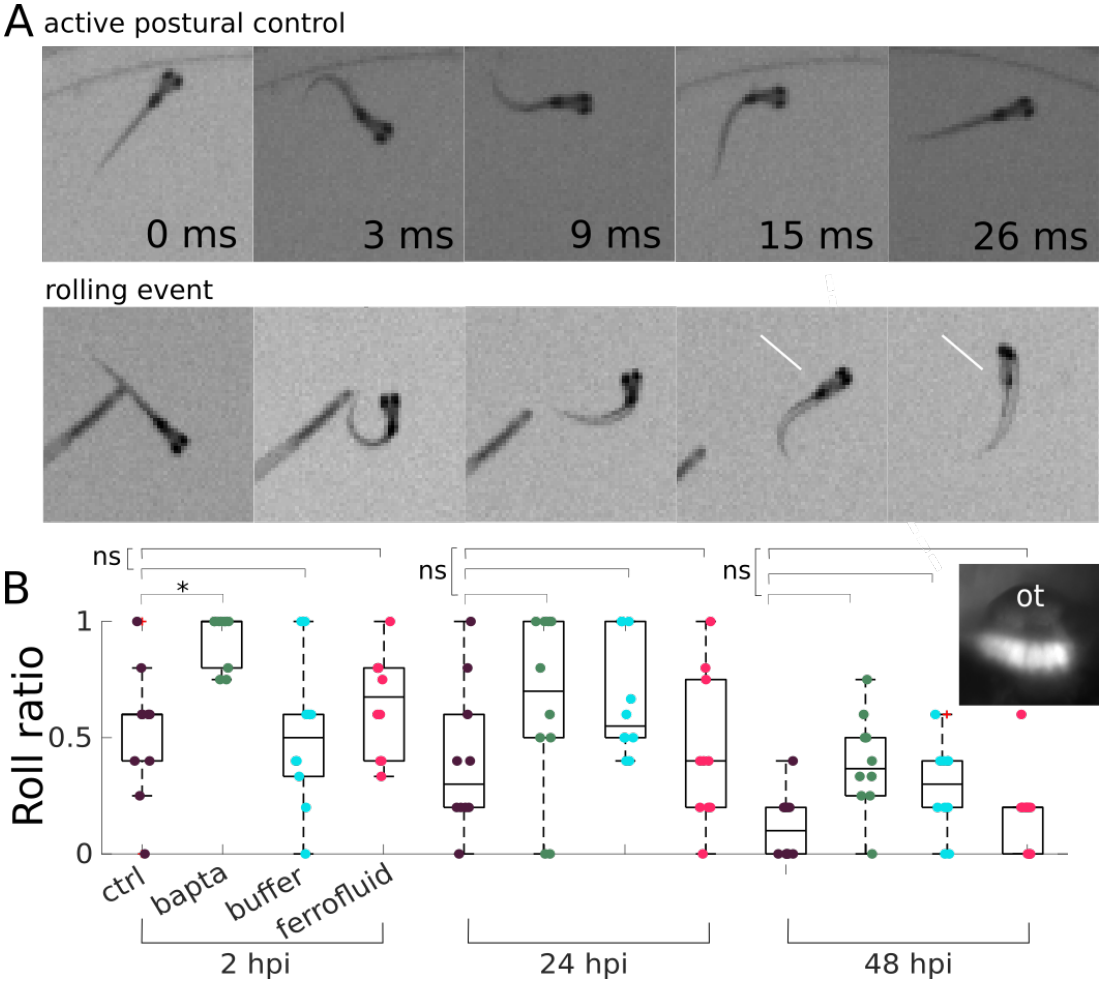

Figure 2: Control experiments probing the impact of the injection procedure on vestibular functionality **A** Image sequence recorded during evoked startle response behaviors for a non-injected control fish illustrating active postural control (top) as well as for BAPTA injected fish illustrating a roll event (bottom). **B** Roll ratio during an evoked startle response measured 2, 24 and 48 hours post bilateral injection (hpi) of BAPTA, ferrofluid or buffer compared to non-injected control fish from the same batch, respectively.

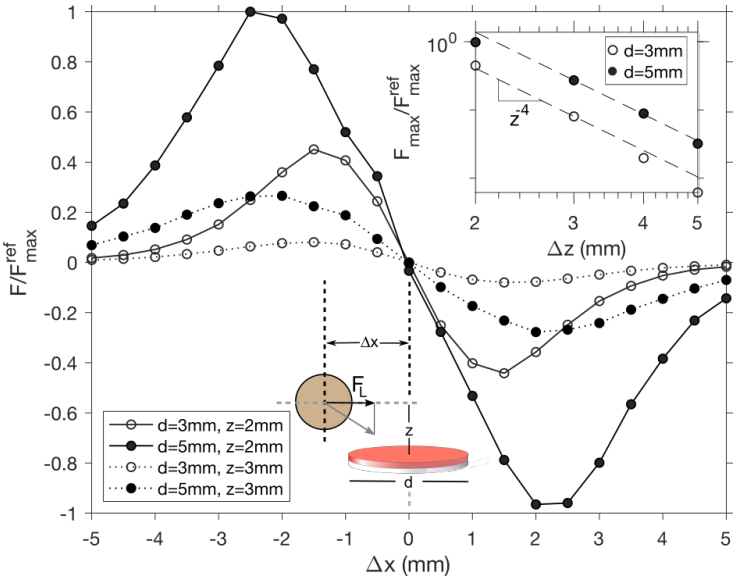

Figure 3: Simulations. Finite element simulation of the lateral force, F, exerted on a paramagnetic particle by a magnet as a function of the lateral distance (Δx) of the particle to the magnet's center axis. Shown are force-displacement relationships for two magnet diameters, d, and two z-distances, z, between the magnet and the particle. The calculated forces were normalized by the maximum of the force-displacement relation, F^{ref}_{max}, extracted from the configuration with the 5 mm in diameter magnet positioned at a distance of 2 mm. Inset: Dependency of the maximal lateral magnetic force, F_{max}, as function of the z-distance between the particle and the magnet, calculated for two magnet diameters.

Brain-wide functional imaging during magnetic vestibular stimulation and behavioral monitoring

One of the assets of our stimulation technique is its low footprint, which facilitates a combination with any functional recording technique. Here we used a setup that enables the application of controlled fictive vestibular stimuli in head-tethered larval zebrafish while recording the behavioral responses as well as the evoked brain-wide neuronal activity using light-sheet imaging (Figure 4A).

We first recorded the neuronal activity, evoked in mechanosensitive inner ear hair cells. In order to do so, we used the transgenic line *α-tubulin:Gal4-VP16;UAS:GCaMP7*, which expresses the GCaMP7 calcium indicator in hair cells of the inner ear [30]. Both inner ears of these fish were injected with ferrofluid, embedded in agarose, and placed in the experimental setup one day after the injection. We generated a fictive vestibular roll stimulus by moving the magnet sinusoidally along the left-right body axis at 0.5 Hz and 2.5 mm amplitude. Hair cells in the anterior macula (AM, utricle) showed a modulation of the fluorescence signal, phase-coupled to the stimulus (Figure 4B). In contrast, hair cells in the posterior macula (PM), which are part of the saccule that senses vertical oscillations at higher (auditory) frequencies, showed no detectable response indicating that they were likely not stimulated. These observations are consistent with the anatomical orientation of the mechanosensitive axes of the two vestibular organs.

Next, we recorded the brain-wide neuronal dynamics elicited upon fictive vestibular stimulation using the pan-neuronal nuclear localized *Tg(elavl3:H2B-GCaMP6f)* transgenic line. This stimulus evoked neuronal activity throughout the brain (see Movie 5). As an example, we show activity time traces recorded from vestibulo-spinal neurons and from the oculomotor nucleus nIII (Figure 4C). We quantified the brain-wide vestibular response pattern by computing a phase map as described in Migault *et al.* [4]. Briefly, we estimated, for each voxel (0.6x0.6x10μm), the amplitude and the phase relation of the evoked signal relative to the stimulus waveform. These two parameters were displayed in the form of a phase map, where color represents the relative phase of the neuronal response to the stimulus and intensity encodes the amplitude of the response. Hence, a phase shift of 0° applies to neurons whose activity is locked to the applied force, whereas a phase shift of 90° corresponds to neurons responding to the time-derivative of the force signal. Figure 4D shows the phase map for several selected layers and their z-projection, recorded in a single fish and registered on the Z-brain atlas [31]. Vestibular-induced activity is clearly visible in the tangential vestibular nucleus and in vestibulo-spinal neurons. The observed ocular motoneuron activity is consistent with the monitored compensatory eye movements. Active regions also include the nucleus of the medial longitudinal fascicle, as well as hindbrain pre-motor neuronal populations involved in tail motion. Cerebellar and inferior olivary neurons were also clearly recruited. This response map was found to be stereotypic and reproducible for all injected fish as shown by the sharpness of the average phase map, which combines the observations in 14 larvae (Figure 4E). This average phase map shows a close similarity with the brain-wide response recorded during natural vestibular stimulation using a rotating light-sheet microscope (Figure 4F and Figure 4 in Migault *et al.* [4].

This new stimulation method offers, as optical tweezers but in contrast to a natural stimulation, the opportunity to stimulate a single ear at a time, by injecting the ferrofluid only unilaterally. Figure 4G show the average phase map for fish injected with ferrofluid into the right ear only. Interestingly, the response appears rather similar to that evoked by bilateral fictive vestibular stimulation, albeit with a relatively lower intensity. The marked antisymmetric activity in the medial octovolateralis nucleus (MON) reflects a strong activity of commissural connections between both sides of the brain and suggests a pronounced contralateral inhibitory connectivity in the hindbrain.

We finally performed control experiments with non-injected fish. At the stimulation frequency, no signal was detectable in the average phase map (Figure 4H). This rules out the possibility that the recorded activity may in part reflect the visual stimulus caused by the moving magnet, which could have been possible as the blue (488 nm) laser forming the light sheet also illuminates the sample chamber.

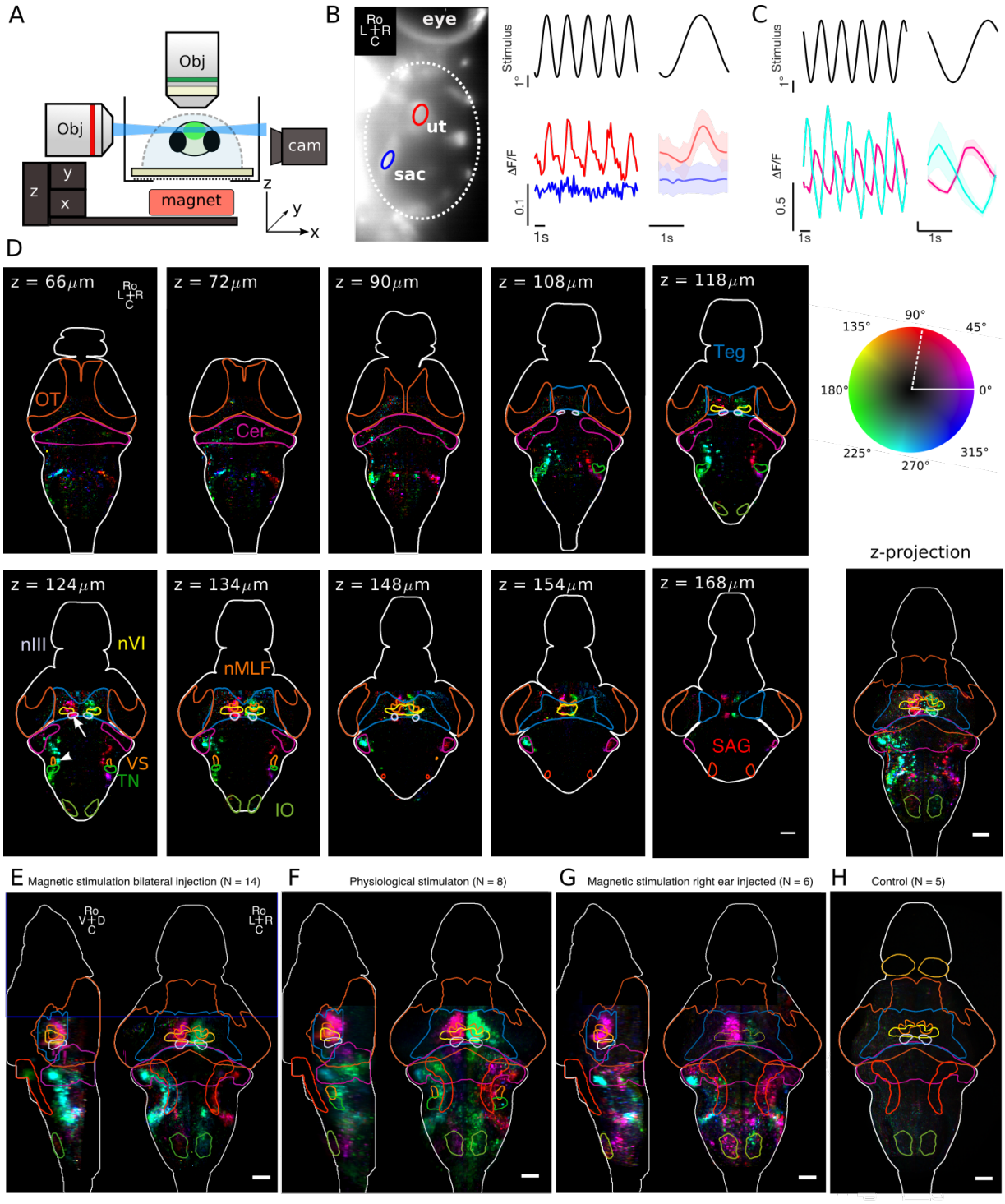

Figure 4: Brain-wide neuronal responses evoked by magnetic vestibular stimulation. Caption continues next page.

Figure 4: (Continued) **A** For functional imaging a light-sheet (blue) excites the fluorescence GCaMP6 sensor genetically encoded in the brain (green). The fluorescence is collected by an objective perpendicular to the light-sheet. **B** Calcium responses recorded in the otic vesicle from the utricle (red) and the saccule (blue) in response to a sinusoidal fictive roll stimulus (black). The trial-averaged response with std (N = 75 repetitions) is shown on the right. The ROIs from which the fluorescent signals were extracted are indicated with red and blue circles respectively. **C** Neuronal responses to the same stimulus as in **B** but measured in vestibulo-spinal neurons (white arrowhead in panel D) and extraocular motoneurons in the oculomotor nucleus (white arrow in panel **D** bottom left). **D** Selected layers of the phase map of the brain-wide response recorded in one fish. OT: optic tectum, Cer: cerebellum, Teg: tegmentum, nIII and nIV: oculomotor and trochlear nucleus, nMLF: nucleus of the medial longitudinal fascicle, SAG: statoacoustic ganglion, IO: inferior olive, TN: tangential nucleus, VS: vestibulo-spinal neurons. The color map indicates the phase of the neuronal response relative to the stimulus after correction for the phase delay introduced by the GCaMP6f calcium sensor $\Delta\phi = \arctan(-2\pi f \tau_{GCaMP6f})$(decay time $\tau_{GCaMP6f} \approx 1.8\,\mathrm{s}$). Without this correction the zero degree phase shift would be at the position indicated by the dashed white line. Bottom right: Maximum z-projection of the entire phase map shown of this fish. **E** Average phase map in response to bilateral fictive vestibular stimulation (N = 14 fish). **F** Average phase map recorded during natural vestibular stimulation with a rotating light-sheet microscope [4]. **G** Average phase map in response to unilateral (only right ear injected) fictive vestibular stimulation. **H** Control phase map recorded under the same conditions as **E and H** but without injected ferrofluid into the inner ear. Transgenic lines: *Tg(a-tubulin:Gal4-VP16 ;UAS:GCaMP7a)* panel B, *Tg(elavl3:H2B-GCaMP6f)* panel C-H.

3 Discussion

Our work demonstrates that injecting a ferrofluid solution into the inner ears of larval zebrafish allows to subsequently apply controlled forces to the utricular otolith *in vivo*, thus mimicking natural motion-like vestibular stimuli in immobilized animals. A small permanent magnet was sufficient to elicit robust motor responses to both fictive vestibular roll and tilt stimulation that were indistinguishable from those observed during natural motion stimulation. Cross-talk between the two stimulus directions was negligible, provided that the magnet was well centered beneath the fish.

Control experiments confirmed that the injection procedure did not damage the vestibular system and left the swimming behavior and postural control performance unaffected 24 hours after the injection. This robustness of the method reflects the minor interference of the injection procedure with the functionality of the system but may in part be related to the capacity of non-mammalian hair cells for self-repair [29]. Hence, even if tip-links were damaged by the injection procedure, the vestibular apparatus is likely fully functional 24 - 48 h post injection. In addition to potential tip-link repair, non-mammalian inner ear hair cells can regenerate destroyed hair cell bundles [32] and even full hair cells with restored sensory function after cell death [33, 34, 35]. In the adult zebrafish utricle, the full regeneration of the utricular macula after induced damage takes about 13 days [36]. This is too slow to explain the observed high performance of the vestibular system after injections leading to the conclusion that the injections did not cause substantial and functionally detrimental cell death.

Our proposed mechanism underpinning the fictive stimulation is based on the irreversible binding of nanoparticles onto the surface of the otolith. This thin magnetized coating can then be acted upon using magnetic field gradients. We reported direct evidence of the effective magnetization of the otolith and that the corresponding magnetic force is in the same order of magnitude as the gravitational force imposed during macroscopic body rotation. In the present study, we only tested two different concentrations of injected ferrofluid, and the strongest response was obtained already at the lowest concentration. This observation suggests that a relatively small number of nanoparticles is sufficient to entirely cover the otolith with a compact monolayer. Any further particles are then likely to be repelled from the surface due to electrostatic repulsion between the citric acid-coated nanoparticles.

A complementary mechanism may be at play that would rely on the magnet-induced motion of freely floating nanoparticles in the endolymphatic otic environment. The induced fluid motion would then impose a drag force onto the otolith. Given the nano-bead dimensions, the associated flow would be in the low Reynolds number regime and the particles are thus expected to reach their terminal velocity in less than a millisecond when placed in a field gradient. The resulting drag force, proportional to this particle velocity, would vary with the magnet position and could not be distinguished from the direct magnetic actuation on the otolith. However, an estimate of the particle terminal velocity results in a value of $\approx 0.1\,\mu m/s$, which in turn yields a drag force orders of magnitude smaller than the force exerted by the particles attached to the otolith. This suggests that this second mechanism is probably negligible.

In zebrafish, the utricular otolith is spherical. For a spherical mass, the gravitational force grows with the radius cubed while the magnetic force acting on a thin surface coating grows with the radius squared. One may thus anticipate that this magnetic actuation method should become relatively inefficient for larger animals (with larger otoliths). However, in most animals other than teleost fish, the otolithic membrane is covered with small carbon crystals called otoconia yielding a flat meshwork of extended mass. This leads to a much higher surface to volume ratio, which is more favorable for the actuation via surface-bound nanoparticles. Our method could thus work also in larger animals such as for instance *Xenopus* larvae, lampreys or even mammalian species provided that sufficiently strong magnetic fields and field gradients can be delivered. In fact, a pilot study on an isolated *in vitro* preparation of *Xenopus* tadpoles at mid-larval stage, demonstrated that solutions of citrate-coated ferromagnetic nanoparticles can be reliably injected and distributed throughout the duct system of the inner ear. Repetitive displacement of a permanent point magnet above the transparent otic capsule in different directions, elicited faithful and robust eye movements also in these animals (see Movie 4), which are an order of magnitude larger than larval zebrafish. The known functionality of all inner ear organs at this developmental stage ([37]), however, renders an identification of the recruited vestibular organ(s) more difficult but potentially derives from the magnetic stimulation of multiple inner ear organs.

This magnetic actuation method was implemented to fictively stimulate a slow tilt or roll of the fish body. However, the same approach could be used to mimic translational accelerations experienced by the larvae during free swimming. Larval zebrafish swimming patterns consist of discrete swim bouts that last for $100 - 200\,\text{ms}$ interspersed by $\sim 1\,\text{s}$-long resting periods. Owing to the Einstein principle, otoliths are

actuated during these transient linear accelerations: forward acceleration of the animal produces a backwards pointing force on the otolith while a deceleration corresponds to a forward pointing force. The reported peak acceleration during a bout is in the range of $0.3 - 2\,\mathrm{m/s^2} = 0.03 - 0.2\,\mathrm{g}$ [38, 39], which corresponds to a force on the otolith in the range of $50 - 300\,\mathrm{pN}$, i.e., within the accessible range of our instrument. To mimic acceleration forces encountered during a swim bout, the magnet has to be moved by $0.3 - 2\,\mathrm{mm}$ in about 50 ms, which is also compatible with the performance of our mechanical stages. Our system can thus be used to emulate vestibular signals associated with fictive self motion in head-fixed animals. It could thus be included into closed-loop virtual reality assays, mitigating sensory mismatch and enhancing the quality of virtual environments. This will open new possibilities to study sensorimotor processing.

Unlike other approaches, such as optical tweezers, the reported method could potentially be implemented in freely swimming configurations as well. A large scale magnetic field gradient could be used to create a sufficiently large force onto the magnetized otolith coating to counteract the gravitational force acting on it. One could thus create a zero gravity condition or mimic inverted gravity and study how fish adapt to and learn to cope with this change of physical parameters. As only injected fish will be sensitive to the applied magnetic field gradients, social behavior experiments can be envisioned to study how conspecific fish react to behavioral changes of a single fish when the latter experiences a perturbation of the vestibular sensation. But one may even go beyond and investigate how animals can learn to use this novel sensation of magnetic field gradients, e.g. for navigational strategies.

We have demonstrated that our vestibular stimulation method is compatible with simultaneous whole-brain functional imaging using light-sheet microscopy. In response to the fictive vestibular stimulus, we observed consistent neuronal activity in the vestibular nucleus and in downstream nuclei throughout the brain. The evoked neuronal response map in bilaterally injected fish was comparable to the one that was obtained during actual vestibular motion stimulation with a rotating light-sheet microscope. This confirms that the magnetic force acts without delay onto the otolith in the same manner as gravitational forces when the animal is e.g., rolled along its longitudinal body axis. The recorded average phase maps during unilateral stimulation suggests the presence of a pronounced commissural inhibition between the two vestibular nuclei, typically conserved in all vertebrates [40]. Sinusoidal magnetic stimulation of the right ear shows that pulling the right otolith laterally activates neurons located in the right vestibular nucleus and downstream regions such as the ipsilateral vestibular cerebellum, and on the contralateral side oculomotor motoneurons, neurons in the nMLF as well as hindbrain neuronal populations probably projecting to the spinal chord. This activity pattern and profile is consistent with the highly conserved axonal projections from the vestibular nucleus to these brain regions [41, 42]. This activation pattern has a mirror-symmetric counterpart with a mean activity that is 180 degrees phase-shifted and thus exhibits a mean activity that is minimal when the mirror-symmetric neuronal correlate is maximally active. This suggests that the vestibular nucleus inhibits the contralateral vestibular nucleus, which leads to a reduced activity in downstream nuclei. The latter result is consistent with the description of inhibitory commissural projections in cats between vestibular neurons of the utricular pathway [43], which are thought to contribute to the sensitivity of vestibular neurons through a disinhibition [43]. In larval zebrafish, commissural projections have been described as originating from the tangential vestibular nucleus [8], with a likely inhibitory function as evidenced by our results.

In summary, our magnet-based vestibular stimulation method is inexpensive, easy to implement, and can be developed as an add-on device for existing microscopes and visual virtual reality setups. Since the magnet is small and operates beneath the fish, the whole experimental chamber is accessible for all types of microscopes, optogenetic tools, electrophysiological setups, other sensory stimulation methods or behavioral monitoring. Accordingly, our method uniquely expands the toolbox of widely accessible sensory stimulation methods for zebrafish systems neuroscience but also for neuroscientific studies in other species.

4 Movie legends

Movie 1

Behavioral responses to fictive magnetic vestibular stimulation with a hand-held magnet.
Part I: Behavioral response to fictive vestibular roll stimulation recorded by top view monitoring. The fish is tethered with the agarose that was removed around the tail and eyes to allow free movements. The movie was obtained with a stereomicroscope immediately after ferrofluid injection. The magnet was hand-held and moved beneath the fish along the left-right body axis to mimic a vestibular roll stimulus.
Part II: Same fish as in Part I, with the magnet moved along the rostro-caudal body axis to mimic a tilt stimulus (nose-up, nose-down).
Eyes and tail perform marked compensatory movements in response to these fictive vestibular stimuli.

Movie 2

Behavioral responses to fictive vestibular roll and tilt stimuli generated and recorded in an automatized setup. Ferrofluid was bilaterally injected at 5 dpf and movies were recorded the next day at 6 dpf. The magnet was moved sinusoidally at 0.5 Hz and with 2.5 mm amplitude. **Part I:** Front view of evoked eye movements in response to a fictive roll stimulus.
Part II: Side view of evoked eye movements in response to a fictive roll stimulus. The eye rotates only along the roll axis and not along the tilt axis, demonstrating the absence of cross-talk between the two stimulation axes.
Part III: Side view of evoked eye movements in response to a fictive tilt stimulus. **Part IV:** Top view of evoked tail movements in response to a fictive roll stimulus. Note that the magnet created a shadow under the fish, which allows to see the correlation between magnet displacement and tail movement.

Movie 3

Impaired postural control along the roll axis after BAPTA injection compared to wild-type control fish with an intact vestibular system.
Part I: The movie shows a fish two hours after bilateral injection of the calcium chelator BAPTA. The fish was placed freely in a Petri dish filled with embryonic medium E3 and recorded from the top. A startle response was elicited by touching the fish with a fine glass tip. During the startle response and also during successive swimming bouts, the fish lost its dorsal position and rolled around its longitudinal body axis.

Part II: Recording of a wild-type control fish under the same conditions as in Part I. Throughout the sequence and including the startle response, the fish maintained its dorsal side-up posture.

Movie 4

Free swimming behavior of fish, injected bilaterally with ferrofluid, compared to wild-type control fish (Recording frame rate = 70 fps):
Part I: Wild-type fish (N = 10) swimming freely in a Petri dish.
Part II: Fish after bilateral injection of ferrofluid into the inner ears (N = 7), swimming freely in a Petri dish.

Movie 5

Brain-wide neuronal responses during a fictive sinusoidal roll stimulus.
The movie shows in a loop the neuronal response averaged over 40 stimulus cycles. Six sections of the brain are shown.
Experimental parameters: Ferrofluid was injected bilaterally at 5 dpf into a fish of the Tg(elav3-H2B:GCaMP6f) transgenic line. The movie was recorded the next day at 6 dpf. The magnet was moved sinusoidally at a frequency of 0.5 Hz and with an amplitude of 2.5 mm.

The phase map in Figure 4D was calculated from this recording.

Movie 6

Pilot study in a *Xenopus* tadpole.
The movie shows a dorsal view of an isolated *in vitro* preparation of a *Xenopus* tadpole prepared following the protocol in Lambert *et al.* 2008 [37]. Ferrofluid was injected into the left inner ear (red-orange color). A permanent point magnet was displaced in close proximity above the inner ear. The magnet motion provoked eye rotations via the vestibulo-ocular reflex. Only the left eye responded as the right eye was partly immobilized to hold the preparation in place.

5 Materials and Methods

5.1 Key resources table

REAGENT OR RESOURCES	SOURCE	IDENTIFIER
Chemicals		
Low melting point agarose	Sigma-Aldrich	A9414-50G
Tricaine	Sigma-Aldrich	E10521-10G
Ferrofluid	custom made	[22]
BAPTA	Sigma-Aldrich	14510-100MG-F
2-Di-4-Asp	Sigma-Aldrich	D3418-500MG
Ultrapure Low Melting Point Agarose	Invitrogen	16520050
Experimental Models: Organisms/Strains		
Tg(a-tubulin:Gal4-VP16 ;UAS:GCaMP7a)		Köster and Fraser 2001 [30]
Tg(elav3-H2B:GCaMP6f)		Vladimirov et al. 2014 [44]
Software and Algorithms		
Matlab	The MathWorks	https://www.mathworks.com/products.html
CMTK	Rohlfing and Maurer, 2003 (citation)	https://www.nitrc.org/projects/cmtk/
FIJI	(ImageJ) NIH	https://fiji.sc/
ZBrain atlas	Randlett et al., 2015	https://zebrafishexplorer.zib.de/home/
Comsol Multiphysics	Comsol	https://www.comsol.com/
Other		
Pneumatic PicoPump	World Precision Instruments	SYS-PV830
Glass capillaries to pull micropipettes	Warner Instruments	GC100F-10
Micropipette puller	Narishige	PC-100
Motorized stages	Physik Instrumente PI	PIMag® Linear Stage: V-408.132020, V-408.232020
Behavior tracking: Camera	Point Grey	BFLY-U3-05S2M-CS
Behavior tracking: Objective	Navitar	1-61449
Behavior tracking: 2x Adaptor	Navitar	1-61450
Magnet (D=5 mm, thickness 1 mm, 3 magnets stacked)	RS Components	N837RS
Micro knife 22,5° cutting angle	Fine Science Tools	10316-14

Table 1: Key resource table

5.2 Animal husbandry

All experiments were performed on 5-7 dpf larvae. Adult fish were maintained at 28°C in system water (ph 7-7.5 and conductivity between 300 and 350 μS)) in the fish facility of the Institut de Biologie Paris-Seine. Eggs were collected in the morning and then kept in a Petri dish with E3 at 28°C in a 14h/10h light/dark cycle. Larvae were fed with paramecia or powder from 5 dpf on. Calcium imaging experiments were carried out in two different transgenic lines: *elavl3:H2B-GCaMP6f* [44] (kindly provided by Misha Arhens) and *α-tubulin:Gal4-VP16 ;UAS:GCaMP7* [30] (kindly provided by Teresa Nicolson) both in Nacre background. Experiments were approved by Le Comité d'Éthique pour l'Expérimentation Animale Charles Darwin C2EA-05 (02601.01 and 32423-202107121527185 v3).

5.3 Ferrofluid

The ferrofluid, a suspension of γ-Fe_2O_3 iron oxide nanoparticles, was produced by Christine Ménager and Aude Michel Tourgis (Sorbonne Université, Laboratoire PHENIX, CNRS UMR 8234) following the protocol described by Massart et al. [22] and kindly provided to us for our experiments. The hydrodynamic diameter measured by dynamic light scattering (DLS) was 22 nm with a polydispersity index of 0.15. This corresponds to a physical diameter of 11 nm, usually measured by TEM after drying the sample. The particles were dispersed in water and stabilized with citrate molecules at pH 7 to prevent agglomeration.

5.4 Ear injections

Either ferrofluid, BAPTA or 4-Di-1-ASP were injected into the inner ear with a glass micropipette held by a micromanipulator (Narishige MN-153) using a pneumatic Pico-pump (World Precision Instruments PV830). Capillaries (1 mm outer diameter, Warner Instruments GC100F-10) were pulled to obtain fine tip micropipettes (tip diameter = 1 - 2 μm) using a Narishige PC-100 puller with the following parameters: 2 steps, Heater N°1 = 52,4; Heater N°2 = 55,7, position 2 mm, 2 heavy and 1 light weights. Micropipettes were loaded with 2 μL of ferrofluid diluted in buffer (NaCl 0.178 M, sodium citrate 0.023 M, HEPES 0.01 M) at 0,019 μM. Injections were performed in 5 dpf fish. Larvae were mounted dorsal side up in 2 % LMP agarose on top of a microscope glass slide. Using a small piece of metal as support, the slide was rolled 45 degrees to access the fish's left ear. For the ferrofluid, 3 pulses (10 psi for 500 ms) were injected into the otic vesicle, corresponding to a total volume of 1,2 nL. After the left ear injection, the glass slide was rolled onto the other side to inject the right ear. For injection of BAPTA and DiASP the protocol was the same except for different concentrations of the solutions. We used 50 mM BAPTA dissolved in extracellular solution containing (in mM) 134 NaCl, 2.9 KCl, 1.2 $MgCl_2$, 2.1 $CaCl_2$, 10 HEPES, and 10 glucose, at 290 mOsm, adjusted to a pH 7.8 with NaOH. For 4-Di-1-ASP, a 50 mM solution of diluted E3 medium containing 1% ethanol was injected. After the injections, larvae were freed from the agarose using a fine tip (Dumont n°5) and maintained in E3 medium until the experiments commenced.

5.5 Free swimming control

We analyzed the free swimming behavior of ferrofluid-injected and control fish. Seven larvae were injected at 5 dpf. 24 hours later they were placed in a Petri dish to record the swimming behavior during 1 hour at 30 fps. The movies were tracked using FastTrack [45]. Individual fish were not tracked throughout the whole movie but rather split into wall-to-wall trajectories. For each trajectory, discrete swim bouts were detected when the instantaneous swim speed exceeded two times the overall variance of the speed. Putative bouts were then filtered on a distance criterion: bouts with a linear displacement – measured in a time window of $\pm$0.5 s centered on the bout velocity peak – less than 0.3 mm or greater than 18 mm were rejected) and on a temporal criterion (bouts occurring within 0.4 s after a bout were rejected. Bout onset was defined at 80 ms before the velocity peak. From positions, time and body angles before and after an event, the inter-bout interval, displacement and turn angles associated with each bout were computed. These values were then averaged over trajectories and the means were displayed as boxplots. Mean square displacement (MSD) was

computed using the MATLAB package msdanalyzer [46]. (x,y) sequences were pooled by condition (control and injected), a MSD was computed for each sequence and the ensemble average is presented along with the standard error of the mean.

5.6 Roll ratio essay

The larvae were placed in a 5 cm Petri dish positioned under a high magnification objective and recorded at 300 fps. Approaching the larvae with a fin glass tip evoked a startle response. Each larva was subjected to five trials. The roll behavior was assessed for each trial. The roll ratio was calculated as the number of trials the animal rolled during an escape divided by the number of trials the animal attempted an escape [27].

5.7 Finite element simulations and force generation mechanism

Force of a ferrofluid particle in a magnetic field gradient The ferrofluid particles are so small that nanoparticles consist only of a single magnetic domain giving the particle a giant magnetic moment. In the absence of an external magnetic field, the direction of this moment changes randomly depending on the temperature. The average magnetisation is zero and the particle is in a superparamagnetic state. In an external magnetic field, the giant magnetic moment becomes progressively aligned against the thermal agitation, and the average net magnetization increases. The macroscopic magnetization of a ferrofluid particle or of a ferrofluid droplet is characterized by the macroscopic magnetic moment, $\vec{m}$, which depends on the volume V of the particle or of a ferrofluid droplet, and the external field B. In a weak magnetic field the macroscopic magnetization is given by

$$\vec{m}(\vec{B}) = \frac{V\chi}{\mu_0}\vec{B}$$

with χ the magnetic susceptibility and μ_0 the vacuum permeability. And the force exerted on the droplet reads

$$\vec{F} = \nabla\left(\vec{m}(\vec{B})\cdot\vec{B}\right) = \nabla\left(\frac{V\chi}{\mu_0}\vec{B}^2\right) = 2\frac{V\chi}{\mu_0}\vec{B}\nabla\vec{B}$$

In a strong field that saturates the magnetization the force exerted on the droplet is

$$\vec{F} = \nabla\left(\vec{m}_{sat}\cdot\vec{B}\right) = \vec{m}_{sat}\nabla\vec{B}$$

Finite element simulations We used Comsol Multiphysics to calculate the magnetic force applied by the magnet to the ferrofluid. Lateral force-displacement curves were calculated for cylindrical magnets of different diameters and z-distance to a spherical droplet of the ferrofluid with a diameter of 200 μm. The spherical droplet was considered perfectly rigid. The droplet volume was chosen arbitrarily. The force, acting on the droplet depends linearly on the volume of the droplet. Therefore uncertainty with respect to the droplet volume will change the maximum force reached but not the linear dependence of force on the magnet position. The relationship between magnetic flux density and magnetic field strength (B-H curve) is defined

for the ferrofluid by a magnetization curve (Figure S3). The magnetic flux density is fixed for the magnets. For the simulations, we started with a mesh size of 500 μm and then iteratively reduced the mesh size until the results converged. Parametric sweeps were realized for different distances and diameters.

The simulation gives a maximal lateral force of $F_{D=200\,\mu} = 4 \cdot 10^{-4} N$ exerted on the ferrofluid droplet with a diameter of $D = 200\,\mu m$ placed 2 mm above our 5 mm in diameter magnet. As the force depends linearly on the volume we estimated that the force exerted on a single nanoparticle with a diameter of $D = 11\,nm$ is $F_p = 0.007\,\text{fN}$.

Drag force on an otolith pulled through water To estimate the maximum force that can be delivered to the otolith, we measured the velocity in water of an isolated otolith (obtained after dissection of an injected larvae) submitted to a comparable magnetic field as in the *in vivo* experiment. Taking into account the otolith diameter that controls the drag force, we obtained an estimated force of

$$F_{drag} = 6\pi\eta R v = 0.9\,\text{nN}$$

with η the viscosity of water $R = 27.5\,\mu$m, the radius of the otolith and v the speed at which the otolith was dragged by the magnet through the aqueous solution.

Given the force that the magnet exerts on a single particle of the ferrofluid suspension $F_p = 0.007\,\text{fN}$ we can estimate the number of particle bound to the otolith

$$N = \frac{F_{drag}}{F_p} = 1.3 \cdot 10^8$$

A monolayer of particles on the otolith surface corresponds to

$$N \approx \frac{4\pi R_{otolith}^2}{D_p} = 0.8 \cdot 10^8$$

particles. Thus we estimate that ~ 1.6 monolayers of particles have bound to the otolith.

However, due to the small diameter of the particles, the mass change of the otolith is negligible with

$$\frac{m_{monolayer}}{m_{otolith}} = \frac{4\pi R_{otolith}^2 D_p \cdot \rho_{Fe_2O_3}}{4/3\pi R_{otolith}^3} = 2 \cdot 10^{-4}$$

Gravitational force F_g exerted onto the otolith during roll motion When the fish is rolled under natural conditions along the rostro-caudal body axis, gravity acts on the otoliths pulling them along the left-right body axis. The magnitude of this lateral component of the gravitational force F_g depends on the roll angle and on the density of the otolith

$$F_g = (\rho_o - \rho_w) V_o g \sin(\alpha)$$

with the density of the otolith $\rho_o = 2.83\,\mathrm{g\,cm^{-3}}$, the density of water $\rho_o = 1\,\mathrm{g\,cm^{-3}}$, the otolith volume $V_o = \frac{4}{3}\pi R_o^3$, the otolith radius $R_o = 27\,\mathrm{nm}$, the gravitational acceleration $g = 9.81\,\mathrm{m\,s^{-2}}$ and the angle α by which the animal is rolled relative to its dorsal side-up position.

At $\alpha = 90°$ the lateral force on the otolith is maximal with:

$$F_g(\alpha = 90°) = 1.6\,nN$$

Because the mean behavioral response in the fictive roll motion experiments compares to the mean evoked response when rolling fish with a sinusoidally modulated excursion of ±15°, we can estimate that we exerted *in vivo* with our experimental parameters in average a force of $< F_{max} >= 1.6\,\mathrm{nN} \cdot \sin(15°) = 400\,\mathrm{pN}$ on the otolith when displacing the magnet $2.5\,mm$.

Time constant at which a particle reaches its terminal velocity when accelerated by a constant force in a viscous solution. Freely floating particles in the inner ear will be accelerated by the magnet. However, due to the interaction with the surrounding water molecules they will reach a terminal velocity after a characteristic time

$$\tau = \frac{m_p}{6\pi\eta R_p} = \frac{2\rho_p R_p^2}{9\eta} = 516\,\mathrm{ps}$$

with the particle mass m_p, the hydrodynamic particle radius $R_p = 22\,nm$ and the viscosity of water η. The terminal velocity reached is

$$v = \frac{F}{6\pi\eta R_p} = 0.1\,\mu\mathrm{m\,s}{-}1$$

with the hydrodynamic particle radius $R_p = 22\,nm$ and the viscosity of water η and with the estimated maximal force $F_p = 0.007\,\mathrm{fN}$ exerted on a ferrofluid nanoparticle placed 2 mm over the edge of our 5 mm in diameter magnet.

5.8 Sample preparation

24 hours after ferrofluid injection larvae were mounted in 2 % low melting point agarose dorsal side-up on top of a small acrylic holder (1mm thick). Then, the holder was placed inside an acrylic chamber filled with E3. For behavioral experiments, the agarose was removed from the eyes and tail using a micro knife (FST Micro Knife - Plastic Handle/22.5° Cutting Angle).

5.9 The setup

We built a platform with two motorized stages (PI instruments) to precisely control the magnet position and hence the fictive vestibular stimulation. A third manual stage allowed to position the magnet beneath the fish as close as possible in the vertical plane in order to maximize the accessible range of force. For the experiments shown in Figure 1 and 4 we used a magnet 5 mm in diameter and 3 mm in height. Injected

fish were mounted in a drop of 2% low melting point agarose on top of a transparent acrylic holder (1 mm thick). The agarose was removed from around the eyes and tail to allow unimpaired movements. Then, the holder was placed into the sample chamber filled with embryonic medium E3. The bottom of the sample chamber was formed by a 220μm thick coverslip glass. A front and a side camera were installed to record eye movements. To record tail movements, we used the same camera as for the neural recordings, equipped with a 4x objective. The entire platform was mounted on a light-sheet microscope system to perform simultaneous brain-wide neuronal activity recordings.

5.10 Behavioral protocol

In order to move the magnet in a controlled manner, we used 2 stages for x and y axis movements (Physik Instrumente, V-408 PIMag Linear Stage). To simulate a roll-like motion, we moved the magnet along the transverse axis, starting from the center and extending 2.5 mm towards each side of the fish. To simulate a tilt-like motion, we moved the magnet along the longitudinal axis, using the same amplitude. The stimulation frequency was 0.5 Hz.

5.11 Imaging Setup

The imaging setup was built around a microscope frame (Scientifica Slicescope Pro) fitted with an Olympus BX-URA fluorescence illuminator and a custom light-sheet forming unit adapted from Migault et al. [4]. Functional imaging was performed with a Leica HC FLUOTAR L 25x/0,95 W VISIR objective and a Hamamatsu Orca-Flash4.0 V3. Images were recorded with HCImage software (Hamamatsu) and the light-sheet was controlled with a custom application written in Matlab (MathWorks). Top view behavioral recordings used the microscope's light path and camera with a Nikon CFI Achro 4x objective. Side and front view behavioral recordings used separate systems of Point Grey cameras (BFLY-U3-05S2M-CS) with Navitar Precise Eye objectives (1-61450 with 1-61449).

5.12 Registration onto the Z-Brain atlas

We used the Computational Morphometry ToolKit CMTK (http://www.nitrc.org/projects/cmtk/) to compute for every fish the morphing transformation from the average brain stack (anatomical stack) to the Elavl3:H2B-RFP stack of the zBrain atlas [31]. This allowed mapping the functional data onto the Z-Brain Viewer, to overlay the region outlines and to calculate averages across animals.

We computed first the affine transformation, which we used then as initialization to compute the warp transformation between the two stacks. The used commands and options are listed in table 2.

5.13 Data and code availability

Data and code are available on request to the lead author: volker.bormuth@sorbonne-universite.fr

Tool	Options	Description
cmtk registration	–Initxlate –dofs 6,9,12 –sampling 3 –coarsest 25 –omit-original-data –accuracy 3 –exploration 25.6	Calculate affine transformation
cmtk warp	-v -–fast –grid-spacing 40 –refine 2 –jacobian-weight 0.001 –coarsest 6.4 –sampling 3.2 –accuracy 3.2 –omit-original-data	Use affine transformation as initialization
reformatx		Apply transformation to other stacks

Table 2: CMTK commands and options

Acknowledgements

We thank Christine Ménager and Aude Michel Tourgis (Sorbonne Université, Laboratoire PHENIX, CNRS UMR 8234) who kindly provided the ferrofluid. We thank the IBPS fish facility staff for the fish maintenance, in particular Stéphane Tronche and Alex Bois. We thank Misha Ahrens and Teresa Nicolson for providing transgenic fish lines. We are grateful to Carounagarane Dore for his contribution to the design of the experimental setup. We thank Claire Wyart and Marcus Ghosh for their comments on the manuscript. This project has received funding from the European Research Council (ERC) under the European Union's Horizon 2020 research innovation program grant agreement number 715980, and was partially funded by the CNRS, Sorbonne Université, and by the German Science Foundation through the collaborative research center 870 (CRC 870). H.M., G.M., and P.T. had a PhD fellowship from the Doctoral School in Physics, Ile de France (EDPIF). G.L.G. had a PhD fellowship from the Systems Biology Network of Sorbonne Université.

Authors contribution

N.B., H.S., N.D, G.D. and V.B designed the project. N.B., H.M., G.M. and P.T. performed the zebrafish experiments. N.B. T.Panier, T. Pujol, G.M, and V.B. built the experimental setup. T.Pujol performed the finite element simulations. N.B., H.M., G.M., G.L.G., P.T., G.D., V.B. analyzed the data, N.D. and H.S. performed the *Xenopus* experiment. N.B., G.D., V.B wrote the manuscript with input from all the authors.

Declaration of interests

The authors declare no competing interests.

References

1. Angelaki DE and Cullen KE. Vestibular system: the many facets of a multimodal sense. English. Annual review of neuroscience 2008; 31:125–50. DOI: 10.1146/annurev.neuro.31.060407.125555
2. Cullen KE. The vestibular system: Multimodal integration and encoding of self-motion for motor control. Trends in Neurosciences 2012; 35:185–96. DOI: 10.1016/j.tins.2011.12.001. Available from: http://dx.doi.org/10.1016/j.tins.2011.12.001
3. Panier T, Romano SA, Olive R, Pietri T, Sumbre G, Candelier R, and Debrégeas G. Fast functional imaging of multiple brain regions in intact zebrafish larvae using Selective Plane Illumination Microscopy. English. Frontiers in neural circuits 2013; 7:65. DOI: 10.3389/fncir.2013.00065
4. Migault G, Plas TL van der, Trentesaux H, Panier T, Candelier R, Proville R, Englitz B, Debrégeas G, and Bormuth V. Whole-Brain Calcium Imaging during Physiological Vestibular Stimulation in Larval Zebrafish. Current Biology 2018. DOI: 10.1016/j.cub.2018.10.017
5. Favre-Bulle IA, Vanwalleghem G, Taylor MA, Rubinsztein-Dunlop H, and Scott EK. Cellular-Resolution Imaging of Vestibular Processing across the Larval Zebrafish Brain. Current Biology 2018 Dec; 28:3711–3722.e3. DOI: 10.1016/j.cub.2018.09.060
6. Ahrens MB, Orger MB, Robson DN, Li JM, and Keller PJ. Whole-brain functional imaging at cellular resolution using light-sheet microscopy. English. Nature methods 2013; 10:413–20. DOI: 10.1038/nmeth.2434
7. Beck JC, Gilland E, Tank DW, and Baker R. Quantifying the ontogeny of optokinetic and vestibuloocular behaviors in zebrafish, medaka, and goldfish. Journal of Neurophysiology 2004 Dec; 92:3546–61. DOI: 10.1152/jn.00311.2004. Available from: https://www.physiology.org/doi/10.1152/jn.00311.2004
8. Bianco IH, Ma LH, Schoppik D, Robson DN, Orger MB, Beck JC, Li JM, Schier AF, Engert F, and Baker R. The tangential nucleus controls a gravito-inertial vestibulo-ocular reflex. Current Biology 2012; 22:1285–95. DOI: 10.1016/j.cub.2012.05.026
9. Favre-Bulle IA, Stilgoe AB, Rubinsztein-Dunlop H, and Scott EK. Optical trapping of otoliths drives vestibular behaviours in larval zebrafish. Nature Communications 2017; 8. DOI: 10.1038/s41467-017-00713-2. Available from: http://dx.doi.org/10.1038/s41467-017-00713-2
10. Mo W, Chen F, Nechiporuk A, and Nicolson T. Quantification of vestibular-induced eye movements in zebrafish larvae. BMC neuroscience 2010; 11:110. DOI: 10.1186/1471-2202-11-110
11. Ehrlich DE and Schoppik D. Control of Movement Initiation Underlies the Development of Balance. Current Biology 2017 Feb; 27:334–44. DOI: 10.1016/j.cub.2016.12.003

12. Voit W, Kim DK, Zapka W, Muhammed M, and Rao KV. Magnetic behavior of coated superparamagnetic iron oxide nanoparticles in ferrofluids. MRS Online Proceedings Library 2011; 676:78. DOI: 10.1557/PROC-676-Y7.8. Available from: https://doi.org/10.1557/PROC-676-Y7.8

13. Shapiro B, Kulkarni S, Nacev A, Sarwar A, Preciado D, and Depireux D. Shaping Magnetic Fields to Direct Therapy to Ears and Eyes. Annual Review of Biomedical Engineering 2014; 16:455–81. DOI: 10.1146/annurev-bioeng-071813-105206

14. Desprat N, Supatto W, Pouille PA, Beaurepaire E, and Farge E. Tissue Deformation Modulates Twist Expression to Determine Anterior Midgut Differentiation in Drosophila Embryos. Developmental Cell 2008; 15:470–7. DOI: 10.1016/j.devcel.2008.07.009

15. Doubrovinski K, Swan M, Polyakov O, and Wieschaus EF. Measurement of cortical elasticity in Drosophila melanogaster embryos using ferrofluids. Proceedings of the National Academy of Sciences of the United States of America 2017 Jan; 114:1051–6. DOI: 10.1073/PNAS.1616659114

16. Fernández-Sánchez ME, Barbier S, Whitehead J, Béalle G, Michel A, Latorre-Ossa H, Rey C, Fouassier L, Claperon A, Brullé L, Girard E, Servant N, Rio-Frio T, Marie H, Lesieur S, Housset C, Gennisson JL, Tanter M, Ménager C, Fre S, Robine S, and Farge E. Mechanical induction of the tumorigenic β-catenin pathway by tumour growth pressure. Nature 2015; 523:92–5. DOI: 10.1038/nature14329. Available from: https://doi.org/10.1038/nature14329

17. Mitrossilis D, Röper JC, Le Roy D, Driquez B, Michel A, Ménager C, Shaw G, Le Denmat S, Ranno L, Dumas-Bouchiat F, Dempsey NM, and Farge E. Mechanotransductive cascade of Myo-II-dependent mesoderm and endoderm invaginations in embryo gastrulation. Nature Communications 2017; 8:13883. DOI: 10.1038/ncomms13883. Available from: https://doi.org/10.1038/ncomms13883

18. Serwane F, Mongera A, Rowghanian P, Kealhofer DA, Lucio AA, Hockenbery ZM, and Campàs O. In vivo quantification of spatially varying mechanical properties in developing tissues. Nature Methods 2017; 14:181–6. DOI: 10.1038/nmeth.4101. Available from: https://doi.org/10.1038/nmeth.4101

19. Strick TR, Allemand JF, Bensimon D, Bensimon A, and Croquette V. The Elasticity of a Single Supercoiled DNA Molecule. Science 1996; 271:1835–7. DOI: 10.1126/science.271.5257.1835. eprint: https://science.sciencemag.org/content/271/5257/1835.full.pdf. Available from: https://science.sciencemag.org/content/271/5257/1835

20. Adhikari AS, Chai J, and Dunn AR. Mechanical Load Induces a 100-Fold Increase in the Rate of Collagen Proteolysis by MMP-1. Journal of the American Chemical Society 2011 Feb; 133:1686–9. DOI: 10.1021/ja109972p. Available from: https://doi.org/10.1021/ja109972p

21. Nimpf S, Nordmann GC, Kagerbauer D, Malkemper EP, Landler L, Papadaki-Anastasopoulou A, Ushakova L, Wenninger-Weinzierl A, Novatchkova M, Vincent P, Lendl T, Colombini M, Mason MJ, and Keays DA. A Putative Mechanism for Magnetoreception by Electromagnetic Induction in the Pigeon Inner Ear. Current Biology 2019; 29:4052–4059.e4. DOI: 10.1016/j.cub.2019.09.048

22. Massart R, Dubois E, Cabuil V, and Hasmonay E. Preparation and properties of monodisperse magnetic fluids. Journal of Magnetism and Magnetic Materials 1995; 149:1–5. DOI: 10.1016/0304-8853(95)00316-9

23. Schuknecht HF and Montandon P. Pathology of the ear in pneumococcal meningitis. Archiv für klinische und experimentelle Ohren-, Nasen-und Kehlkopfheilkunde 1970; 195:207–25

24. Riley BB and Moorman SJ. Development of utricular otoliths, but not saccular otoliths, is necessary for vestibular function and survival in zebrafish. Journal of Neurobiology 2000 Jun; 43:329–37. DOI: 10.1002/1097-4695(20000615)43:4<329::AID-NEU2>3.0.CO;2-H

25. Bagnall MW and McLean DL. Modular organization of axial microcircuits in zebrafish. Science 2014; 343:197–200. DOI: 10.1126/science.1245629

26. Roberts R, Elsner J, and Bagnall MW. Delayed Otolith Development Does Not Impair Vestibular Circuit Formation in Zebrafish. JARO - Journal of the Association for Research in Otolaryngology 2017; 18:415–25. DOI: 10.1007/s10162-017-0617-9

27. Hubbard JM, Böhm UL, Prendergast A, Tseng PEB, Newman M, Stokes C, and Wyart C. Intraspinal Sensory Neurons Provide Powerful Inhibition to Motor Circuits Ensuring Postural Control during Locomotion. Current Biology 2016; 26:2841–53. DOI: 10.1016/j.cub.2016.08.026

28. Assad JA, Shepherd GM, and Corey DP. Tip-link integrity and mechanical transduction in vertebrate hair cells. Neuron 1991; 7:985–94. DOI: 10.1016/0896-6273(91)90343-X

29. Zhao YD, Yamoah EN, and Gillespie PG. Regeneration of broken tip links and restoration of mechanical transduction in hair cells. Proceedings of the National Academy of Sciences of the United States of America 1996 Dec; 93:15469–74. DOI: 10.1073/pnas.93.26.15469. Available from: /pmc/articles/PMC26428/%20/pmc/articles/PMC26428/?report=abstract%20https://www.ncbi.nlm.nih.gov/pmc/articles/PMC26428/

30. Köster RW and Fraser SE. Tracing transgene expression in living zebrafish embryos. Developmental Biology 2001 May; 233:329–46. DOI: 10.1006/dbio.2001.0242

31. Randlett O, Wee CL, Naumann EA, Nnaemeka O, Schoppik D, Fitzgerald JE, Portugues R, Lacoste AMB, Riegler C, Engert F, and Schier AF. Whole-brain activity mapping onto a zebrafish brain atlas. Nature methods 2015; 12:1039–46. DOI: 10.1038/nmeth.3581

32. Harris Ja, Cheng AG, Cunningham LL, MacDonald G, Raible DW, and Rubel EW. Neomycin-induced hair cell death and rapid regeneration in the lateral line of zebrafish (Danio rerio). Journal of the Association for Research in Otolaryngology : JARO 2003 Jun; 4:219–34. DOI: 10.1007/s10162-002-3022-x. Available from: http://www.pubmedcentral.nih.gov/articlerender.fcgi?artid=3202713&tool=pmcentrez&rendertype=abstract

33. Cotanche DA. Regeneration of hair cell stereociliary bundles in the chick cochlea following severe acoustic trauma. Hearing research 1987; 30:181–95

34. Girod DA, Duckert LG, and Rubel EW. Possible precursors of regenerated hair cells in the avian cochlea following acoustic trauma. Hearing research 1989; 42:175–94

35. Jones JE and Corwin JT. Regeneration of sensory cells after laser ablation in the lateral line system: hair cell lineage and macrophage behavior revealed by time-lapse video microscopy. eng. The Journal of neuroscience : the official journal of the Society for Neuroscience 1996 Jan; 16:649–62. DOI: 10.1523/JNEUROSCI.16-02-00649.1996

36. Jimenez E, Slevin CC, Colón-Cruz L, and Burgess SM. Vestibular and Auditory Hair Cell Regeneration Following Targeted Ablation of Hair Cells With Diphtheria Toxin in Zebrafish. Frontiers in Cellular Neuroscience 2021; 15:721950. DOI: 10.3389/fncel.2021.721950

37. Lambert FM, Beck JC, Baker R, and Straka H. Semicircular Canal Size Determines the Developmental Onset of Angular Vestibuloocular Reflexes in Larval Xenopus. Journal of Neuroscience 2008; 28:8086–95. DOI: 10.1523/jneurosci.1288-08.2008

38. Ehrlich DE and Schoppik D. A primal role for the vestibular sense in the development of coordinated locomotion. eLife 2019 Oct; 8. DOI: 10.7554/eLife.45839

39. Pozo Ad, Manuel R, Gonzalez ABI, Koning HK, Habicher J, Zhang H, Allalou A, Kullander K, and Boije H. Behavioral Characterization of dmrt3a Mutant Zebrafish Reveals Crucial Aspects of Vertebrate Locomotion through Phenotypes Related to Acceleration. eNeuro 2020; 7:ENEURO.0047–20.2020. DOI: 10.1523/eneuro.0047-20.2020

40. Malinvaud D, Vassias I, Reichenberger I, Rossert C, and Straka H. Functional Organization of Vestibular Commissural Connections in Frog. Journal of Neuroscience 2010; 30:3310–25. DOI: 10.1523/jneurosci.5318-09.2010

41. Highstein SM, Goldberg JM, Moschovakis AK, and Fernandez C. Inputs from regularly and irregularly discharging vestibular nerve afferents to secondary neurons in the vestibular nuclei of the squirrel monkey. II. Correlation with output pathways of secondary neurons. Journal of Neurophysiology 1987; 58:719–38. DOI: 10.1152/jn.1987.58.4.719

42. Straka H and Baker R. Vestibular blueprint in early vertebrates. Frontiers in Neural Circuits 2013; 7:1–9. DOI: 10.3389/fncir.2013.00182. Available from: http://journal.frontiersin.org/article/10.3389/fncir.2013.00182/abstract

43. Uchino Y, Sato H, Zakir M, Kushiro K, Imagawa M, Ogawa Y, Ono S, Meng H, Zhang X, Katsuta M, Isu N, and Wilson VJ. Commissural effects in the otolith system. Experimental Brain Research 2001; 137:421–30. DOI: 10.1007/s002210000611

44. Vladimirov N, Mu Y, Kawashima T, Bennett DV, Yang CT, Looger LL, Keller PJ, Freeman J, and Ahrens MB. Light-sheet functional imaging in fictively behaving zebrafish. English. Nature methods 2014; 11:883–4. DOI: 10.1038/nmeth.3040

45. Gallois B and Candelier R. FastTrack: An open-source software for tracking varying numbers of deformable objects. PLoS Computational Biology 2021; 17:e1008697. DOI: 10.1371/journal.pcbi.1008697. eprint: 2011.06837

46. Tarantino N, Tinevez JY, Crowell EF, Boisson B, Henriques R, Mhlanga M, Agou F, Israël A, and Laplantine E. TNF and IL-1 exhibit distinct ubiquitin requirements for inducing NEMO–IKK supramolecular structures. The Journal of Cell Biology 2014; 204:231–45. DOI: 10.1083/jcb.201307172

Supplementary Information

Supplementary figures

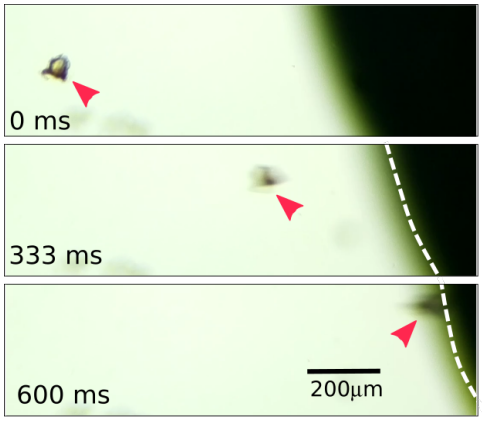

Figure S1: Image sequence of the dissected otolith (red arrowheads) with attached magnetic nanoparticles being attracted by a magnet (d = 5 mm) over time (dashed line indicates the magnet's edge).

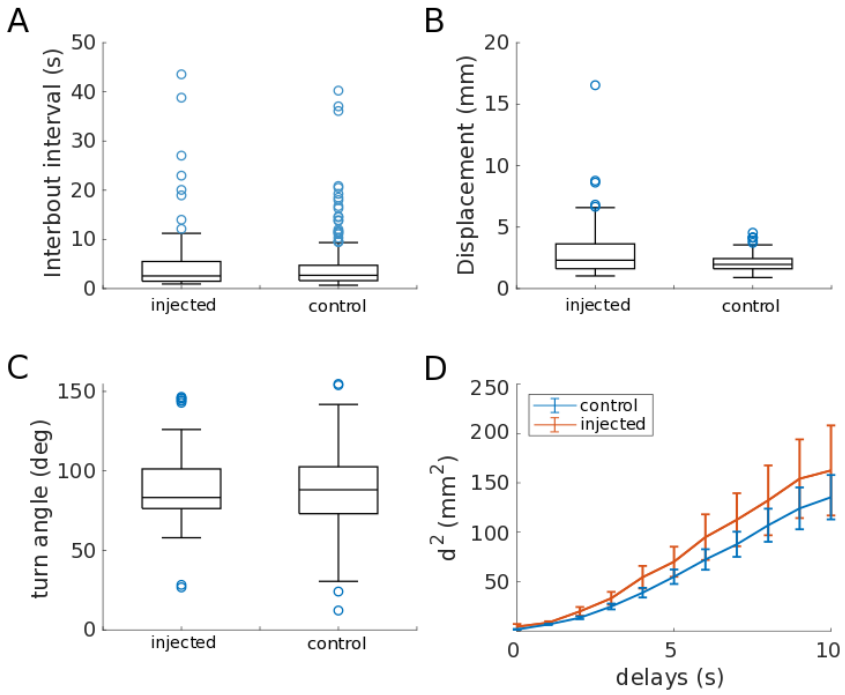

Figure S2: Effect of ferrofluid injection on swimming behavior. **(A-C)** Boxplots showing: **(A)** the distribution of the inter-bout interval, which is the time in seconds elapsed between two consecutive swimming events, **(B)** the mean displacement after a swim bout in mm, and **(C)** the turn angle in degrees. **(D)** Plot showing the mean of the mean square distance for 10 different time delay. The results were obtained by tracking two different batches of injected and non-injected fish. The fish were filmed swimming freely during 1 h (75 fps). P-values : ib-interval p = 0.846, displacement p = 0.00077, turn angle p = 0.366. N = 6 injected fish, 11 control non-injected fish.

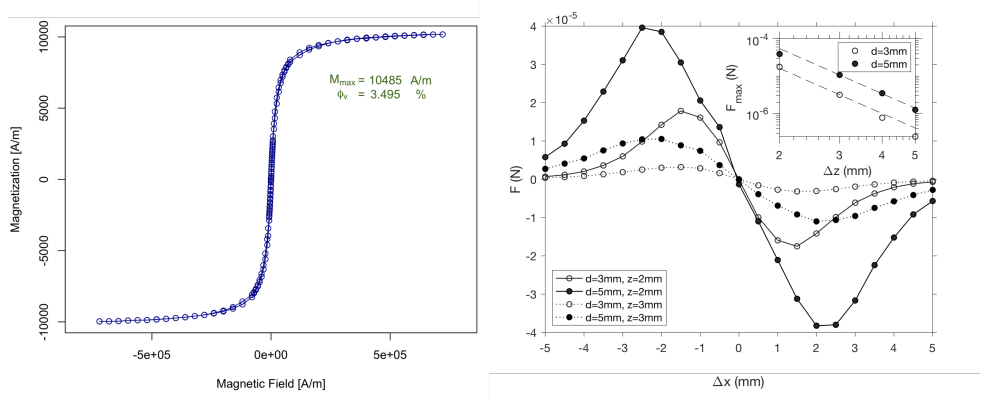

Figure S3: Left: Magnetization of the ferrofluid as a function of the magnetic field intensity (H). In vacuum, magnetic field intensity and magnetic flux density are linked by $\vec{B} = \mu_0 \vec{H}$. Right: Non-normalized simulation results from Figure 3.

Bibliography

[1] H. B. Barlow; «Possible Principles Underlying the Transformations of Sensory Messages»; . 3

[2] G. Gingras, B. A. Rowland & B. E. Stein; «The Differing Impact of Multisensory and Unisensory Integration on Behavior»; (2009). 3

[3] T. Ohyama, C. M. Schneider-Mizell, R. D. Fetter, J. V. Aleman, R. Franconville, M. Rivera-Alba, B. D. Mensh, K. M. Branson, J. H. Simpson, J. W. Truman, A. Cardona & M. Zlatic; «A multilevel multimodal circuit enhances action selection in Drosophila»; Nature 2015 520:7549 **520**, p. 633–639 (2015). ISSN 1476-4687. https://www.nature.com/articles/nature14297. 3

[4] A. M. Peiffer, J. L. Mozolic, C. E. Hugenschmidt & P. J. Laurienti; «Age-related multisensory enhancement in a simple audiovisual detection task»; NeuroReport **18**, p. 1077–1081 (2007). ISSN 09594965. https://journals.lww.com/neuroreport/Fulltext/2007/07020/Age_related_multisensory_enhancement_in_a_simple.26.aspx. 3

[5] D. Alais, F. N. Newell & P. Mamassian; «Multisensory Processing in Review: from Physiology to Behaviour»; Seeing and Perceiving **23**, p. 3–38 (2010). ISSN 1878-4763. https://brill.com/view/journals/sp/23/1/article-p3_2.xml. 3

[6] Y. H. Song, J. H. Kim, H. W. Jeong, I. Choi, D. Jeong, K. Kim & S. H. Lee; «A Neural Circuit for Auditory Dominance over Visual Perception»; Neuron **93**, p. 940–954.e6 (2017). ISSN 0896-6273. 3, 30

[7] L. Shams & A. R. Seitz; «Benefits of multisensory learning»; Trends in Cognitive Sciences **12**, p. 411–417 (2008). ISSN 1364-6613. 3, 29

[8] M. Gori; «Multisensory Integration and Calibration in Children and Adults with and without Sensory and Motor Disabilities»; Multisensory Research **28**, p. 71–99 (2015). ISSN 2213-4808. https://brill.com/view/journals/msr/28/1-2/article-p71_5.xml. 3

[9] S. Martínez-Sanchis; «Neurobiological foundations of multisensory integration in people with autism spectrum disorders: The role of the medial prefrontal cortex»; Frontiers in Human Neuroscience **8**, p. 970 (2014). ISSN 16625161. 3

[10] M. O. Ernst & H. H. Bülthoff; «Merging the senses into a robust percept»; (2004). 3, 4

[11] M. M. Mesulam; «From sensation to cognition.»; Brain **121**, p. 1013–1052 (1998). ISSN 0006-8950. https://academic.oup.com/brain/article/121/6/1013/280347. 4

[12] A. Zaidel, W. J. Ma & D. E. Angelaki; «Supervised Calibration Relies on the Multisensory Percept»; Neuron **80**, p. 1544–1557 (2013). ISSN 0896-6273. 4

[13] D. E. Angelaki, Y. Gu & G. C. DeAngelis; «Multisensory integration: psychophysics, neurophysiology, and computation»; Current Opinion in Neurobiology **19**, p. 452–458 (2009). ISSN 0959-4388. 4

[14] M. O. Ernst & M. S. Banks; «Humans integrate visual and haptic information in a statistically optimal fashion»; Nature 2002 415:6870 **415**, p. 429–433 (2002). ISSN 1476-4687. https://www.nature.com/articles/415429a. 4

[15] D. Alais & D. Burr; «The Ventriloquist Effect Results from Near-Optimal Bimodal Integration»; Current Biology **14**, p. 257–262 (2004). ISSN 0960-9822. 4

[16] M. A. Meredith & B. E. Stein; «Interactions Among Converging Sensory Inputs in the Superior Colliculus»; Science **221**, p. 389–391 (1983). ISSN 00368075. https://www.science.org/doi/10.1126/science.6867718. 4

[17] T. R. Stanford, S. Quessy & B. E. Stein; «Behavioral/Systems/Cognitive Evaluating the Operations Underlying Multisensory Integration in the Cat Superior Colliculus»; (2005). 4, 31

[18] C. R. Fetsch, G. C. Deangelis & D. E. Angelaki; «Bridging the gap between theories of sensory cue integration and the physiology of multisensory neurons»; (2013). 4, 19, 30

[19] N. A. Steinmetz, C. Aydin, A. Lebedeva, M. Okun, M. Pachitariu, M. Bauza, M. Beau, J. Bhagat, C. Böhm, M. Broux, S. Chen, J. Colonell, R. J. Gardner, B. Karsh, F. Kloosterman, D. Kostadinov, C. Mora-Lopez, J. O'Callaghan, J. Park, J. Putzeys, B. Sauerbrei, R. J. van Daal, A. Z. Vollan, S. Wang, M. Welkenhuysen, Z. Ye, J. T. Dudman, B. Dutta, A. W. Hantman, K. D. Harris, A. K. Lee, E. I. Moser, J. O'Keefe, A. Renart, K. Svoboda, M. Häusser, S. Haesler, M. Carandini & T. D. Harris; «Neuropixels 2.0: A miniaturized high-density probe for stable, long-term brain recordings»; Science (New York, N.Y.) **372** (2021). ISSN 10959203. /pmc/articles/PMC8244810//pmc/articles/PMC8244810/?report=abstracthttps://www.ncbi.nlm.nih.gov/pmc/articles/PMC8244810/. 4

[20] J. Driver & T. Noesselt; «Multisensory Interplay Reveals Crossmodal Influences on 'Sensory-Specific' Brain Regions, Neural Responses, and Judgments»; Neuron **57**, p. 11–23 (2008). ISSN 0896-6273. 5, 30, 56

[21] G. A. Calvert, E. T. Bullmore, M. J. Brammer, R. Campbell, S. C. Williams, P. K. McGuire, P. W. Woodruff, S. D. Iversen & A. S. David; «Activation of Auditory Cortex During Silent Lipreading»; Science **276**, p. 593–596 (1997). ISSN 00368075. https://www.science.org/doi/10.1126/science.276.5312.593. 5, 6, 30

[22] G. A. Calvert & T. Thesen; «Multisensory integration: methodological approaches and emerging principles in the human brain»; Journal of Physiology-Paris **98**, p. 191–205 (2004). ISSN 0928-4257. 5

[23] A. P. Alivisatos, M. Chun, G. M. Church, R. J. Greenspan, M. L. Roukes & R. Yuste; «The Brain Activity Map Project and the Challenge of Functional Connectomics»; Neuron **74**, p. 970–974 (2012). ISSN 0896-6273. 5

[24] T. Panier, S. A. Romano, R. Olive, T. Pietri, G. Sumbre, R. Candelier & G. Debrégeas; «Fast functional imaging of multiple brain regions in intact zebrafish

larvae using selective plane illumination microscopy»; Frontiers in Neural Circuits **7**, p. 65 (2013). ISSN 16625110. 5, 16, 17, 18

[25] M. B. Ahrens, M. B. Orger, D. N. Robson, J. M. Li & P. J. Keller; «Whole-brain functional imaging at cellular resolution using light-sheet microscopy»; nature methods | **10**, p. 413 (2013). 5

[26] M. W. Bagnall & D. Schoppik; «Development of vestibular behaviors in zebrafish»; Current Opinion in Neurobiology **53**, p. 83–89 (2018). ISSN 18736882. 5, 14

[27] D. G. Zeddies & R. R. Fay; «Development of the acoustically evoked behavioral response in zebrafish to pure tones»; Journal of Experimental Biology **208**, p. 1363–1372 (2005). ISSN 0022-0949. https://journals.biologists.com/jeb/article/208/7/1363/16005/Development-of-the-acoustically-evoked-behavioral. 7

[28] S. C. Neuhauss; «Zebrafish vision: Structure and function of the zebrafish visual system»; Fish Physiology **29**, p. 81–122 (2010). ISSN 1546-5098. 7

[29] A. J. Sefton, B. Dreher, A. R. Harvey & P. R. Martin; «Visual System»; The Rat Nervous System: Fourth Edition p. 947–983 (2015). 7

[30] S. G. Solomon & M. G. Rosa; «A simpler primate brain: The visual system of the marmoset monkey»; Frontiers in Neural Circuits **8**, p. 96 (2014). ISSN 16625110. 7

[31] S. Prasad & S. L. Galetta; «Anatomy and physiology of the afferent visual system»; Handbook of Clinical Neurology **102**, p. 3–19 (2011). ISSN 0072-9752. 7

[32] S. R. y Cajal & D. Sánchez; «Contribución al conocimiento de los centros nerviosos de los insectos / por S.R. Cajal y D. Sánchez.»; Contribución al conocimiento de los centros nerviosos de los insectos / por S.R. Cajal y D. Sánchez. (1915). 7

[33] G. Gestri, B. A. Link & S. C. Neuhauss; «The visual system of zebrafish and its use to model human ocular Diseases»; Developmental Neurobiology **72**, p. 302–327 (2012). ISSN 1932-846X. https://onlinelibrary.wiley.com/doi/full/10.

1002/dneu.20919https://onlinelibrary.wiley.com/doi/abs/10.1002/dneu.20919https://onlinelibrary.wiley.com/doi/10.1002/dneu.20919. 7

[34] V. C. Fleisch & S. C. Neuhauss; «Visual Behavior in Zebrafish»; https://home.liebertpub.com/zeb **3**, p. 191–201 (2006). ISSN 15458547. https://www.liebertpub.com/doi/10.1089/zeb.2006.3.191. 7

[35] S. S. Easter & G. N. Nicola; «The Development of Vision in the Zebrafish (Danio rerio)»; Developmental Biology **180**, p. 646–663 (1996). ISSN 0012-1606. 7, 26, 29

[36] S. S. Easter & G. N. Nicola; «The Development of Eye Movements in the Zebrafish (Danio rerio)»; Developmental Psychobiology **31**, p. 267–276 (1997). ISSN 00121630. 7, 29

[37] I. H. Bianco, L. H. Ma, D. Schoppik, D. N. Robson, M. B. Orger, J. C. Beck, J. M. Li, A. F. Schier, F. Engert & R. Baker; «The Tangential Nucleus Controls a Gravito-inertial Vestibulo-ocular Reflex»; Current Biology **22**, p. 1285–1295 (2012). ISSN 0960-9822. 7, 21, 24

[38] D. E. Ehrlich & D. Schoppik; «Control of Movement Initiation Underlies the Development of Balance»; Current Biology **27**, p. 334–344 (2017). ISSN 0960-9822. 7

[39] D. E. Angelaki & K. E. Cullen; «Vestibular System: The Many Facets of a Multimodal Sense»; (2008). www.annualreviews.org. 7

[40] M. Beraneck, F. M. Lambert & S. G. Sadeghi; «Functional Development of the Vestibular System: Sensorimotor Pathways for Stabilization of Gaze and Posture»; Development of Auditory and Vestibular Systems: Fourth Edition p. 449–487 (2014). 7

[41] K. E. Cullen; «Vestibular processing during natural self-motion: implications for perception and action»; (2019). www.nature.com/nrn. 7, 21

[42] W. Mo, F. Chen, A. Nechiporuk & T. Nicolson; «Quantification of vestibular-induced eye movements in zebrafish larvae.»; BMC neuroscience **11**, p. 110 (2010). ISSN 14712202. https://bmcneurosci.biomedcentral.com/articles/10.1186/1471-2202-11-110. 7, 21

[43] W. Graf & F. Klam; «Le système vestibulaire : anatomie fonctionnelle et comparée, évolution et développement»; Comptes Rendus Palevol **5**, p. 637–655 (2006). ISSN 1631-0683. 7

[44] H. Straka & R. Baker; «Vestibular blueprint in early vertebrates»; Frontiers in Neural Circuits **7**, p. 182 (2013). ISSN 16625110. 7, 24

[45] G. Migault, T. L. van der Plas, H. Trentesaux, T. Panier, R. Candelier, R. Proville, B. Englitz, G. Debrégeas & V. Bormuth; «Whole-Brain Calcium Imaging during Physiological Vestibular Stimulation in Larval Zebrafish»; Current Biology **28**, p. 3723–3735.e6 (2018). ISSN 09609822. 7, 14, 21, 57, 87, 120

[46] M. F. Glasser, T. S. Coalson, E. C. Robinson, C. D. Hacker, J. Harwell, E. Yacoub, K. Ugurbil, J. Andersson, C. F. Beckmann, M. Jenkinson, S. M. Smith & D. C. V. Essen; «A multi-modal parcellation of human cerebral cortex»; Nature 2016 536:7615 **536**, p. 171–178 (2016). ISSN 1476-4687. https://www.nature.com/articles/nature18933. 8

[47] S. R. y Cajal & L. Azoulay; «Histologie du systeme nerveux de l'homme et des vertebrés»; p. 2v–2v (1909). 9

[48] T. Tyrrell & D. Willshaw; «Cerebellar cortex: its simulation and the relevance of Marr's theory»; Philosophical Transactions of the Royal Society of London. Series B: Biological Sciences **336**, p. 239–257 (1992). ISSN 09628436. https://royalsocietypublishing.org/doi/10.1098/rstb.1992.0059. 9, 34

[49] B. J. Cook, A. D. H. Peterson, W. Woldman & J. R. Terry; «Neural Field Models: A mathematical overview and unifying framework»; (2021). http://arxiv.org/abs/2103.10554http://dx.doi.org/10.46298/mna.7284. 10

[50] L. Weissman, N. C. de Souza-Pinto, T. Stevnsner & V. A. Bohr; «DNA repair, mitochondria, and neurodegeneration»; Neuroscience **145**, p. 1318–1329 (2007). ISSN 03064522. https://www.researchgate.net/publication/6703948_DNA_repair_mitochondria_and_neurodegeneration. 10

[51] S. F. Cooke & T. V. Bliss; «Plasticity in the human central nervous system»; Brain **129**, p. 1659–1673 (2006). ISSN 0006-8950. https://academic.oup.com/brain/article/129/7/1659/300527. 11

[52] S. Behnke; «Neurobiological Background»; p. 17–33 (2003). https://www.researchgate.net/publication/251299196_Neurobiological_Background. 12

[53] H. Eichenbaum, T. Otto & N. J. Cohen; «The hippocampus—what does it do?»; Behavioral and Neural Biology **57**, p. 2–36 (1992). ISSN 0163-1047. 12

[54] A. M. Graybiel; «The basal ganglia»; (2000). 12

[55] M. T. Herrero, C. Barcia & J. M. Navarro; «Functional anatomy of thalamus and basal ganglia»; Child's Nervous System **18**, p. 386–404 (2002). ISSN 02567040. https://link.springer.com/article/10.1007/s00381-002-0604-1. 12

[56] Y. B. Saalmann & S. Kastner; «The cognitive thalamus»; (2015). 12

[57] C. B. Saper & B. B. Lowell; «The hypothalamus»; Current Biology **24**, p. R1111–R1116 (2014). ISSN 0960-9822. 12

[58] P. D. Gamlin; «The pretectum: connections and oculomotor-related roles»; Progress in Brain Research **151**, p. 379–405 (2006). ISSN 0079-6123. 12

[59] L. Cazin, W. Precht & J. Lannou; «Pathways mediating optokinetic responses of vestibular nucleus neurons in the rat»; Pflügers Archiv European Journal of Physiology **384**, p. 19–29 (1980). ISSN 00316768. https://link.springer.com/article/10.1007/BF00589510. 12

[60] K. J. Berkley & D. C. Mash; «Somatic sensory projections to the pretectum in the cat»; Brain Research **158**, p. 445–449 (1978). ISSN 0006-8993. 12

[61] T. Isa, E. Marquez-Legorreta, S. Grillner & E. K. Scott; «The tectum/superior colliculus as the vertebrate solution for spatial sensory integration and action»; Current Biology **31**, p. R741–R762 (2021). ISSN 0960-9822. 13, 30, 56

[62] O. K. Faull, H. H. Subramanian, M. Ezra & K. T. Pattinson; «The midbrain periaqueductal gray as an integrative and interoceptive neural structure for breath-

ing»; Neuroscience Biobehavioral Reviews **98**, p. 135–144 (2019). ISSN 0149-7634. 13

[63] S. Lammel, B. K. Lim, C. Ran, K. W. Huang, M. J. Betley, K. M. Tye, K. Deisseroth & R. C. Malenka; «Input-specific control of reward and aversion in the ventral tegmental area»; Nature 2012 491:7423 **491**, p. 212–217 (2012). ISSN 1476-4687. https://www.nature.com/articles/nature11527. 13

[64] K. Takakusaki, R. Chiba, T. Nozu & T. Okumura; «Brainstem control of locomotion and muscle tone with special reference to the role of the mesopontine tegmentum and medullary reticulospinal systems»; Journal of Neural Transmission 2015 123:7 **123**, p. 695–729 (2015). ISSN 1435-1463. https://link.springer.com/article/10.1007/s00702-015-1475-4. 13

[65] M. I. COHEN & S. C. WANG; «RESPIRATORY NEURONAL ACTIVITY IN PONS OF CAT»; https://doi.org/10.1152/jn.1959.22.1.33 **22**, p. 33–50 (1959). ISSN 00223077. https://journals.physiology.org/doi/10.1152/jn.1959.22.1.33. 13

[66] A. S. Lim, E. Moro, A. M. Lozano, C. Hamani, J. O. Dostrovsky, W. D. Hutchison, A. E. Lang, R. A. Wennberg & B. J. Murray; «Selective enhancement of rapid eye movement sleep by deep brain stimulation of the human pons»; Annals of Neurology **66**, p. 110–114 (2009). ISSN 1531-8249. https://onlinelibrary.wiley.com/doi/full/10.1002/ana.21631https://onlinelibrary.wiley.com/doi/abs/10.1002/ana.21631https://onlinelibrary.wiley.com/doi/10.1002/ana.21631. 13

[67] E. J. Fine, C. C. Ionita & L. Lohr; «The history of the development of the cerebellar examination»; Seminars in Neurology **22**, p. 375–384 (2002). ISSN 02718235. http://www.thieme-connect.com/products/ejournals/html/10.1055/s-2002-36759http://www.thieme-connect.de/DOI/DOI?10.1055/s-2002-36759. 13

[68] J. D. Schmahmann & D. Caplan; «Cognition, emotion and the cerebellum»; Brain **129**, p. 290–292 (2006). ISSN 0006-8950. https://academic.oup.com/brain/article/129/2/290/292272. 13

[69] S. D. Waldman; «The Medulla Oblongata»; Pain Review p. 208 (2009). 13

[70] C. Houart; «Zebrafish as an Experimental Organism»; eLS (2001). https://onlinelibrary.wiley.com/doi/full/10.1038/npg.els.0002094https://onlinelibrary.wiley.com/doi/abs/10.1038/npg.els.0002094https://onlinelibrary.wiley.com/doi/10.1038/npg.els.0002094. 14

[71] H. Bielen; «Zebrafish as an Experimental Organism»; eLS p. 1–7 (2015). https://onlinelibrary.wiley.com/doi/full/10.1002/9780470015902.a0002094.pub2https://onlinelibrary.wiley.com/doi/abs/10.1002/9780470015902.a0002094.pub2https://onlinelibrary.wiley.com/doi/10.1002/9780470015902.a0002094.pub2. 14

[72] D. Y. Stainier & M. C. Fishman; «The zebrafish as a model system to study cardiovascular development»; Trends in Cardiovascular Medicine **4**, p. 207–212 (1994). ISSN 1050-1738. 14

[73] T. J. Chico, P. W. Ingham & D. C. Crossman; «Modeling Cardiovascular Disease in the Zebrafish»; Trends in Cardiovascular Medicine **18**, p. 150–155 (2008). ISSN 1050-1738. 14

[74] N. S. Trede, D. M. Langenau, D. Traver, A. T. Look & L. I. Zon; «The Use of Zebrafish to Understand Immunity»; Immunity **20**, p. 367–379 (2004). ISSN 1074-7613. 14

[75] B. C. Das, L. McCormick, P. Thapa, R. Karki & T. Evans; «Use of zebrafish in chemical biology and drug discovery»; Future medicinal chemistry **5**, p. 2103–2116 (2013). ISSN 1756-8927. https://pubmed.ncbi.nlm.nih.gov/24215349/. 14

[76] S. C. Baraban; «A zebrafish-centric approach to antiepileptic drug development»; DMM Disease Models and Mechanisms **14** (2021). ISSN 17548411. https://journals.biologists.com/dmm/article/14/7/dmm049080/270828/A-zebrafish-centric-approach-to-antiepileptic-drug. 14

[77] R. W. Friedrich, C. Genoud & A. A. Wanner; «Analyzing the structure and function of neuronal circuits in zebrafish»; Frontiers in Neural Circuits **7**, p. 71 (2013). ISSN 16625110. 14

[78] T. Roeser & H. Baier; «Visuomotor Behaviors in Larval Zebrafish after GFP-Guided Laser Ablation of the Optic Tectum»; Journal of Neuroscience **23**, p. 3726–3734 (2003). ISSN 0270-6474. https://www.jneurosci.org/content/23/9/3726https://www.jneurosci.org/content/23/9/3726.abstract. 14

[79] O. Rinner, J. M. Rick & S. C. Neuhauss; «Contrast sensitivity, spatial and temporal tuning of the larval zebrafish optokinetic response»; Investigative Ophthalmology and Visual Science **46**, p. 137–142 (2005). ISSN 01460404. 14, 29, 36, 93

[80] E. A. Naumann, J. E. Fitzgerald, T. W. Dunn, J. Rihel, H. Sompolinsky & F. Engert; «From Whole-Brain Data to Functional Circuit Models: The Zebrafish Optomotor Response»; Cell **167**, p. 947–960.e20 (2016). ISSN 10974172. 14, 26, 57

[81] S. Wolf, W. Supatto, G. Debrégeas, P. Mahou, S. G. Kruglik, J. M. Sintes, E. Beaurepaire & R. Candelier; «Whole-brain functional imaging with two-photon light-sheet microscopy»; Nature Methods 2015 12:5 **12**, p. 379–380 (2015). ISSN 1548-7105. https://www.nature.com/articles/nmeth.3371. 14

[82] V. Pérez-Schuster, A. Kulkarni, M. Nouvian, S. A. Romano, K. Lygdas, A. Jouary, M. Dippopa, T. Pietri, M. Haudrechy, V. Candat, J. Boulanger-Weill, V. Hakim & G. Sumbre; «Sustained Rhythmic Brain Activity Underlies Visual Motion Perception in Zebrafish»; Cell Reports **17**, p. 1098–1112 (2016). ISSN 2211-1247. 14

[83] L. Avitan, Z. Pujic, J. Mölter, M. V. D. Poll, B. Sun, H. Teng, R. Amor, E. K. Scott & G. J. Goodhill; «Spontaneous Activity in the Zebrafish Tectum Reorganizes over Development and Is Influenced by Visual Experience»; Current Biology **27**, p. 2407–2419.e4 (2017). ISSN 0960-9822. 14

[84] M. Haesemeyer, D. N. Robson, J. M. Li, A. F. Schier & F. Engert; «A Brain-wide Circuit Model of Heat-Evoked Swimming Behavior in Larval Zebrafish»; Neuron **98**, p. 817–831.e6 (2018). ISSN 0896-6273. 14

[85] M. Privat, S. A. Romano, T. Pietri, A. Jouary, J. Boulanger-Weill, N. Elbaz, A. Duchemin, D. Soares & G. Sumbre; «Sensorimotor Transformations in the Zebrafish Auditory System»; Current Biology **29**, p. 4010–4023.e4 (2019). ISSN 0960-9822. 14

[86] R. Candelier, M. S. Murmu, S. A. Romano, A. Jouary, G. Debrégeas & G. Sumbre; «A microfluidic device to study neuronal and motor responses to acute chemical stimuli in zebrafish»; Scientific Reports 2015 5:1 **5**, p. 1–10 (2015). ISSN 2045-2322. https://www.nature.com/articles/srep12196. 14

[87] F. Svara, D. Förster, F. Kubo, M. Januszewski, M. dal Maschio, P. J. Schubert, J. Kornfeld, A. A. Wanner, E. Laurell, W. Denk & H. Baier; «Automated synapse-level reconstruction of neural circuits in the larval zebrafish brain»; Nature Methods 2022 19:11 **19**, p. 1357–1366 (2022). ISSN 1548-7105. https://www.nature.com/articles/s41592-022-01621-0. 15

[88] N. Jurisch-Yaksi, E. Yaksi & C. Kizil; «Radial glia in the zebrafish brain: Functional, structural, and physiological comparison with the mammalian glia»; Glia **68**, p. 2451–2470 (2020). ISSN 1098-1136. https://onlinelibrary.wiley.com/doi/full/10.1002/glia.23849https://onlinelibrary.wiley.com/doi/abs/10.1002/glia.23849https://onlinelibrary.wiley.com/doi/10.1002/glia.23849. 15

[89] C. B. Kimmel, J. Patterson & R. O. Kimmel; «The development and behavioral characteristics of the startle response in the zebra fish»; Developmental Psychobiology **7**, p. 47–60 (1974). ISSN 1098-2302. https://onlinelibrary.wiley.com/doi/full/10.1002/dev.420070109https://onlinelibrary.wiley.com/doi/abs/10.1002/dev.420070109https://onlinelibrary.wiley.com/doi/10.1002/dev.420070109. 14

[90] J. A. Lister, C. P. Robertson, T. Lepage, S. L. Johnson & D. W. Raible; «Nacre encodes a zebrafish microphthalmia-related protein that regulates neural-crest-derived pigment cell fate»; Development **126**, p. 3757–3767 (1999). ISSN 0950-1991. https://journals.biologists.com/dev/article/126/17/3757/40374/nacre-encodes-a-zebrafish-microphthalmia-related. 16, 17

[91] J. Nakai, M. Ohkura & K. Imoto; «A high signal-to-noise Ca2+ probe composed of a single green fluorescent protein»; Nature Biotechnology 2001 19:2 **19**, p. 137–141 (2001). ISSN 1546-1696. https://www.nature.com/articles/nbt0201_137. 16

[92] M. B. Ahrens, J. M. Li, M. B. Orger, D. N. Robson, A. F. Schier, F. Engert & R. Portugues; «Brain-wide neuronal dynamics during motor adaptation in zebrafish»; Nature **485** (2012). 16, 17, 34, 97

[93] J. P. García-Cambero, F. J. Beltrán, A. Encinas, F. J. Rivas & A. L. Oropesa; «The added value of a zebrafish embryo–larval model in the assessment of wastewater tertiary treatments»; Environmental Science: Water Research Technology **5**, p. 2269–2279 (2019). ISSN 2053-1419. https://pubs.rsc.org/en/content/articlehtml/2019/ew/c9ew00411dhttps://pubs.rsc.org/en/content/articlelanding/2019/ew/c9ew00411d. 16

[94] S. I. Higashijima, M. A. Masino, G. Mandel & J. R. Fetcho; «Imaging Neuronal Activity during Zebrafish Behavior with a Genetically Encoded Calcium Indicator»; Journal of Neurophysiology **90**, p. 3986–3997 (2003). ISSN 00223077. https://journals.physiology.org/doi/10.1152/jn.00576.2003. 16

[95] C. Grienberger & A. Konnerth; «Imaging Calcium in Neurons»; Neuron **73**, p. 862–885 (2012). ISSN 0896-6273. 16

[96] T. W. Chen, T. J. Wardill, Y. Sun, S. R. Pulver, S. L. Renninger, A. Baohan, E. R. Schreiter, R. A. Kerr, M. B. Orger, V. Jayaraman, L. L. Looger, K. Svoboda & D. S. Kim; «Ultrasensitive fluorescent proteins for imaging neuronal activity»; Nature 2013 499:7458 **499**, p. 295–300 (2013). ISSN 1476-4687. https://www.nature.com/articles/nature12354. 16

[97] M. Renz; «Fluorescence microscopy—A historical and technical perspective»; Cytometry Part A **83**, p. 767–779 (2013). ISSN 1552-4930. https://onlinelibrary.wiley.com/doi/full/10.1002/cyto.a.22295https://onlinelibrary.wiley.com/doi/abs/10.1002/cyto.a.22295https://onlinelibrary.wiley.com/doi/10.1002/cyto.a.22295. 17

[98] J. R. Fetcho & D. M. O'Malley; «Visualization of active neural circuitry in the spinal cord of intact zebrafish»; https://doi.org/10.1152/jn.1995.73.1.399 **73**, p. 399–406 (1995). ISSN 00223077. https://journals.physiology.org/doi/10.1152/jn.1995.73.1.399. 17

[99] E. M. Hillman, V. Voleti, K. Patel, W. Li, H. Yu, C. Perez-Campos, S. E. Benezra, R. M. Bruno & P. T. Galwaduge; «High-speed 3D imaging of cellular activity in the brain using axially-extended beams and light sheets»; Current Opinion in Neurobiology **50**, p. 190–200 (2018). ISSN 0959-4388. 17

[100] P. A. Santi; «Light sheet fluorescence microscopy: A review»; Journal of Histochemistry and Cytochemistry **59**, p. 129–138 (2011). ISSN 00221554. https://journals.sagepub.com/doi/full/10.1369/0022155410394857. 17

[101] R. M. Power & J. Huisken; «A guide to light-sheet fluorescence microscopy for multiscale imaging»; Nature Methods 2017 14:4 **14**, p. 360–373 (2017). ISSN 1548-7105. https://www.nature.com/articles/nmeth.4224. 17

[102] P. J. Keller & M. B. Ahrens; «Visualizing Whole-Brain Activity and Development at the Single-Cell Level Using Light-Sheet Microscopy»; Neuron **85**, p. 462–483 (2015). ISSN 0896-6273. 17

[103] S. L. Renninger & M. B. Orger; «Two-photon imaging of neural population activity in zebrafish»; Methods **62**, p. 255–267 (2013). ISSN 1046-2023. 17

[104] J. Huisken & D. Y. Stainier; «Selective plane illumination microscopy techniques in developmental biology»; Development **136**, p. 1963–1975 (2009). ISSN 0950-1991. https://journals.biologists.com/dev/article/136/12/1963/65234/Selective-plane-illumination-microscopy-techniques. 18

[105] O. Randlett, C. L. Wee, E. A. Naumann, O. Nnaemeka, D. Schoppik, J. E. Fitzgerald, R. Portugues, A. M. Lacoste, C. Riegler, F. Engert & A. F. Schier; «Whole-brain activity mapping onto a zebrafish brain atlas»; Nature Methods 2015 12:11 **12**, p. 1039–1046 (2015). ISSN 1548-7105. https://www.nature.com/articles/nmeth.3581. 18, 69, 71, 80, 87, 138, 139

[106] H. Straka, B. Fritzsch & J. C. Glover; «Connecting Ears to Eye Muscles: Evolution of a 'Simple' Reflex Arc»; Brain, Behavior and Evolution **83**, p. 162–175 (2014). ISSN 0006-8977. https://www.karger.com/Article/FullText/357833https://www.karger.com/Article/Abstract/357833. 19, 21

[107] T. G. Deliagina, P. V. Zelenin, I. N. Beloozerova & G. N. Orlovsky; «Nervous mechanisms controlling body posture»; Physiology Behavior **92**, p. 148–154 (2007). ISSN 0031-9384. 19

[108] S. S. Desai & A. Dua; «History of Research in the Vestibular System: A 400-Year-Old Story»; Anatomy Physiology: Current Research **4**, p. 1–5 (2013). ISSN 2161-0940. https://www.longdom.org/open-access/history-of-research-in-the-vestibular-system-a-400yearold-story-21094.htmlhttps://www.longdom.org/abstract/history-of-research-in-the-vestibular-system-a-htmlhttps://www.longdom.org/. 19

[109] B. Fritzsch; «Evolution of the Vestibulo-Ocular System»; http://dx.doi.org/10.1016/S0194-5998(98)70053-1 **119**, p. 182–192 (2016). ISSN 01945998. https://journals.sagepub.com/doi/abs/10.1016/S0194-5998(98)70053-1. 19

[110] V. J. Wilson; «Physiological Pathways Through the Vestibular Nuclei»; International Review of Neurobiology **15**, p. 27–81 (1972). ISSN 0074-7742. 19

[111] A. M. Howard & D. M. Fragaszy; «Applying the bicoded spatial model to nonhuman primates in an arboreal multilayer environment»; Behavioral and Brain Sciences **36**, p. 552–553 (2013). ISSN 0140525X. 20

[112] S. M. Highstein, R. R. Fay & A. N. Popper; «The Vestibular System»; **19** (2008). http://link.springer.com/10.1007/b97280. 20

[113] L. Abbas & T. T. Whitfield; «The zebrafish inner ear»; Fish Physiology **29**, p. 123–171 (2010). ISSN 1546-5098. 20

[114] M. Inoue, M. Tanimoto & Y. Oda; «The role of ear stone size in hair cell acoustic sensory transduction»; Scientific Reports 2013 3:1 **3**, p. 1–5 (2013). ISSN 2045-2322. https://www.nature.com/articles/srep02114. 20

[115] R. R. Gacek & M. Lyon; «The Localization of Vestibular Efferent Neurons in the Kitten with Horseradish Peroxidase»; http://dx.doi.org/10.3109/00016487409124603 **77**, p. 92–101 (2009).

ISSN 00016489. https://www.tandfonline.com/doi/abs/10.3109/00016487409124603. 21

[116] R. S. Swenson; «The Vestibular System»; Conn's Translational Neuroscience p. 167–183 (2017). 22

[117] C. Haddon & J. Lewis; «Early Ear Development in the Embryo of the Zebrafish, Danio rerio»; THE JOURNAL OF COMPARATIVE NEUROLOGY **365**, p. 113–125 (1996). https://onlinelibrary.wiley.com/doi/10.1002/. 21

[118] F. M. Lambert, J. C. Beck, R. Baker & H. Straka; «Semicircular canal size determines the developmental onset of angular vestibuloocular reflexes in larval Xenopus»; The Journal of neuroscience : the official journal of the Society for Neuroscience **28**, p. 8086–8095 (2008). ISSN 1529-2401. https://pubmed.ncbi.nlm.nih.gov/18685033/. 21

[119] B. B. Riley & S. J. Moorman; «Development of Utricular Otoliths, but not Saccular Otoliths, Is Necessary for Vestibular Function and Survival in Zebrafish»; J Neurobiol **43**, p. 329–337 (2000). https://onlinelibrary.wiley.com/terms-and-conditions. 21

[120] T. D. M. Roberts; *The Neurophysiology of Postural Mechanisms* (1978). 21

[121] T. Nicolson; «The genetics of hearing and balance in zebrafish»; Annual Review of Genetics **39**, p. 9–22 (2005). ISSN 00664197. https://www.researchgate.net/publication/7482282_The_Genetics_of_Hearing_and_Balance_in_Zebrafish. 23

[122] F. Auer & D. Schoppik; «The Larval Zebrafish Vestibular System Is a Promising Model to Understand the Role of Myelin in Neural Circuits»; Frontiers in Neuroscience **16**, p. 625 (2022). ISSN 1662453X. 24

[123] J. C. Beck, E. Gilland, D. W. Tank & R. Baker; «Quantifying the ontogeny of optokinetic and vestibuloocular behaviors in zebrafish, medaka, and goldfish»; Journal of Neurophysiology **92**, p. 3546–3561 (2004). ISSN 00223077. https://journals.physiology.org/doi/10.1152/jn.00311.2004. 21

[124] G. D. Paige & E. W. Sargent; «Visually-induced adaptive plasticity in the human vestibulo-ocular reflex»; Experimental Brain Research **84**, p. 25–34 (1991). ISSN 00144819. https://link.springer.com/article/10.1007/BF00231759. 21

[125] D. E. Angelaki & B. J. M. Hess; «Organizational Principles of Otolith- and Semicircular Canal-Ocular Reflexes in Rhesus Monkeys»; Annals of the New York Academy of Sciences **781**, p. 332–347 (1996). ISSN 1749-6632. https://onlinelibrary.wiley.com/doi/full/10.1111/j.1749-6632.1996.tb15711.xhttps://onlinelibrary.wiley.com/doi/abs/10.1111/j.1749-6632.1996.tb15711.xhttps://nyaspubs.onlinelibrary.wiley.com/doi/10.1111/j.1749-6632.1996.tb15711.x. 21

[126] F. M. Lambert, J. Bacqué-Cazenave, A. L. Seach, J. Arama, G. Courtand, M. Tagliabue, S. Eskiizmirliler, H. Straka & M. Beraneck; «Stabilization of Gaze during Early Xenopus Development by Swimming-Related Utricular Signals»; Current Biology **30**, p. 746–753.e4 (2020). ISSN 0960-9822. 21

[127] D. Schoppik, I. H. Bianco, D. A. Prober, A. D. Douglass, D. N. Robson, J. M. Li, J. S. Greenwood, E. Soucy, F. Engert & A. F. Schier; «Gaze-Stabilizing Central Vestibular Neurons Project Asymmetrically to Extraocular Motoneuron Pools»; Journal of Neuroscience **37**, p. 11 353–11 365 (2017). ISSN 0270-6474. https://www.jneurosci.org/content/37/47/11353https://www.jneurosci.org/content/37/47/11353.abstract. 24

[128] M. Posner & R. M. Klein; «Visual dominance: An information-processing account of its origins and significance»; (1976). https://www.researchgate.net/publication/22375771. 24

[129] M. F. Land & R. D. Fernald; «THE EVOLUTION OF EYES»; **15**, p. 1–29 (1992)www.annualreviews.org/aronline. 24

[130] N. Unal & O. Elcioglu; «Anatomy of the eye from the view of Ibn Al-Haitham (965-1039). The founder of modern optics»; (2009). https://pubmed.ncbi.nlm.nih.gov/19271057/. 24

[131] W. Jaeger; «[Johannes Kepler's contributions to ophthalmologic optics]»; Klinische Monatsblatter fur Augenheilkunde **188**, p. 163–166 (1986). ISSN 0023-2165. https://pubmed.ncbi.nlm.nih.gov/3520121/. 24

[132] C. G. Gross; «How Inferior Temporal Cortex Became a Visual Area»; Cerebral Cortex **4**, p. 455–469 (1994). ISSN 1047-3211. https://academic.oup.com/cercor/article/4/5/455/332213. 24

[133] P. H. Schiller; «The central visual system»; Vision Research **26**, p. 1351–1386 (1986). ISSN 0042-6989. 24

[134] R. J. Love & W. G. Webb; «Neurosensory Organization of Speech and Hearing»; Neurology for the Speech-Language Pathologist p. 59–80 (1992). 25

[135] R. Armstrong & R. Cubbidge; «The Eye and Vision: An Overview»; Handbook of Nutrition, Diet, and the Eye p. 3–14 (2019). 25

[136] Y. Han, J. M. Kebschull, R. A. Campbell, D. Cowan, F. Imhof, A. M. Zador & T. D. Mrsic-Flogel; «The logic of single-cell projections from visual cortex»; Nature 2018 556:7699 **556**, p. 51–56 (2018). ISSN 1476-4687. https://www.nature.com/articles/nature26159. 25

[137] A. Resulaj; «Projections of the Mouse Primary Visual Cortex»; Frontiers in Neural Circuits **15**, p. 133 (2021). ISSN 16625110. 25

[138] J. K. Bowmaker & H. J. Dartnall; «Visual pigments of rods and cones in a human retina.»; The Journal of Physiology **298**, p. 501–511 (1980). ISSN 1469-7793. https://onlinelibrary.wiley.com/doi/full/10.1113/jphysiol.1980.sp013097https://onlinelibrary.wiley.com/doi/abs/10.1113/jphysiol.1980.sp013097https://physoc.onlinelibrary.wiley.com/doi/10.1113/jphysiol.1980.sp013097. 25

[139] J. Dowling; «Retina: An Overview»; Reference Module in Biomedical Sciences (2015). 25

[140] C. Salesse; «Physiologie du signal visuel rétinien : de la phototransduction jusqu'au cycle visuel»; Journal Français d'Ophtalmologie **40**, p. 239–250 (2017). ISSN 0181-5512. 25

[141] D. Purves, G. J. Augustine, D. Fitzpatrick, L. C. Katz, A.-S. LaMantia, J. O. McNamara & S. M. Williams; *Neuroscience, 2nd edition* (Sinauer Associates) (2001); ISBN 0-87893-742-0. https://www.ncbi.nlm.nih.gov/books/NBK10799/. 26

[142] G. Twig, H. Levy & I. Perlman; «Color opponency in horizontal cells of the vertebrate retina»; Progress in Retinal and Eye Research **22**, p. 31–68 (2003). ISSN 1350-9462. 26

[143] L. Lagnado; «Retinal processing: Amacrine cells keep it short and sweet»; Current Biology **8**, p. R598–R600 (1998). ISSN 09609822. http://www.cell.com/article/S0960982298703859/fulltexthttp://www.cell.com/article/S0960982298703859/abstracthttps://www.cell.com/current-biology/abstract/S0960-9822(98)70385-9. 26

[144] R. H. Masland; «The Neuronal Organization of the Retina»; Neuron **76**, p. 266–280 (2012). ISSN 0896-6273. 26

[145] E. N. Pugh; «The Nature and Identity of the Internal Excitational Transmitter of Vertebrate Phototransduction»; Annual Review of Physiology **49**, p. 715–741 (1987). ISSN 0066-4278. https://www.researchgate.net/publication/20124361_The_Nature_and_Identity_of_the_Internal_Excitational_Transmitter_of_Vertebrate_Phototransduction. 27

[146] J. Malicki, S. C. F. Neuhauss, A. F. Schier, L. Solnica-Krezel, D. L. Stemple, D. Y. R. Stainier, S. Abdelilah, F. Zwartkruis, Z. Rangini & W. Driever; «Mutations affecting development of the zebrafish retina»; (1997). https://www.researchgate.net/publication/14201818_Mutations_affecting_development_of_the_zebrafish_retina. 26, 28

[147] T. Baden; «Circuit mechanisms for colour vision in zebrafish»; Current Biology **31**, p. R807–R820 (2021). ISSN 0960-9822. 26

[148] N. A. Mundell, K. T. Beier, Y. A. Pan, S. W. Lapan, D. G. Aytürk, V. K. Berezovskii, A. R. Wark, E. Drokhlyansky, J. Bielecki, R. T.

Born, A. F. Schier & C. L. Cepko; «Vesicular stomatitis virus enables gene transfer and transsynaptic tracing in a wide range of organisms»; Journal of Comparative Neurology **523**, p. 1639–1663 (2015). ISSN 10969861. https://www.researchgate.net/publication/279962110_Mundell_et_al-2015-Journal_of_Comparative_Neurology. 26

[149] F. Kubo, B. Hablitzel, M. DalMaschio, W. Driever, H. Baier & A. B. Arrenberg; «Functional architecture of an optic flow-responsive area that drives horizontal eye movements in zebrafish»; Neuron **81**, p. 1344–1359 (2014). ISSN 10974199. 26, 29, 57

[150] E. I. Dragomir, V. Štih & R. Portugues; «Evidence accumulation during a sensorimotor decision task revealed by whole-brain imaging»; Nature Neuroscience **23**, p. 85–93 (2020). ISSN 15461726. 26

[151] T. W. Dunn, Y. Mu, S. Narayan, O. Randlett, E. A. Naumann, C. T. Yang, A. F. Schier, J. Freeman, F. Engert & M. B. Ahrens; «Brain-wide mapping of neural activity controlling zebrafish exploratory locomotion»; eLife **5** (2016). ISSN 2050084X. 26

[152] T. R. Thiele, J. C. Donovan & H. Baier; «Descending Control of Swim Posture by a Midbrain Nucleus in Zebrafish»; Neuron **83**, p. 679–691 (2014). ISSN 0896-6273. 26

[153] K. Matsuda & F. Kubo; «Circuit Organization Underlying Optic Flow Processing in Zebrafish»; Frontiers in Neural Circuits **15**, p. 73 (2021). ISSN 16625110. 28

[154] Y.-Y. Huang & S. C. F. Neuhauss; «The optokinetic response in zebrafish and its applications»; Frontiers in Bioscience **13**, p. 1899 (2008). 29

[155] O. A. Masseck & K. P. Hoffmann; «Comparative Neurobiology of the Optokinetic Reflex»; Annals of the New York Academy of Sciences **1164**, p. 430–439 (2009). ISSN 1749-6632. https://onlinelibrary.wiley.com/doi/full/10.1111/j.1749-6632.2009.03854.xhttps://onlinelibrary.wiley.com/doi/abs/10.1111/j.1749-6632.2009.03854.xhttps://nyaspubs.onlinelibrary.wiley.com/doi/10.1111/j.1749-6632.2009.03854.x. 29

[156] R. Portugues, C. E. Feierstein, F. Engert & M. B. Orger; «Whole-brain activity maps reveal stereotyped, distributed networks for visuomotor behavior»; Neuron **81**, p. 1328–1343 (2014). ISSN 10974199. 29, 57

[157] V. I. Petkova, M. Björnsdotter, G. Gentile, T. Jonsson, T. Q. Li & H. H. Ehrsson; «From Part- to Whole-Body Ownership in the Multisensory Brain»; Current Biology **21**, p. 1118–1122 (2011). ISSN 0960-9822. 29

[158] L. D. Knogler, D. A. Markov, E. I. Dragomir, V. Štih & R. Portugues; «Sensorimotor Representations in Cerebellar Granule Cells in Larval Zebrafish Are Dense, Spatially Organized, and Non-temporally Patterned»; Current Biology **27**, p. 1288–1302 (2017). ISSN 09609822. 29, 56

[159] N. S. Sankrithi & D. M. O'Malley; «Activation of a multisensory, multifunctional nucleus in the zebrafish midbrain during diverse locomotor behaviors»; Neuroscience **166**, p. 970–993 (2010). ISSN 03064522. 30, 56

[160] P. Coen, T. P. H. Sit, M. J. Wells, M. Carandini & K. D. Harris; «Mouse frontal cortex mediates additive multisensory decisions»; . https://doi.org/10.1101/2021.04.26.441250. 30, 56

[161] J. D. Schmahmann & D. N. Pandya; «Anatomic Organization of the Basilar Pontine Projections from Prefrontal Cortices in Rhesus Monkey»; Journal of Neuroscience **17**, p. 438–458 (1997). ISSN 0270-6474. https://www.jneurosci.org/content/17/1/438https://www.jneurosci.org/content/17/1/438.abstract. 30

[162] Y. Cao, C. Summerfield, H. Park, B. L. Giordano & C. Kayser; «Causal Inference in the Multisensory Brain»; Neuron **102**, p. 1076–1087.e8 (2019). ISSN 10974199. 30

[163] A. A. Ghazanfar & C. E. Schroeder; «Is neocortex essentially multisensory?»; Trends in Cognitive Sciences **10**, p. 278–285 (2006). ISSN 1364-6613. 30

[164] C. Kayser & L. Shams; «Multisensory Causal Inference in the Brain»; PLOS Biology **13**, p. e1002075 (2015). ISSN 1545-7885. https://journals.plos.org/plosbiology/article?id=10.1371/journal.pbio.1002075. 30

[165] E. Macaluso & J. Driver; «Multisensory spatial interactions: a window onto functional integration in the human brain»; Trends in Neurosciences **28**, p. 264–271 (2005). ISSN 0166-2236. 30, 56

[166] N. P. Holmes & C. Spence; «Multisensory Integration: Space, Time and Superadditivity»; Current Biology **15**, p. R762–R764 (2005). ISSN 0960-9822. 30, 31

[167] A. A. Kardamakis, J. P. R.-F. Ndez & S. Grillner; «Spatiotemporal interplay between multisensory excitation and recruited inhibition in the lamprey optic tectum»; (2016). 30

[168] G. Oikonomou, M. Altermatt, R. wei Zhang, G. M. Coughlin, C. Montz, V. Gradinaru & D. A. Prober; «The Serotonergic Raphe Promote Sleep in Zebrafish and Mice»; Neuron **103**, p. 686–701.e8 (2019). ISSN 10974199. http://www.cell.com/article/S089662731930491X/fulltexthttp://www.cell.com/article/S089662731930491X/abstracthttps://www.cell.com/neuron/abstract/S0896-6273(19)30491-X. 30

[169] T. Kawashima, M. F. Zwart, C. T. Yang, B. D. Mensh & M. B. Ahrens; «The Serotonergic System Tracks the Outcomes of Actions to Mediate Short-Term Motor Learning»; Cell **167**, p. 933–946.e20 (2016). ISSN 10974172. 30, 35, 117

[170] G. Vanwalleghem, L. A. Heap & E. K. Scott; «A profile of auditory-responsive neurons in the larval zebrafish brain»; Journal of Comparative Neurology **525**, p. 3031–3043 (2017). ISSN 1096-9861. https://onlinelibrary.wiley.com/doi/full/10.1002/cne.24258https://onlinelibrary.wiley.com/doi/abs/10.1002/cne.24258https://onlinelibrary.wiley.com/doi/10.1002/cne.24258. 30

[171] P. M. Henriques, N. Rahman, S. E. Jackson & I. H. Bianco; «Nucleus Isthmi Is Required to Sustain Target Pursuit during Visually Guided Prey-Catching»; Current Biology **29**, p. 1771–1786.e5 (2019). ISSN 0960-9822. 30

[172] C. V. Parise & M. O. Ernst; «Correlation detection as a general mechanism for multisensory integration»; Nature Communications 2016 7:1 **7**, p. 1–9 (2016). ISSN 2041-1723. https://www.nature.com/articles/ncomms11543. 30

[173] D. B. Polley; «Multisensory Conflict Resolution: Should I Stay or Should I Go?»; Neuron **93**, p. 725–727 (2017). ISSN 0896-6273. 30

[174] P. R. Jones; «A tutorial on cue combination and Signal Detection Theory: Using changes in sensitivity to evaluate how observers integrate sensory information - ScienceDirect»; (2016). https://www.sciencedirect.com/science/article/pii/S0022249616300165. 31

[175] M. Kouh & T. Poggio; «A Canonical Neural Circuit for Cortical Nonlinear Operations»; Neural Computation **20**, p. 1427–1451 (2008). ISSN 0899-7667. https://direct.mit.edu/neco/article/20/6/1427/7322/A-Canonical-Neural-Circuit-for-Cortical-Nonlinear. 31

[176] D. J. Heeger; «Normalization of cell responses in cat striate cortex»; Visual Neuroscience **9**, p. 181–197 (1992). ISSN 1469-8714. https://www.cambridge.org/core/journals/visual-neuroscience/article/abs/normalization-of-cell-responses-in-cat-striate-cortex/0851FEE8DEE00514E1A432123E703643. 31

[177] S. R. Olsen, V. Bhandawat & R. I. Wilson; «Divisive Normalization in Olfactory Population Codes»; Neuron **66**, p. 287–299 (2010). ISSN 0896-6273. 31

[178] M. Carandini & D. J. Heeger; «Normalization as a canonical neural computation»; Nature reviews. Neuroscience **13**, p. 51 (2012). ISSN 1471003X. /pmc/articles/PMC3273486//pmc/articles/PMC3273486/?report=abstracthttps://www.ncbi.nlm.nih.gov/pmc/articles/PMC3273486/. 31

[179] O. Schwartz & E. P. Simoncelli; «Natural signal statistics and sensory gain control»; Nature Neuroscience 2001 4:8 **4**, p. 819–825 (2001). ISSN 1546-1726. https://www.nature.com/articles/nn0801_819. 31

[180] T. Ohshiro, D. E. Angelaki & G. C. Deangelis; «A normalization model of multisensory integration»; Nature Neuroscience 2011 14:6 **14**, p. 775–782 (2011). ISSN 1546-1726. https://www.nature.com/articles/nn.2815. 31

[181] B. E. Stein, T. R. Stanford, M. T. Wallace, J. W. Vaughan & W. Jiang; «Crossmodal spatial interactions in subcortical and cortical circuits»; (2004). https://philpapers.org/rec/STECSI-2. 31

[182] T. R. Stanford & B. E. Stein; «Superadditivity in multisensory integration: Putting the computation in context»; NeuroReport **18**, p. 787–792 (2007). ISSN 09594965. https://journals.lww.com/neuroreport/Fulltext/2007/05280/Superadditivity_in_multisensory_integration_.13.aspx. 31

[183] P. J. Laurienti, T. J. Perrault, T. R. Stanford, M. T. Wallace & B. E. Stein; «On the use of superadditivity as a metric for characterizing multisensory integration in functional neuroimaging studies»; Experimental Brain Research **166**, p. 289–297 (2005). ISSN 00144819. https://link.springer.com/article/10.1007/s00221-005-2370-2. 31, 56

[184] I. Skaliora, T. P. Doubell, N. P. Holmes, F. R. Nodal & A. J. King; «Functional Topography of Converging Visual and Auditory Inputs to Neurons in the Rat Superior Colliculus»; J Neurophysiol **92**, p. 2933–2946 (2004). www.jn.org. 31, 56

[185] C. F. Stevens & J. F. Wesseling; «Augmentation Is a Potentiation of the Exocytotic Process»; Neuron **22**, p. 139–146 (1999). ISSN 0896-6273. 32

[186] S. L. Jackman & W. G. Regehr; «The Mechanisms and Functions of Synaptic Facilitation»; Neuron **94**, p. 447–464 (2017). ISSN 0896-6273. 32

[187] R. Xue, D. A. Ruhl, J. S. Briguglio, A. G. Figueroa, R. A. Pearce & E. R. Chapman; «Doc2-mediated superpriming supports synaptic augmentation»; Proceedings of the National Academy of Sciences of the United States of America **115**, p. E5605–E5613 (2018). ISSN 10916490. https://www.pnas.org/doi/abs/10.1073/pnas.1802104115. 32

[188] R. S. Zucker & W. G. Regehr; «Short-term synaptic plasticity.»; Annual review of physiology **64**, p. 355–405 (2002). ISSN 00664278. 32

[189] T. J. Teyler & P. Discenna; «LONG-TERM POTENTIATION History and Definition»; (1987)www.annualreviews.org. 32

[190] T. V. Bliss & T. Lømo; «Long-lasting potentiation of synaptic transmission in the dentate area of the anaesthetized rabbit following stimulation of the perforant path»; The Journal of Physiology **232**, p. 331–356 (1973). ISSN 1469-7793. https://onlinelibrary.wiley.com/doi/full/10.1113/jphysiol.1973.sp010273https://onlinelibrary.wiley.com/doi/abs/10.1113/jphysiol.1973.sp010273https://physoc.onlinelibrary.wiley.com/doi/10.1113/jphysiol.1973.sp010273. 32

[191] T. Dunwiddie & G. Lynch; «Long-term potentiation and depression of synaptic responses in the rat hippocampus: localization and frequency dependency.»; The Journal of Physiology **276**, p. 353–367 (1978). ISSN 1469-7793. https://onlinelibrary.wiley.com/doi/full/10.1113/jphysiol.1978.sp012239https://onlinelibrary.wiley.com/doi/abs/10.1113/jphysiol.1978.sp012239https://physoc.onlinelibrary.wiley.com/doi/10.1113/jphysiol.1978.sp012239. 32

[192] M. Baudry; «Long-term Potentiation (Hippocampus)»; International Encyclopedia of the Social Behavioral Sciences p. 9081–9083 (2001). 32

[193] A. Maffei; «Long-Term Potentiation and Long-Term Depression»; Oxford Research Encyclopedia of Neuroscience (2018). https://. 32

[194] T. Masquelier, R. Guyonneau & S. J. Thorpe; «Spike Timing Dependent Plasticity Finds the Start of Repeating Patterns in Continuous Spike Trains»; PLOS ONE **3**, p. e1377 (2008). ISSN 1932-6203. https://journals.plos.org/plosone/article?id=10.1371/journal.pone.0001377. 33

[195] K. Grill-Spector; «Selectivity of Adaptation in Single Units: Implications for fMRI Experiments»; Neuron **49**, p. 170–171 (2006). ISSN 0896-6273. 33

[196] J. Benda; «Neural adaptation»; Current Biology **31**, p. R110–R116 (2021). ISSN 0960-9822. 33

[197] S. Martinez-Conde, S. L. Macknik & D. H. Hubel; «The role of fixational eye movements in visual perception»; Nature Reviews Neuroscience 2004 5:3 **5**, p. 229–240 (2004). ISSN 1471-0048. https://www.nature.com/articles/nrn1348. 33

[198] G. G. Consalez, D. Goldowitz, F. Casoni & R. Hawkes; «Origins, Development, and Compartmentation of the Granule Cells of the Cerebellum»; Frontiers in Neural Circuits **14**, p. 88 (2021). ISSN 16625110. 33

[199] Y. K. Bae, S. Kani, T. Shimizu, K. Tanabe, H. Nojima, Y. Kimura, S. ichi Higashijima & M. Hibi; «Anatomy of zebrafish cerebellum and screen for mutations affecting its development»; Developmental Biology **330**, p. 406–426 (2009). ISSN 1095564X. 33

[200] A. Gómez, E. Durán, C. Salas & F. Rodríguez; «Cerebellum lesion impairs eyeblink-like classical conditioning in goldfish»; Neuroscience **166**, p. 49–60 (2010). ISSN 0306-4522. 33

[201] M. Ito; «Mechanisms of motor learning in the cerebellum»; Brain Research **886**, p. 237–245 (2000). ISSN 0006-8993. 33, 34

[202] J. I. Wadiche & C. E. Jahr; «Multivesicular release at climbing fiber-Purkinje cell synapses»; Neuron **32**, p. 301–313 (2001). ISSN 08966273. http://www.cell.com/article/S0896627301004883/fulltexthttp://www.cell.com/article/S0896627301004883/abstracthttps://www.cell.com/neuron/abstract/S0896-6273(01)00488-3. 34

[203] R. Shadmehr; «Population coding in the cerebellum: A machine learning perspective»; Journal of Neurophysiology **124**, p. 2022–2051 (2020). ISSN 15221598. https://journals.physiology.org/doi/10.1152/jn.00449.2020. 34

[204] C. I. D. Zeeuw, C. C. Hoogenraad, S. K. Koekkoek, T. J. Ruigrok, N. Galjart & J. I. Simpson; «Microcircuitry and function of the inferior olive»; Trends in Neurosciences **21**, p. 391–400 (1998). ISSN 0166-2236. 34

[205] C. Habas; «Functional Imaging of the Deep Cerebellar Nuclei: A Review»; (2009). 34

[206] J. Diedrichsen, S. Maderwald, M. Küper, M. Thürling, K. Rabe, E. R. Gizewski, M. E. Ladd & D. Timmann; «Imaging the deep cerebellar nuclei: A probabilistic atlas and normalization procedure»; NeuroImage **54**, p. 1786–1794 (2011). ISSN 1053-8119. 34

[207] E. J. Lang; «Coordination of Reaching Movements: Cerebellar Interactions with Motor Cortex»; The Neuronal Codes of the Cerebellum p. 197–217 (2016). 34

[208] M. Ito; «LONG-TERM DEPRESSION»; (1989)www.annualreviews.org. 34

[209] M. Kawato, S. Ohmae, H. Hoang & T. Sanger; «50 Years Since the Marr, Ito, and Albus Models of the Cerebellum»; Neuroscience **462**, p. 151–174 (2021). ISSN 0306-4522. 34

[210] P. Strata; «David Marr's theory of cerebellar learning: 40 years later»; The Journal of Physiology **587**, p. 5519 (2009). ISSN 00223751. /pmc/articles/PMC2805361/ https://www.ncbi.nlm.nih.gov/pmc/articles/PMC2805361/. 34

[211] D. Marr; «A theory of cerebellar cortex»; The Journal of Physiology **202**, p. 437 (1969). ISSN 14697793. /pmc/articles/PMC1351491/?report=abstracthttps://www.ncbi.nlm.nih.gov/pmc/articles/PMC1351491/. 34

[212] A. Valente, K.-H. Huang, R. Portugues & F. Engert; «Ontogeny of classical and operant learning behaviors in zebrafish»; . http://www.learnmem.org/cgi/doi/10.1101/lm.025668.112. 34

[213] S. Narayanan, A. Varma & V. Thirumalai; «Rapid acquisition of internal models of timing by Purkinje cells enables faster behavioral responses»; bioRxiv p. 2021.04.28.441782 (2021). https://www.biorxiv.org/content/10.1101/2021.04.28.441782v2https://www.biorxiv.org/content/10.1101/2021.04.28.441782v2.abstract. 34

[214] D. A. Markov, L. Petrucco, A. M. Kist & R. Portugues; «A cerebellar internal model calibrates a feedback controller involved in sensorimotor control»; Nature Communications 2021 12:1 **12**, p. 1–21 (2021). ISSN 2041-1723. https://www.nature.com/articles/s41467-021-26988-0. 34, 104

[215] A. M. Pastor, R. R. D. L. Cruz & R. Baker; «Cerebellar role in adaptation of the goldfish vestibuloocular reflex»; Article in Journal of Neurophysiology (1994). https://www.researchgate.net/publication/15392426. 35, 97

[216] A. M. Pastor, R. R. D. L. Cruz & R. Baker; «Characterization and adaptive modification of the goldfish vestibuloocular reflex by sinusoidal and velocity step

vestibular stimulation»; Article in Journal of Neurophysiology (1992). https://www.researchgate.net/publication/21664975. 35, 97, 99

[217] Y. Mu, D. V. Bennett, M. Rubinov, S. Narayan, C. T. Yang, M. Tanimoto, B. D. Mensh, L. L. Looger & M. B. Ahrens; «Glia Accumulate Evidence that Actions Are Futile and Suppress Unsuccessful Behavior»; Cell (2019). ISSN 10974172. 35

[218] J. P. Hornung; «The human raphe nuclei and the serotonergic system»; Journal of Chemical Neuroanatomy **26**, p. 331–343 (2003). ISSN 0891-0618. 35

[219] G. Migault; «Whole-Brain Calcium Imaging during Physiological Vestibular Stimulation in Larval Zebrafish»; (2020). https://hal.science/tel-03179291https://hal.science/tel-03179291/document. 38, 41

[220] G. L. Goc; «Exploration of larval zebrafish internal states using temperature»; (2021). https://hal.science/tel-03404623https://hal.science/tel-03404623/document. 38, 41

[221] R. Olive; «Flow and vibration perception in zebrafish larva : behavioral study and imaging»; (2015). https://theses.hal.science/tel-01293005https://theses.hal.science/tel-01293005/document. 38, 41

[222] L. Ronconi, L. Casartelli, S. Carna, M. Molteni, F. Arrigoni & R. Borgatti; «When one is Enough: Impaired Multisensory Integration in Cerebellar Agenesis»; (2016). 56

[223] M. Kunst, E. Laurell, N. Mokayes, A. Kramer, F. Kubo, A. M. Fernandes, D. Förster, M. D. Maschio & H. Baier; «A Cellular-Resolution Atlas of the Larval Zebrafish Brain»; Neuron **103**, p. 21–38.e5 (2019). ISSN 0896-6273. 70, 71

[224] F. A. Miles & B. B. Eighmy; «Long-term adaptive changes in primate vestibuloocular reflex. I. Behavioral observations.»; https://doi.org/10.1152/jn.1980.43.5.1406 **43**, p. 1406–1425 (1980). ISSN 00223077. https://journals.physiology.org/doi/10.1152/jn.1980.43.5.1406. 96

[225] R. J. Egan, C. L. Bergner, P. C. Hart, J. M. Cachat, P. R. Canavello, M. F. Elegante, S. I. Elkhayat, B. K. Bartels, A. K. Tien, D. H. Tien,

S. Mohnot, E. Beeson, E. Glasgow, H. Amri, Z. Zukowska & A. V. Kalueff; «Understanding behavioral and physiological phenotypes of stress and anxiety in zebrafish»; Behavioural Brain Research **205**, p. 38–44 (2009). ISSN 0166-4328. 117

[226] C. Beppi, G. Beringer, D. Straumann & S. Y. Bögli; «Light-stimulus intensity modulates startle reflex habituation in larval zebrafish»; Scientific Reports 2021 11:1 **11**, p. 1–7 (2021). ISSN 2045-2322. https://www.nature.com/articles/s41598-021-00535-9. 117

[227] C. Beppi, D. Straumann & S. Y. Bögli; «A model-based quantification of startle reflex habituation in larval zebrafish»; Scientific Reports 2021 11:1 **11**, p. 1–14 (2021). ISSN 2045-2322. https://www.nature.com/articles/s41598-020-79923-6. 117

[228] R. G. Foster, M. S. Grace, I. Provencio, W. J. Degrip & J. M. Garcia-Fernandez; «Identification of vertebrate deep brain photoreceptors»; Neuroscience Biobehavioral Reviews **18**, p. 541–546 (1994). ISSN 0149-7634. 117

[229] H. A. Moore & D. Whitmore; «Circadian Rhythmicity and Light Sensitivity of the Zebrafish Brain»; PLOS ONE **9**, p. e86 176 (2014). ISSN 1932-6203. https://journals.plos.org/plosone/article?id=10.1371/journal.pone.0086176. 117

[230] A. M. Fernandes, K. Fero, A. B. Arrenberg, S. A. Bergeron, W. Driever & H. A. Burgess; «Deep Brain Photoreceptors Control Light-Seeking Behavior in Zebrafish Larvae»; Current Biology **22**, p. 2042–2047 (2012). ISSN 0960-9822. 117

[231] V. S. tih ID, L. I. Petrucco, A. M. K. ID & R. I. Portugues; «Stytra: An open-source, integrated system for stimulation, tracking and closed-loop behavioral experiments»; (2019). https://doi.org/10.1371/journal.pcbi.1006699. 147